The Development and Validation of a Hydrodynamic Model of False Bay

by

Fawaaz Coleman

Thesis presented in fulfilment of the requirements for the degree of

Master of Engineering in the Faculty of

Civil Engineering at Stellenbosch University

Supervisor: Dr. Andre K. Theron

Co-supervisor: Dr. Gerhardus P. J. Diedericks

April 2019

UNIVERSITEIT•STELLENBOSCH•UNIVERSITY
jou kennisvennoot • your knowledge partner

PLAGIARISM DECLARATION

1 Plagiaat is die oorneem en gebruik van die idees, materiaal en ander intellektuele eiendom van ander persone asof dit jou eie werk is.

Plagiarism is the use of ideas, material and other intellectual property of another's work and to present is as my own.

2 Ek erken dat die pleeg van plagiaat 'n strafbare oortreding is aangesien dit 'n vorm van diefstal is.

I agree that plagiarism is a punishable offence because it constitutes theft.

3 Ek verstaan ook dat direkte vertalings plagiaat is.

also understand that direct translations are plagiarism.

4 Dienooreenkomstig is alle aanhalings en bydraes vanuit enige bron (ingesluit die internet) volledig verwys (erken). Ek erken dat die woordelikse aanhaal van teks sonder aanhalingstekens (selfs al word die bron volledig erken) plagiaat is.

Accordingly all quotations and contributions from any source whatsoever (including the internet) have been cited fully. I understand that the reproduction of text without quotation marks (even when the source is cited) is plagiarism.

5 Ek verklaar dat die werk in hierdie skryfstuk vervat, behalwe waar anders aangedui, my eie oorspronklike werk is en dat ek dit nie vantevore in die geheel of gedeeltelik ingehandig het vir bepunting in hierdie module/werkstuk of 'n ander module/werkstuk nie.

declare that the work contained in this assignment, except where otherwise stated, is my original work and that I have not previously (in its entirety or in part) submitted it for grading in this module/assignment or another module/assignment.

Studentenommer / *Student number*	**Handtekening / *Signature***
Voorletters en van / *Initials and surname* F COLEMAN	**Datum / *Date*** April 2019

ABSTRACT

False Bay is located in the Western Cape and is the largest coastal embayment along the South African coastline. The location of the bay is unique in that it is influenced by a complex wind regime and by both the Benguela and Agulhas currents. In recent years, False Bay has become the focus of numerous studies investigating engineering and environmental issues such as water quality issues, storm events, wave focusing and rip currents at certain beaches. In order to understand and assess these issues, physical processes, such as coastal hydrodynamics, within False Bay needs to be well defined.

The findings of a comprehensive literature review revealed that despite the notable contributions of various historical studies on the analysis of bay circulation and the physical processes driving them, there remains significant uncertainty mainly due to these studies being undertaken over short durations and on limited spatial scales. Most importantly, regarding coastal hydrodynamics, few historical studies have investigated the effect(s) of the spatially varying wind field in False Bay which has been regarded as a significant hindrance in providing robust simulation of hydrodynamics. One of the major objectives of this thesis was therefore to address the shortcomings of historical studies by providing a thorough evaluation of intra-annual hydrodynamics within False Bay with particular emphasis on defining (1) current circulation; (2) horizontal thermal structure (sea surface temperatures); and (3) vertical thermal structure.

In order to evaluate the three hydrodynamic processes above, a three-dimensional hydrodynamic model was developed, calibrated and verified. The modelling approach included the influence of the spatially-varying wind field, daily averaged temperature-depth profiles on the boundaries and atmospheric heat exchange.

The model results relating to current circulation were consistent with historical studies which described a cyclonic (clockwise) circulation within the bay under south-easterly wind conditions. The development of this cyclonic pattern is due to the spatially varying wind field. During warmer months, upwelling events were noted at Cape Hangklip. Interestingly, under north-westerly wind conditions, the model results deviated from historical findings by showing a spatially-uniform current field across the bay. Under these conditions, strong bottom return currents are generated which contribute significantly to cold water intrusion events within the bay.

Analysis of model results revealed that the horizontal thermal structure is uniform during colder months (June to August). In summer months, surface temperatures were progressively warmer toward the northern shore. This finding was consistent with composite satellite measurements.

Furthermore, upwelling cells were identified at Cape Point, along the eastern shore and at Cape Hangklip.

Regarding the vertical thermal structure of the bay, the model results indicated that at the entrance of False Bay, the influence of Rocky Bank was very apparent. This feature segregates warmer western and colder eastern waters. Due to the asymmetry of bathymetry at the entrance, bottom waters are approximately 1-2℃ colder east of Rocky Bank under well-mixed (isothermic) and stratified conditions. In warmer months, under stratified conditions, the north-westerly winds significantly contribute to stratification in the bay due to cold water advection from offshore to the middle of the bay.

Sensitivity analyses were undertaken to investigate the potential engineering application of hydrodynamic modelling of False Bay. It was found that a two-dimensional hydrodynamic model of False Bay would be suitable for the simulation of hydrodynamics under well-mixed conditions. In addition, the sensitivity results proved that spatially uniform wind fields are not sufficient in characterising hydrodynamic processes within False Bay. Furthermore, the sensitivity analyses indicated that monthly-averaged temperature-depth profiles on the boundary provided results that were comparable to those from daily-averaged temperature-depth profiles.

OPSOMMING

Valsbaai is in die Wes-Kaap geleë en is die grootste baai langs die Suid-Afrikaanse kuslyn. Die ligging van die baai is uniek aangesien dit beïnvloed word deur ‘n komplekse windregime en deur beide die Benguela en Agulhas strome. In die verlede was Valsbaai die onderwerp van talle studies rakende ingenieurs- en omgewingsaangeleenthede soos byvoorbeeld waterkwaliteit, storms, fokussering van golwe en sleurstrome by sommige strande. Om hierdie prosesse te verstaan en te kwantifiseer moet die fisiese prosesse, soos kushidrodinamika, in Valsbaai goed gedefinieer word.

‘n Omvattende literatuurstudie het aangetoon dat, benewens die noemenswaardige bydraes van verskeie historiese studies oor die analise van sirkulasie in die baai en die fisiese prosesse wat dit veroorsaak, is daar nog steeds beduidende onsekerheid hoofsaaklik omdat hierdie studies oor kort periodes en op beperkte fisiese skaal uitgevoer is. Die belangrikste tekortkoming, wat kushidrodinamika aanbetref, is dat daar te min studies is wat ondersoek ingestel het oor die effekte van wind wat ruimtelik oor die baai varieer wat beskou word as die hoofbeperking om akkurate hidrodinamiese simulasies te doen. Een van die hoofdoelwitte van hierdie tesis was om die tekortkominge van die historiese studies aan te spreek deur middel van ‘n deeglike ondersoek van hidrodinamika wat binne ‘n tydskaal van ‘n jaar verander in Valsbaai met spesifieke klem op die definiëring van (1) stroomsirkulasie (2) seevlak temperature; en (3) vertikale temperature.

Om bogenoemde drie hidrodinamiese prosesse te evalueer, is ‘n drie-dimensionele hidrodinamiese model opgestel, gekalibreer en geverifieer. Die modellering ondersoeke het die invloed van winde wat ruimtelik varieer ingesluit asook diepte-profiele van daaglikse gemiddelde temperature op die grense van die model en atmosferiese hitte-uitruiling.

Die model- resultate rakende stroomsirkulasie was in ooreenstemming met historiese studies wat ‘n sikloniese (kloksgewyse) sirkulasie in die baai beskryf tydens ‘n suidooste wind toestand. Die sikloniese sirkulasie is ‘n gevolg van die windveld wat ruimtelik varieer. Gedurende warmer maande, is opstuwing by Hangklip opgemerk. Onder noordweste winde wyk die model resultate af van historiese studies deur ‘n ruimtelik uniforme stroomveld oor die baai aan te toon. Onder hierdie omstandighede word sterk trustrome op die bodem opgewek wat ‘n beduidende invloed het op koue water wat in die baai inbeweeg.

‘n Analise van die model resultate het ook aangedui dat die seevlak temperature uniform is gedurende kouer maande (Junie tot Augustus). Gedurende somer maande word die temperature op die oppervlak progressief warmer in die rigting van die noordelike strande. Die bevindinge is in ooreenstemming met satellietmetings. Verder is opstuwing langs Kaappunt opgemerk asook langs die oostelike strande en Hangklip.

Wat die vertikale temperatuur verspreiding in die baai aanbetref, dui die model resultate daarop dat by die ingang tot die baai het Rocky Bank ‘n beduidende invloed. Hierdie rotsbank verdeel warme westelike vloei van koue oostelike vloei. As gevolg van die feit dat die dieptes by die ingang tot die baai nie simmetries is nie, is die water op die bodem ongeveer 1-2^{o}C kouer oos van Rocky Bank onder toestande waar die water beide vermeng is en ook gestratifiseer is. In warmer maande, onder toestande waar die water gelaag (gestratifiseer) is, dra noordweste winde by tot die stratifikasie in die baai deur adveksie van koue water vanaf die diepsee tot in die middel van die baai.

‘n Sensitiwiteitsanalise is onderneem om ondersoek in te stel na die moontlike ingenieurs toepassings van die hidrodinamiese model van Valsbaai. Daar is bevind dat ‘n twee-dimensionele hidrodinamiese model van Valsbaai toepaslik sal wees vir simulasies wanneer die water vermeng is. Verder het die sensitiwiteitsanalise ook getoon dat winde wat ruimtelik uniform is, nie voldoende is om hidrodinamiese prosesse in Valsbaai te karakteriseer nie. Die sensitiwiteitsanalise het ook aangetoon dat maandelikse gemiddelde temperatuurprofiele oor die diepte op die grense van die model resultate lewer wat vergelykbaar is met resultate gebaseer op daaglikse gemiddelde temperatuurprofiele.

ACKNOWLEGDEMENTS

The financial assistance provided by my employer, Prestedge Retief Dresner Wijnberg (PRDW), for my complete master's degree is hereby acknowledged. I would also like to extend my thanks and gratitude for the company's continual support and encouragement.

I would like to thank the South African Weather Service (SAWS), Prestedge Retief Dresner Wijnberg (PRDW), Council for Scientific and Industrial Research (CSIR) and Institute for Maritime Technology (IMT) for providing me with data crucial to this study. In addition, I would like to extend enormous thanks and gratitude to Dr. Chris Lennard from the University of Cape Town's (UCT) Climate Systems Analysis Group (CSAG) who provided me with high quality wind datasets which underpin this study.

I would like to thank DHI South Africa for providing me with a MIKE student software license. Without the MIKE software suite, this study would not have been possible.

My supervisors Dr. Andre Theron and Dr. Gerhardus Diedericks are greatly acknowledged for their support, guidance and patience. I am very grateful for their genuine interest in my work and their willingness to assist throughout the course of this study. In addition, I would like to thank Mr. Stephen Luger for his assistance, guidance and providing me with valuable insight into hydrodynamic modelling.

Lastly, I would like to thank my close friends and family for their continual support and guidance. Without their support, the commencement and development of my master's degree would not be possible.

CONTENTS	Page Number

TABLES

FIGURES

LIST OF ABBREVIATIONS AND ACRONYMS

ADCP:	Acoustic Doppler Current Profiler
AGL:	Above Ground Level
CD:	Chart Datum
CSAG:	Climate Systems Analysis Group (University of Cape Town)
CSIR:	The Council for Scientific and Industrial Research
CTD:	Conductivity, Temperature and Depth (Measurement Instrument)
Deg:	Degrees
DHI:	Danish Hydraulics Institute
ECMWF:	European Centre for Medium-Range Weather Forecasts
HAT:	Highest Astronomical Tide
H_s:	Significant Wave Height
HYCOM:	Hybrid Coordinate Ocean Model
LAT:	Lowest Astronomical Tide
m:	Metre
m^2:	Metre Squared
m/s:	Metre(s) per second
MSL:	Mean Sea Level
NOAA:	National Oceanic and Atmospheric Administration
SST:	Sea Surface Temperature
T_p:	Peak Wave Period
TN:	True Norh
WASA:	Wind Atlas of South Africa Project
WOA:	World Ocean Atlas

GLOSSARY AND DEFINITIONS

Advection:	The transfer of a property such as heat by the movement of water
Bathymetry:	Underwater depth of the ocean bed
Coriolis force:	A force that as a result of the earth's rotation deflects moving objects
Current:	Flow of water in a specific direction
Current Direction:	The direction towards which the current is flowing, measured clockwise from true north
Hydrodynamics:	The movement of fluid
Salinity:	The measure of all the salts dissolved in water
Significant wave height:	The significant wave height, determined from the zeroth moment of the wave energy spectrum. It is approximately equal to the average of the highest one-third of the waves in a given sea state
Stratification:	Formation of water layers based on salinity and temperature
Upwelling:	An oceanographic phenomenon that involves wind- and Coriolis-driven motion of dense, cooler, and usually nutrient-rich water towards the ocean surface, replacing the warmer, usually nutrient-depleted surface water
Wave direction:	The direction from which the wave is coming, measured clockwise from true north
Well-mixed:	Isothermic or uniform temperature distribution throughout the water column
Wind direction:	The direction from which the wind is coming, measured clockwise from true north
Wind setup:	The vertical rise in the still water level on the leeward side of a body of water caused by wind stresses on the surface of the water.

CHAPTER 1: INTRODUCTION AND BACKGROUND

1.1 Background

False Bay is a natural coastal embayment in the Western Cape, near Cape Town, that serves many functions which support the livelihoods of a rapidly growing population of over 4 million people. Fishing activities, including recreational and subsistence fishing are very popular with many fishing harbours dotted along the coastline. Popular recreational activities in the region include surfing, swimming, scuba diving and sailing with sailing clubs located in Fish Hoek, Simons Town, Gordons Bay and Strand. The bay also serves a variety of marine life including dolphins, whales, sharks, seabirds and Cape fur seals which occupy Seal Island near the northern coastline.

The bay is the largest along the South African coastline (Rundgren, 1992) and is almost square in shape with each side approximately 30 - 35 kilometres in length with the southern entrance to the Atlantic Ocean being approximately 35 km wide. The locality map of False Bay is shown in Figure 1-1. The location of False Bay is unique in that it is influenced by the Agulhas Current and the Benguela Current. In addition, due to the surrounding mountainous topography, the meteorology of the region is complex with wind fields creating a persistent upwelling region within the bay during summer months (Dufois & Rouault, 2012). These regional influences fundamentally affect circulation in the bay which may be regarded as highly complex (Nicholson, 2011).

Current environmental issues facing False Bay include erosion along the northern coastline, water quality issues, extreme storm events (particularly storm surge), wave focussing and rip currents at certain beaches (Taljaard et al., 2000). These issues emphasise the need for a contemporary evaluation of physical processes occurring in False Bay.

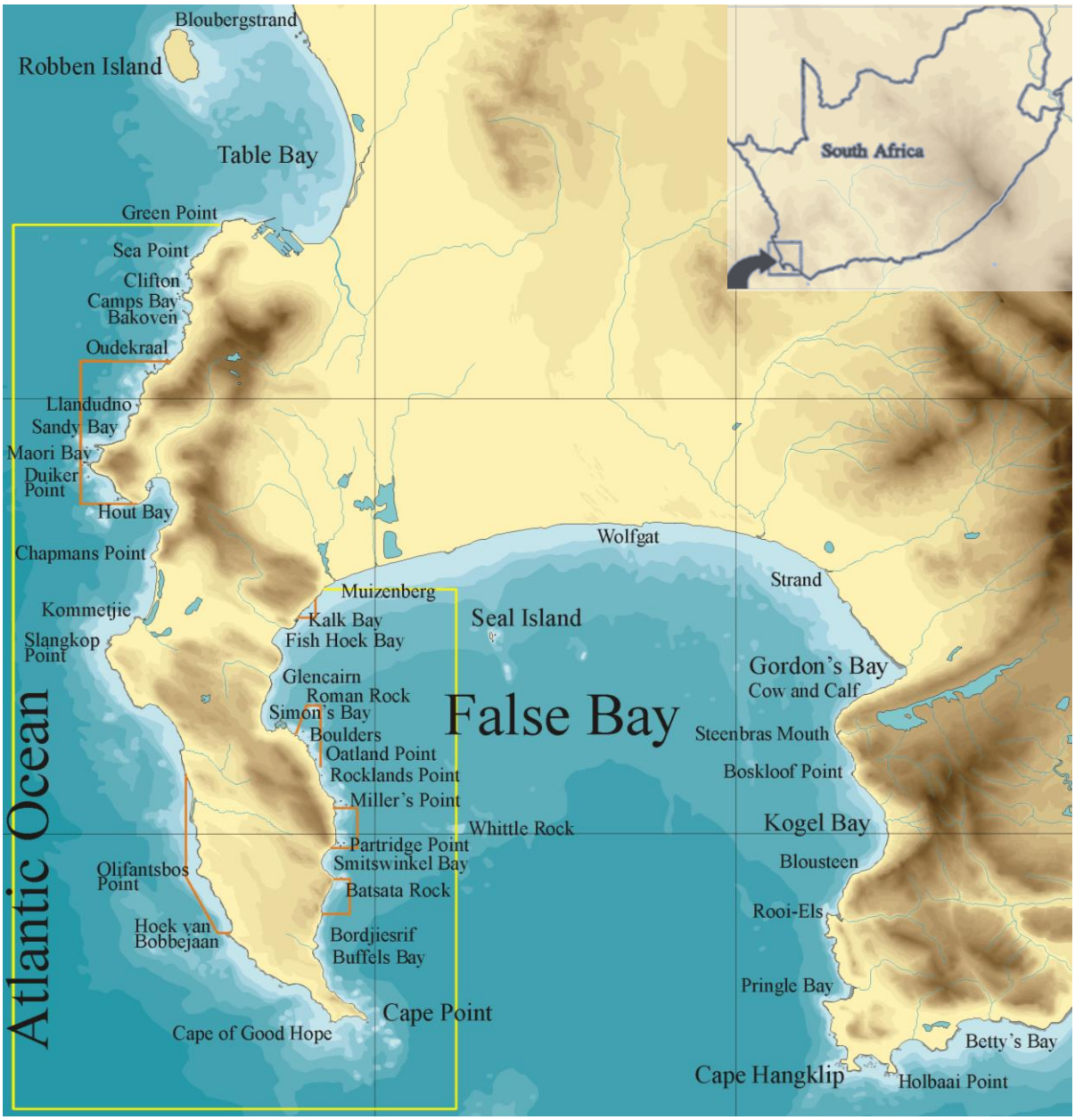

Figure 1-1: Locality Map of False Bay (Jones, 2008)

1.2 Significance of the Study

During the 1970s to early 1990s False Bay was the focus of many observational studies (Shannon et al., (1983); Jury, (1985); Jury, (1986); Botes, (1988); Gründlingh et al., (1989); Gründlingh & Largier, (1991); Gründlingh & Potgieter, (1993)) focusing on the collection of measurement data and establishing a database and understanding of the broader physical characteristics of the bay, particularly current circulation patterns. However, despite these numerous studies, the analysis of circulation in the bay, and the physical processes driving it, there remains significant uncertainty mainly due to:

- The short duration of measurement campaigns underpinning these studies; and

- The limited spatial scale of measurement campaigns.

Hydrodynamic models are capable of overcoming the shortcomings listed above by resolving long-term coastal hydrodynamic processes over a large spatial scale. In addition, due to recent developments in numerical algorithms and increases in computational processing power, high resolution three-dimensional hydrodynamic models are commonly formulated to resolve mesoscale coastal circulation features robustly and proficiently (Penven, et al., 2001).

During recent years, various hydrodynamic modelling studies have investigated aspects affecting False Bay (Nicholson, 2011). However, a major limitation of these models is insufficient calibration and verification against measurement data. In addition, spatially varying wind forcing has not been considered in these studies which has been regarded as a serious hindrance in providing robust simulation of the hydrodynamics of False Bay (Taljaard et al., 2000). Therefore, the current study is one of the first studies to investigate the influence of spatially varying wind forcing on the coastal hydrodynamics of False Bay.

1.3 Aims, Objectives and Limitations

The aim of this thesis is to add to the existing body of knowledge on False Bay's physical processes with particular emphasis on bay circulation and hydrodynamic processes such as spatially varying wind forcing and intra-annual variability of sea temperature. In addition, this thesis was developed to assist potential engineering applications of hydrodynamic modelling of False Bay. Lastly, it is envisaged that this thesis will serve as a basis for the potential development of an operational forecast model(s).

This study comprises the development of a three-dimensional (3D) hydrodynamic model which considers wind forcing, tidal forcing, temperature-depth profiles on the boundary and atmospheric inputs. However, the model does not consider wave coupling and the resulting physical processes such as wave breaking and longshore currents. In addition, the model is driven by a smooth tidal signal on the boundaries which excludes the effect of other water level constituents such as coastally trapped waves, long waves, short waves, smaller timescale gusting events etc. This means these perturbations in water level and subsequently current variation are not captured.

The model mesh is reasonably course and does not resolve hydrodynamics in the surf zone.

1.4 Thesis Structure

The thesis structure comprises eight chapters. Chapter 1 introduces the thesis topic and study motivation. Chapter 2 provides the literature review which includes a description of False Bay physical processes and a review of historical observational studies. Chapter 3 summarises background literature on hydrodynamic models. Chapter 4 describes the hydrodynamic model methodology which comprises the model description, model inputs and simulation period. Chapter 5 provides the model calibration and model verification results which include the calibration and verification of water levels, atmospheric conditions, currents and sea temperature. Chapter 6 presents the hydrodynamic model results and sensitivity analyses which comprise a comprehensive description of the intra-annual (seasonal) current circulation, vertical thermal structure and sea surface temperature. Chapter 7 concludes the thesis and provides recommendations for future studies. Chapter 8 provides the references used in the study.

CHAPTER 2: LITERATURE REVIEW

False Bay is categorised as an approximately rectangular shaped body of water bound by coastlines on the western, northern and eastern extents. Mountains flank the bay, notably the Cape Peninsula Mountain Chain to the west and the Hottentots-Holland Mountains to the east. The Northern area accommodates the Cape Flats which is a sandy featureless region connecting the western and eastern mountain ranges. The bay encloses an approximate area of 35 km x 30 km which is less than 100 m deep. It has been estimated that the mean depth of the bay is approximately -41 m MSL (Taljaard et al., 2000). There are few rivers discharging into the bay with an estimated 1% of bay volume comprising annual river runoff.

Coastal embayments such as False Bay are unlike the coastal ocean mainly due to their surrounding topography and bathymetry. Water circulation inside these embayments differs from an exposed coast mainly due to tidal flow and regional coastal currents (Hearn, 2008). Therefore, more temperature and salinity variation is present than along an open coast. Furthermore, the complex mountainous topography surrounding False Bay results in a complex wind field that contributes to complex hydrodynamic behaviour within the bay such as seasonal upwelling. Moreover, the geographic position of the bay is in a rare location that is significantly influenced by both the warm Agulhas current and the cold Benguela current. The interaction of these two currents further adds to the complexity of the hydrodynamics within False Bay. This hydrodynamic interaction and the complex wind-induced upwelling, has resulted in False Bay being the focus of a number of studies over the last four decades (Cram, (1970); Atkins, (1970a); Shannon et al,. (1983); Jury, (1985); Jury, (1986); Botes, (1988); Gründlingh et al., (1989); Gründlingh & Largier, (1991); Gründlingh & Potgieter, (1993); Nicholson, (2011); Dufois et al., (2012)).

This section is a prelude to the hydrodynamic modelling of the bay by providing a summary of the hydrodynamics of False Bay comprising coastal basin physical processes such as current circulation, the wind climate, wave driven currents, wind driven currents and sea temperature.

2.1 Initial Description of Site Conditions

This section serves as an introduction to key physical processes in False Bay. More detailed descriptions of physical processes are presented in subsequent sections.

2.1.1 Bathymetry

False Bay is characterised by long northern beaches spanning between Muizenberg and Gordons Bay which are briefly interrupted by cliffs at Swartklip (refer to Figure 1-1). This section of the bay has a sandy bottom to the west with a fragmented rocky bottom towards the

east. To the south of the bay, steep headlands flank either side of the bay, namely Cape Point to the west and Cape Hangklip to the east. The deepest point in the bay is near the mouth with a depth of approximately -90 m MSL and becomes shallower toward the northern boundary. The eastern and western boundaries comprise steep rocky shorelines with small bays dotted along these boundaries, notably Simons Town and Gordons Bay.

The major topographic features in the bay influencing the hydrodynamics of the bay, include (Taljaard et al., 2000):

- A vast shallow rocky region at less than -22 m MSL known as Rocky Bank located at the mouth of the bay;
- The shallow rocky region spanning 20 km from Cape Hangklip which is named the Hangklip Ridge;
- The shallow rocky region of Cape Point; and
- Deep water channels on either side of Rocky Bank which occasionally lead to focusing of waves, especially on the east coast.

The features above directly influence the shelf-bay exchange and the wave climate of the False Bay region. Other features within the bay include (Taljaard et al., 2000):

- Seal Island and York Shoal to the north of False Bay;
- Whittle Rock which is located in the western half of the bay and is surrounded by a number of isolated rocks covering an extensive area;
- East Shoal located near the middle of northern False Bay; and
- The series of ridges with a north-south orientation in the eastern side of the bay.

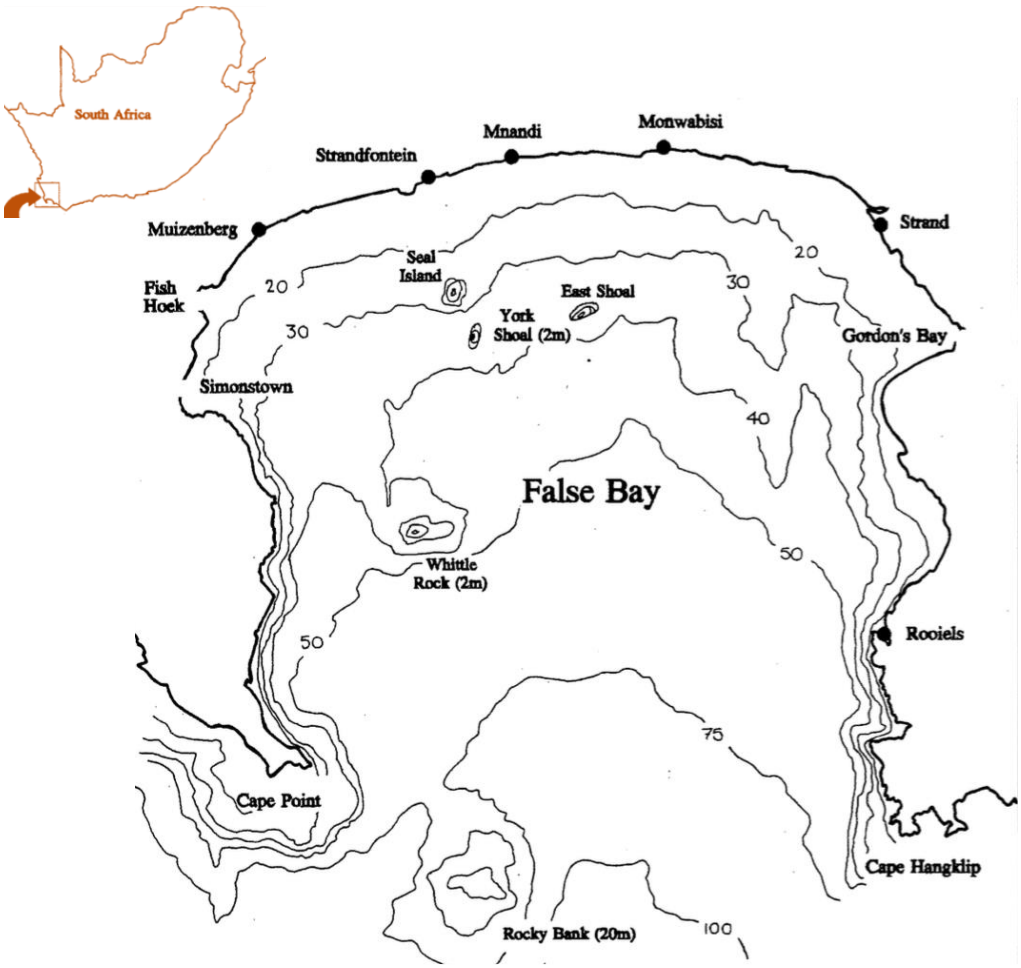

Figure 2-1: Overview of Bathymetric Features of False Bay (Rundgren, 1992)

One of the more recent studies investigating the influence of False Bay's bathymetry on metocean conditions was a study by Nicholson (2011). The study involved the set-up of a hydrodynamic model of False Bay with the aim of forming a comparative analysis of a (1) "constant bathymetry scenario", which assumed an average depth of -50 m MSL across the entire domain, with a (2) "realistic bathymetry" scenario, which considered the actual bathymetry of False Bay. The results of the comparative analysis showed that the there was an apparent "seasonal decoupling" in the realistic bathymetry scenario i.e. the surface currents and bottom currents behaved independently of one another in summer months. This phenomenon was determined to be partly due to the influence of the unique bathymetry of False Bay. More specifically, shallow regions within the bay, such as Rocky Bank, contribute significantly to the flow regime and therefore the thermal structure, seasonal stratification and circulation in the bay.

2.1.2 Wind Climate

The wind regime within False Bay is seasonally bimodal with a dominant south-easterly wind in summer months and a dominant north-westerly wind in the winter months. This seasonality

in wind conditions is due to major atmospheric pressure systems which move northwards in winter meaning that the predominant wind conditions change from the typical south-to-south east winds associated with the South Atlantic high-pressure system, to north-to-north west associated with the mid-latitude cyclones and coastal lows (Taljaard et al., 2000).

2.1.3 Wave Climate

Wave conditions significantly influence sediment transport within the bay primarily due to turbulence and the generation of longshore currents around the periphery of the bay. The wave interaction with Rocky Bank has been the focus of a few studies, particularly the focusing of waves between the Steenbras River mouth and Cape Hangklip (Taljaard et al., 2000). This focusing is prevalent during the refraction of south westerly swells into the bay.

2.1.4 Seasonality and Stratification

During thermal stratification, large water bodies such as bays are characterised by a water column that exhibits a warm upper layer and a colder denser bottom layer. The layer of water between these extremes is termed the thermocline which is subject to rapid changes in temperature in relation to depth. The major factors governing vertical stratification are buoyancy inputs, mixing produced by winds and tides, and the interaction of vertically sheared currents with a horizontal density gradient i.e. tidal straining (Cheng, et al., 2010a). In coastal environments, including bays, where freshwater influences are absent, the main driver of stratification is atmospheric input of heat (solar radiation) at the water surface which leads to seasonal changes in vertical stratification. In addition, coastal upwelling due to wind forcing plays a major role in driving water temperature and density stratification in coastal embayments (Cheng, et al., 2010a). Due to the unique location of False Bay, water temperature is influenced by the interaction of the Benguela and Agulhas currents.

During the summer months (December to February), False Bay is characterized by thermal stratification while in winter months (June to August), the water column is isothermal (Dufois & Rouault, 2012). During summer months, a temperature differential of 5-9˚C is typically expected between the surface and -50 m water depth (Atkins, 1970a). A rapid intensification of the thermocline is generally observed in late December (Gründlingh et al., 1989).

A process-orientated modelling study, employing the Regional Oceanic Modelling System (ROMS) model, was undertaken by Nicholson (2011) which investigated the seasonality and stratification within False Bay. The model considered tidal forcing and unidirectional sustained wind forcing. The results of the study showed that the bathymetry of False Bay significantly influences the circulation within the bay which consequently influences the thermal structure of the water column. In addition, the results showed that within summer months the circulation

in the bay is “decoupled” meaning that bottom and surface flows act independently of one another. More specifically, with a stratified water column in summer, the flow had a two-layered structure with a stronger cyclonic flow at the surface and a weaker cyclonic flow in the bottom layers (<5 cm/s) (Nicholson, 2011). The maximum mean summer velocities were in an order of 10 cm/s. Conversely the results showed that, during winter months when the water column was well-mixed (isothermic), the flow was weaker and uniform with depth.

Figure 2-2 presents a vertical section at the mouth of the bay which indicates the seasonal mean v-component current velocity (north-south) of flow for the first three months JFM (January, February and March) and median months JAS (July, August and September) of the year. Current magnitude is presented as a heat map with northward flow being positive (indicated as red) and southward flow being negative (indicated as blue). In addition, isotherms are overlaid in 0.5˚ C increments on the figure.

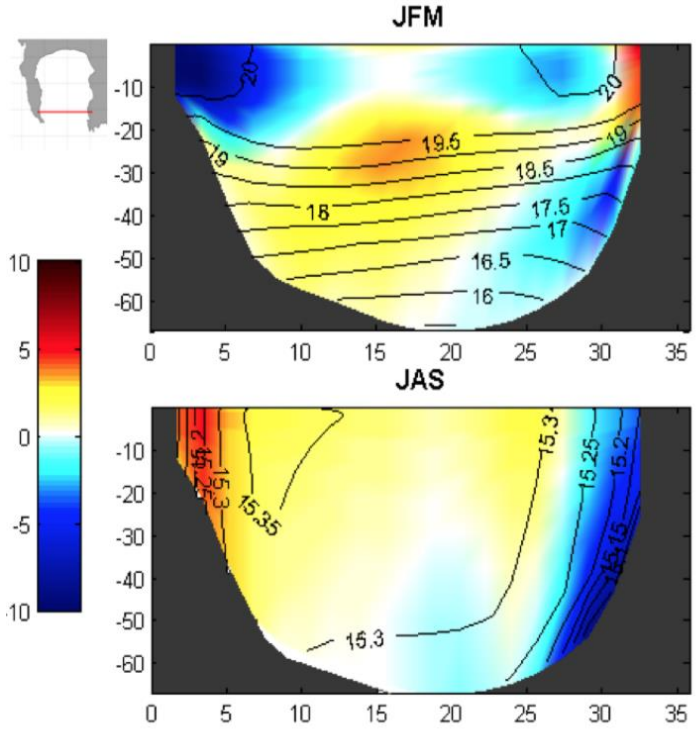

Figure 2-2: The North-South Seasonal Mean Current Velocities (cm/s) Presented as a Heatmap and overlaid with Isotherms (◦C) for JFM and winter JAS (Nicholson, 2011)

2.1.5 Tides

Tidal circulation is more significant during periods of calmer wave and wind conditions (Atkins, 1970a). In addition, tidally-driven current magnitudes are believed to be stronger at the entrance of the bay, at complex bathymetric features and at shallower regions within the bay

(Taljaard et al., 2000). The tidal range is approximately 1.6 m and 0.8 m during spring and neap tide cycles respectively (Gründlingh et al., 1989).

2.2 Observational Studies

2.2.1 Background

During the 1970s to early 1990s False Bay was the focus of many observational studies (Shannon et al., (1983); Jury, (1985); Jury, (1986); Botes, (1988); Gründlingh et al., (1989); Gründlingh & Largier, (1991); Gründlingh & Potgieter, (1993)). These studies focused on the collection of measurement data and establishing a database and a body of knowledge of the broader physical characteristics of the bay, particularly current circulation patterns.

2.2.2 Sea Temperature

2.2.2.1 Sea surface temperature (SST)

Some of the earliest temperature circulation measurements, using airborne infra-red radiation thermometry (ART), were collected by Cram (1970) who confirmed an upwelling zone comprising cold water plumes off Cape Hangklip during the summer where the predominant wind direction is south-easterly. This zone was identified by recognising sea surface temperature anomalies of -6° C to -7° C relative to surrounding surface water.

The data collected from ART measurements was calibrated against conventional recorded sea surface measurements to create temperature plots. Figure 2-3 below shows an example of one of the plots from Cram's (1970) study.

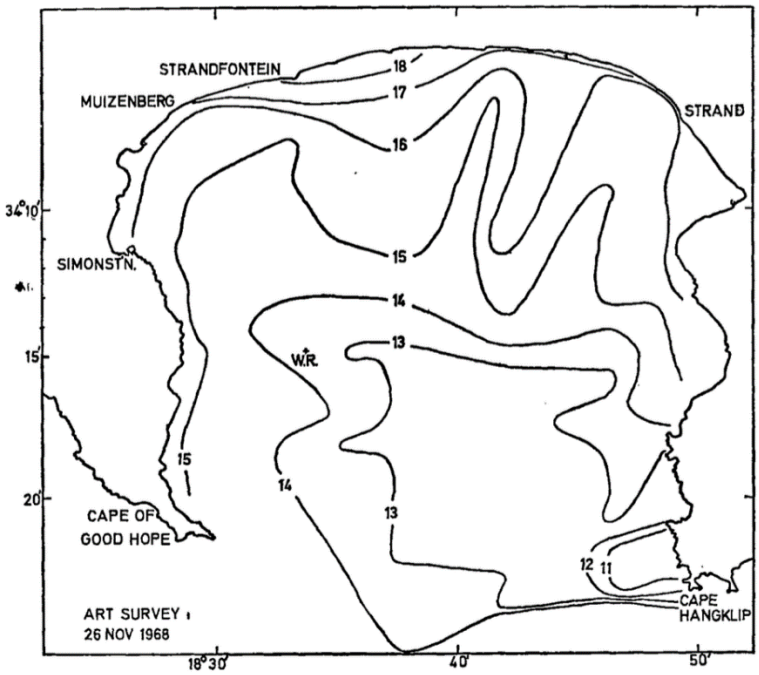

Figure 2-3: Sea Surface Temperature Chart Generated from ART Measurements (Cram, 1970)

In addition, Cram (1970) successfully confirmed the findings by Atkins (1970a) who identified bottom temperatures in False Bay off Cape Hangklip as being less than 12° C.

A more recent study by Dufois et al. (2012) focused on calibrating sea surface temperature data collected from satellite measurements, namely Pathfinder version 5.0 and MODIS/TERRA. The study included a comparative analysis against thermometer sea surface temperature measurements at Gordans Bay. This comparative analysis was done over long datasets spanning decades. The results showed a bias of up to 3° C in the Pathfinder dataset. In addition, the results highlighted the high intra-annual variability in sea surface temperature in the southern half of the bay during summer represented by upwelling cells at Cape Point and Cape Hangklip. An overview of monthly sea surface temperature composite plots derived from satellite measurements spanning 2000-2010 is presented in Figure 2-4.

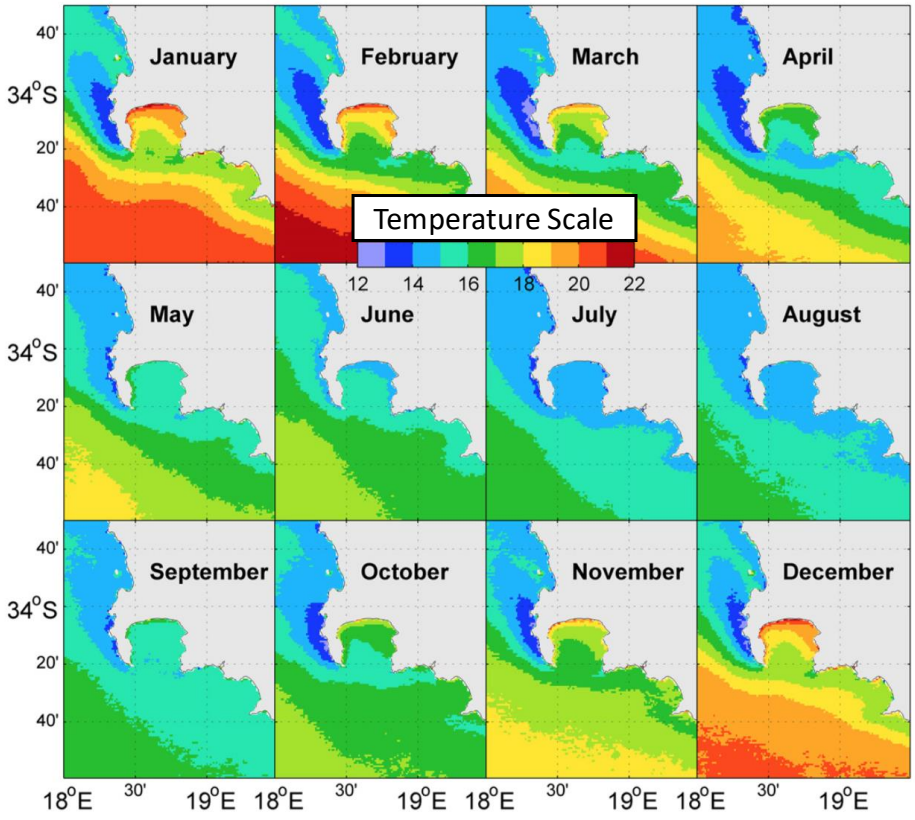

Figure 2-4: Monthly SST (°C) spanning 2000-2010 generated from Composite Satellite Measurements (Dufois et al., 2012)

2.2.2.2 Vertical thermal structure

Gründlingh et al. (1989) investigated temperature gradients at the entrance of the bay with multiple CTD measurements to generate a vertical section temperature plots. These plots are presented in Figure 2-5.

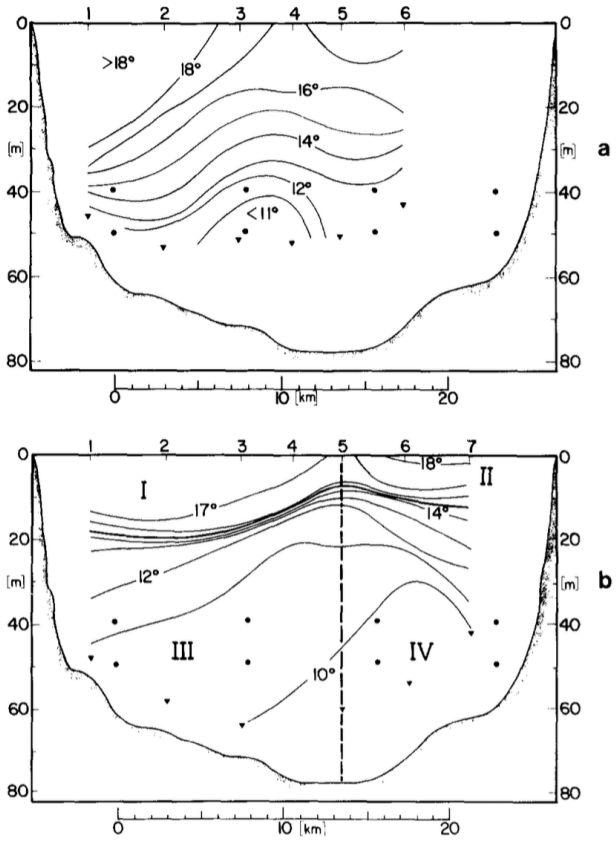

Figure 2-5: Vertical Sections across the Entrance of False Bay during (a) 3 December 1987 and (b) 12 March 1987

From Figure 2-5, the two vertical sections show notable seasonal development of the vertical thermal structure. More specifically, compared to the thermocline in December, the thermocline observed in March is more extreme down to -20 m MSL. In both vertical sections, an average stratification of approximately 0.16° C per meter may be inferred.

2.2.3 Wind Climate

Within False Bay, high variability is present between wind stations around the bay. Wainman et al. (1987) analysed time series data sources from measurement devices at locations around the bay and concluded that correlation was generally poor (less than 0.6). It is also believed that this complex spatially varying wind pattern over False Bay significantly influences the hydrodynamics of the bay. More specifically, it has been postulated that this wind regime is responsible for localised upwelling which results in mixing or stratification of the water column at multiple locations in the bay.

The generation of the spatially varying wind over False Bay may be best described as a synoptic sequence as outlined by Jury (1984):

- *South-west regime*: South-westerly winds are associated with the leading edge of a ridging anticyclone following a cold front. These winds tend to flow uniformly across False Bay and strengthen with time.
- *Deep south-east regime*: Two south-east wind phases follow the south-westerly winds as the anticyclone ridges eastwards south of the subcontinent. First deep south-easterly winds prevail over False Bay. However, a low-level subsidence inversion develops which confines the south-easterly winds to below the Hottentots-Holland and Cape Peninsula mountains. Under deep south easterly conditions winds speeds are accelerated across the bay and a strong downslope jet with a strong easterly component develops in the lee of the Kogelberg mountains.
- *Shallow south-east regime*: During the period of the ridging of the South Atlantic high, the subsidence inversion lowers in height, typically from 1 800 m to 600 m over a period of three days (Jury, 1984). The wind is then prevented from rising over the coastal mountains causing the airflow to deflect seawards, causing an acceleration of the wind past Cape Hangklip and a wind shadow to develop along the eastern side of the bay (Wainman et al., 1987). Wind speeds also decrease from south to north across the bay (Jury, 1984). The wind velocities at Cape Point and Cape Hangklip being approximately twice the magnitude of those along the northern shore. Wainman et al. (1987) described the wind variations across the bay under south-easterly winds using wind data recorded on two survey vessels in False Bay. It was shown that south-easterly winds are deflected on entering the bay to more southerly winds.
- *North-west regime*: This phase follows the passage of the coastal low and signals the approach of a cold front. During this phase the north-westerly winds curl around Table Mountain, becoming more northerly over False Bay. At the mouth of the bay these north to north-westerly winds develop a strong westerly component.

This synoptic sequence described above is presented diagrammatically in Figure 2-6 below. Dashed contours represent isobars and arrows represent predominant wind direction.

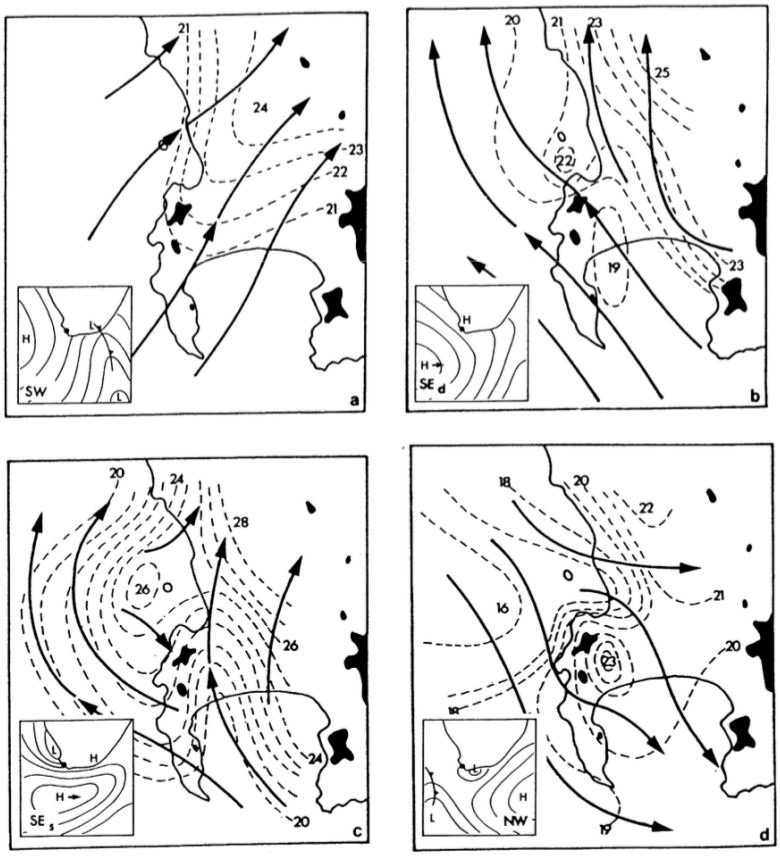

Figure 2-6: A Typical Sequence of the Four Primary Wind Phases Over False Bay (Jury, 1984)

2.2.4 Circulation

Shannon and Chapman (1983) postulated that the dominant inflow into the bay was due to the south-easterly wind and suggested that False Bay could be influenced by the Agulhas Bank as most drifters in their site investigation drifted into False Bay.

Van Forrest and Jury (1985) developed a depth-averaged circulation model, assuming steady-state fixed synoptic conditions and a barotropic water column, which suggested a clockwise circulation within the bay which was consistent with studies around the same time (Cram, (1970); Atkins, (1970a); Shannon et al., (1983) and Botes, (1988)).

Wainman et al. (1987) sought to validate the modelled current behaviour suggested by the above studies by placing four current meter moorings around False Bay between February 1985 and May 1985 namely, two bouys on the -40 m MSL contour between Gordons Bay and Simons Town and another two buoys located on the -60 m MSL contour just off Cape Point and Cape Hangklip, respectively. Generally, the sub-surface measurements at these locations showed that current flow within the bay was more dynamic than previously thought. More specifically, the current measurements at Cape Hangklip and Cape Point showed a southerly

current which challenged the wind-driven cyclonic behaviour derived in Van Forrest and Jury's (1985) numerical model.

Gründlingh et al. (1989) conducted a study incorporating current mooring measurements with fine temporal resolution and multiple CTDs near the entrance of False Bay. The deployment period was from November 1986 to March 1987. An overview of the measurement locations considered in the study is provided in Figure 2-7.

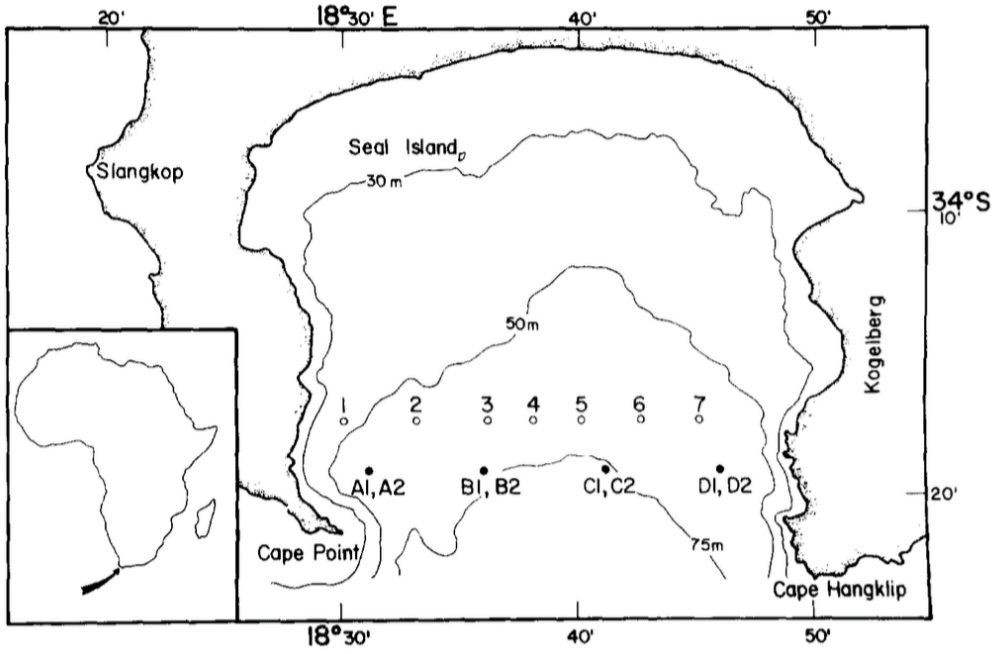

Figure 2-7: Overview of Measurement Locations of CTD (1-7) and Current Moorings (A1-D2) (Gründlingh et al, 1989)

The study further added to the results by Wainman et al. (1987) who postulated a dominant south to south-easterly flow at a current mooring location 5 km south-east of mooring A1/A2 by postulating a "bifurcated" flow pattern at Cape Point which was first postulated by Atkins (1970a). An overview of this bifurcated flow pattern is provided in Figure 2-8.

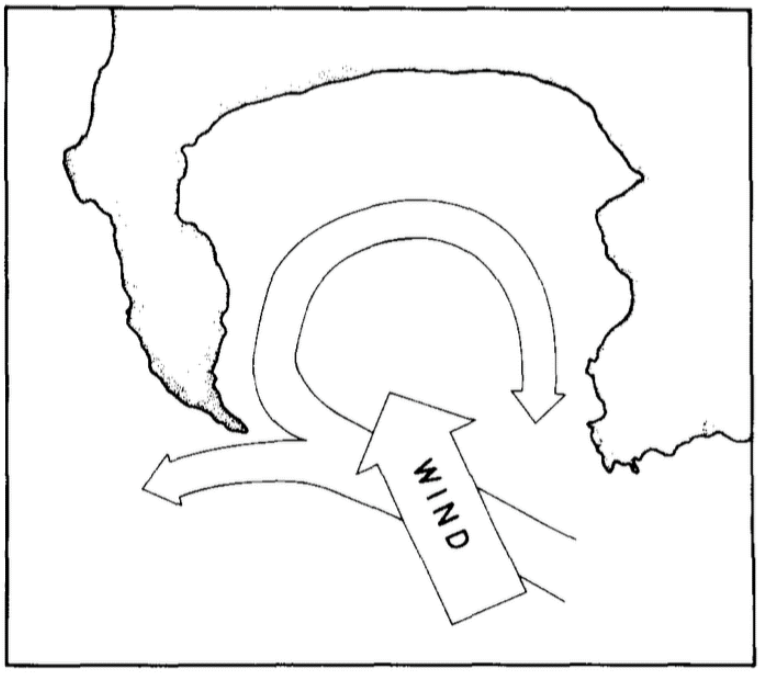

Figure 2-8: Simplified Representation of Bifurcated Flow Pattern Postulated by Gründlingh et al. (1989)

This circulation pattern was later referenced by Gründlingh et al. (1991) as being responsible for biotic plumes generated off the north coast. The study also acknowledged the various time scales, spatial scales and the lack of consistency between previous studies.

In summary, the present understanding of circulation within False Bay is characterised by a predominantly bimodal behaviour which is dependent on the prevailing wind regime over the bay, namely:

- South-easterly wind generated: surface and bottom currents are generated in a cyclonic motion with a small anti-cyclonic gyre formed near Gordons Bay. It is believed that the south-easterly circulation pattern persists under calm and weaker north-westerly wind conditions; and
- North-westerly wind generated: surface and bottom currents are generated in an anticyclonic motion with a small cyclonic gyre formed near Gordons Bay. It should be noted that the correlation between current circulation and north-westerly winds is believed to be weaker than south-easterly generated circulation patterns (Taljaard et al., 2000).

An overview of the above circulation patterns was formulated diagrammatically by Taljaard et al. (2000) and summarises historical observations and empirical relationships of

wind forcing. This overview is provided in Figure 2-9 and Figure 2-10 which refers to the south-easterly and north-westerly wind generated circulation patterns respectively.

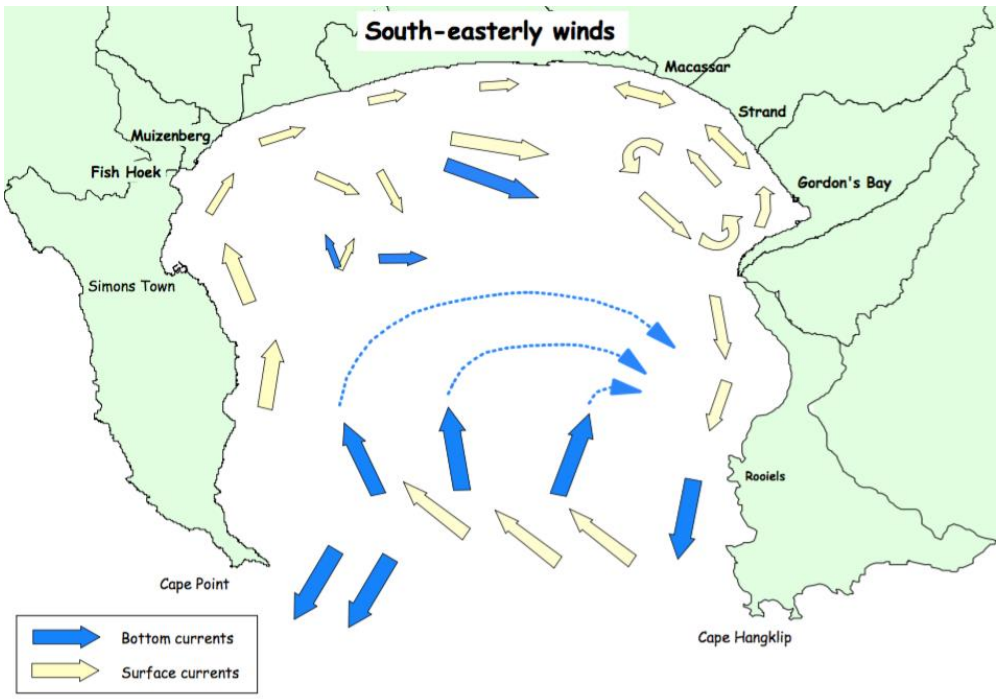

Figure 2-9: Schematic South-easterly Wind Generated Circulation Pattern of Surface and Bottom Flows Inferred from Previous Observational Studies (Taljaard et al., 2000)

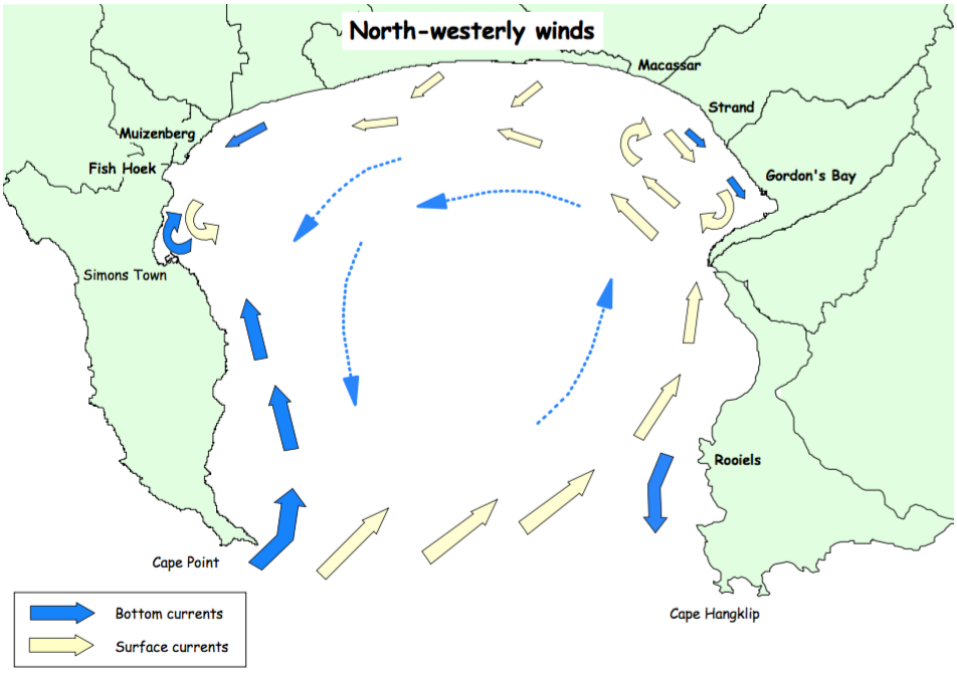

Figure 2-10: Schematic North-westerly Wind Generated Circulation Pattern of Surface and Bottom Flows Inferred from Previous Observational Studies (Taljaard et al., 2000)

The persistence of the south-easterly circulation pattern is believed to be due to the following possibilities (Taljaard et al., 2000):

- Density structures remain during calm and weaker north-westerly wind conditions; and
- Wave-driven currents along the northern shore promote a cyclonic circulation pattern.

It should be noted that the influence of wave-drive currents is believed to be more significant in shallower waters with wind-driven currents being more dominant in deeper waters in the central region and along the deeper western and eastern boundaries of the bay.

2.2.5 Wave-driven Longshore Currents

Wave-driven longshore currents in the surf zone due to obliquely incident wave and/or wave-set up are summarised from a CSIR (1982) study in Figure 2-11. The northern shore of False Bay comprises several sandy beaches with a wide surf zone where wave-driven currents and turbulence dominates. The influence of wave-driven currents is believed to be more significant in shallower waters with wind-driven currents being more dominant in deeper waters in the central region and along the deeper western and eastern boundaries of the bay.

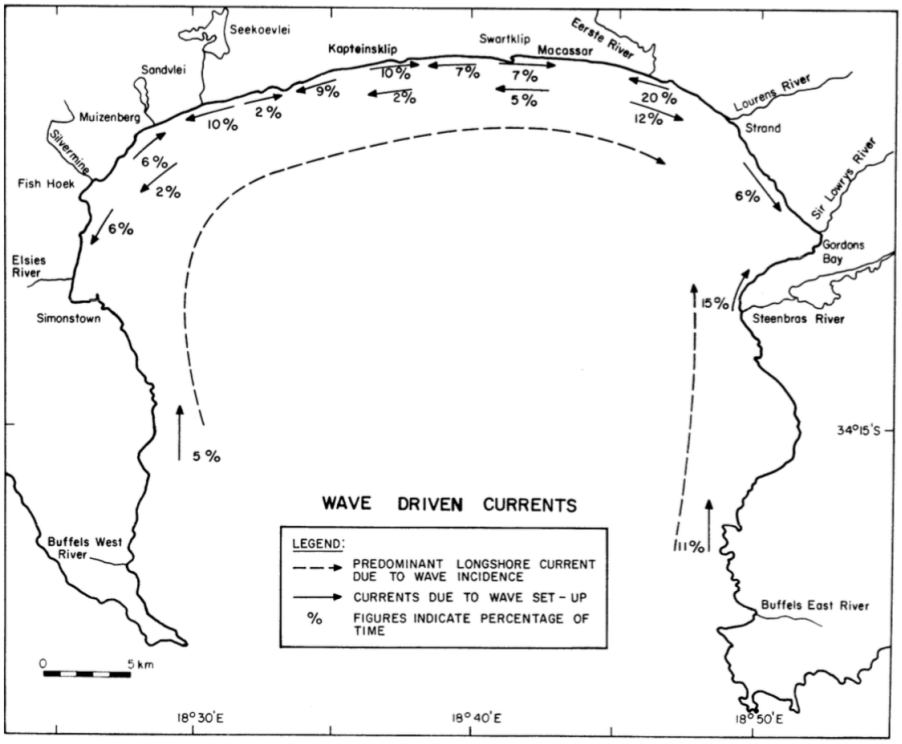

Figure 2-11: Summary of Wave-Driven Currents and Percentage Occurrence Based on Refraction of Deep Water Wave Conditions (CSIR, 1982)

From Figure 2-11, it was postulated by CSIR (1982) that wave driven currents tend to generate a clockwise (cyclonic) circulation pattern in False Bay with predominant easterly and northerly flow along the northern and western shorelines respectively.

Current measurements in the north-east corner of the bay (i.e. Strand and Gordon's Bay) generally indicate a north-westerly current direction, with a maximum current speed of 0.6 m/s and 0.3 m/s at the surface and seabed (10 m depth) respectively, under predominant south to south-easterly wind directions (Taljaard et al., 2000). Conversely, a south-easterly current direction has been observed during a predominantly north-westerly wind with a maximum current speed of 0.2 m/s and 0.1 m/s at the surface and seabed (10 m depth), respectively.

2.3 Discussion

A review of relevant information pertaining to coastal hydrodynamics was presented comprising coastal basin physical processes such as current circulation, the wind climate and sea temperature. In addition, the review included a summary of numerous historical observational studies. Despite the notable contributions of these historical studies regarding the analysis of bay circulation, and the physical processes driving them - there remains significant uncertainty mainly due to:

- The short duration of measurement campaigns underpinning these studies; and
- The limited spatial scale of measurement campaigns.

Besides the historical studies listed in this section, few modern studies (Nicholson (2011); Dufois et al. (2012)) have been carried out to determine hydrodynamic physical processes, such as current circulation and temperature variability in False Bay over a long time period. More specifically, although these studies contributed to the overall understanding of physical processes within False Bay, various important issues were not addressed such as a detailed description and evolution of intra-annual hydrodynamic processes. This shortcoming is emphasised from the findings of Wainman et al. (1987) (refer to Section 2.2.4) that showed the lack of consensus regarding complex circulation patterns in False Bay.

The development of the complex wind field over False Bay has been well documented in historical studies (Jury, (1984); Jury and Van Foreest, (1985)). However, hydrodynamic models driven by spatially varying wind forcing has not been considered (Jury and Van Foreest, (1985); Nicholson, (2011)) which has been regarded as a serious hindrance in providing robust simulation of hydrodynamics of False Bay (Taljaard et al., 2000).

Therefore, the hydrodynamic modelling work proposed in this thesis aims to address the shortcomings elucidated above while contributing to the existing body of knowledge of False Bay.

CHAPTER 3: HYDRODYNAMIC MODELLING

Hydrodynamic models are process-based numerical coastal area modelling systems which are generally used to determine key physical processes and baseline conditions within coastal areas such as estuaries, rivers, natural bays, port environments etc. Hydrodynamic models consist of a number of modules which resolve physical processes comprising wave and current propagation, sediment transport and morphodynamic bed updating.

This chapter provides an overview of the key components of hydrodynamic modelling as they pertain to physical processes comprising nearshore currents and water elevations. Other hydrodynamic modules relating to sediment transport, morphological evolution, wave-driven currents etc. are not discussed due to these modules being outside the scope of the current study (refer to Section 1.3).

3.1 Model Objectives

Hydrodynamic models are used extensively in the determination of impacts to the marine environment. Most hydrodynamic models can be linked to other models such as spectral wave models, sediment models and water quality models etc. (Sutherland et al., 2004). The main objectives of a hydrodynamic model can be broadly split into two categories, namely:

- Spatial and temporal domain: the model is capable of resolving physical characteristics anywhere and at any time within the model domain;
- Prediction (or forecasting): the model is able to predict how characteristics change relative to an action within the extent of the model.

The development of a hydrodynamic model can be summarised in a staged process as presented diagrammatically in Figure 3-1.

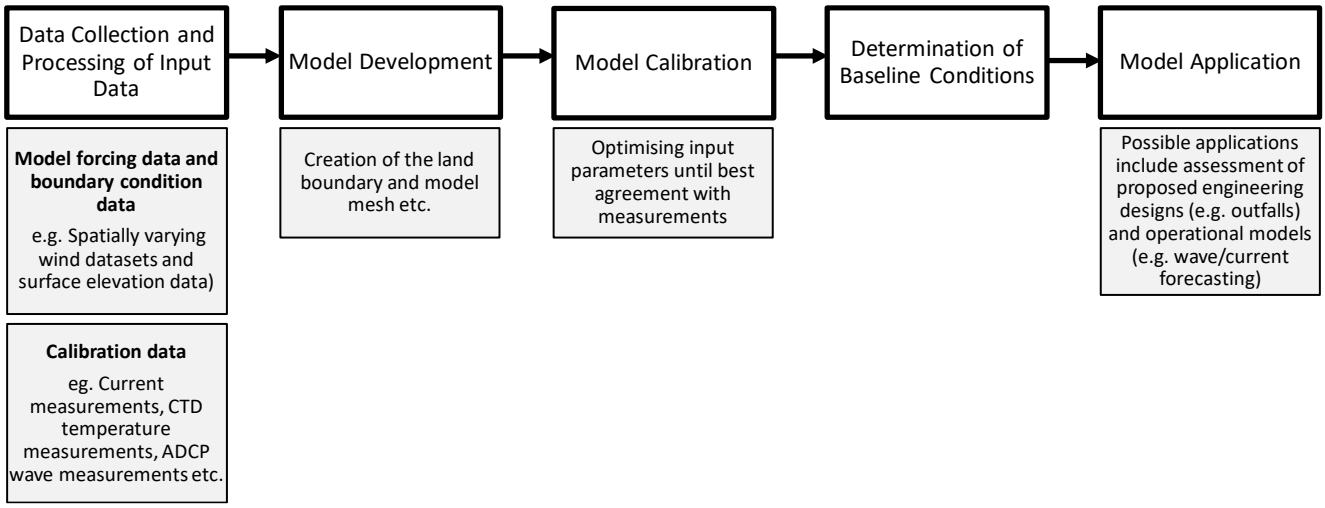

Figure 3-1: High-level Diagrammatic Development of a Typical Hydrodynamic Model

3.2 Types of Hydrodynamic Models

Hydrodynamic models applied to coastal environments generally include two- or three-dimensional models. Two-dimensional models are underpinned by depth-averaged wave and current equations and neglect the vertical variations of waves and currents (Nam et al., 2011). A single velocity vector is computed for each horizontal cell in the computational domain which defines an area(s) of surface flow (Nam et al., 2011). Two-dimensional models are applicable in cases where the water column is well-mixed (or isothermic) or in cases with minimal stratification. A degree of three-dimensionality may be incorporated into 2D models. These models are referred to as quasi-3D and compute the vertical current velocity at a given location which is determined by local forcing and depth-integrated flow (Nam et al., 2011).

Three-dimensional models include both the horizontal and vertical variations of waves and currents. Three-dimensional hydrodynamic models are generally applied to cases where the current distribution/structure through the water column is non-uniform e.g. in applications where bottom and surface currents flow in different directions. In addition, 3D hydrodynamic models are applied to cases where there are vertical temperature and salinity gradients which create density driven currents. Typically, 3D hydrodynamic models are significantly more computationally intensive than 2D models and are therefore used less frequently for the modelling of large coastal areas (Sutherland et al., 2004).

For the hydrodynamic modelling of embayments (comprising bays, lakes and other large regions of water bodies) that are significantly influenced by complex wind regimes and subsequent upwelling, it is imperative that 3D models be employed to capture variations in currents, circulation and temperature and salinity profiles to an acceptable degree of accuracy.

3.3 Model Description

Processed-based models make predictions by solving the discretised empirical or Newtonian equations related to conservation of momentum and mass in a fluid namely, the Navier-Stokes equations (NOAA, 2017). These equations are derived from Newton's laws of motion and describe the action of force applied to the fluid; that is, the resulting changes in flow. This is the property of conservation of momentum. Process-based numerical coastal area modelling systems also impose the continuity principle i.e. mass and energy are conserved within the model domain. The three-dimensional continuity equation solved by the numerical model is written below (DHI, 2017a):

$$\frac{\partial u}{\partial x}+\frac{\partial v}{\partial y}+\frac{\partial w}{\partial z}=S \tag{1}$$

All equations are provided in cartesian coordinates i.e. (x, y, z) with related velocity components i.e. (u, v, w).

The governing momentum equations as they relate to the x and y directions are provided in equation (2) and (3) respectively (DHI, 2017a).

$$\frac{\partial u}{\partial t}+\frac{\partial u^2}{\partial x}+\frac{\partial vu}{\partial y}+\frac{\partial wu}{\partial z}=fv-g\frac{\partial \eta}{\partial x}-\frac{1}{\rho_0}\frac{\partial p_a}{\partial x}-\frac{g}{\rho_0}\int_z^{\eta}\frac{\partial \rho}{\partial x}dz-\frac{1}{\rho_0 h}\left(\frac{\partial s_{xx}}{\partial x}+\frac{\partial s_{xy}}{\partial x}\right)+F_u+\frac{\partial}{\partial z}\left(\upsilon_t\frac{\partial u}{\partial z}\right)+u_sS \tag{2}$$

$$\frac{\partial v}{\partial t}+\frac{\partial v^2}{\partial x}+\frac{\partial uv}{\partial y}+\frac{\partial wv}{\partial z}=fu-g\frac{\partial \eta}{\partial y}-\frac{1}{\rho_0}\frac{\partial p_a}{\partial y}-\frac{g}{\rho_0}\int_z^{\eta}\frac{\partial \rho}{\partial y}dz-\frac{1}{\rho_0 h}\left(\frac{\partial s_{yx}}{\partial x}+\frac{\partial s_{yy}}{\partial y}\right)+F_v+\frac{\partial}{\partial z}\left(\upsilon_t\frac{\partial v}{\partial z}\right)+v_sS \tag{3}$$

where:

f refers to the Coriolis parameter;

u_t is the vertical turbulent viscosity;

h is the total water depth;

ρ and ρ_0 refers to the water density and reference water density respectively;

p_a is the atmospheric pressure and u_s and v_s are resulting discharge velocities;

S refers to a point source related velocity magnitude;

g is gravitational acceleration; and

s_{xx}, s_{xy}, s_{yx} and s_{yy} are stress tensor components.

For processed-based numerical models, the Navier-Stokes equations are simplified by the specific properties of the coastal ocean, primarily by the formulation of the shallow water equations which are termed due to the relative scale of features in the horizontal plane as being much greater than in the vertical. For example, oceans and bays are much larger in length and width than they are in depth (NOAA, 2017). Some processed-based numerical models use the cell centered finite volume method to discretise the shallow water equations. The “equation of state” formulation is used for elucidating the state of incompressible flow which describes the relationship between density, temperature and salinity, written in equation (4).

The transport equations defining the salinity and heat balance are provided in equation (5) and (6) respectively (DHI, 2017a).

$$\rho = \rho(T, S) \tag{4}$$

$$\frac{\partial \mathrm{T}}{\partial \mathrm{t}} + \frac{\partial \mathrm{uT}}{\partial \mathrm{x}} + \frac{\partial \upsilon \mathrm{T}}{\partial \mathrm{y}} + \frac{\partial \mathrm{wT}}{\partial \mathrm{z}} = F_T + \frac{\partial}{\partial \mathrm{z}}\left(D_\upsilon \frac{\partial \mathrm{T}}{\partial \mathrm{z}}\right) + H + T_s S \tag{5}$$

$$\frac{\partial \mathrm{s}}{\partial \mathrm{t}} + \frac{\partial \mathrm{us}}{\partial \mathrm{x}} + \frac{\partial \upsilon \mathrm{s}}{\partial \mathrm{y}} + \frac{\partial \mathrm{ws}}{\partial \mathrm{z}} = F_s + \frac{\partial}{\partial \mathrm{z}}\left(D_\upsilon \frac{\partial \mathrm{s}}{\partial \mathrm{z}}\right) + s_s S \tag{6}$$

Where:

D is the turbulent diffusion coefficient;

H refers to the heat exchange;

T and T_S are temperature and temperature of the source respectively;

s and s_S are salinity and source salinity; and

F_T and F_S are the horizontal diffusion of temperature and salinity.

3.4 Wind Forcing and Current Generation

This section provides an introduction to the relationship between wind forcing and current generation as applied in process-based hydrodynamic models.

Wind forcing has a significant effect on the hydrodynamics of large water bodies such as False Bay. Wind forcing is usually responsible for the generation of surface currents and surface

gravity waves which are a result of shear forces exerted on the water surface by the wind (Apel, 1999). This relationship may be represented by the following formulation (Hearn, 2008):

$$\tau = c_d . \rho_u . |u_w| . u_w$$

where:

τ is the water surface shear stress due to wind;

u_w is the wind velocity;

ρ_u is the density of air; and

c_d is a dimensionless quantity called the aerodynamic drag coefficient.

As wind blows over a coastal basin, surface currents are generated in the wind direction and water set-up forms due to surface shear stress of the wind blowing over water. Bottom currents are then formed and act against the wind direction. The difference in set-up in the direction of wind and subsequent set-down in the opposite direction of wind, creates a tilting water surface profile. This phenomenon induces a pressure gradient which is responsible for the bottom return current and can be approximated by the hydrostatic equation of pressure and water elevation (Hearn, 2008):

$$p(z) = g\rho(\eta - z)$$

Where:

$p\ (z)$ is the hydrostatic pressure;

$\eta - z$ is the vertical length of the water column above a reference point at height z;

ρ is the density of seawater; and

g is the acceleration due to gravity.

The pressure gradient due to water set-up with respect to any height (x) produces a force (per unit volume) parallel to the x-axis which is equal to the pressure gradient. This relationship is shown in the equation below (Hearn, 2008):

$$-\frac{\partial p}{\partial x} = -gp\frac{\partial \eta}{\partial x}$$

The total force due to pressure summed over the entire water column may therefore represented as (Hearn, 2008):

$$-\int_{-h}^{\eta} \frac{\partial p}{\partial x} dz = -gp(h + \eta)\frac{\partial \eta}{\partial x}$$

The force above should equal the water surface shear force due to wind with the assumption that the bottom stress is negligible. This relationship is shown in the equation below (Hearn, 2008):

$$\tau = -gp(h+\eta)\frac{\partial \eta}{\partial x}$$

This relationship between surface set-up and wind forcing describes a common response to forcing within a coastal basin and represents the steady state solution i.e. where the wind has blown over a coastal basin sufficiently so that the total volume flux is zero. However, wind forcing is more complicated than a simplified balance between the pressure gradient associated with a set-up and the wind stress at the surface (Pond & Pickard, 1978). Factors such as time variations, the effect of bathymetry and non-linear effects of shallow water and site-specific factors are important in influencing the c_d term. It should be noted that the relationships above are only valid for cases involving an irrotational basin i.e. where the Coriolis force is negligible, where the basin is closed and where the basin is of uniform depth. Furthermore, bottom friction is assumed negligible in the formulations above. If bottom friction is included, then assuming a total volume flux of zero (steady state), the bottom frictional stress would counter the bottom return current's direction and therefore act in the direction of the wind. The added component of bottom friction would increase surface set-up (Hearn, 2008).

Hydrodynamic numerical models solve equations similar to the above taking into account multiple factors. These models resolve hydrodynamics at near-stead state conditions i.e. when a set of primary boundary conditions dominate, namely (DHI, 2017a):

- Pressure (or surface elevation); and
- Velocities.

CHAPTER 4: MODELLING METHODOLOGY

4.1 Introduction

As stated in previous sections, one of the main objectives of this thesis is to develop a greater understanding and better quantification of False Bay physical processes, through hydrodynamic modelling of bay circulation and hydrodynamic processes such as spatially varying wind forcing and intra-annual variability of sea temperature.

The methodology used for the setup of the hydrodynamic model, to achieve the objectives above, is introduced in this chapter with technical detail provided for model inputs.

4.2 Numerical Modelling

4.2.1 Model Description

The three-dimensional MIKE 3 Flow Flexible Mesh Model is used for the modelling of False Bay. The general application of the model is described in the User Manual (DHI, 2017b), while full details of the physical processes being simulated and the numerical solution techniques are described in the MIKE 3 Scientific Documentation (DHI, 2017a) and in Section 3.3.

The model is based on the numerical solution of the three-dimensional incompressible Reynolds averaged Navier-Stokes equations invoking the assumptions/approximation of Boussinesq and of hydrostatic pressure (for further detail on the model description refer to Section 3.3). The model comprises the continuity, momentum, temperature, salinity and density equations and is closed by a k-ε vertical turbulence closure scheme. Horizontal eddy viscosity is modelled with the Smagorinsky formulation.

The time integration of the shallow water equations and the transport equations is performed using a semi-implicit scheme, where the horizontal terms are treated explicitly and the vertical terms are treated implicitly. In the vertical direction a structured mesh, based on a sigma-coordinate transformation is used, while the geometrical flexibility of the unstructured flexible mesh comprising triangles or quadrangles is utilised in the horizontal plane.

The MIKE 3 Flow Flexible Mesh Model for the present study includes the following physical phenomena:

- Currents due to tides;
- Currents due to wind stress on the water surface;
- Currents due to density gradients;
- Coriolis forcing;
- Bottom friction;

- Flooding and drying; and
- Heat exchange.

4.3 Model Inputs

This section summarises the data requirements and the datasets used as input into the hydrodynamic model. A summary of available datasets is provided in Table 4-1. It should be noted that the measurement and hindcast datasets were used for model calibration and assisted in defining the calibration period. This is discussed further in Section 5.1.

Table 4-1: Summary of Available Datasets

Data Type	Data Source	Data Location(s)	Dataset Period	Considered for Calibration
Wind	CSIR	Cape Point	1994-1997 (4 years)	
		Seal Island	1987-1988 (1 year)	
		Simons Town (IMT)	1995 (3 months)	
		Roman Rock	1995 (2 months)	
		Steenbras	1995 (2 months)	
	UCT CSAG	Atmospheric Model*	2005 - 2013 (8 years)	X
	South African Weather Service Data	Cape Point	1973-2017 (44 years)	X
		Cape Town International Airport	1949-2017 (68 years)	X
		Simons Town (IMT)	1949-1950 (1 year)	
		Strand	2000-2017 (17 years)	X
	IMT	Roman Rock	2007-2013 (6 years)	X
Current	CSIR	Simons Town	2008-05-14 - 2008-06-03 (20 days)	X
		Simons Town	2010-09-29 - 2010-10-22 (23 days)	X
		Gordons Bay	2010-08-20 - 2010-09-13 (24 days)	X

*Hindcast dataset

The datasets provided in Table 4-1 refer to multiple measurement locations within False Bay. An overview of these measurement locations is presented in Figure 4-1.

Figure 4-1: Overview of Measurement Locations in False Bay

4.3.1 Bathymetry and Model Mesh

To capture hydrodynamic processes within a reasonable computational timescale, optimisation of the model mesh (a form of model reduction) was necessary. For example, calibration runs required a high grid resolution in the areas of measurement locations to resolve local-scale hydrodynamic processes while the remaining domain needed a large enough spatial extent to describe regional-scale hydrodynamics.

The WGS84 coordinate system was considered for the present study. All spatial plots show x- and y-coordinates in metres in the WGS84 coordinate system (Hartebeesthoek 1994 Datum, coordinate zone WG19). True north is shown to be pointing upwards in all plots. Seabed levels and water levels were provided relative to the Mean Sea Level (MSL).

Bathymetric data was obtained from the CMAP Electronic Chart database (DHI, 2017c). The bathymetry and computational mesh used for the model simulation runs are presented in Figure 4-2 and Figure 4-3 respectively. In addition, Figure 4-4 and Figure 4-5 present the mesh detail near Gordons Bay and Simons Town respectively. Both locations coincide with ADCP instrument measurement locations.

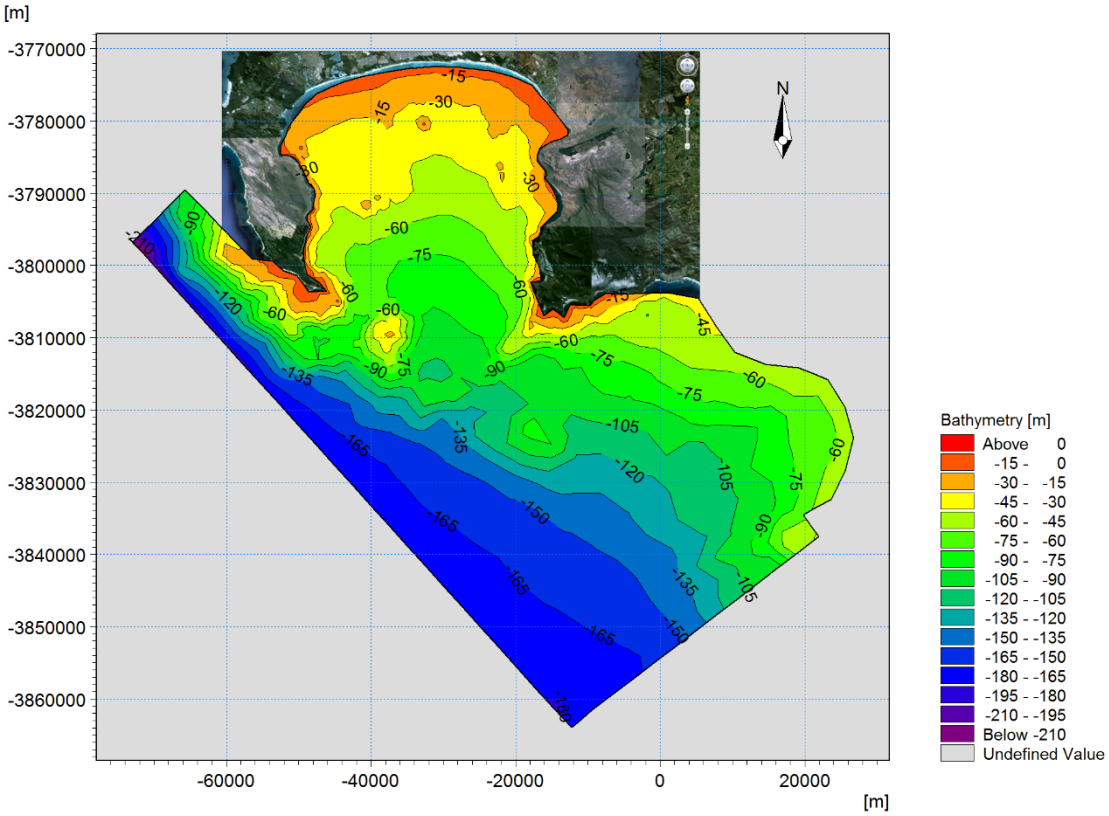

Figure 4-2: Bathymetric Mesh Generated from C-MAP Database

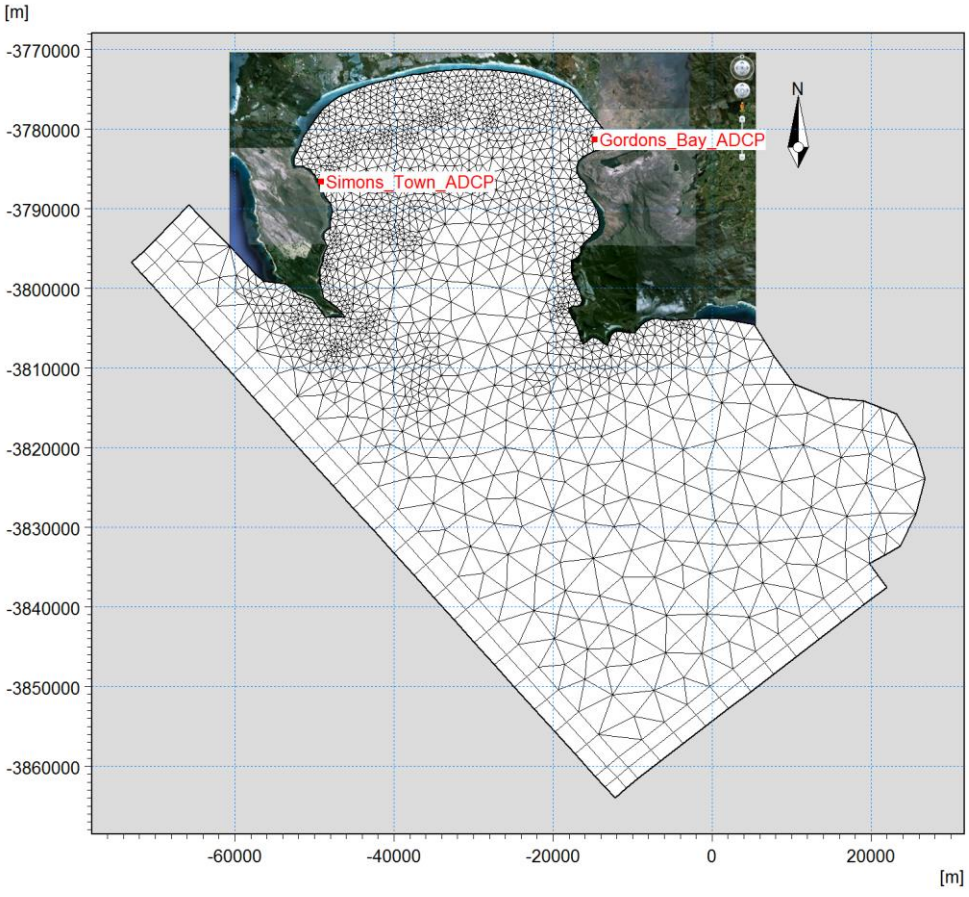

Figure 4-3: Computational Mesh Considered for Simulation Runs

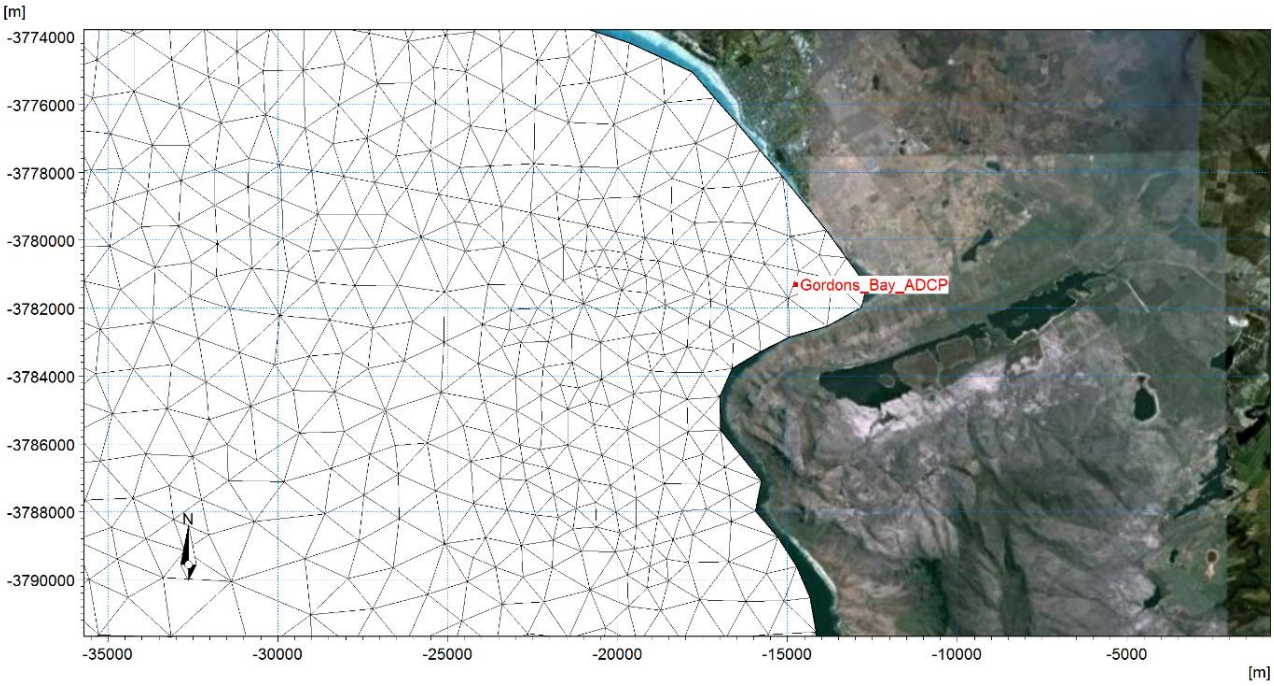

Figure 4-4: Computational Mesh Considered for Calibration Runs – Detail (Gordons Bay)

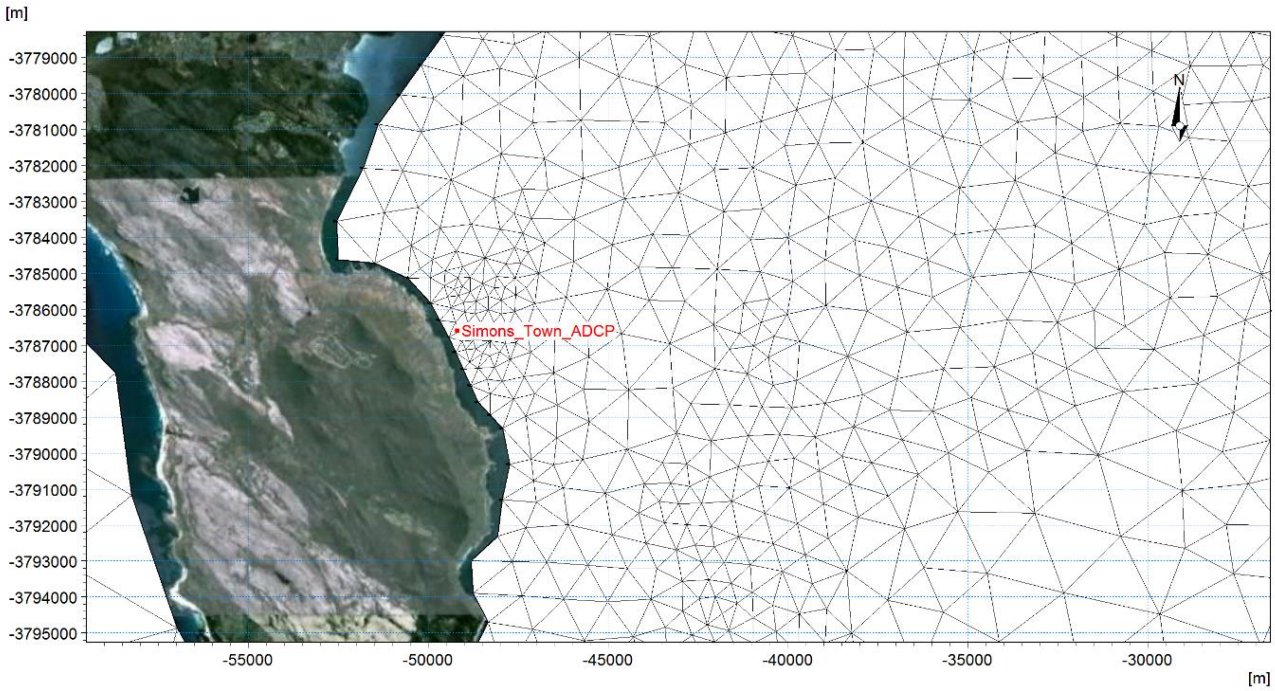

Figure 4-5: Computational Mesh Considered for Calibration Runs – Detail (Simons Town)

The horizontal mesh resolution for the calibration model varies from approximately 10 km at the offshore boundary to 500 m in areas of interest i.e. bathymetric features such as Rocky

Bank, Cape Point and Cape Hangklip, shallow regions near the measurement locations etc. The vertical mesh is comprised of 20 sigma layers with equal layer thicknesses.

4.3.2 Water Levels

Predicted tidal water levels were extracted from the DTU10 global tide model which includes 12 major tidal constituents (Cheng & Andersen, 2010a) and were applied as time-varying water levels along the model boundaries. Corrections for wind setup and Coriolis force were applied to the water levels prescribed along the seaward model boundaries. These corrections are built into the MIKE 3 model and allow for tilting of the water level (due to wind setup and Coriolis force) along the model boundaries. The correction along the boundary is calculated based on the steady state Navier Stokes equations.

4.3.3 Boundary Seawater Temperature, Salinity and Current Profiles

Seawater temperature profiles were applied along the seaward model boundaries as depth-varying and time-varying profiles. The boundary conditions were varied over time to account for seasonal trends in water column stratification and to aid in capturing event-scale hydrodynamic processes. The depth-varying sea temperature profiles at the boundaries were extracted from the Hybrid Coordinate Ocean Model (HYCOM) reanalysis dataset (Cummings et al., 2013).

HYCOM is an ocean general circulation model which is based on solving the set of primitive equations comprising continuity, momentum and thermal energy. The HYCOM model is a successor to the Miami Isopycnic-Coordinate Ocean Model (MICOM) which was one of the premier ocean circulation models which was subjected to numerous validation studies (Halliwell, 2002). Vertical coordinates in HYCOM remain isopycnic in the open, stratified ocean. However, they smoothly transition to z-coordinates in the weakly-stratified upper-ocean mixed layer, to terrain-following sigma coordinate in shallow water regions, and back to level coordinates in very shallow water (Halliwell, 2002). The HYCOM reanalysis dataset comprises a spatial resolution of 0.08 degrees and a 24-hour temporal resolution.

An example of the HYCOM temperature depth profiles along the boundaries for the 1st of August 2010 is provided in Figure 4-6. Boundary temperature depth profiles are provided with start and end points following an anticlockwise convention around the model extent.

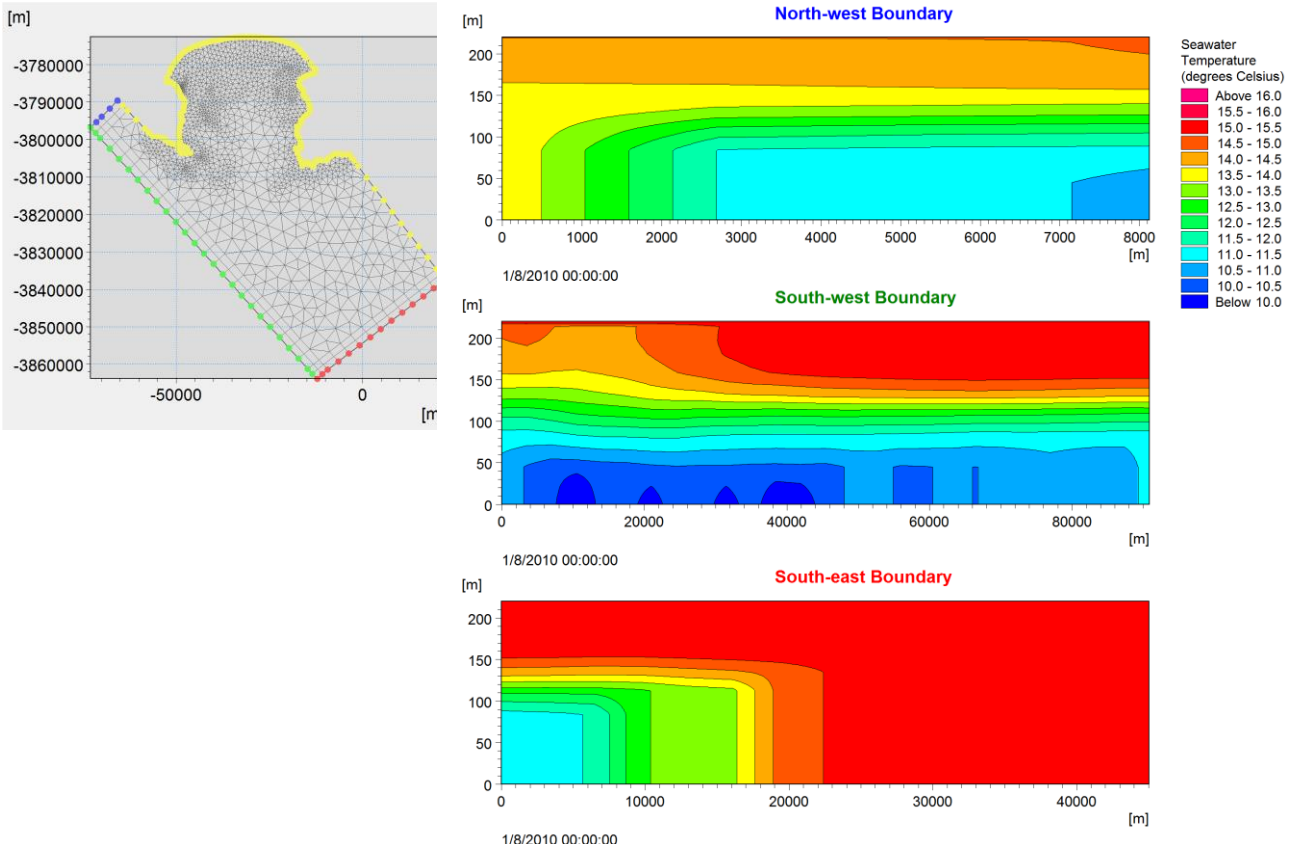

Figure 4-6: Temperature (℃) Depth Profiles along the Boundaries for 1 August 2010

4.3.4 Wind Forcing

A two-dimensional dataset was applied as spatially and time-varying wind input to the model for the generation of wind-driven currents and atmospheric heat exchange. This two-dimensional dataset was derived from calibrated atmospheric modelled data over the period 2005 to 2013. Seasonal wind patterns and transitions from land to sea are therefore included in this dataset which were sourced from the WASA (2014) project (refer to Annexure B). The WASA dataset was developed by the University of Cape Town's (UCT) Climate System Analysis Group (CSAG).

To investigate the suitability of the WASA (2014) dataset, a comparative analysis was undertaken between the WASA (2014) dataset and weather station measurements. It should be noted that the WASA (2014) model was calibrated against purpose-built measurement stations setup around South Africa and was not verified against existing weather stations. Therefore, the current study is the first study to investigate the extent of agreement of the WASA (2014) dataset and existing weather station measurements around False Bay.

A comparative analysis, comprising time series and wind rose analyses, was undertaken for various weather stations around False Bay over the calibration period of 2 months. The weather station measurements were provided by the South African Weather Service (SAWS).

It should be noted that the WASA dataset (modelled) provides atmospheric data at 10 m above ground level (AGL) which is at the same measurement height of the Cape Town International Airport weather station. Therefore, a comparison at the location of the Cape Town International Airport was deemed the most suitable for the comparative analysis. Although other weather stations were compared to the WASA dataset, they are not reported in this section and are instead included in Annexure A. A wind speed time series, wind direction time series and wind rose comparison is presented in Figure 4-7, Figure 4-8 and Figure 4-9 respectively. The wind rose comparison and the time series comparison were undertaken over the calibration period (August 2010 – October 2010). Both wind datasets are hourly averaged.

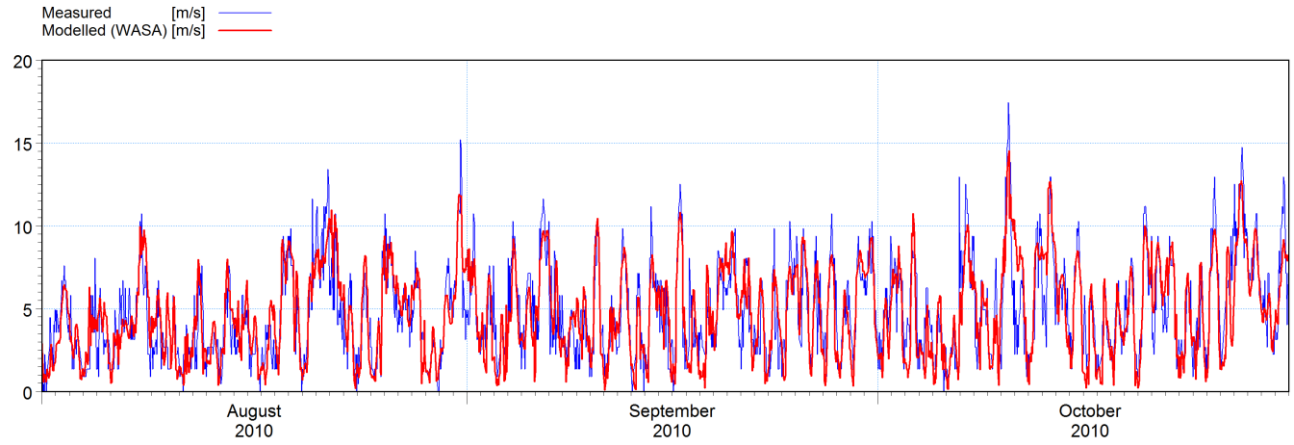

Figure 4-7: Time Series Comparison of Cape Town International Airport Measured Wind Speed vs. Modelled WASA Wind Speed

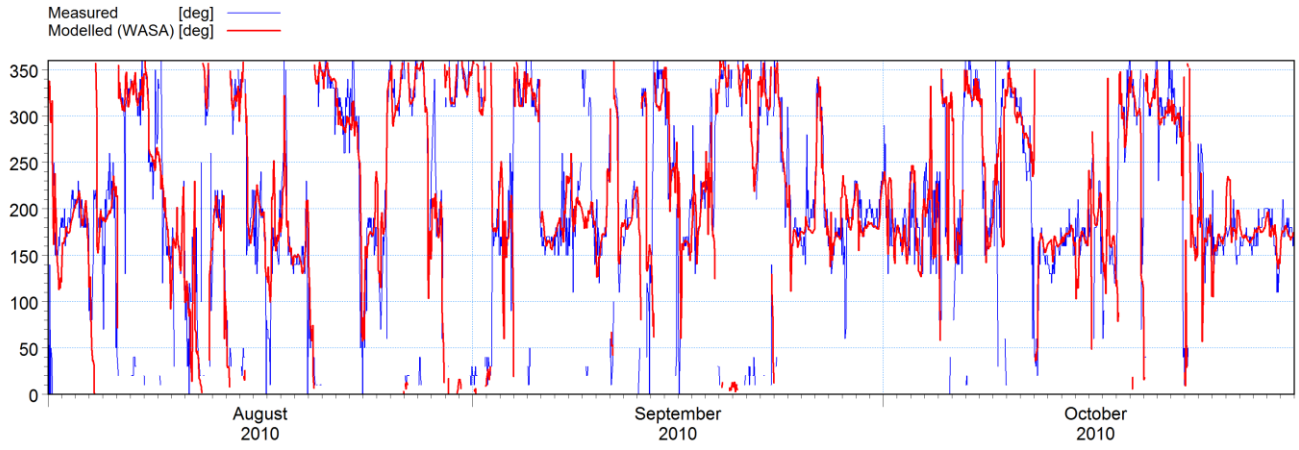

Figure 4-8: Time Series Comparison of Cape Town International Airport Measured Wind Direction vs. Modelled WASA Wind Direction

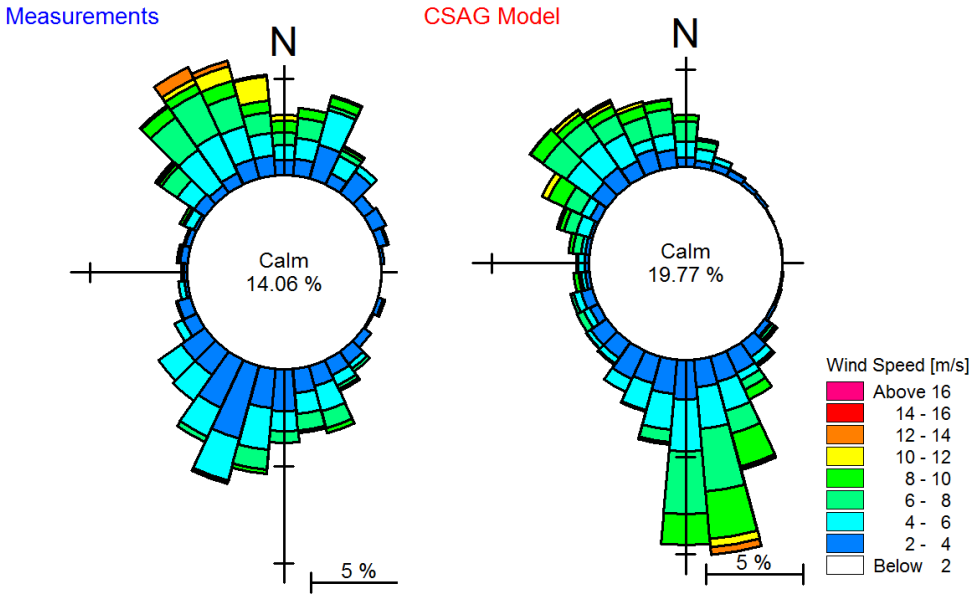

Figure 4-9: Wind Rose Comparison of Cape Town International Airport Measured Wind Data vs. Modelled WASA Wind Data (August to October 2010)

From Figure 4-7, the WASA modelled dataset shows good agreement with Cape Town International Airport weather station data. The WASA model occasionally fails to capture wind spikes below 8 m/s and tends to overestimate wind speeds in these cases. However, generally the model captures the overall wind speed trend over the calibration period and was deemed acceptable with no pre-processing undertaken.

From Figure 4-8 and Figure 4-9, wind direction generally shows good agreement between the measured and modelled datasets. However, the measured dataset does show a greater directional spread over the calibration period. In addition, a south-westerly component is more prominent in the measured data, while the model dataset shows more frequent stronger south-easterly components.

Overall, the time series comparison over the calibration period shows the modelled data following the directional wind trend quite well and was deemed acceptable with no pre-processing undertaken.

4.4 Selection of Run Simulation Period

The significant computational load associated with 3D hydrodynamic models enforces a limit on the duration over which the model can be run. However, it is desirable to simulate hydrodynamics over a wide range of environmental conditions including seasonal variations in seawater temperature, winds, tides and currents.

One of the key model outputs is the seawater temperature profile. The selection of a suitable modelling period is thus based on ensuring that both the well-mixed (isothermic) winter condition and the more stratified summer conditions are well represented. As discussed in Section 3.2, well-mixed winter conditions in False Bay occur between mid-May and mid-September. The most stratified conditions occur at the height of summer between December and February. In addition, since the currents at False Bay are predominantly wind-driven, the selection of the baseline run simulation period needs to ensure that a representative range of tidal water levels and tidal currents are covered as well. The baseline run simulation refers to the simulation of baseline metocean conditions once the model has been successfully calibrated.

In this study, the run-time constraints allowed for the modelling of an entire year of environmental conditions. Subsequent to the simulation duration to be modelled, a representative year needs to be selected. Since the model has been calibrated for the period of August 2010 to October 2010, additional certainty is gained by carrying out baseline run simulations within the same year. Therefore, the year 2010 was selected for the baseline run simulations.

CHAPTER 5: MODEL CALIBRATION

5.1 Calibration and Verification Period

The calibration and verification periods are dependent on the availability of concurrent data over the same periods. To assess the preferred calibration and verification periods, a "data-concurrence" plot was developed which showed where available data overlapped within the available data domain. The data-coexistence plot is provided in Figure 5-1.

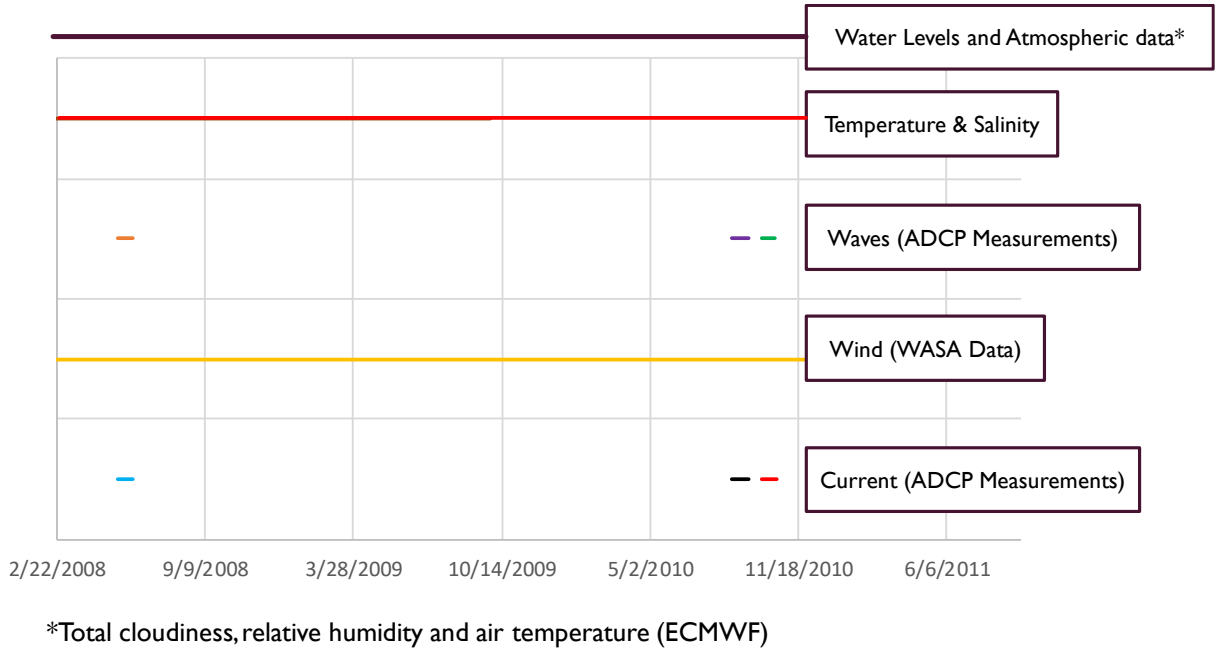

Figure 5-1: Data-concurrence Plot of Available Data for Calibration/Verification

From Figure 5-1, the data periods with the most comprehensive data-concurrence are the periods defining the wave and current ADCP measurements. As a result of this finding, the calibration periods and verification periods were defined as shown in Table 5-1.

Table 5-1: Summary of Selected Calibration and Verification Periods

Parameter	Period		Days
	Start	End	
Calibration	20/8/2010	21/10/2010	62
Verification	14/5/2008	3/6/2008	20

The calibration period spans approximately 2 months during the winter period of the year. Although it would have been desirable to simulate the stratified water column in the summer months (December to February), ADCP measurements were unavailable for this time period

(refer to Table 4-1). Model calibration was necessary to determine model input parameters whereas model verification was used to validate the accuracy of the hydrodynamic model.

5.2 Model Calibration

5.2.1 Water Levels

Modelled water levels were calibrated against measurements at Simons Town (refer to Figure 4-1 for measurement locations). Figure 5-2 presents a time series comparison of measured and modelled water levels at Simons Town.

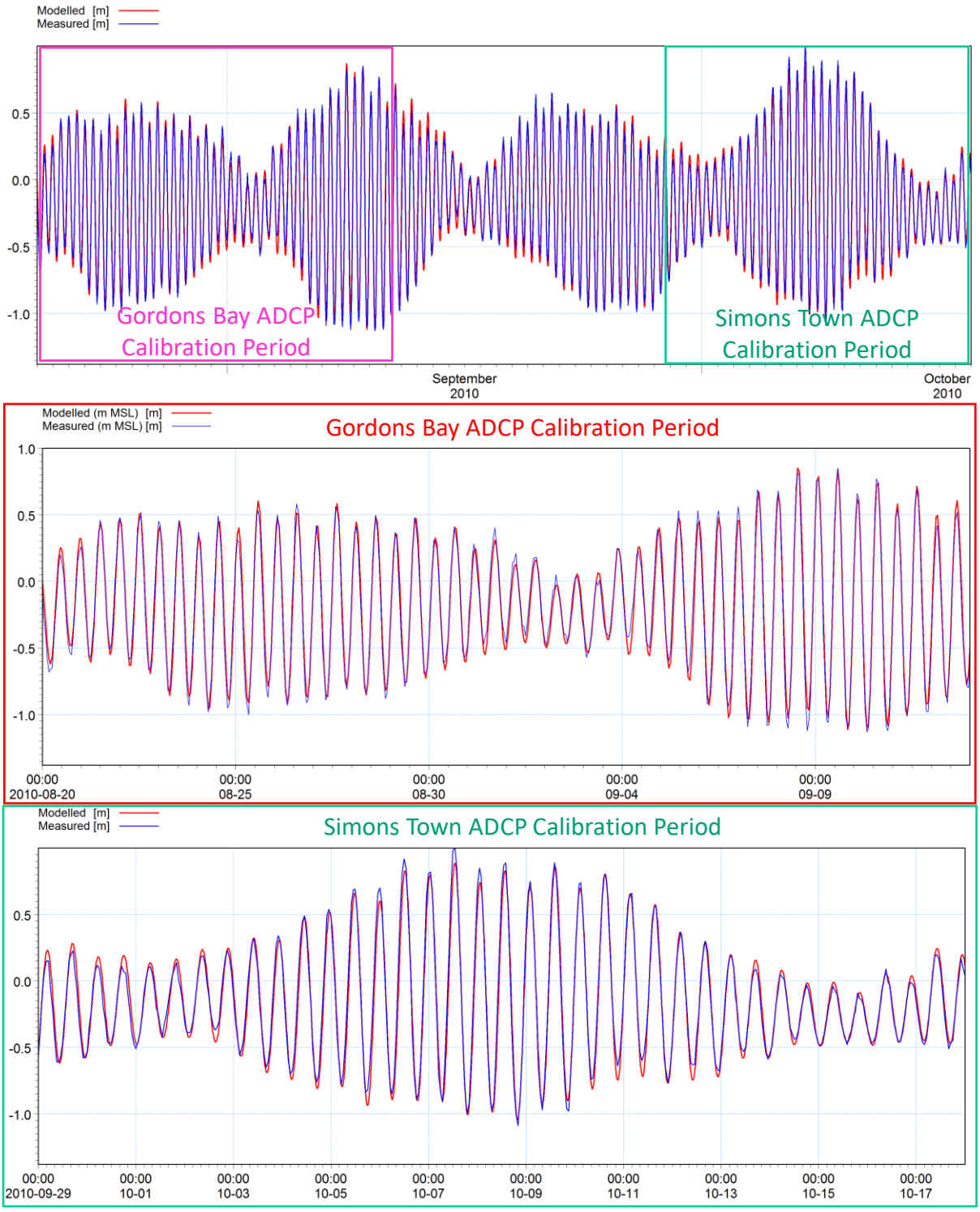

Figure 5-2: Time Series Comparison of Modelled and Measured Water Levels at Simons Town over Calibration Period

From Figure 5-2, the time series plots show that the model accurately reproduces the predicted tidal water levels. It is not clear whether the discrepancies between the predicted and measured water levels is symptomatic of inaccuracies in the predicted water levels applied at the open boundaries or other factors such as localised set-ups or response to wind forcing.

5.2.2 Atmospheric Conditions

Heat exchange between the water and the atmosphere was included in the hydrodynamic model. Total cloud cover and relative humidity data were extracted from the ERA-Interim global atmospheric reanalysis product (i.e. hindcast data) provided by ECMWF (2017) and were applied as space and time varying input conditions in the model.

A relative humidity time series comparison between ECMWF and measurement data at Cape Town International Airport (refer to Figure 4-1) is presented in Figure 5-3.

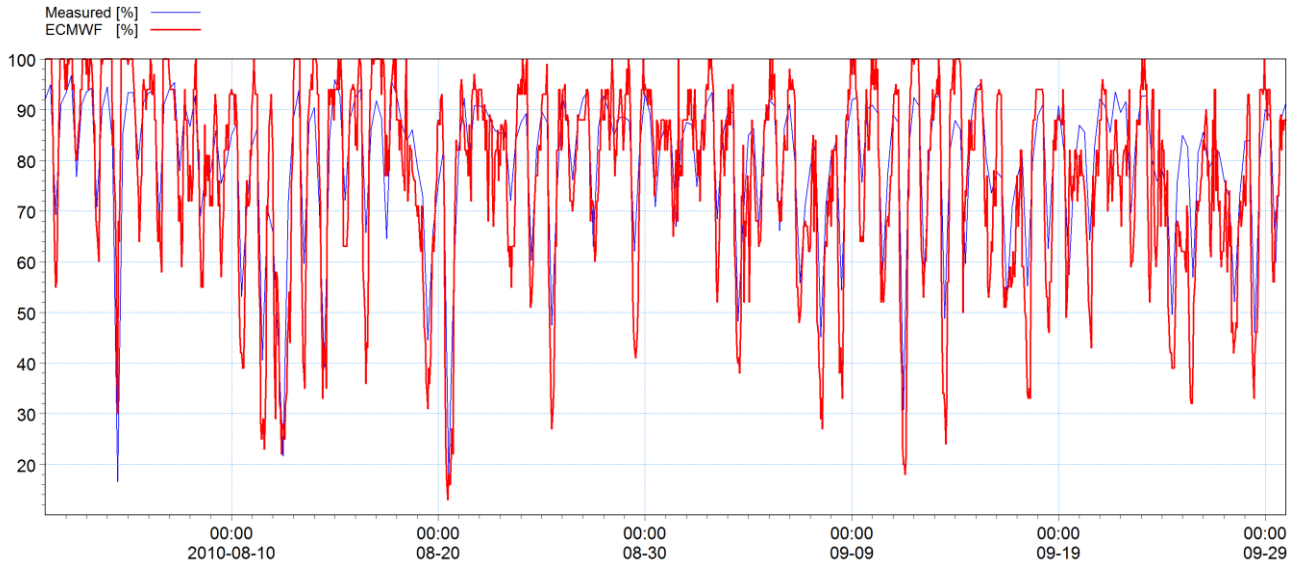

Figure 5-3: Relative Humidity Time Series Comparison Between ECMWF and Measurements (SA Weather Service) at Cape Town International Airport

From Figure 5-3, the time series comparison shows that the ERA-Interim hindcast data provides a good estimation of the general monthly humidity trend.

In addition to relative humidity, the air temperature dataset was applied as spatially-varying and time-varying input to the model. The dataset was extracted from the ERM-Interim reanalysis product provided by ECMWF. An air temperature time series comparison between ECMWF and measurement data at the Cape Town International Airport is presented in Figure 5-4.

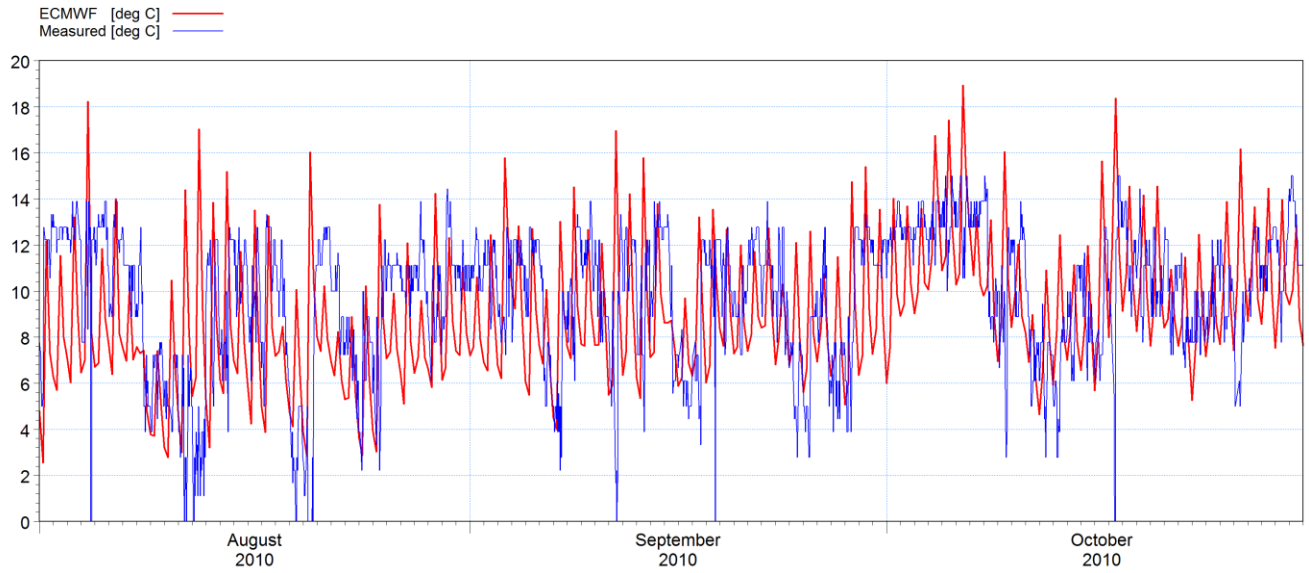

Figure 5-4: Air Temperature Time Series Comparison Between ECMWF and Measurements at Cape Town International Airport

From Figure 5-4, the ERA-Interim hindcast data provides a good estimation of the general monthly air temperature trend. However, day-night cycles do not show a strong correlation as the modelled data shows higher variability in air temperature. In addition, higher temperatures are not captured in the measurement dataset compared to the hindcast dataset.

Overall, the ERA-Interim hindcast dataset was deemed suitable for the purposes of this study due to the general monthly trend in air temperature and relative humidity being captured acceptably.

5.2.3 Currents

Modelled currents were calibrated against ADCP measurements located at Gordons Bay and Simons Town (refer to Figure 4-4 and Figure 4-5 respectively). ADCP measurements were provided in 0.5 m intervals through the water column and at 10-minute intervals from August 2010 to September 2010. Although the model was able to output current speeds and directions at 10-minute timesteps, the wind forcing in the model was at 1-hour timesteps thus effectively limiting resolved current speeds and directions to 1-hour timesteps. Therefore, for the sake of comparison, current measurements were hourly-averaged. For the purposes of calibration, surface and seabed currents were investigated independently.

Measured currents were found to be fairly “noisy” compared to model results. Generally, weaker currents show higher variability (or “noise”) in current direction and are therefore more difficult to measure with ADCP instruments.

Conversely the model results show less variability which is due to the model being driven by a smooth tidal signal. In reality the presence of coastally trapped waves, long waves, short waves etc. would influence water levels and subsequently currents. Therefore, by excluding these factors, the modelled currents appear smoother than measured currents.

Analysis of the Gordons Bay ADCP data revealed a poor correlation with modelled results on initial comparison. Unlike the current speeds, the modelled current directions showed poor agreement with measurements. Upon further analysis of wave measurements from the ADCP, it was determined that the current direction discrepancy was likely due to measurement error. Wave direction at the ADCP location is generally perpendicular to the bathymetry due to wave refraction. A comparison of observed wave direction from satellite imagery and ADCP measurements is presented in Figure 5-5.

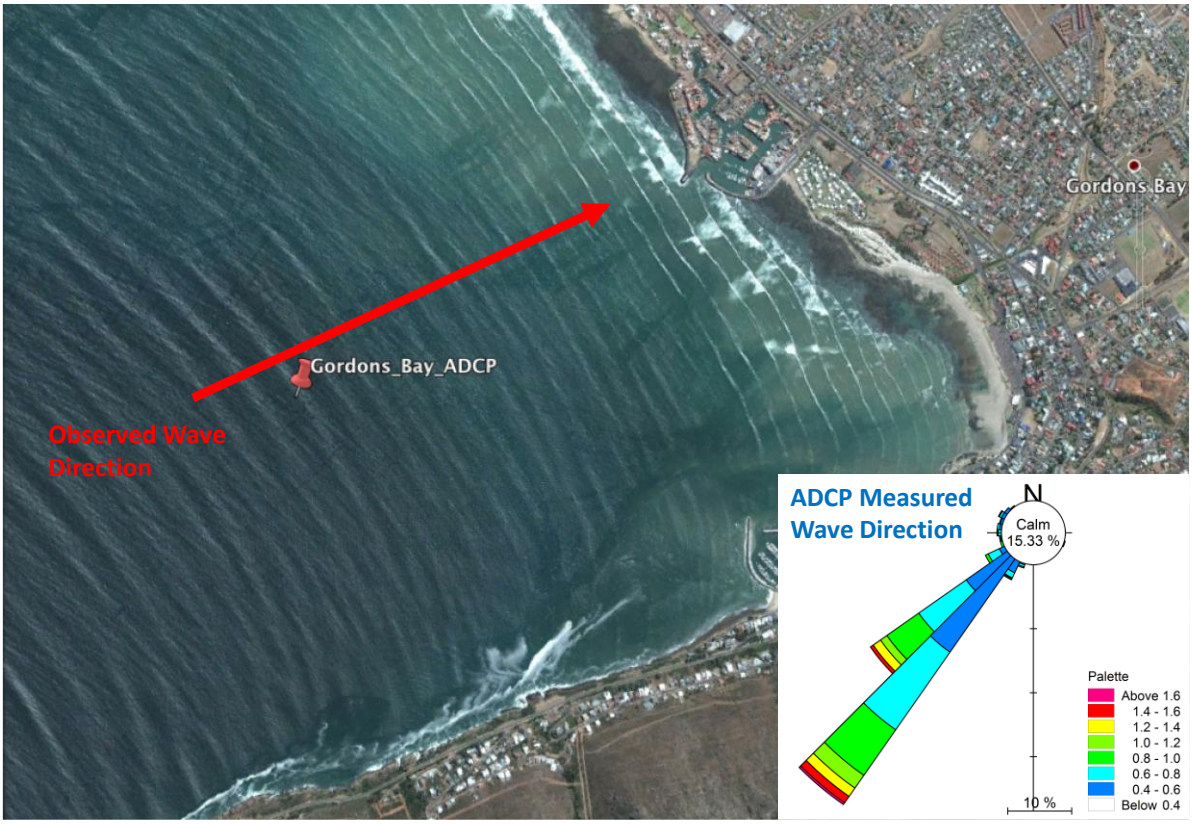

Figure 5-5: Comparison between Observed and ADCP Measured Wave Direction

From Figure 5-5, the predominant wave direction from ADCP measurements is approximately 20-25 degrees less that the observed wave direction. Therefore, a 25-degree correction was applied to the current measurement dataset. After the correction, the model results showed better agreement with the measured dataset.

Gordons Bay time series comparisons of surface (z=3) current speed, current direction, wind speed and wind direction is presented in Figure 5-6. In addition, the Gordons Bay surface (z=3) current rose comparison of modelled and measured data is presented in Figure 5-7.

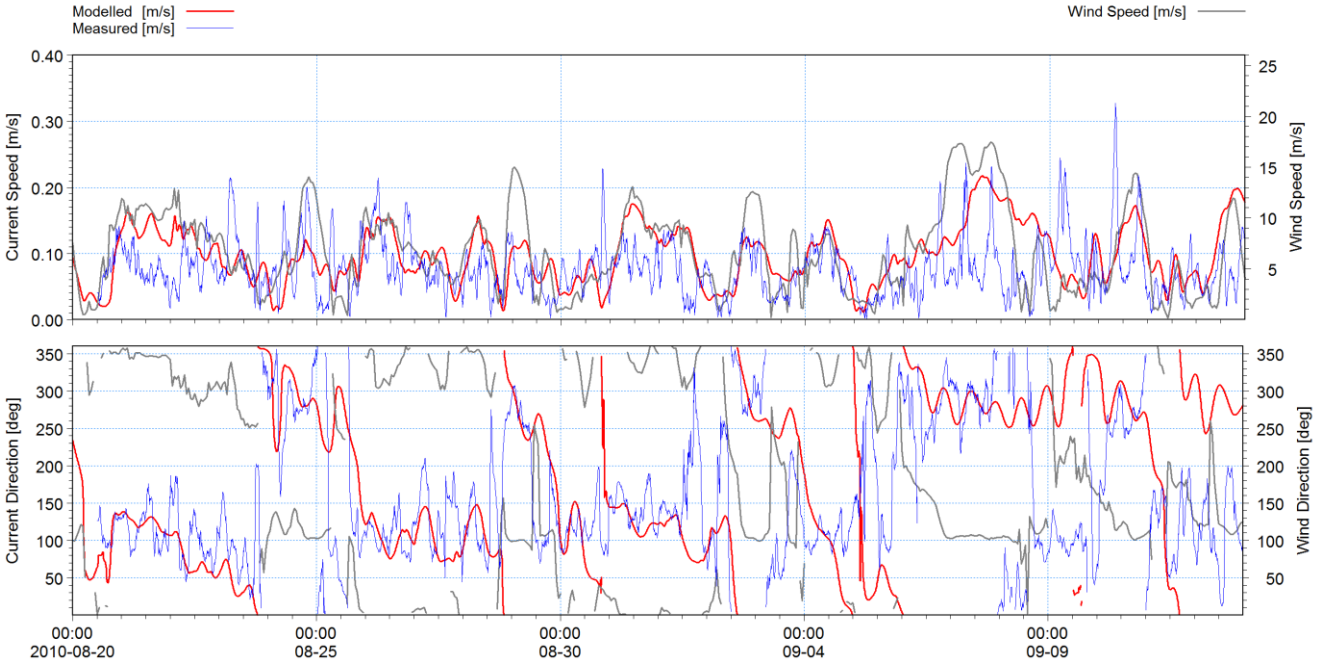

Figure 5-6: Surface (z=3) Current Speed and Direction Time Series Comparison at Gordons Bay

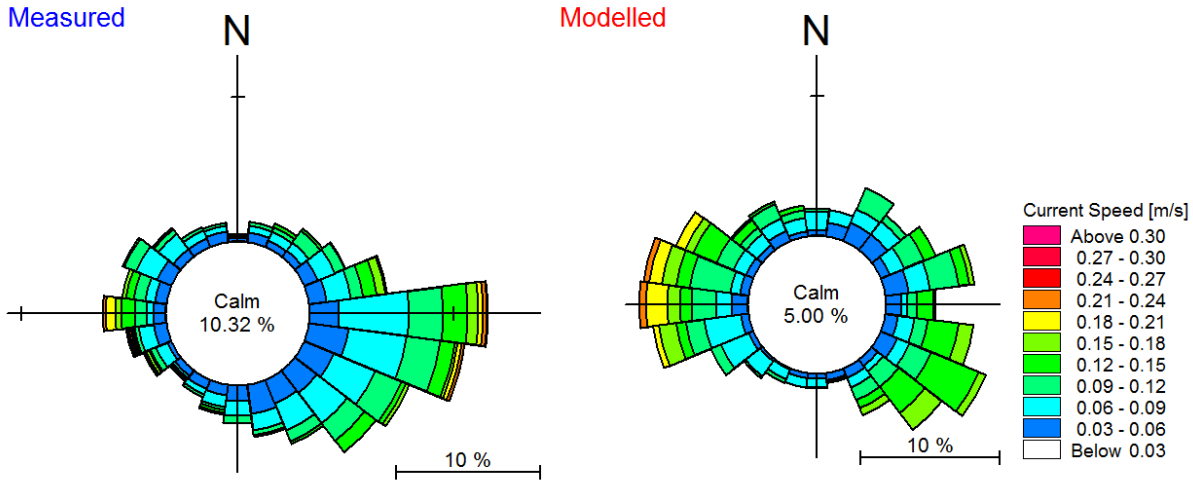

Figure 5-7: Surface (z=3) Current Rose Comparison at Gordons Bay

Gordons Bay time series comparisons of near seabed (z=10) current speed, current direction, wind speed and wind direction are presented in Figure 5-8. In addition, the Gordons Bay seabed (z=10) current rose comparison of modelled and measured data is presented in Figure 5-9.

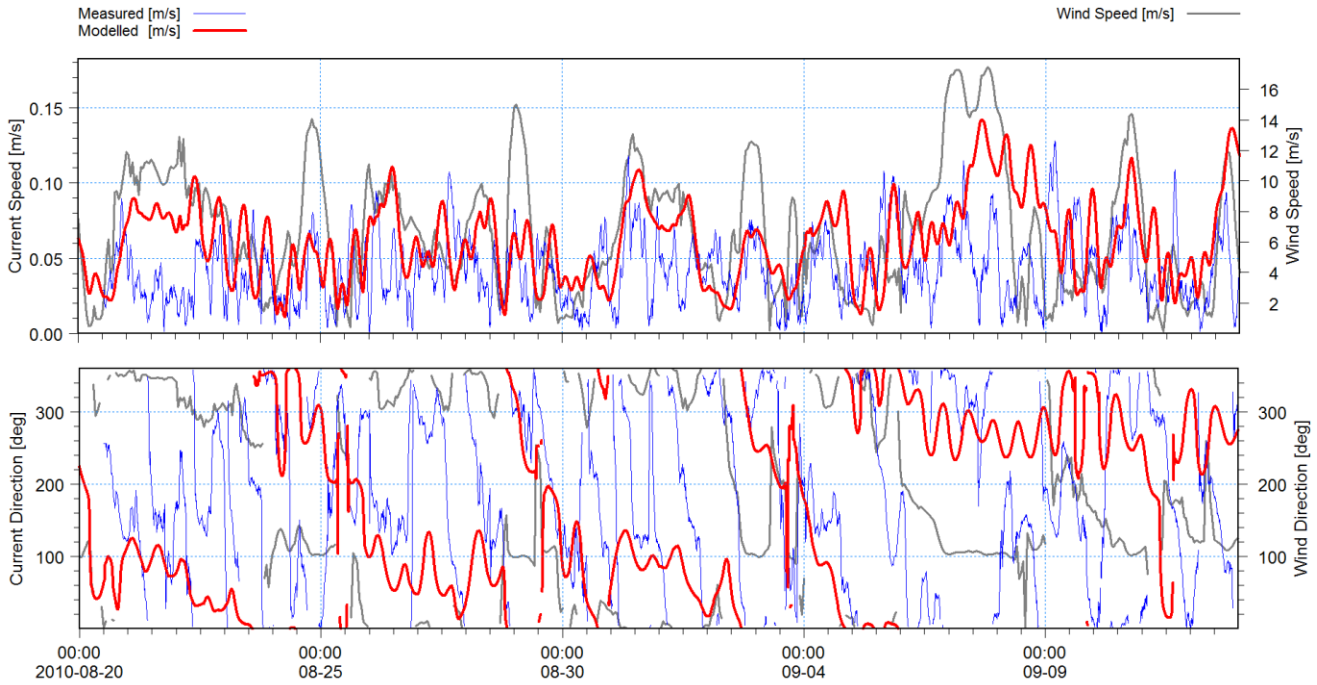

Figure 5-8: Seabed (z=10) Current Speed and Direction Time Series Comparison at Gordons Bay

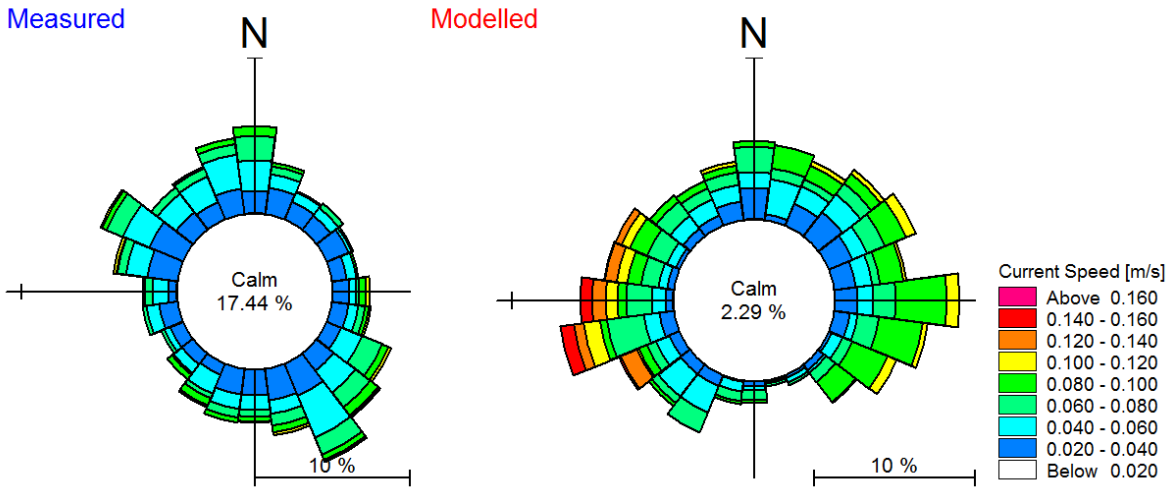

Figure 5-9: Seabed (z=10) Current Rose Comparison at Gordons Bay

Overall, the Gordons Bay modelled and measured current speeds show acceptable agreement at the surface and seabed. It should be noted that surface and seabed measurements are mainly wind-driven.

Simons Town time series comparisons of seabed (z=12) current speed, current direction, wind speed and wind direction is presented in Figure 5-10. In addition, Simons Town surface (z=10) current rose comparison of modelled and measured data is presented in Figure 5-11.

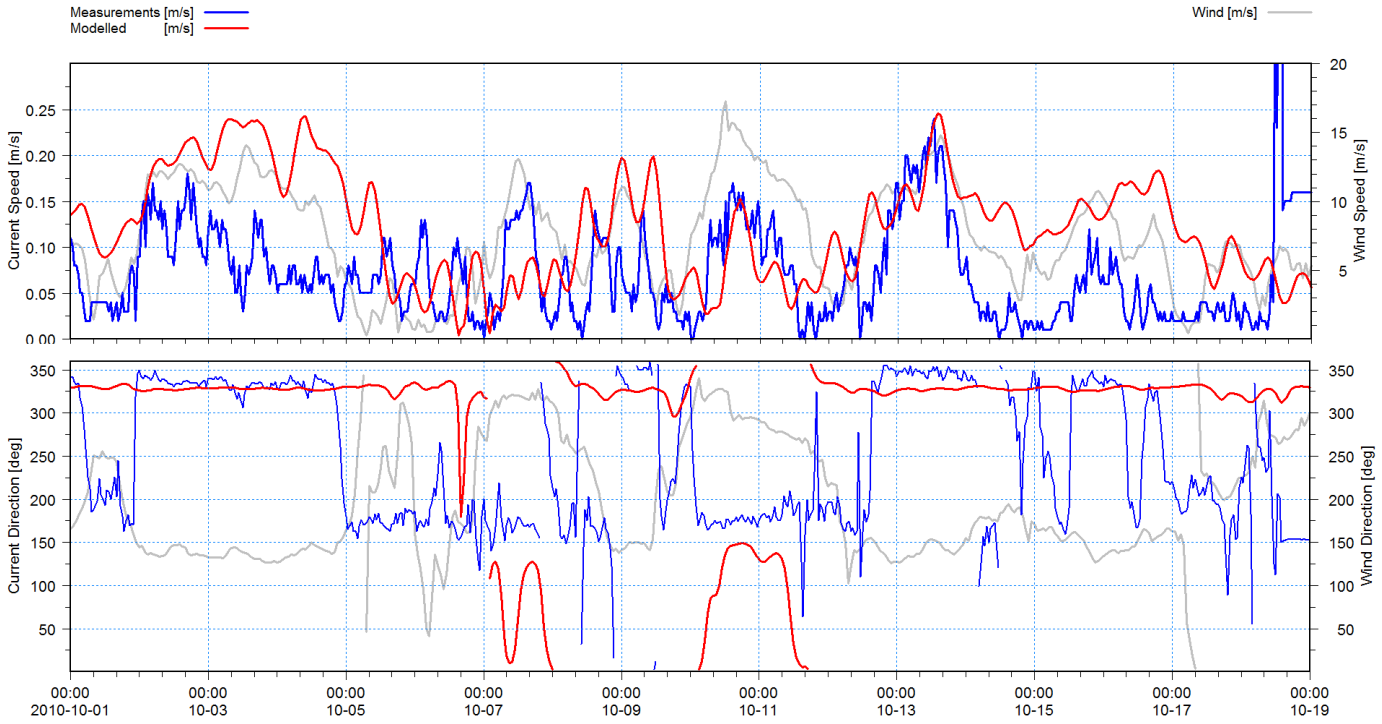

Figure 5-10: Seabed (z=12) Current Speed and Direction Time Series Comparison at Simons Town

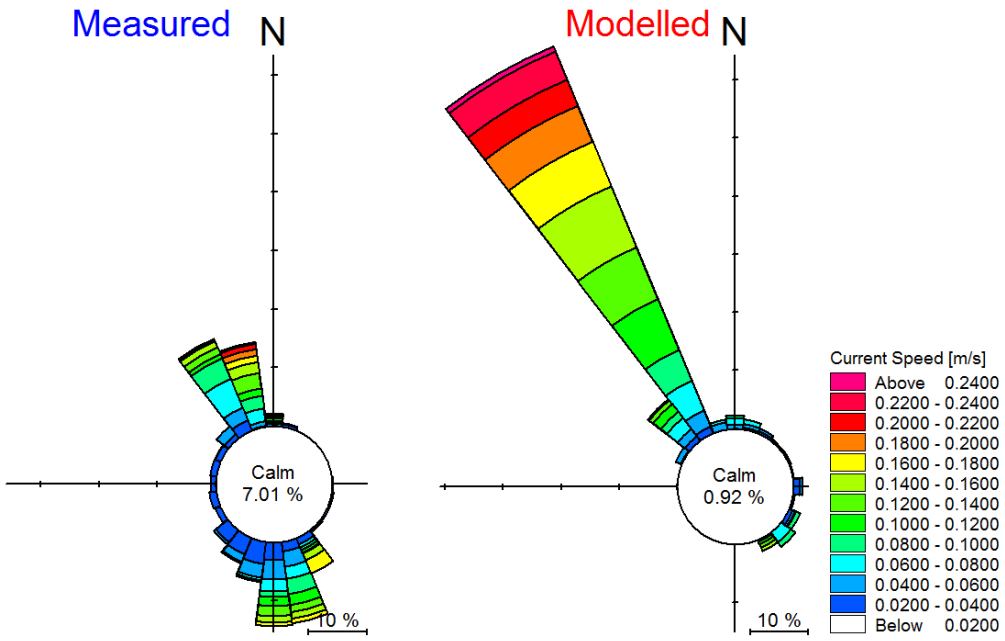

Figure 5-11: Seabed (z=12) Current Rose Comparison at Simons Town

Overall measured currents are predominantly wind-driven and weak (≤0.25 m/s). It should be noted that the model tends to overestimate lower current speeds. From Figure 5-10 and Figure 5-11, the current calibration shows better agreement with stronger current trends but less agreement with weaker current trends which tend to show greater variability in current direction. Generally, weaker currents show higher variability (or “noise”) in current direction and are therefore more difficult to measure with ADCP instruments. This trend is noted in the Gordons Bay measurements as well with stronger currents showing better agreement with the modelled dataset.

5.2.4 Sea Temperature

Modelled sea surface temperature was calibrated against daily measurements sourced from the South African Weather Service at Gordons Bay. In addition, near seabed measurements from the ADCP were calibrated as well.

A time series comparison between the modelled (surface: z=2 m and near seabed: z = 12 m) and measured seawater temperatures is presented in Figure 5-12.

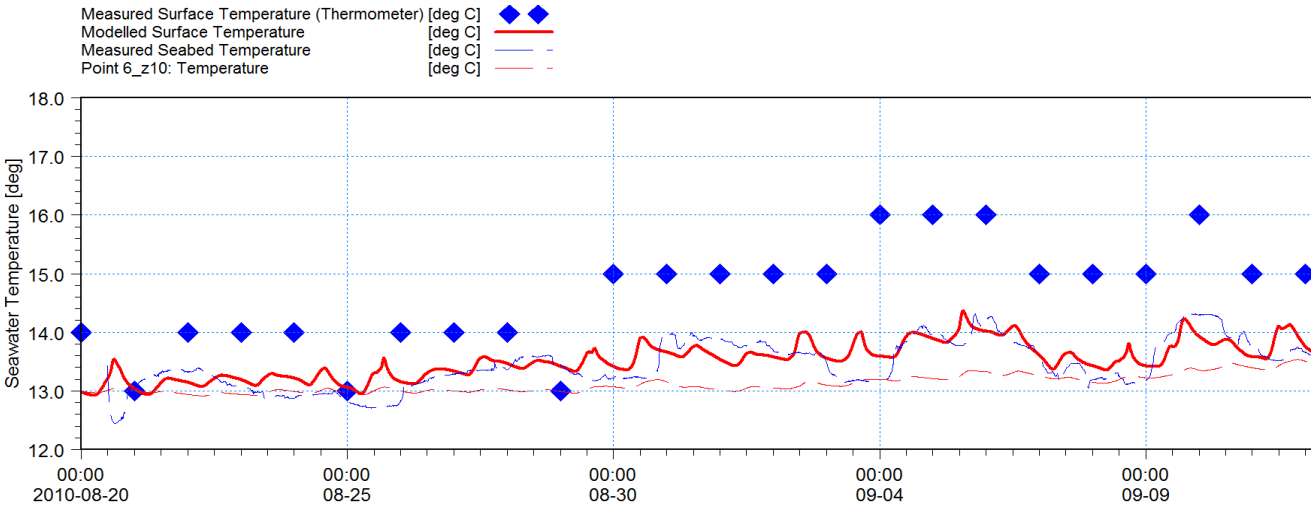

Figure 5-12: Sea Surface Temperature Time Series Comparison of Modelled (ADCP location) and Measurements

From Figure 5-12, the modelled near-surface temperature (z=2) trend compares well with the measured near seabed temperature trend. However, when comparing the modelled and measured near-seabed temperatures, the model results show less fluctuation.

The measured surface temperatures consistently show warmer measurements. However, it should be noted that the measured dataset comprises daily thermometer readings at the harbour in Gordans bay (Dufois & Rouault, 2012). The measurement location is therefore in shallower, more stagnant water than the modelled ADCP location. Thermometer readings are generally coarse and are read to the nearest degree. Overall, this may explain the higher mean temperature and relatively large 1-2℃ fluctuations in sea surface temperature in the measured dataset.

A further calibration was undertaken against near seabed measurements from a previous study undertaken by Nicholson (2011) who deployed four ADCPs near the centre of the bay. The locations of these ADCPs are provided in Figure 5-13. The measurement time series from this study is presented in Figure 5-14. The calibration results are presented as a time series comparison plot presented in Figure 5-15. Wind speed and wind direction are presented on the plot which were extracted from the WASA (CSAG) dataset at a point near the ADCP locations.

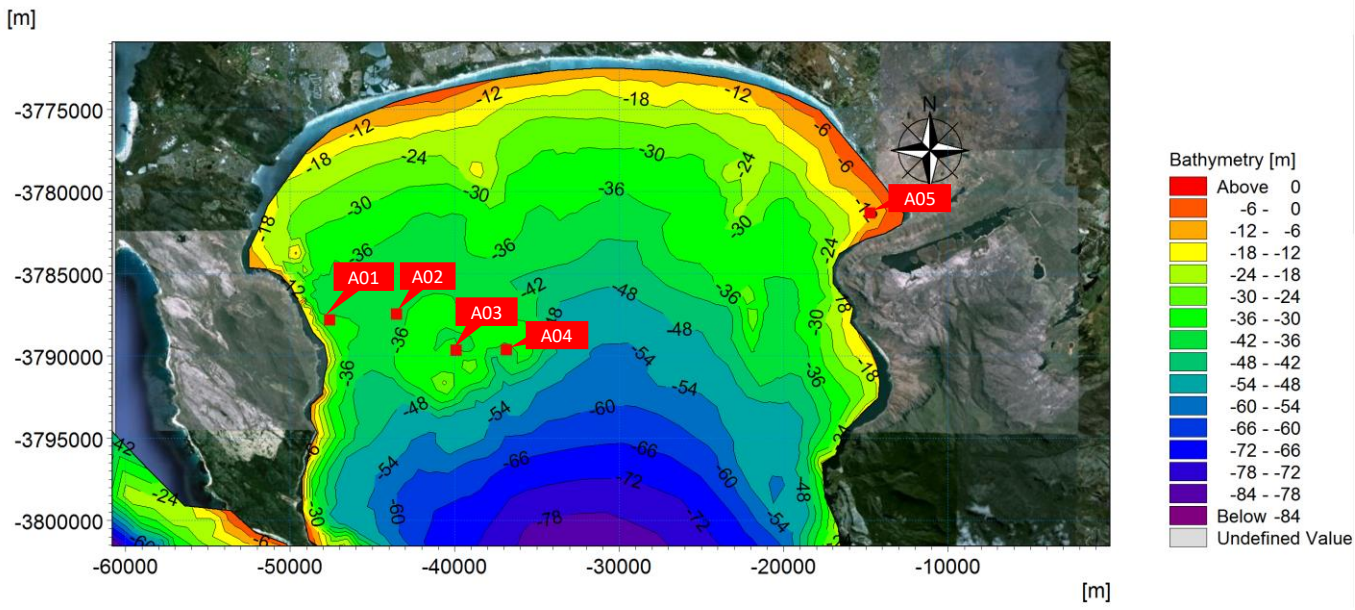

Figure 5-13: Deployed ADCP Locations from Nicholson (2011)

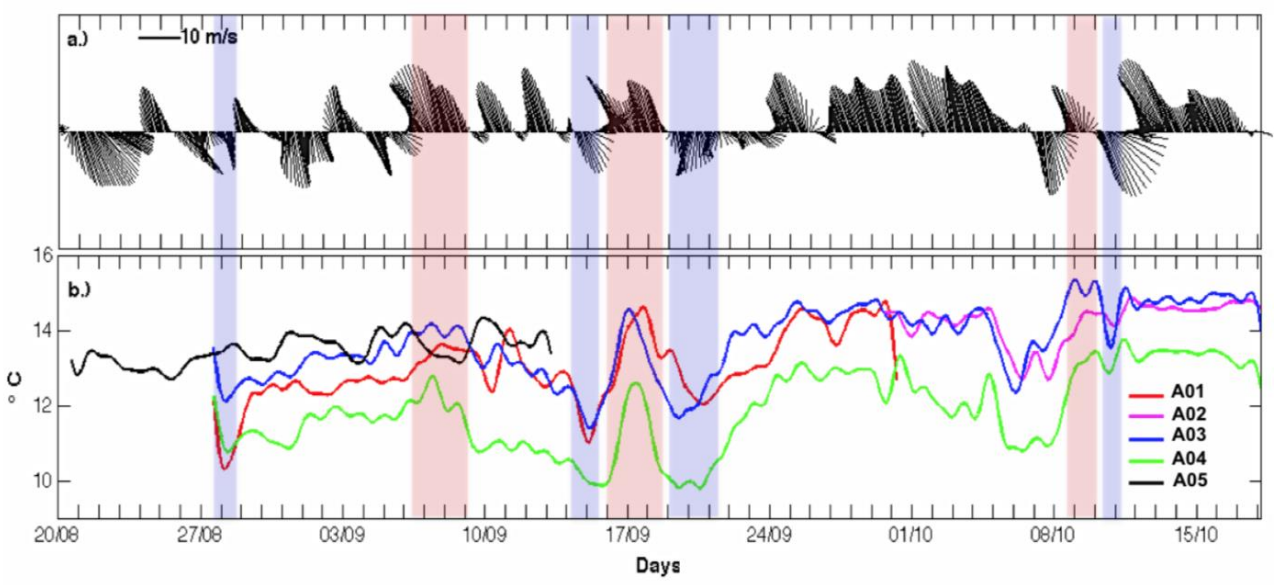

Figure 5-14: Seawater Temperature Measurement Time Series from Nicholson (2011)

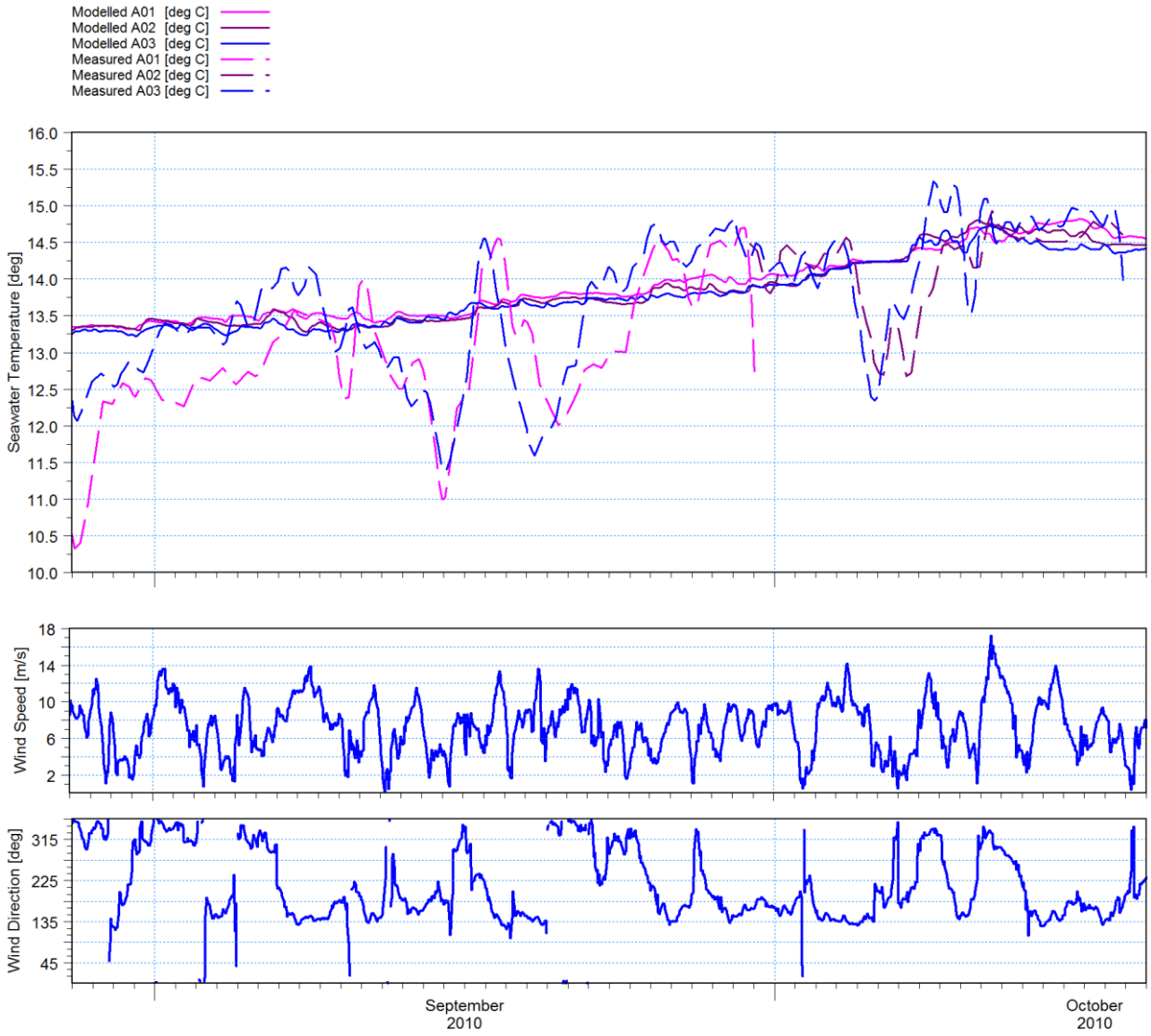

Figure 5-15: Near Seabed Temperature Time Series Comparison of Modelled and Measurements from Nicholson (2011)

From Figure 5-14, the ADCP measurements from the Nicholson (2011) study showed some inconsistency. Notably ADCP A04 which consistently registered colder temperatures when compared to the other ADCP measurements. For example, a minimum of 11℃ was recorded on the 7th October 2010 at ADCP A04 whereas adjacent ADCP measurements, at similar moored depths, during the same period were recording 13.8℃. Therefore, ADCP A04 was excluded from the calibration of model results.

From Figure 5-15, the mean seabed temperature trend agrees with the modelled time series. However, several strong fluctuations in temperature are noted throughout the measured time series. The model was unable to capture these fluctuations in near-seabed temperature.

Nicholson (2011) described the bottom temperature measurements as being dependent on the change in wind direction, namely bottom temperatures decreasing when the wind direction transitioned to a north-westerly and increasing when wind direction transitioned to south-

easterly. However, from the wind time series presented in Figure 5-15, the relationship between wind direction and bottom temperature is weak. Similarly, the relationship between wind speed and bottom temperature is weak. It is therefore postulated that cold water in the bottom layers of the water column were advected from offshore to the centre of the bay during events represented by large bottom temperature fluctuations.

Overall, the model was able to reproduce the mean monthly trends in seawater temperature well but was unable to reproduce the events responsible for the fluctuation in bottom temperature. It should be noted that capturing fluctuations in temperature on an event-scale is also dependent on the spatial and temporal resolution of the seawater temperature-depth boundary conditions.

5.2.5 Summary of Calibration Parameters

The wind friction coefficient and seabed roughness was optimised to physically realistic values which were consistent with the default values in MIKE 3 and yielded the best agreement between modelled and measured currents within False Bay. A summary of calibration parameters is provided in Table 5-2.

Table 5-2: Model Calibration Parameters

Parameter	Value*
Eddy viscosity (horizontal)	Smagorinsky formulation constant of 0.28
Eddy viscosity (vertical)	k-ε formulation with default empirical constants in MIKE 3 HD (FM)
Wind friction coefficient	Interpolated linearly from 0.001255 (7 m/s) to 0.002425 (25 m/s)
Seabed roughness height (m)	0.05
Vertical Dispersion Coefficient (Vertical)	1.0

*All calibration values are MIKE 3 defaults

Typically, the vertical dispersion coefficient set to unity may decrease the decoupling of surface and bottom flows which may in turn reduce upwelling (mixing) events. However, during calibration run testing, a value of 0.1 for the vertical dispersion coefficient yielded less agreement with measurement datasets (in isothermic conditions) and therefore was not preferred. It is possible that a value of 0.1 may be more representative of the decoupling and mixing within False Bay. However, to confirm this, measurement datasets in deeper, less sheltered water would be necessary, especially under stratified conditions. For the purposes of this study, the vertical dispersion coefficient set to unity yielded the best agreement with measurements and was deemed acceptable.

5.3 Model Verification

5.3.1 Water Levels

Modelled water levels were verified against measurements at Simons Town over the verification period May to June 2008 (refer to Table 5-1). Figure 5-16 presents a time series comparison of measured and modelled water levels at Simons Town.

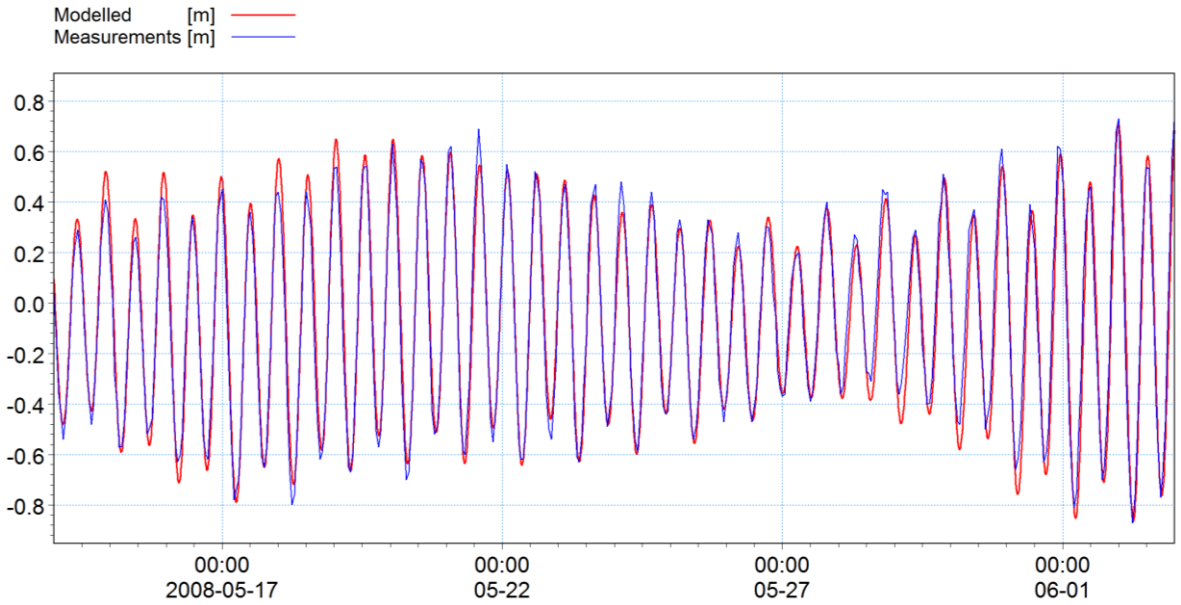

Figure 5-16: Time Series Comparison of Modelled and Measured Water Levels at Simons Town over the Verification Period

From Figure 5-16, the time series plot shows that the model accurately reproduces the predicted tidal water levels.

5.3.2 Currents

Modelled currents were verified against ADCP measurements located at Simons Town (refer to Figure 4-4). ADCP 40-minute measurements were provided near the seabed (-18.0 m CD) over the measurement period May 2010 to June 2010. It should be noted that unlike the Gordons Bay ADCP dataset, the Simons Town ADCP dataset does not contain measurements at varying depths. Instead, depths are only provided near the seabed (-18.0 m CD). Simons Town time series comparisons of near seabed (z=18) current speed, current direction, wind speed and wind direction is presented in Figure 5-17.

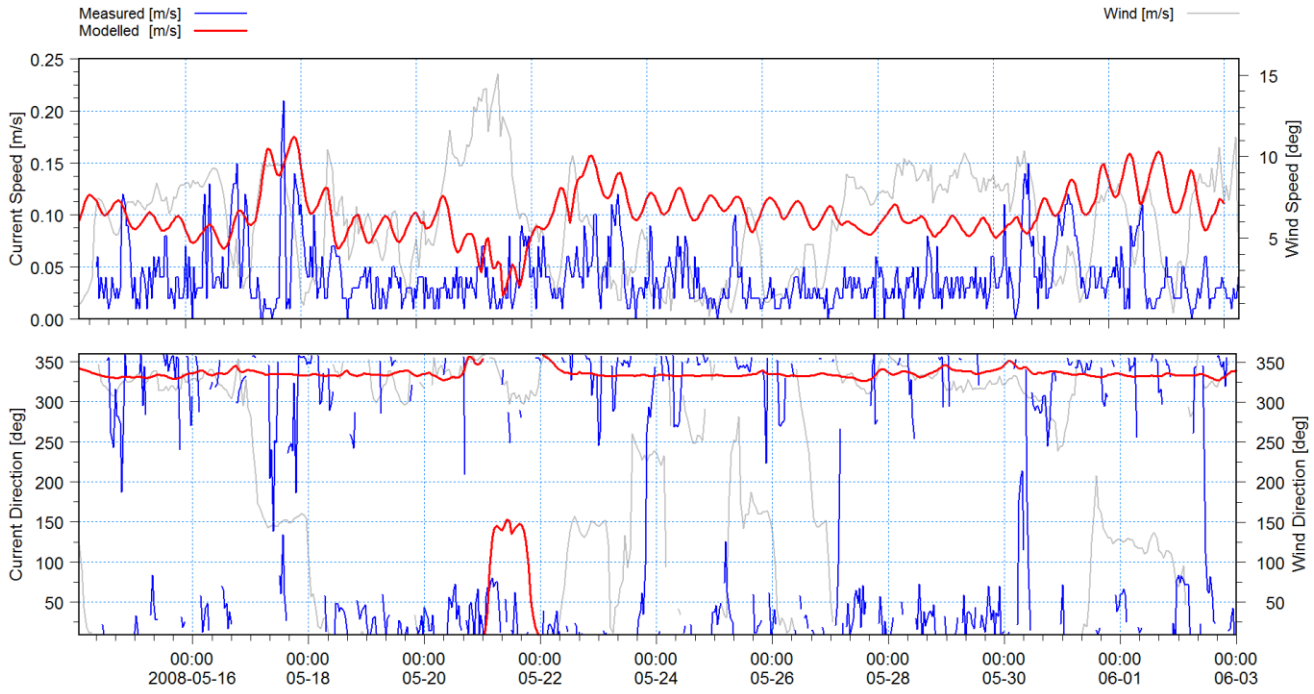

Figure 5-17: Surface (z=18) Current Speed and Direction Time Series Comparison at Simons Town (May to June 2008)

In addition, the Simons Town near seabed (z=18) current rose comparison of modelled and measured data is presented in Figure 5-18.

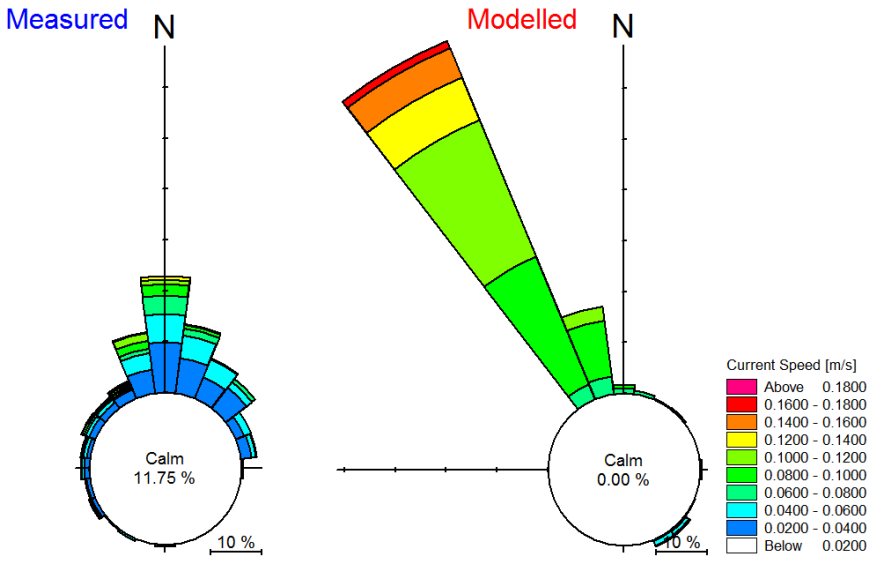

Figure 5-18: Surface (z=18) Current Rose Comparison at Simons Town (May to June 2008)

Overall the measurement data contains mostly weak tidal currents with stronger (>0.1 m/s) wind-generated currents present during south-easterly wind conditions. The weaker tidal

currents are “noisy” with high direction variability. From Figure 5-18, the model results were unable to replicate this variability but does show some agreement with measured northerly (setting) current directions. Similarly, modelled current speed does not show the high variability present in the measured dataset. Instead the model tends to slightly overestimate the weaker tidally driven currents. Overall, the model results are within the measured range of current speed and current directions at the site. Possible reasons for discrepancies in the time series comparison include:

- Smaller timescale gusting events not captured in the CSAG wind dataset;
- The model not including the following water level constituents: coastally trapped waves, long waves, short waves etc.; and
- The measurement instrument (ADCP) being unable to accurately capture current speed and direction parameters of weaker currents.

It is recommended that, in a future study, if the verification and calibration of the model is to be improved, that a measurement campaign considering multiple measurement locations be integrated into the research work. This methodology will aid in ensuring that “data integrity” is consistent across measurement datasets.

5.3.3 Sea Temperature

Modelled sea surface temperature was verified against daily measurements sourced from the South African Weather Service at Gordons Bay over the 2008-year verification period (refer to Table 5-1). A time series comparison between the modelled (near seabed: z =18 m) and measured seawater temperatures in Gordons Bay (refer to Figure 4-4 for measurement location) is presented in Figure 5-19.

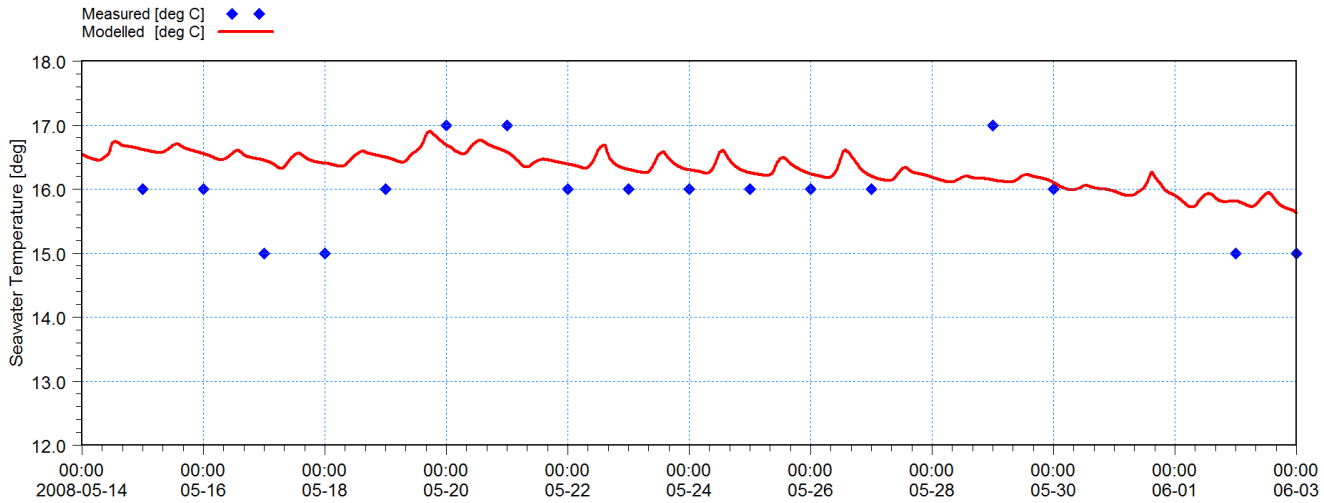

Figure 5-19: Sea Surface Temperature Time Series Comparison of Modelled and Measurements at Gordons Bay

From Figure 5-19, the measured surface temperature trend is captured in the modelled time series. However, as stated previously in Section 5.2.4, the measured dataset comprises daily thermometer readings at the harbour in Gordans bay (Dufois & Rouault, 2012). Thermometer readings are generally coarse and are read to the nearest degree. Therefore, relatively large 1-2℃ fluctuations are present in sea surface temperature measurements.

CHAPTER 6: MODEL RESULTS AND ANALYSIS

This chapter presents the results of the hydrodynamic model considering a complete year (2010) of simulation. Results are presented on an annual scale and event scale. Event scale results were useful for comparison with historical observational studies which elucidated physical processes on similar timescales.

This chapter comprises analysis subsections which address key False Bay hydrodynamic processes relating to the following:

- Event Scale Analysis
  - Current circulation; and
  - Vertical thermal structure.
- Annual Analysis
  - Sea surface temperature; and
  - Vertical thermal structure.

In addition to these results, sensitivity analyses were undertaken to investigate the potential engineering application of hydrodynamic modelling of False Bay. It cannot be guaranteed that all the input data sources considered in this study (e.g. WASA hindcast dataset) will be available for future investigations/studies. Therefore, the sensitivity analyses considered the effects of including or neglecting certain processes or variability, and evaluated the potential errors if such processes/variations are necessarily omitted. With this consideration in mind, the sensitivity analyses comprised the following:

- 2D (depth integrated) model setup and comparison with 3D model;
- Spatially varying wind field and unidirectional wind field comparison; and
- Monthly averaged climatology dataset (World Ocean Atlas) and HYCOM (daily) comparison.

6.1 Event Scale Analysis - Current Circulation

As described previously (refer to Section 2.2.4), circulation patterns within False Bay have historically been characterised by a predominantly bimodal behaviour which is dependent on the prevailing wind regime over the bay, namely south-easterly and north-westerly wind generated circulation. South-easterly and north-westerly conditions predominate during summer and winter respectively (Taljaard et al., 2000). Therefore, this section elucidates south-easterly and north-westerly circulation patterns separately on an event scale.

6.1.1 Tidal Currents

The model results generally show the decoupling of surface and bottom flows. More specifically, surface flows tend to be wind-driven with bottom flows comprising weak (≤0.1 m/s) tide-driven currents. This finding is consistent with Gründlingh et al., (1989) who reported measured tidal bottom current speeds of 0.09-0.11 m/s at the entrance of the bay. Similarly, Wainman et al. (1987) measured tidal bottom currents at Cape Point within the range of 0.0-0.2 m/s which was consistent with model results. However, under strong wind conditions, modelled bottom flows are more wind-driven than tide-driven.

Contour plots of currents for neap ebb, neap flood, spring ebb and spring flood are presented in Figure 6-1, Figure 6-2, Figure 6-3 and Figure 6-4 respectively. To isolate tidal flows, all plots were generated from model results considering no wind forcing, no atmospheric heat exchange and no temperature-depth profiles on the boundaries.

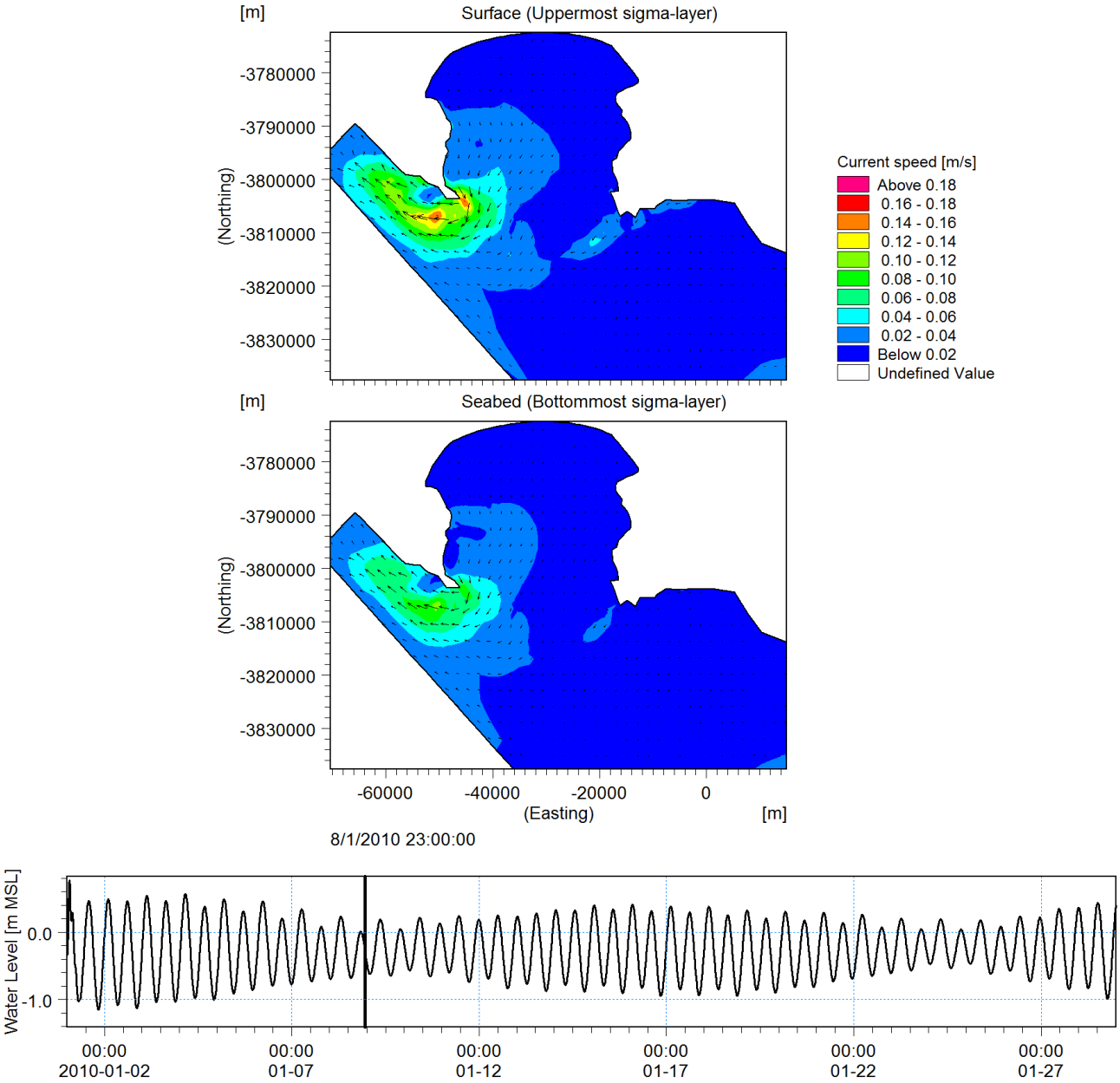

Figure 6-1: Contour and Time Series Plot of Typical Neap Ebb Tide

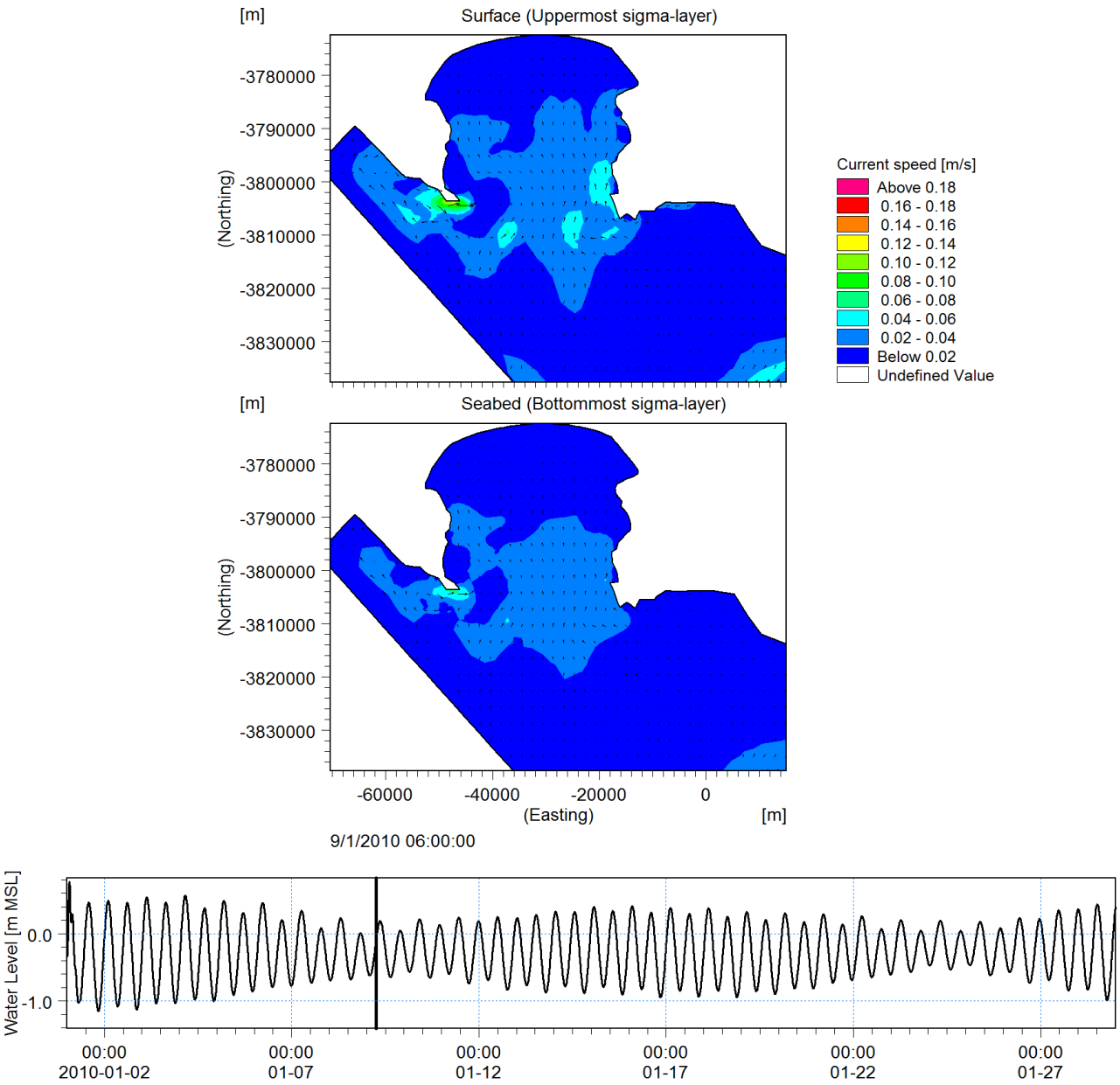

Figure 6-2: Contour and Time Series Plot of Typical Neap Flood Tide

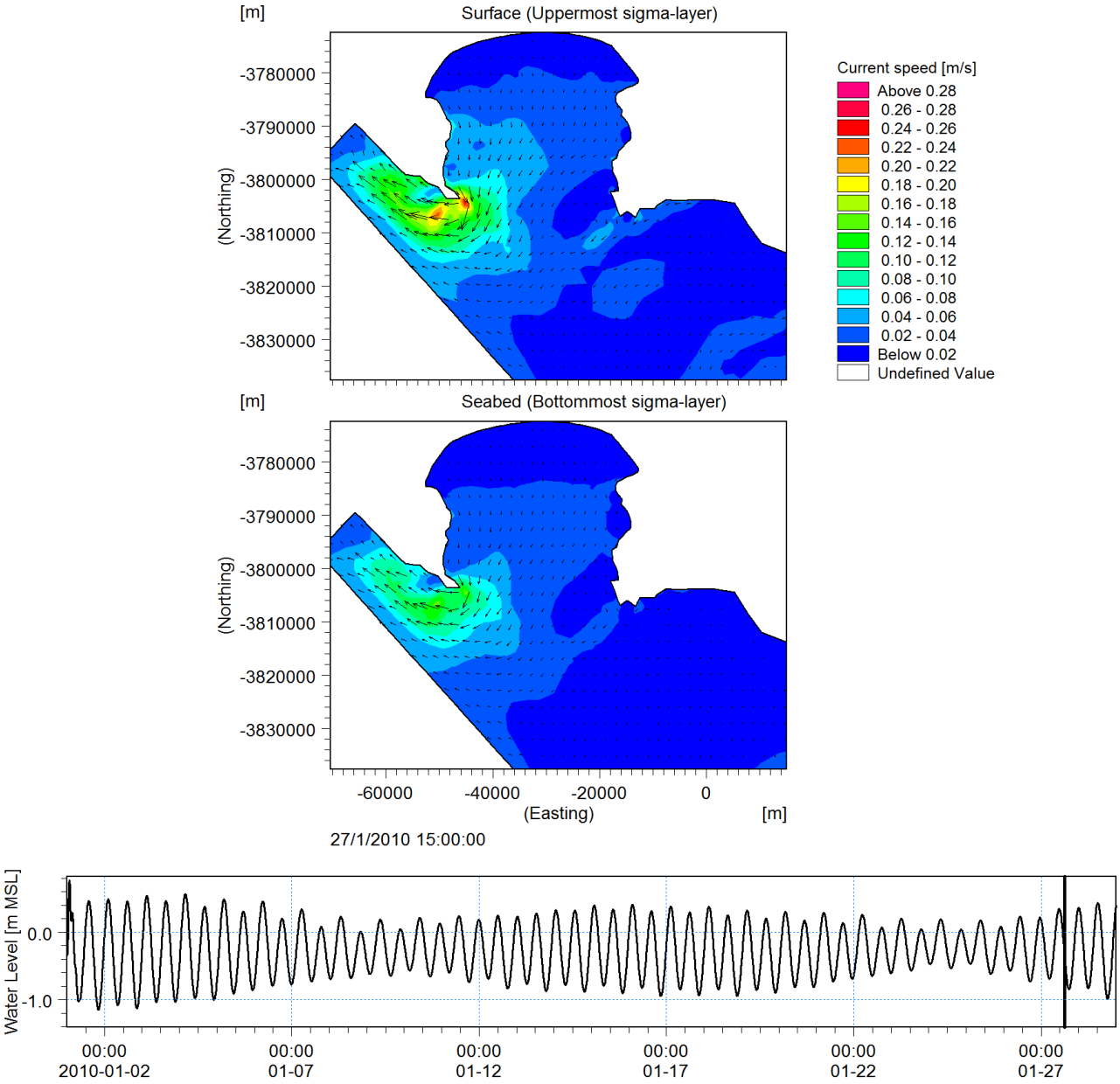

Figure 6-3: Contour and Time Series Plot of Typical Spring Ebb Tide

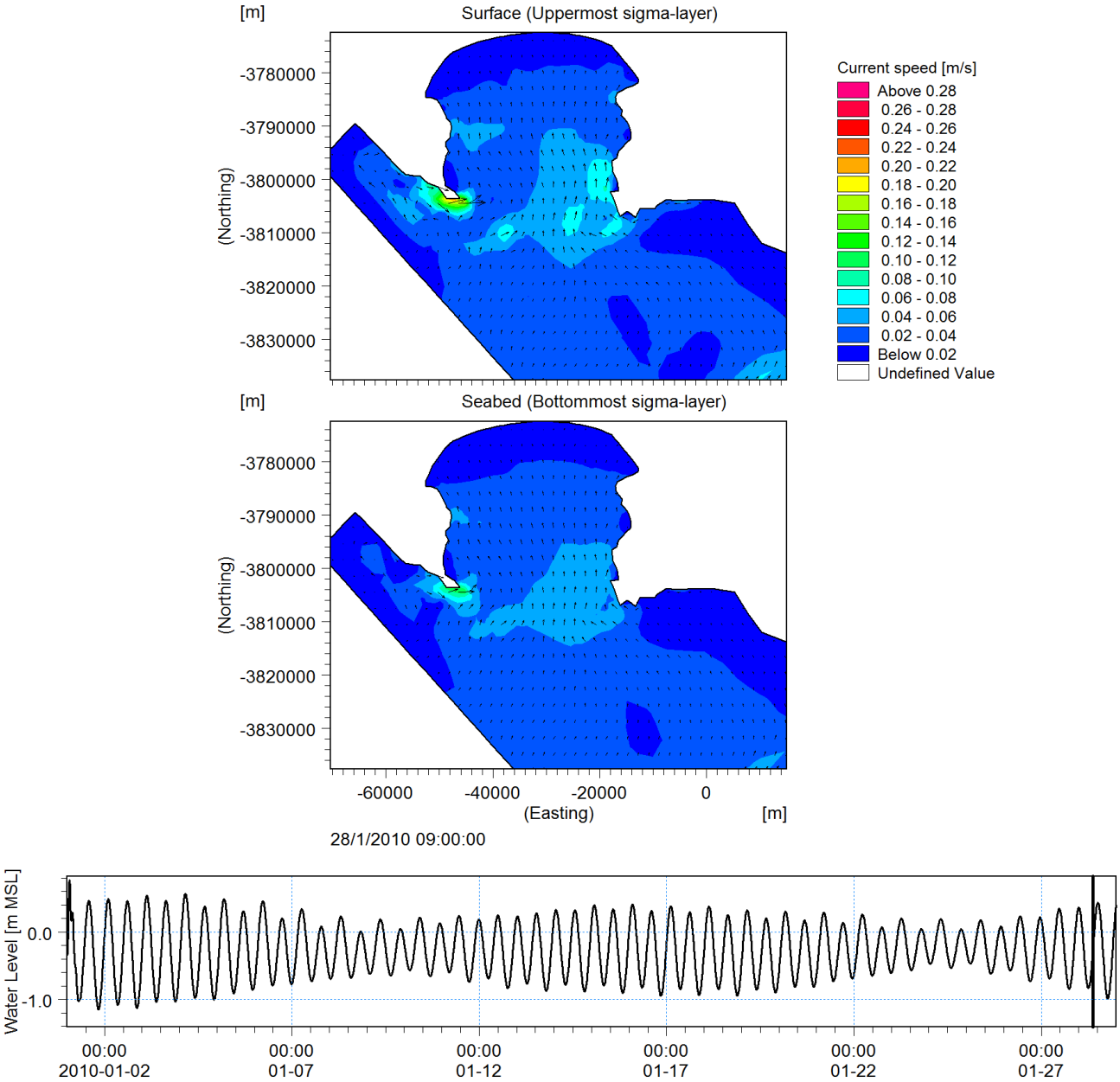

Figure 6-4: Contour and Time Series Plot of Typical Spring Flood Tide

Neap and spring tidal currents are similar under both flood and ebb conditions. Generally, under flood conditions, currents are uniform throughout the bay whereas ebb tidal currents show some variation. Throughout the bay domain, flood tidal currents are weak with typical magnitudes within the range of 0.02-0.1 m/s. Flood tidal currents accelerate while passing around Cape Point, the eastern shore or over Rocky Bank.

Ebb tidal currents are weak with typical magnitudes within the range of 0.02-0.06 m/s. Currents accelerate around Cape Point and over Rocky Bank with a magnitude of 0.1-0.25 m/s.

It is likely that tidal currents around Cape Point intensify slightly due to the proximity of Cape Point to the open model boundaries where the sea levels are imposed. However, in later chapters, with wind forcing applied, this degree of intensification of currents at Cape Point is not present which indicates that the flow regime is more susceptible to wind forcing.

6.1.2 South-easterly Circulation

Circulation patterns are presented on two contour plots: current magnitude and temperature in Figure 6-5 and Figure 6-6 respectively. The plots show near surface and near seabed flows. To characterise the predominant wind climate, a time series was extracted from the WASA (CSAG) hindcast dataset at Roman Rock (refer to Figure 4-1).

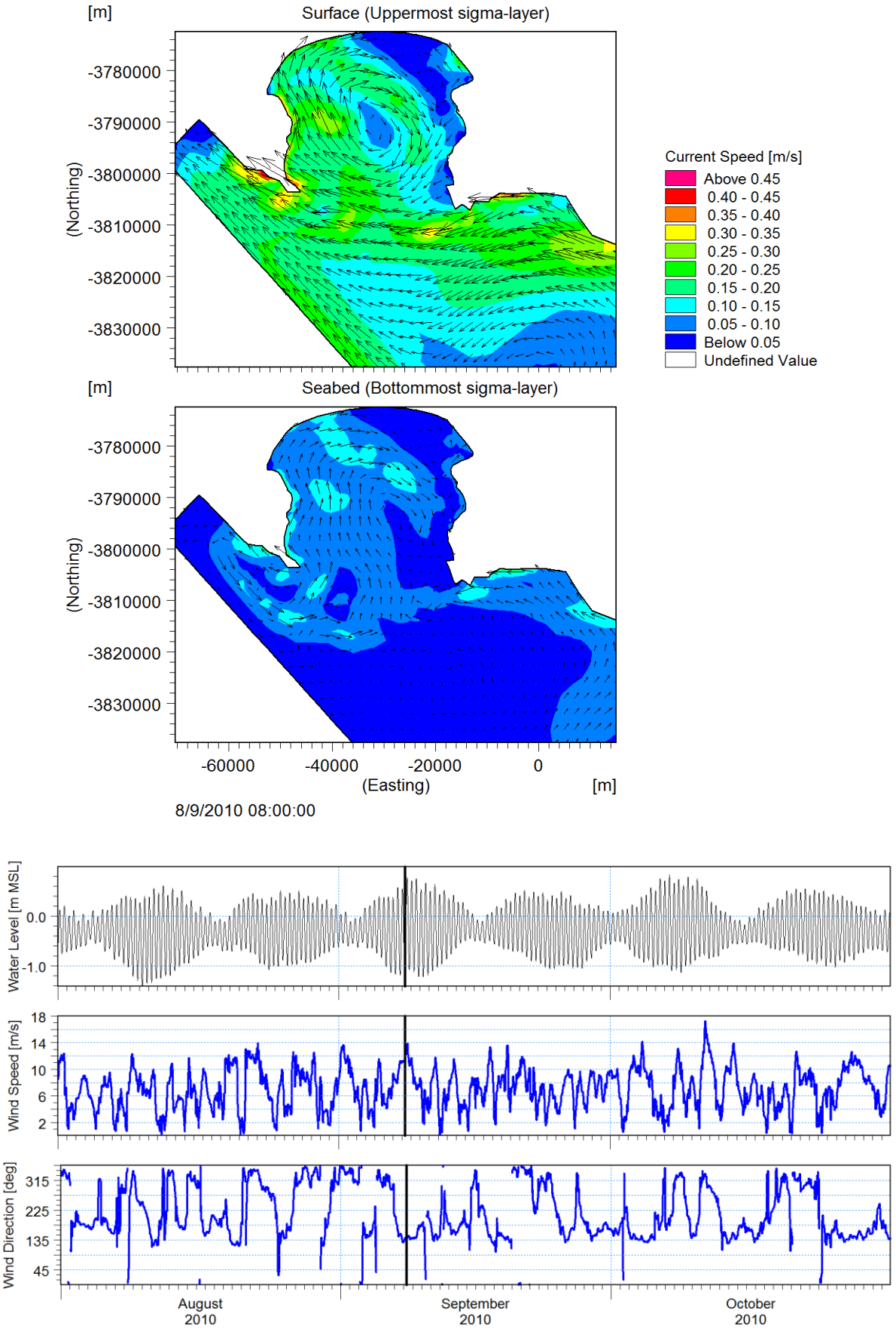

Figure 6-5: Well-mixed South-easterly Generated Current Circulation Pattern

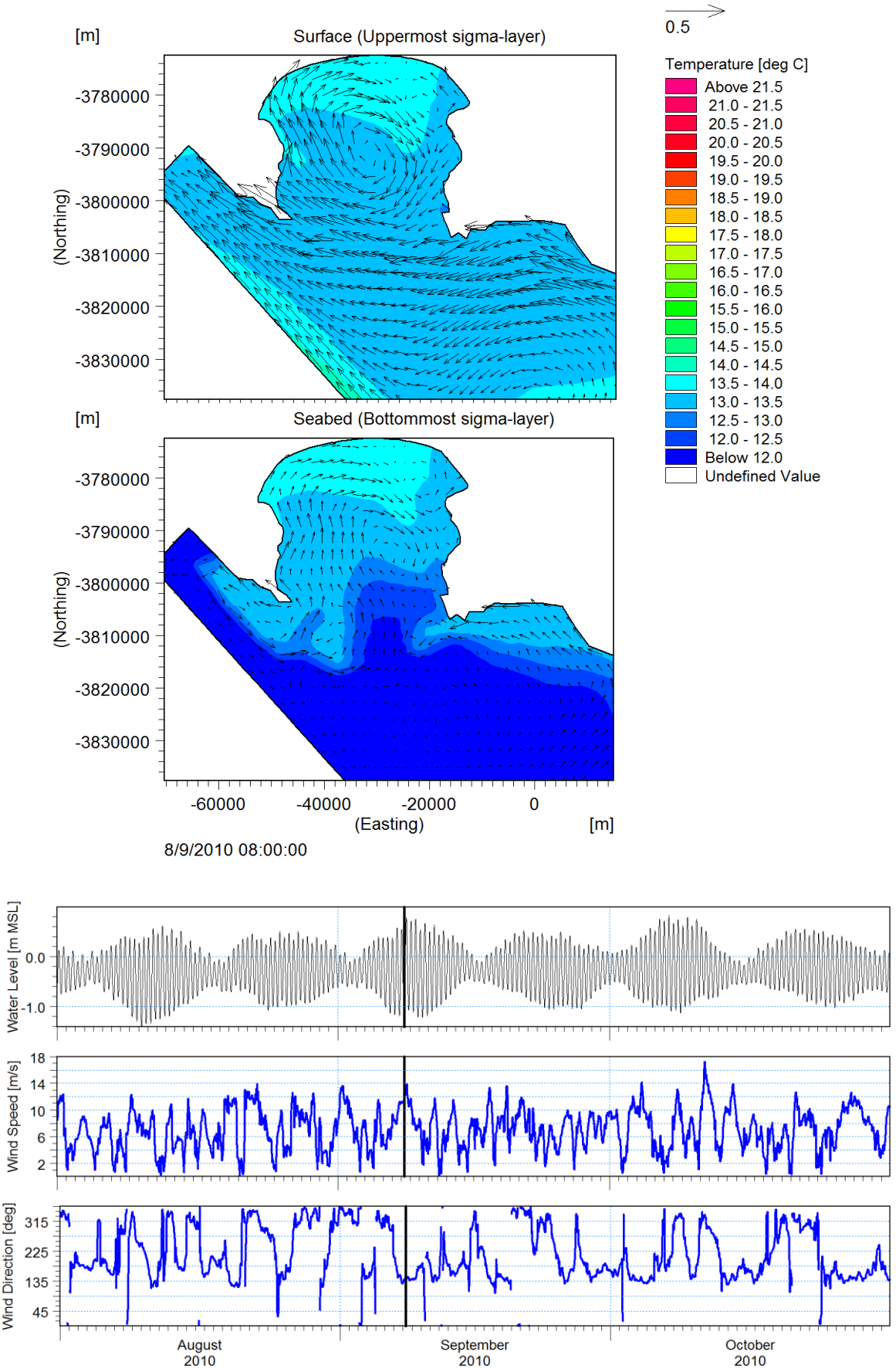

Figure 6-6: Well-mixed South-easterly Generated Current Circulation Pattern with Temperature Contours

Overall, the circulation pattern results are consistent with historical studies which noted the formation of a clockwise gyre under predominant south-easterly wind conditions (Cram, (1970); Atkins, (1970a); Shannon et al., (1983); Van Forrest and Jury, (1985); Wainman et al., (1987) and Botes, (1988). In addition, the bifurcated circulation pattern (refer to Figure 2-8) postulated by Gründlingh et al. (1989) is well represented in Figure 6-6. The formation of this gyre means that there is a net inflow near Cape Point and net outflow at Cape Hangklip. From analysis of the south-easterly circulation pattern presented in Figure 6-8, colder surface waters are advected from offshore through the entrance of the bay at Cape Point toward the middle of the bay. The cyclonic circulation pattern results in warmer nearshore water being advected through the entrance (near Cape Hangklip) toward offshore. However, the results indicated that this circulation pattern is generally fully developed under stronger south-easterly conditions.

Under south-easterly wind conditions, the model results show the formation of a weak anticyclonic gyre near Gordons Bay. This zone shows evidence of a “wind shadow” in this region which stretches from Strand along the Eastern shore up to Cape Hangklip. The presence of a wind shadow under south-easterly conditions was documented by Wainman, et al. (1987). Current magnitudes in this region are typically ≤0.1 m/s and ≤0.05 m/s at the surface and seabed respectively.

Model results correctly reproduced the decoupling of surface and bottom flows which were noted in previous studies (Gründlingh et al., (1993); Taljaard et al., (2000); Nicholson, (2011)). Decoupling of flows refers to surface flows being significantly influenced by wind-forcing compared to weaker bottom flows which flow in a different direction. While the surface flow forms a stronger clockwise (or cyclonic) gyre, the bottom flows show a weaker cyclonic flow. Surface current magnitudes of up to 0.3 m/s are generated under the influence of strong south-easterly winds (approximately 12 m/s). Bottom current magnitudes are weak with a magnitude of 0.05-0.1 m/s.

The results above refer to a well-mixed water column. To investigate the influence of seasonality on the south-easterly circulation pattern, two contour plots showing current speed and seawater temperature are depicted in Figure 6-7 and Figure 6-8 respectively. The results consider stratified conditions in January 2010.

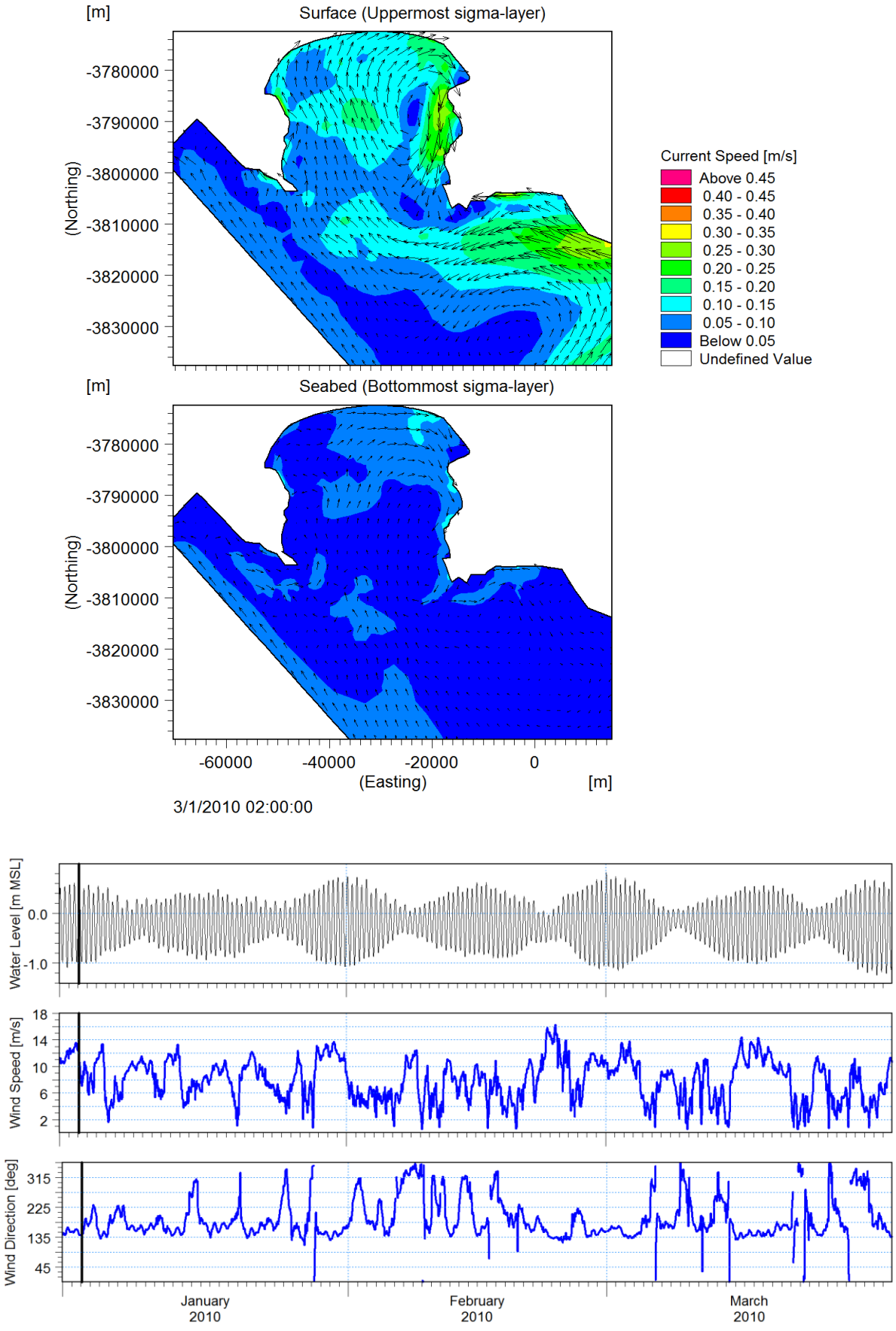

Figure 6-7: Stratified South-easterly Generated Current Circulation Pattern

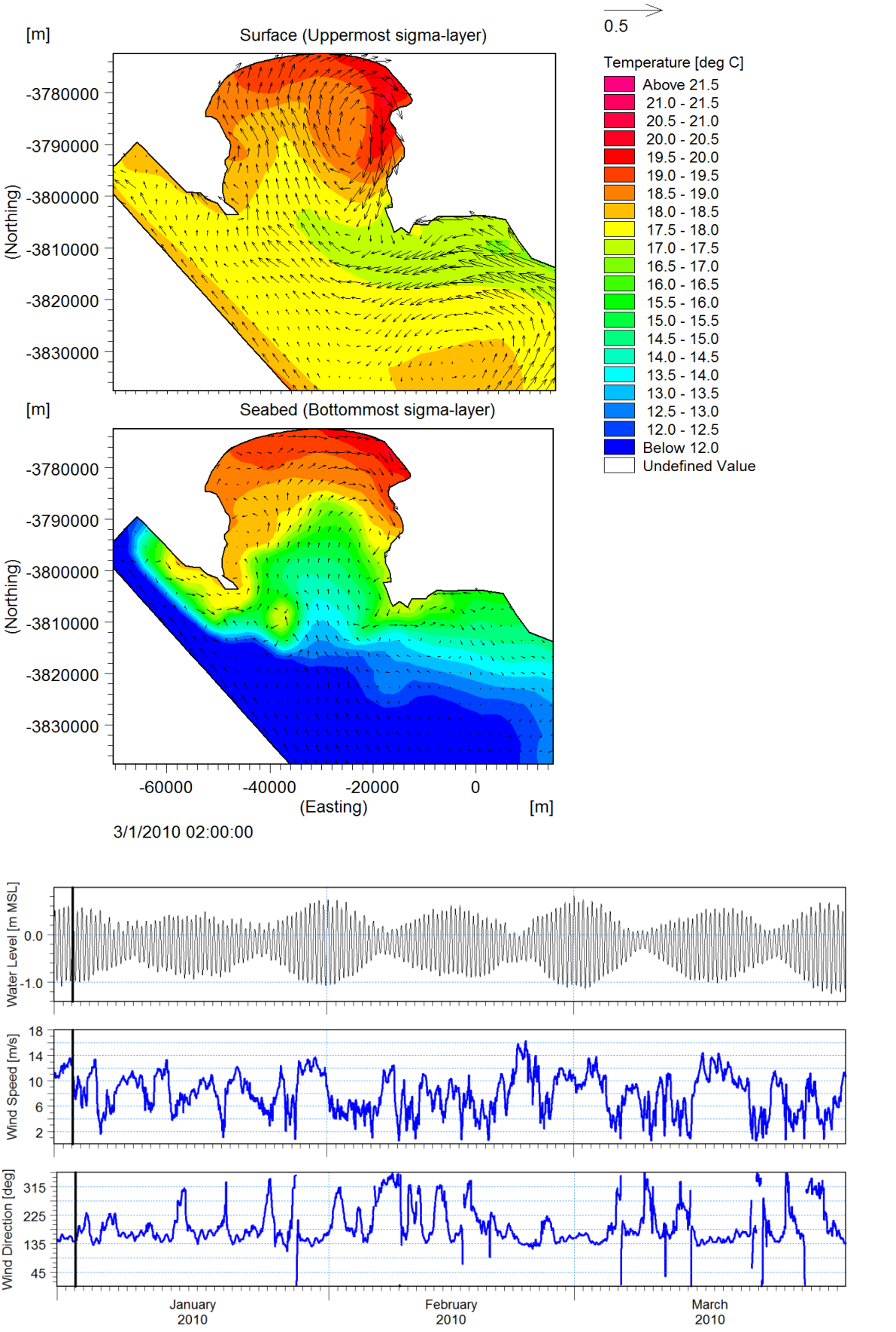

Figure 6-8: Stratified South-easterly Generated Current Circulation Patterns with Temperature Contours

The overall stratified south-easterly circulation pattern is similar to the circulation pattern under well-mixed conditions with some minor differences, notably:

- The surface longshore currents at Cape Hangklip which were significantly stronger (approximately double the magnitude) under stratified conditions;
- The centre (or “eye”) of the cyclonic gyre is pushed more toward Gordons Bay;
- The presence of a “wind shadow” is not present; and
- The formation of a weak anticyclonic gyre at Gordons Bay is not present.

The model results show that under stratified conditions, an upwelling zone is present just off Cape Hangklip which is consistent with historical observational studies (Cram, (1970); Jury, (1985); Wainman et al., (1987); Taljaard et al., (2000)). This upwelling region is shown to be approximately 1-2℃ colder than surrounding sea surface temperatures.

In addition to the findings above, the model results show that the bottom flow regime is greatly influenced by Rocky Bank which tends to steer inflows around it. More specifically, current magnitudes west of Rocky Bank are sometimes double those east of Rocky Bank. This flow dichotomy is mainly due to the bay entrance west of Rocky Bank being narrower and shallower than the bay entrance east of Rocky Bank. The influence of Rocky Bank extends to the horizontal thermal structure as well with bottom waters east of Rocky Bank being approximately 1-3℃ colder than bottom waters west of Rocky Bank. The vertical thermal structure will be described in more detail in Section 6.2.

6.1.3 North-westerly Circulation

Circulation patterns were extracted on two contour plots showing current speed and seawater temperature in Figure 6-9 and Figure 6-10 respectively. To characterise the predominant wind climate, a time series was extracted from the WASA hindcast dataset at Roman Rock (refer to Figure 4-1). An overview of the north-westerly circulation pattern (surface and seabed) during October 2010 is presented in Figure 6-10.

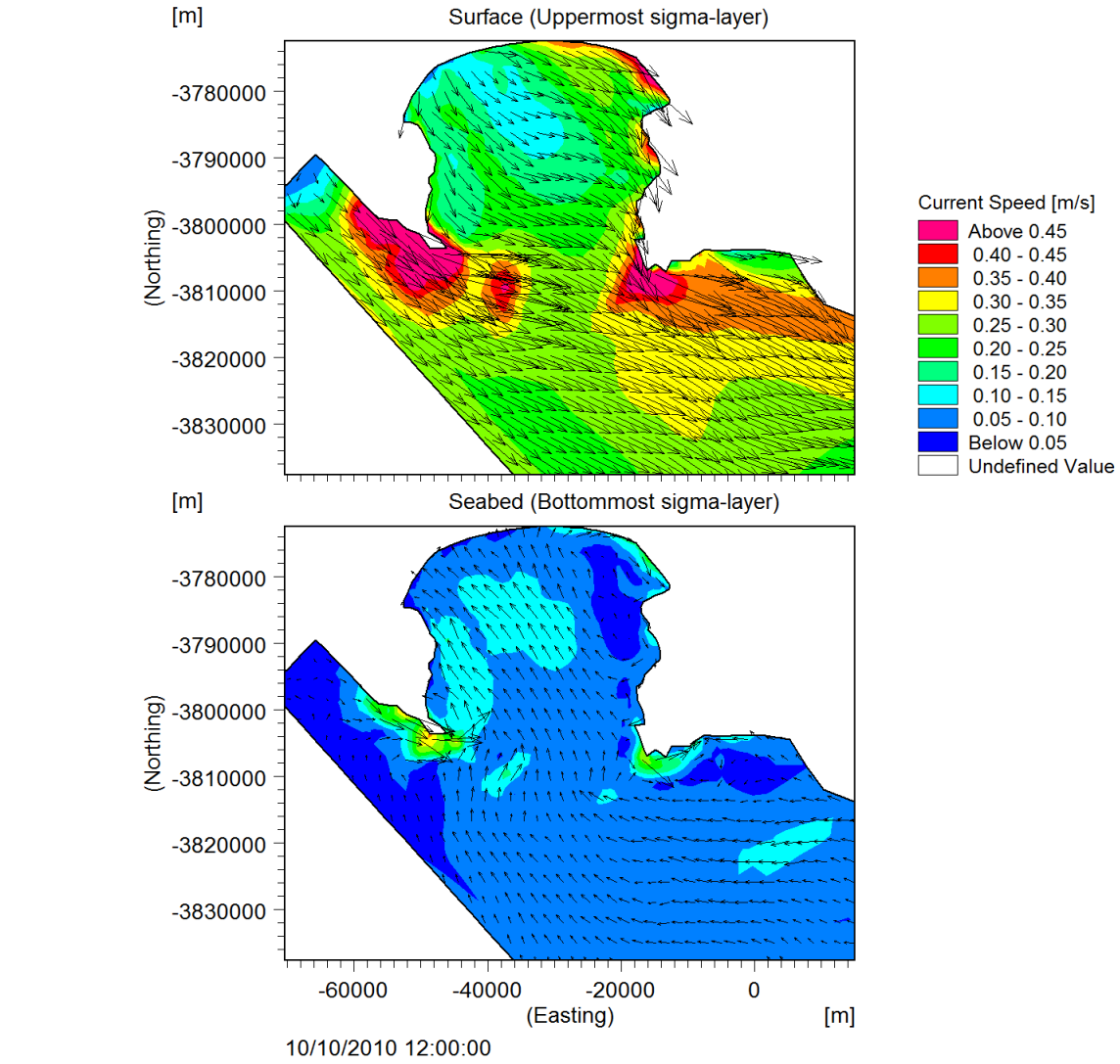

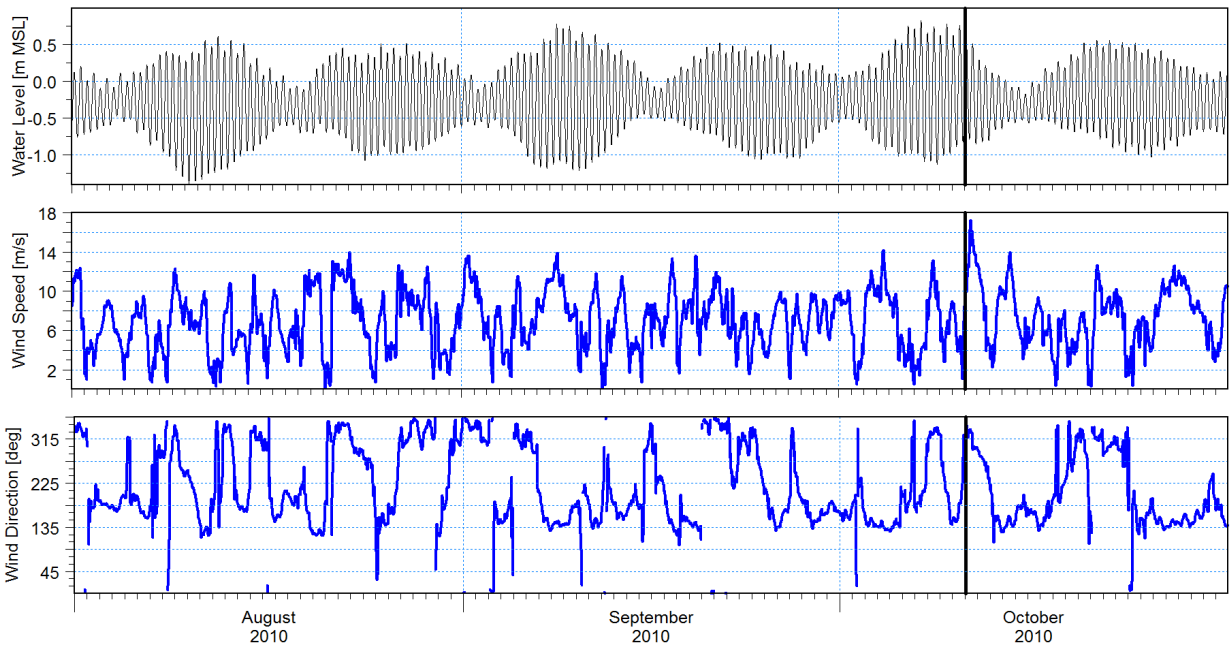

Figure 6-9: Well-mixed North-westerly Generated Current Circulation Pattern

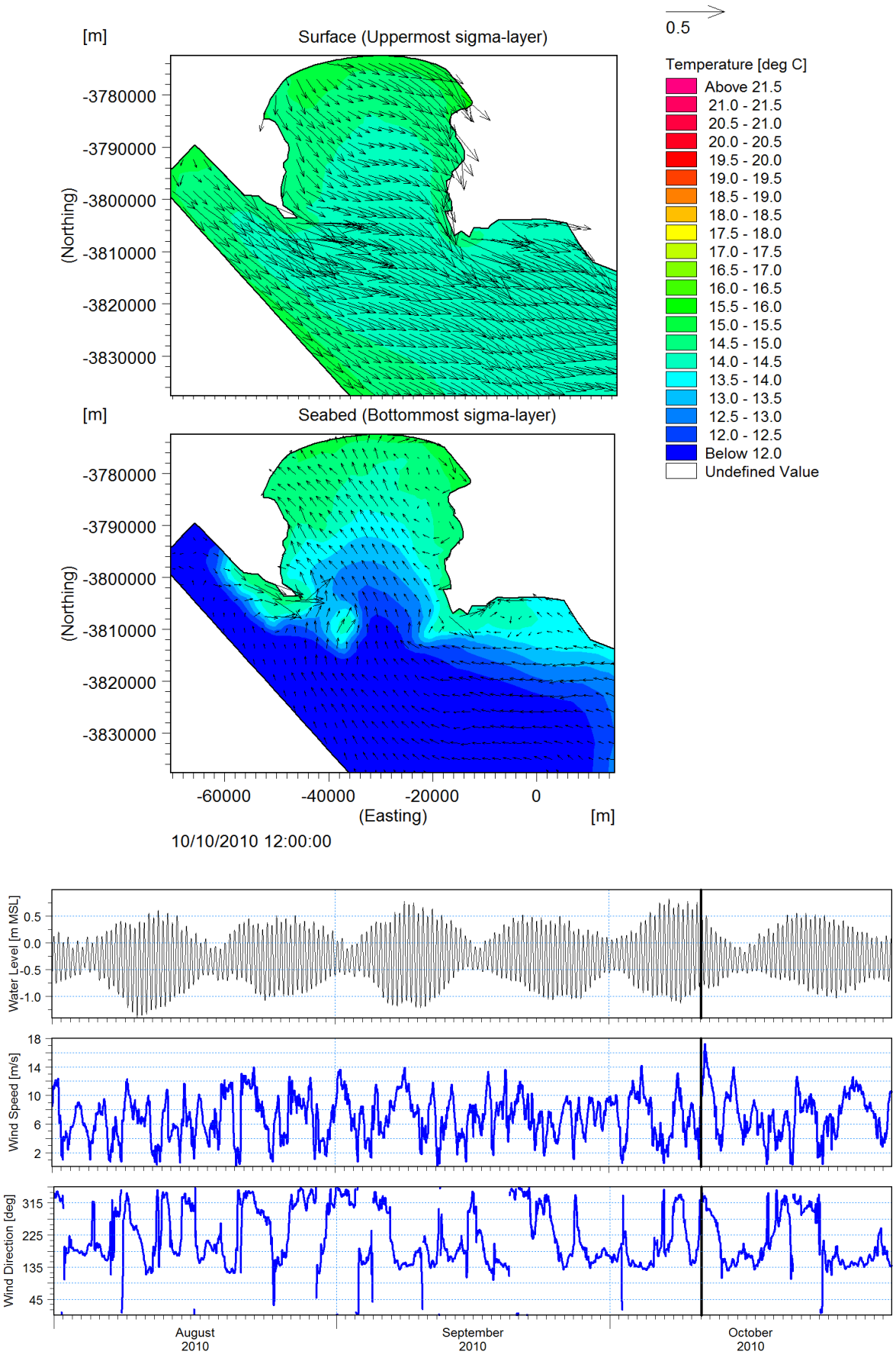

Figure 6-10: Well-mixed North-westerly Generated Current Circulation Pattern with Temperature Contours

Overall, the results show that, under north-westerly conditions, the anti-cyclonic circulation pattern presented in historical observational studies (refer to Figure 2-10) is absent. Instead, the north-westerly wind condition induces a spatially-uniform current field with no distinct gyres forming in the bay. A possible explanation for this finding could be the formation of the north-westerly wind condition which is less spatially-complex than the south-easterly wind condition. Unlike south-easterly winds which are influenced by complex orographic features surrounding False Bay, north-westerly winds are mainly influenced by Table Mountain (Jury, 1984) which is further from the bay. North westerly winds tend to deflect around Table Mountain and across the bay uniformly until they are steered westerly at the entrance of the bay at Cape Point and Cape Hangklip (refer to Figure 2-6).

The north-westerly circulation pattern is generally less persistent than the south-easterly pattern (Taljaard et al., 2000). The model was able to reproduce this behaviour during the year-long simulation. It has been postulated that the north-westerly circulation pattern being less persistent may be due to the setup of persisting seawater density structures during south-easterly winds conditions (Taljaard et al., 2000).

Generally, the model was able to correctly reproduce the decoupling of surface and bottom flows observed in historical studies (Gründlingh, (1993); Taljaard et al., (2000); Nicholson, (2011)) i.e. surface flows being more influenced by wind-forcing compared to weaker bottom flows which flow in a different direction. From Figure 6-9, the results show that under strong north-westerly conditions (>10 m/s), strong south-east setting surface currents exceeding 0.3 m/s are generated. As the north-westerly wind forces surface waters away from the shore and toward the bay entrance, the flow deflects westerly and accelerates at Cape Point, Cape Hangklip and along the eastern shoreline. At these locations current speeds exceeding 0.45 m/s are present.

The results show that under north-westerly conditions, north-westerly-setting bottom return currents are generated throughout the bay domain. This finding was consistent with measurements by Nicholson (2011) who showed the bottom current flowing in the opposite direction under north-westerly conditions near the middle of the bay. As shown in Figure 6-9, the bottom return current magnitudes have a range of 0.05-0.1 m/s. These return currents force bottom water from the entrance to the middle of the bay. Upon entry to the bay, currents accelerate around Cape Point, Cape Hangklip and over Rocky Bank. Current magnitudes at these locations accelerate to approximately 0.3 m/s under strong north-westerly wind conditions. The model results presented in Figure 6-10 indicate that these bottom return currents facilitate advection of cold water through the entrance east of Rocky Bank. This process is described in greater detail in Section 6.2.2

The results and analysis above refer to a well-mixed water column under north-westerly conditions. To investigate the influence of seasonality on the north-westerly circulation pattern, two contour plots showing current speed and seawater temperature are presented in Figure 6-11 and Figure 6-12 respectively. The results consider stratified conditions in February 2010.

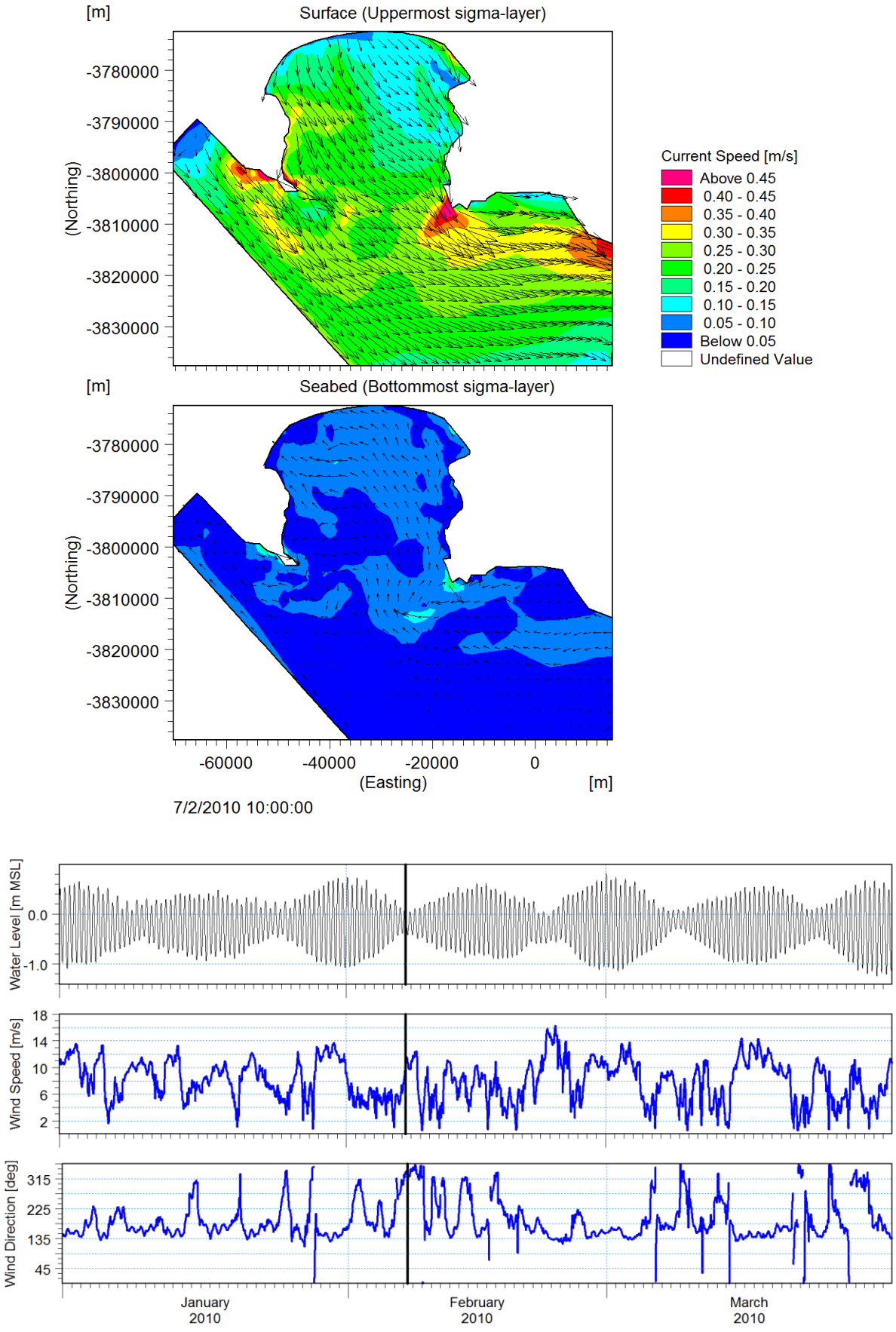

Figure 6-11: Stratified North-westerly Generated Current Circulation Pattern

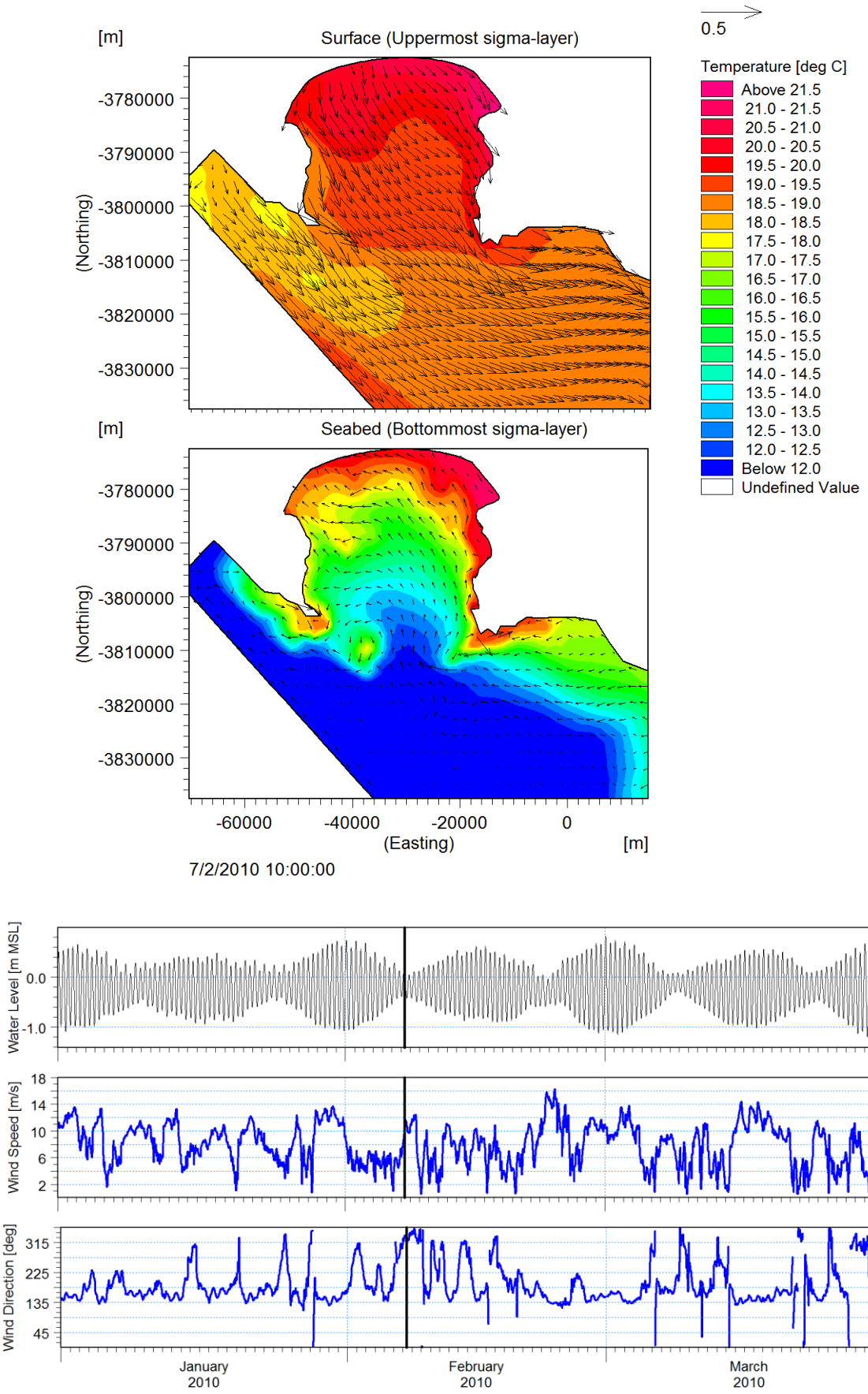

Figure 6-12: Stratified North-westerly Generated Current Circulation Patterns with Temperature Contours

Overall, the stratified north-westerly circulation pattern is nearly identical to the well-mixed circulation pattern. From Figure 6-11, current magnitudes are within a similar range to well-mixed conditions. Once again, even under stratified conditions, the results show that the anticyclonic gyre postulated in historical observational studies (Taljaard et al. (2000)) is absent under stratified conditions.

6.2 Event Scale Analysis - Vertical Thermal Structure

To investigate the event-scale vertical thermal structure further under well-mixed and stratified conditions, three section plots were extracted: one in the nearshore, one near the middle of the bay and one near the entrance of the bay. A summary of these vertical sections is presented in Figure 6-13.

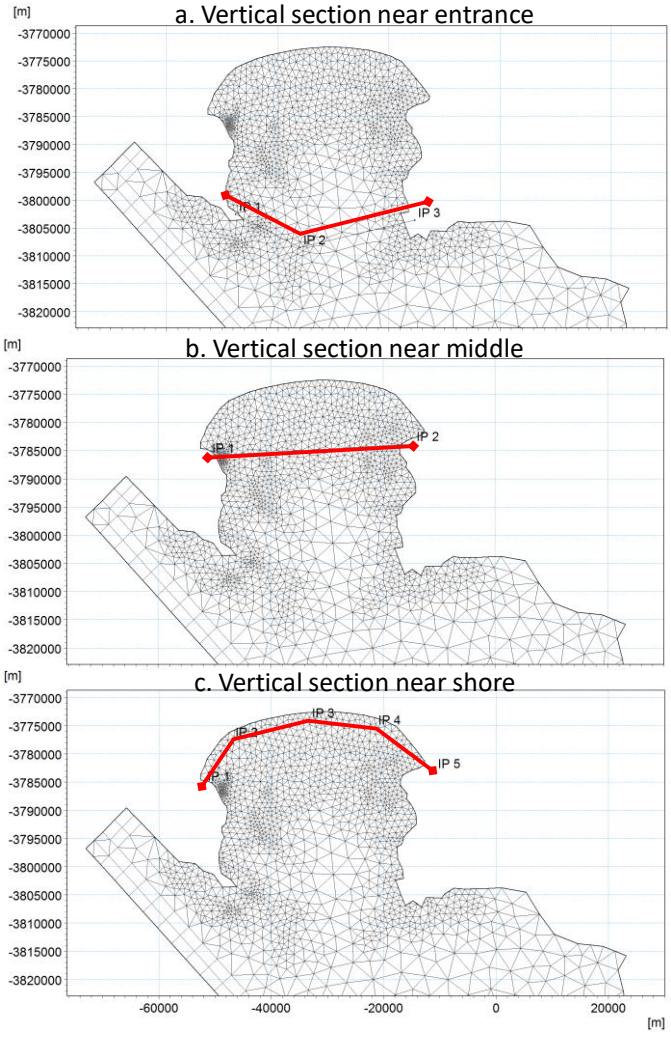

Figure 6-13: Summary of Vertical Sections Considered

The entrance vertical section (a) is v-shaped in plan to include the influence of Rocky Bank. The middle vertical section (b) extends from Simons Town to Gordons Bay. The nearshore vertical section (c) comprises multiple points along the northern shore.

6.2.1 South-easterly Conditions

This section provides the results and analysis of the vertical thermal structure of the bay under south-easterly wind conditions. Vertical sections are presented in Figure 6-14 and Figure 6-15 which provide an overview of vertical thermal structure under well-mixed and stratified conditions respectively. To characterise the predominant wind climate, a time series was extracted from the WASA (CSAG) hindcast dataset at Roman Rock (refer to Figure 4-1).

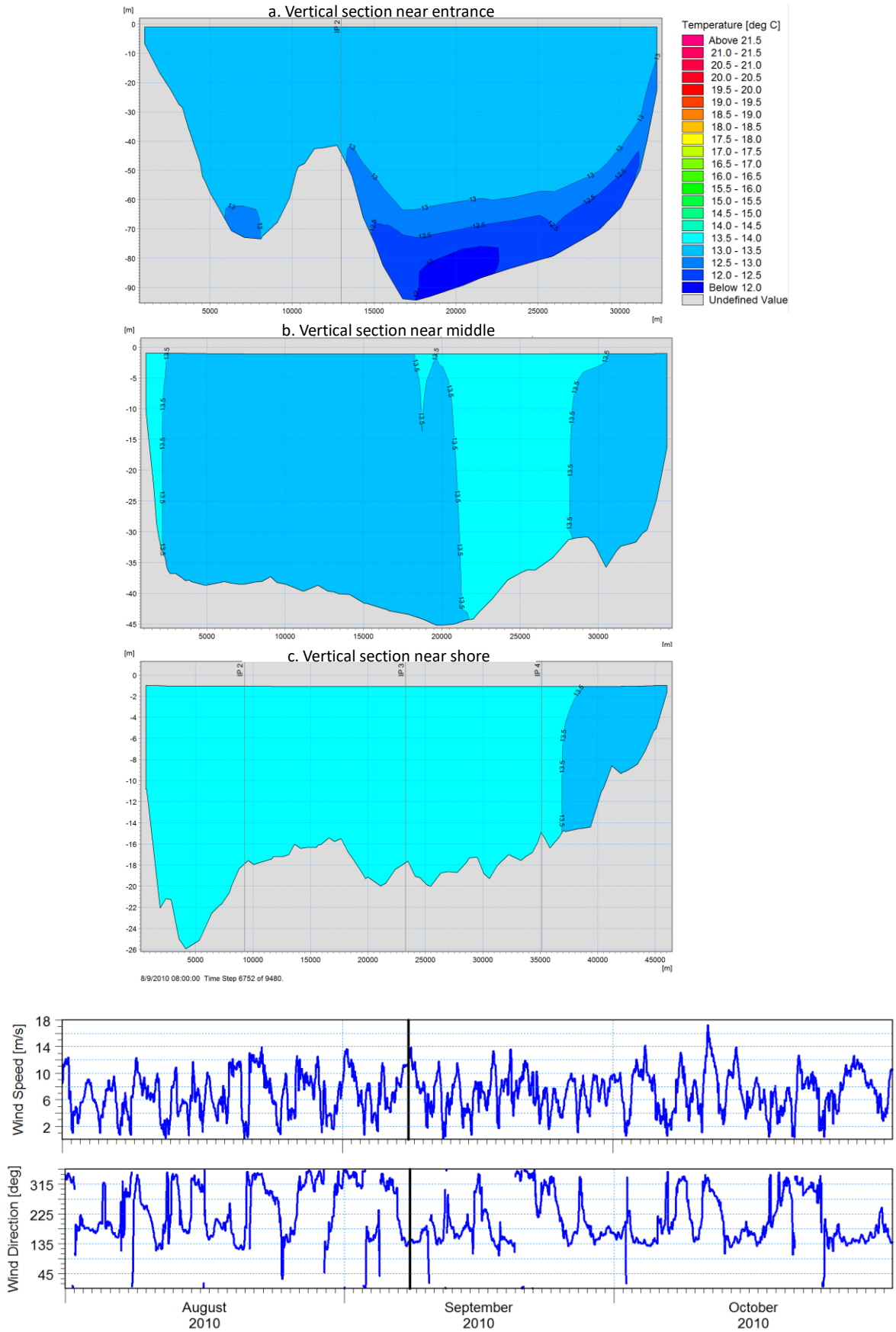

Figure 6-14: Vertical Sections near the Entrance (a), Middle (b) and Northern Shore (c) under Well-Mixed South-easterly Conditions

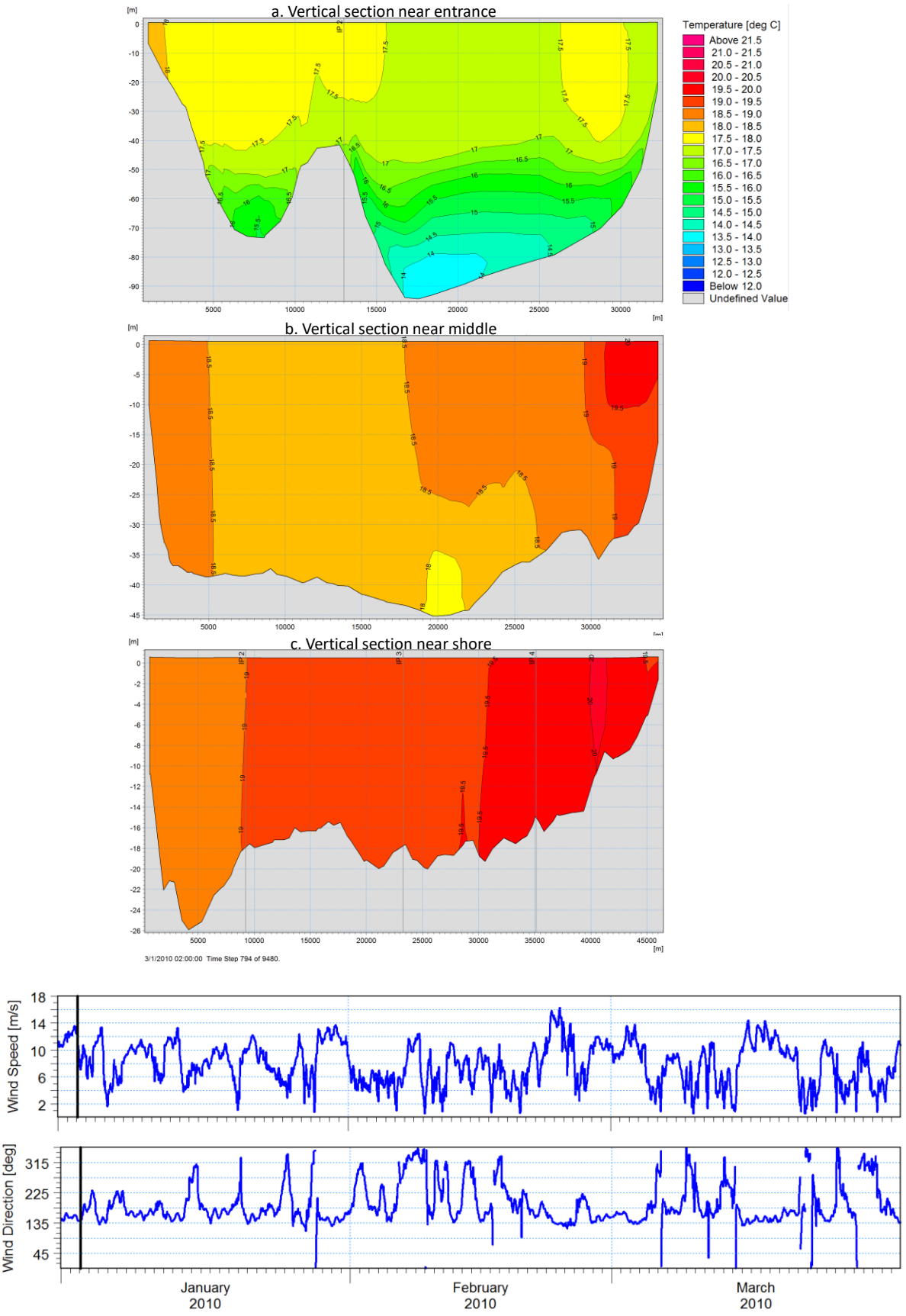

Figure 6-15: Vertical Sections near the Entrance (a), Middle (b) and Northern Shore (c) under Stratified South-easterly Conditions

Overall, the model results show that the vertical sections under well-mixed and stratified conditions show the presence of colder bottom water at the entrance of the bay. From the deep-water entrance to the shallower northern shore, seawater temperatures become progressively warmer. At the entrance, the influence of Rocky Bank is clearly identified in the plots which show how the feature segregates warmer western and colder eastern waters. Due to the asymmetry of bathymetry at the entrance, bottom waters are approximately 1-2℃ colder east of Rocky Bank under well-mixed and stratified conditions.

The model results show that the middle vertical section (b), under both well-mixed and stratified conditions, shows a near-uniform vertical temperature profile. A maximum temperature difference of 1℃ is shown between the surface and seabed. Horizontally, seawater temperatures are warmer along the eastern shore.

Analysis of the near shore vertical section (c), indicates a uniform vertical temperature profile under well-mixed and stratified conditions.

As described in Section 6.1.2, south-easterly winds form a clockwise (cyclonic) gyre covering the entire bay. The formation of this gyre means that there is a net inflow near Cape Point and net outflow at Cape Hangklip. From analysis of the south-easterly circulation pattern presented in Figure 6-8, colder surface waters are advected from offshore through the entrance of the bay at Cape Point toward the middle of the bay. The cyclonic circulation pattern results in warmer nearshore water being advected through the entrance (near Cape Hangklip) toward offshore. Ultimately, this results in surface seawater temperatures along the eastern shore being colder than the western shore. Therefore, from the results presented in this section, it is evident that the model correctly resolved the changes in vertical thermal structure under the south-easterly circulation regime.

6.2.2 North-westerly Conditions

This section provides the results and analysis of the vertical thermal structure of the bay under north-westerly wind conditions. Vertical sections are presented in Figure 6-16 and Figure 6-17 which provide an overview of vertical thermal structure under well-mixed and stratified conditions respectively. In addition, wind time series plots showing wind direction and wind speed are provided.

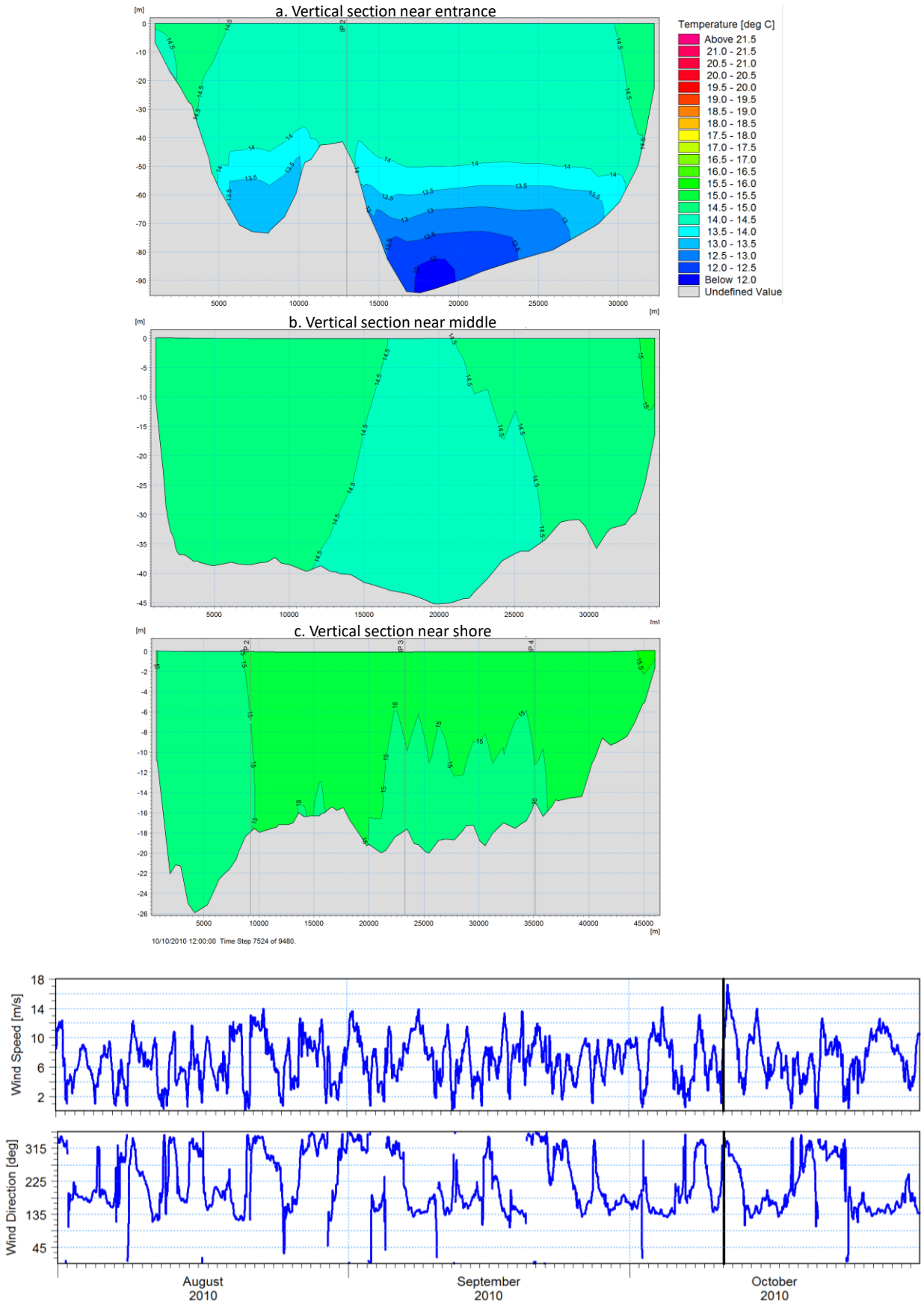

Figure 6-16: Vertical Sections near the Entrance (a), Middle (b) and Northern Shore (c) under Well-Mixed North-westerly Conditions

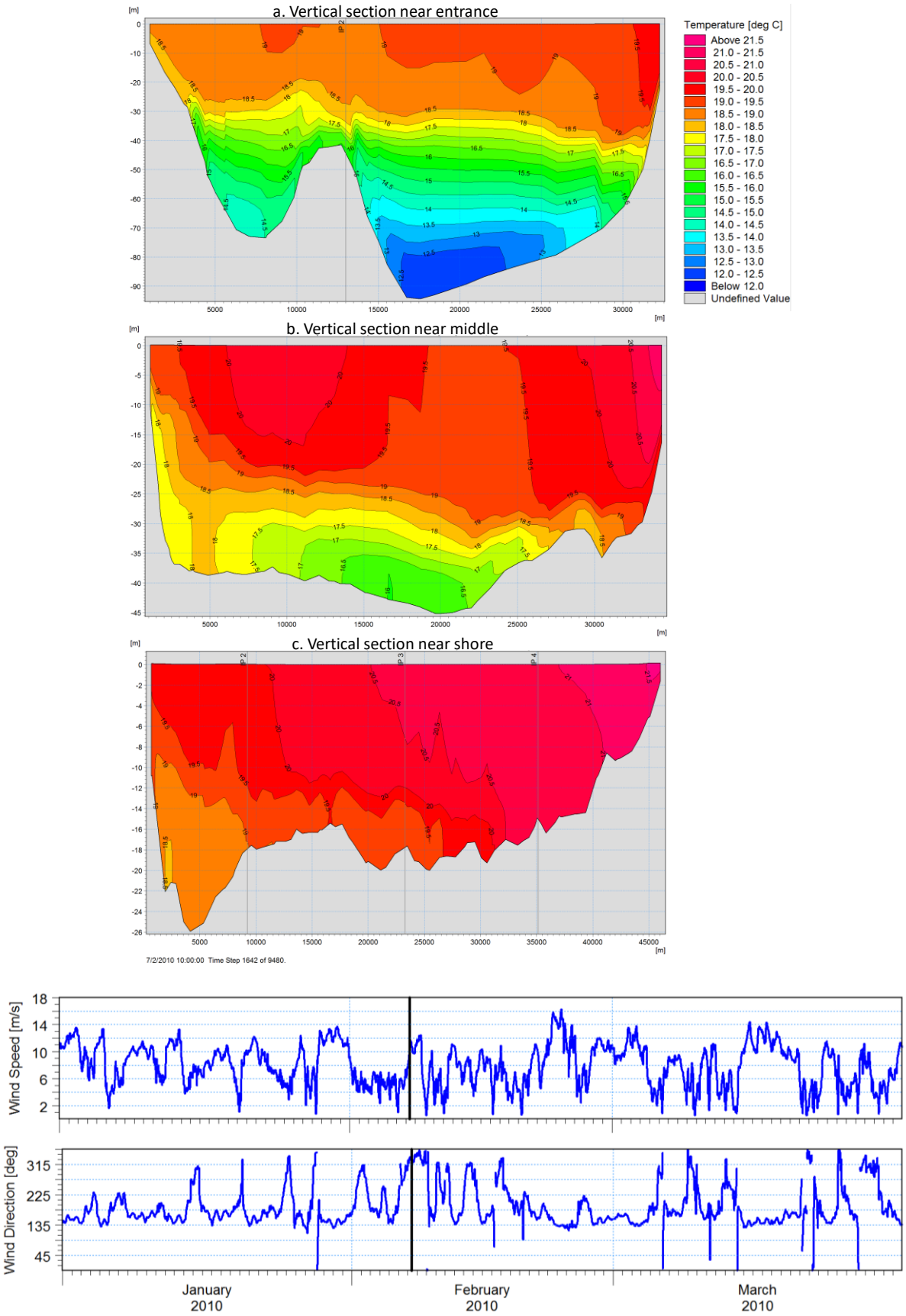

Figure 6-17: Vertical Sections near the Entrance (a), Middle (b) and Northern Shore (c) under Stratified North-westerly Conditions

Overall, the model results show that the vertical sections under well-mixed and stratified conditions show the presence of colder bottom water at the entrance of the bay. From the deep-water entrance to the shallower northern shore, seawater temperatures become progressively warmer. At the entrance, the influence of Rocky Bank is clearly identified in the plots which show how the feature segregates warmer western and colder eastern waters. Due to the asymmetry of bathymetry at the entrance, bottom waters are approximately 1-2℃ colder East of Rocky Bank under well-mixed and stratified conditions. From Figure 6-17, under stratified conditions, a temperature difference of 6-7℃ between surface and bottom layers is noted. This finding is consistent with CTD measurements by Gründlingh et al. (1989) who recorded temperature differences of 7℃ over a similar period during December and March.

The model results show that the middle vertical section (b), under well-mixed conditions, shows a near-uniform vertical temperature profile. However, under stratified conditions, there is significant difference between surface and bottom waters of approximately 3-4℃.

Analysis of the near shore vertical section (c), indicates a uniform vertical temperature profile under well-mixed and stratified conditions. However, the horizontal temperature profile, under stratification conditions, shows the eastern shore to be warmer than the western shore by approximately 2℃.

As described in Section 6.1.3, north-westerly winds result in a spatially-uniform surface current field in the direction of the wind. The formation of this surface current field then induces a bottom return current field in the opposite direction i.e. north-west setting currents. The surface currents force warmer nearshore waters toward the entrance offshore. The induced bottom return currents then advect colder bottom waters from offshore into middle of the bay. This decoupling mechanism between surface and bottom flows leads to significant stratification during warmer months. Therefore, from the results presented in this section, it is evident that the model correctly resolved the vertical thermal structure under the north-westerly flow regime.

6.3 Annual Analysis

6.3.1 Sea Surface Temperature (SST)

Based on historical observational studies and the model results simulating a full year (2010), generally seawater temperature increases seasonally from winter (June to August) to summer months (December to January). A well-mixed water column is present in colder months with a near-uniform temperature profile along the depth. In warmer months, the water column is stratified with a noticeable temperature gradient (thermocline). The thermocline is more

pronounced at deeper regions within the bay. Overall, the model was able to capture the seasonal increase in SST when transitioning from winter to summer months.

The False Bay annual SST trend comprises the transition from warmer months (January to March) to colder months (April to October). Warmer months are characterised by spatially diverse SSTs whereas colder months have more spatially-uniform SSTs. An overview of the minimum and average SST per month over the simulation period of January to December 2010 is presented as contour plots in Figure 6-18 and Figure 6-19 respectively. For the sake of comparison, an overview of monthly mean SST composite plots derived from satellite measurements spanning 2000-2010 (Dufois et al., 2012) is presented in Figure 6-20.

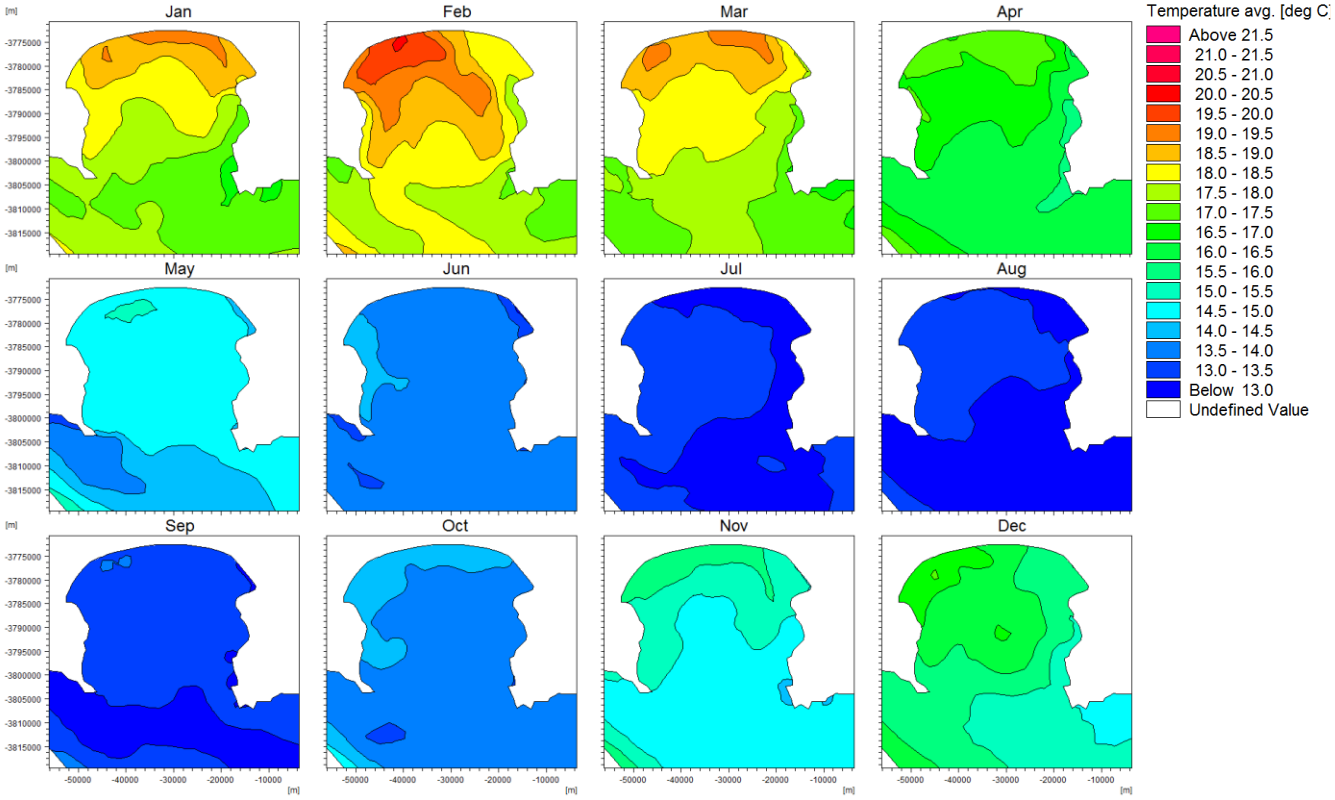

Figure 6-18: Minimum SST per month over the Simulation Period Jan-Dec 2010

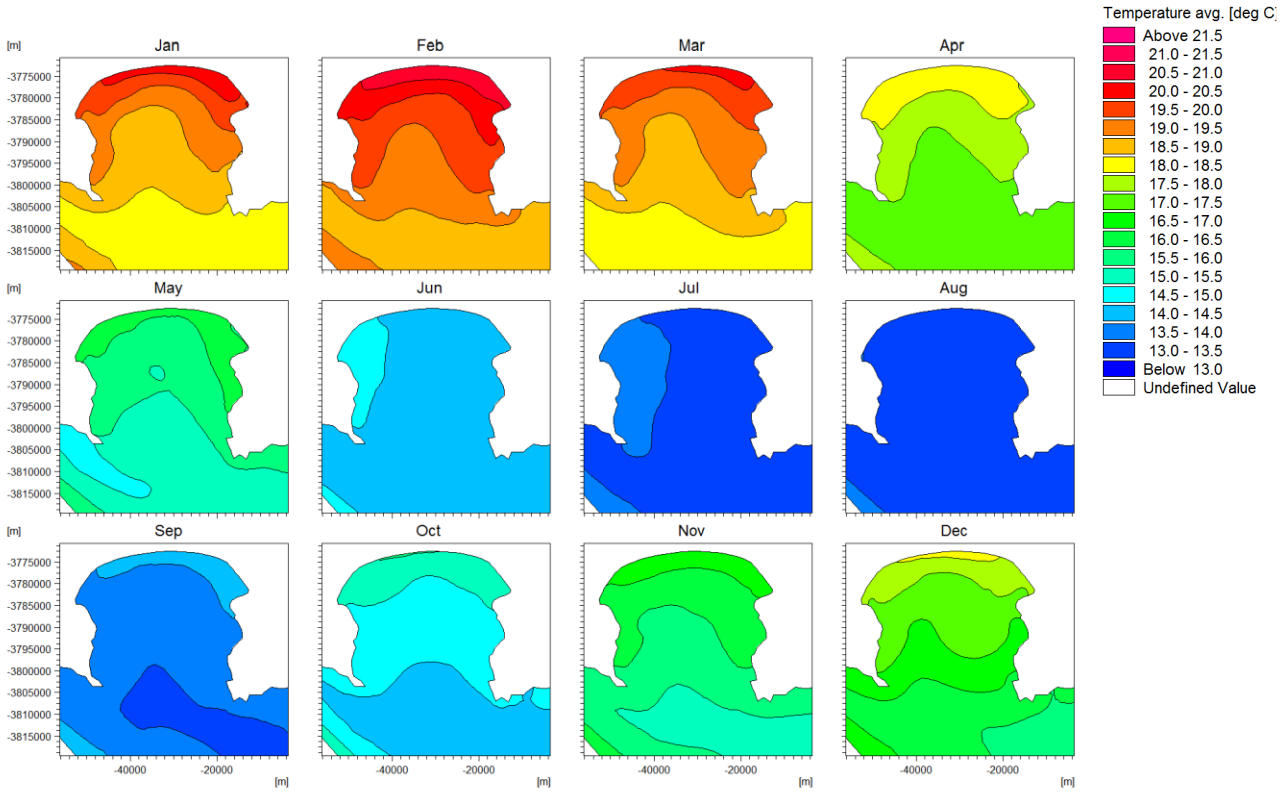

Figure 6-19: Average SST per month over the Simulation Period Jan-Dec 2010

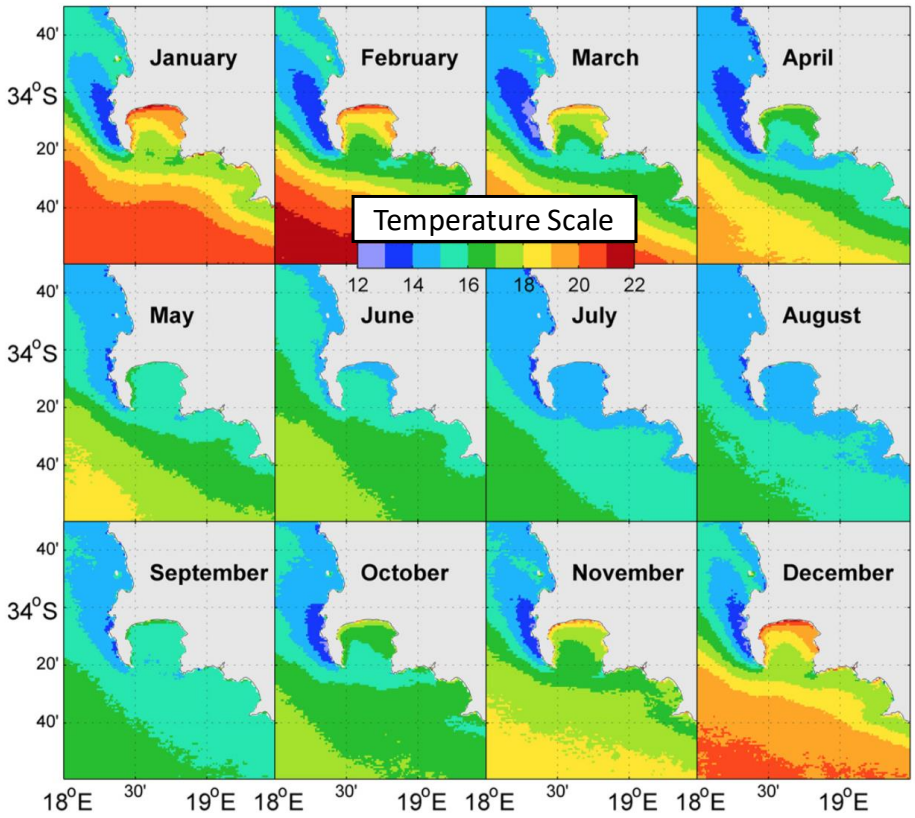

Figure 6-20: Monthly SST (°C) spanning 2000-2010 generated from composites from satellite measurements (Dufois et al., 2012)

From Figure 6-19, it is evident that the model was able to reproduce the annual SST trend present in composite satellite measurements in Figure 6-20. During colder months (May to August), the model results and satellite measurements in the bay show good agreement. The satellite composite measurements show a strong shoreward gradient during warmer months which is apparent in the model results as well (refer to Figure 6-19). Satellite data analysis packages are prone to biases, especially toward the nearshore (Smit, et al., 2013). Compared to in situ measurements, satellite measurements show warmer temperatures of 1-2℃ at Cape Point and Muizenberg (Smit, et al., 2013). Therefore, the reader should be sensitive to the limitations of comparing model results with the presented satellite measurements.

The model results show that the warmest month is February with mean SSTs ranging from 18.5℃ to 21℃ which is consistent with historical studies (Gründlingh et al., (1993)). During colder months (June to October), spatially-uniform SSTs are present with temperature ranges of 13-15℃.

From Figure 6-18, the model results show that during warmer months (November to March), upwelling cells are noted at Cape Point, along the eastern shore and at Cape Hangklip with surface temperatures being approximately 0.5-1℃ less than surrounding SSTs. Although this temperature anomaly may not be significant in isolation, on smaller event scales, upwelling cells are larger and colder under stronger wind conditions (refer to Figure 6-8). However, when comparing minimum SSTs over a month the size and magnitudes of upwelling events are less apparent. The upwelling locations represented in the model results are consistent with historical studies (Cram, (1970); Jury, (1985); Wainman et al., (1987); Taljaard et al., (2000)).

6.3.2 Vertical Thermal Structure

An analysis of the intra-annual vertical thermal structure was undertaken. The analysis considered a time series comparison of two locations in the bay, namely:

- A point off Cape Hangklip was selected since this location has been noted in historical studies (Cram, (1970); Jury, (1985); Wainman et al,. (1987); Taljaard et al., (2000)) as being a region susceptible to upwelling events under stratified conditions; and
- A point near the middle of the bay.

An overview of time series extraction point locations is presented in Figure 6-21. A time series plot showing the seawater temperatures at the near-surface and near-seabed levels of these extraction locations is presented in Figure 6-22. In addition, to characterise the wind climate, a wind speed and direction time series extracted from the WASA (CSAG) dataset at Roman Rock (refer to Figure 4-1) is presented.

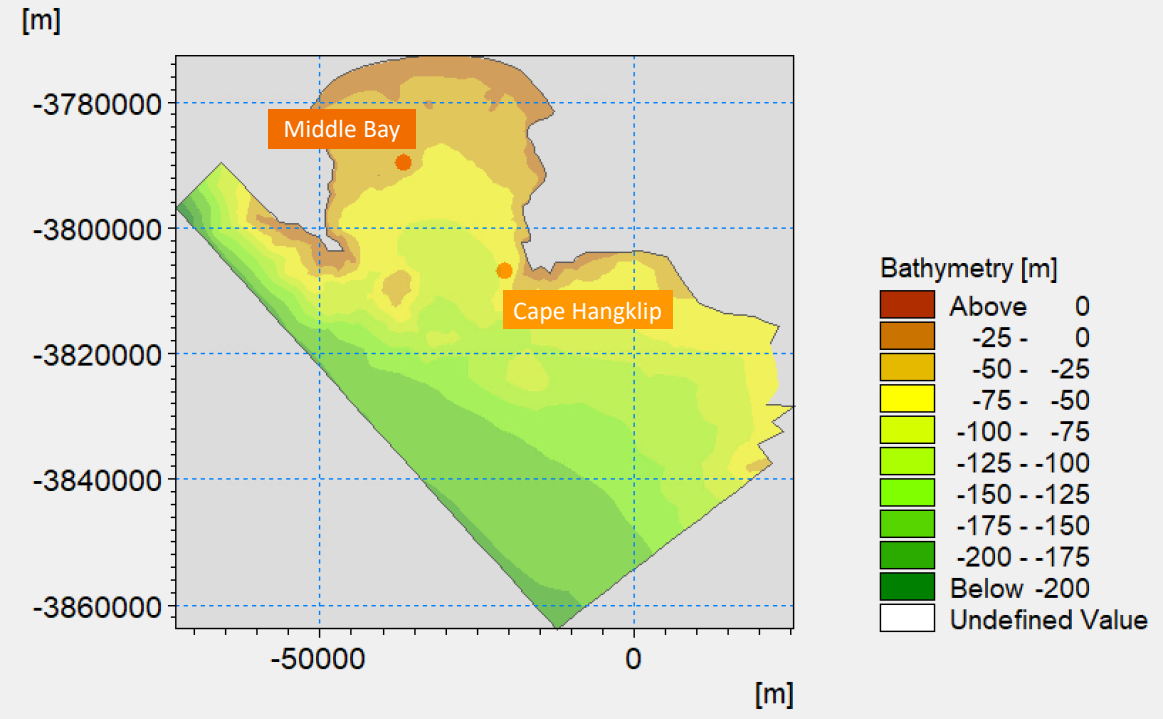

Figure 6-21: Seawater Temperature Time series Extraction Point Locations

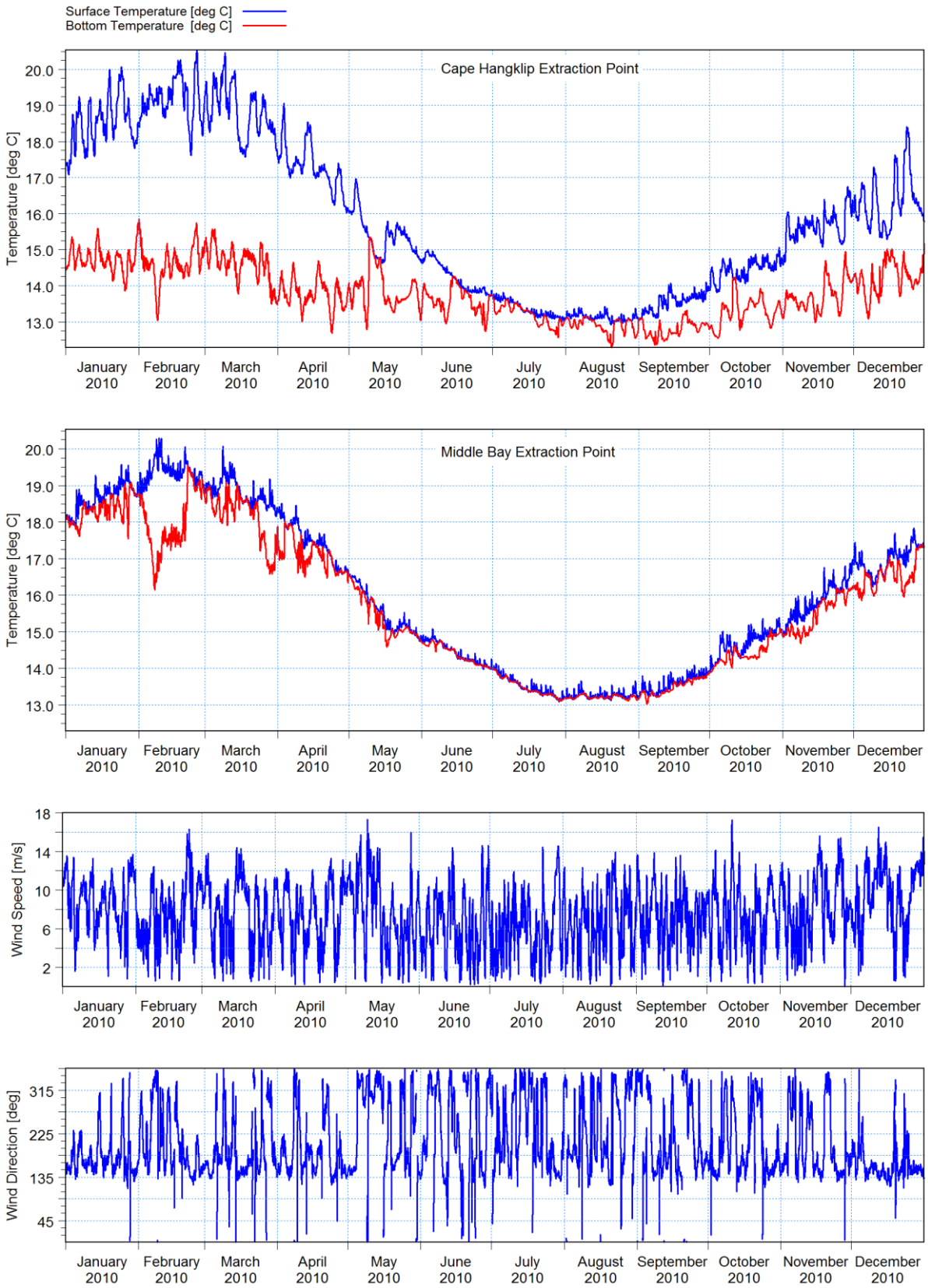

Figure 6-22: Time Series of Surface and Bottom Temperatures at a point near Cape Hangklip and in the Middle of the Bay

Overall, the model results showed that the model was able to identify upwelling and cold-water intrusion events on an annual timescale. Furthermore, the model results show that during warmer months, at the entrance of the bay, bottom temperatures range from 14-15℃. The transition from summer months to winter is marked by an almost linear decline to temperatures in the range of 12-13℃.

From Figure 6-22, it is evident that the Cape Hangklip time series captures sharp surface temperature fluctuations of 2-3℃ during warmer months (January, February and December). These events are synonymous with upwelling events (Cram, 1970). During colder months (June to August), the Cape Hangklip time series indicates a well-mixed water column with surface and bottom temperatures being near-uniform.

Generally, the extracted temperature time series from the middle of the bay shows less fluctuation compared to the Cape Hangklip time series. Furthermore, the middle of the bay is less stratified than at Cape Hangklip during warmer months. It should be noted that the extracted time series does not indicate any upwelling events. However, sharp drops in bottom temperature are noted in warmer months, notably the first week of February 2010 (refer to Figure 6-22). These sharp drops in bottom temperature are attributed to cold-water intrusion into the middle of the bay. Based on analysis of the wind time series, these cold-water intrusion events occur under strong north-westerly conditions. As described in Section 6.1.3, strong bottom return currents are induced under strong north-westerly wind conditions. The results show that these bottom return currents are responsible for cold water advection from the entrance of the bay to the middle of the bay. During colder months (May to September) a well-mixed water column is present in the middle of the bay with temperatures ranging from 13-15℃.

6.4 Model Sensitivities

It is possible that in engineering applications, it may not be feasible to model the hydrodynamics of False Bay considering a 3D model due to the computationally intensive nature of these models (refer to Section 3.2). In addition, the forcing and boundary data considered in this study (e.g. WASA hindcast dataset) cannot be guaranteed and therefore may not be available for future investigations/studies. Therefore, model sensitivities were undertaken to quantify how the level of detail of input data (i.e. temporal and spatial resolution) and the modelling methodology (2D or 3D) may influence the accuracy of modelling hydrodynamic processes within False Bay.

6.4.1 Comparison of 2D vs. 3D Hydrodynamic Modelling of False Bay

This sensitivity provides a comparison of 3D and 2D hydrodynamic modelling of physical processes in False Bay. The major limitation of 2D hydrodynamic models is their inability to

capture seasonal stratification and baroclinicity of the water column due to vertical integration of flow (Nam et al., 2011). In addition, vertical integration of flow means that the decoupling of surface and bottom flows within False Bay during warmer months, is not resolved in 2D hydrodynamic models (Taljaard, et al., 2000). Therefore, considering these main limitations, the results presented in this section are limited to well-mixed (isothermic) conditions (i.e. uniform temperature-depth profiles) which occur from May to October in False Bay.

The 2D model time series results presented in this section covers the period August to September 2010 to allow for comparison with the ADCP measurement datasets.

6.4.1.1 2D Model Parameters

A summary of 2D model parameters is provided in Table 6-1. The default values in MIKE 21 FM yielded the best agreement between modelled and measurements (water levels and currents) within False Bay.

Table 6-1: Model Calibration Parameters

Parameter	Value*
Density	Barotropic
Eddy viscosity (horizontal)	Smagorinsky formulation constant of 0.28
Wind friction coefficient	Interpolated linearly from 0.001255 (7 m/s) to 0.002425 (25 m/s)
Bed resistance (Manning)	32 $m^{1/3}/s$

*All model input parameter values are MIKE 21 FM defaults

6.4.1.2 Water Levels

Modelled water levels were compared against measurements at Simons Town (refer to Figure 4-1 for measurement location). Figure 6-23 presents a time series comparison of measured and modelled water levels (2D model results and 3D model results) at Simons Town.

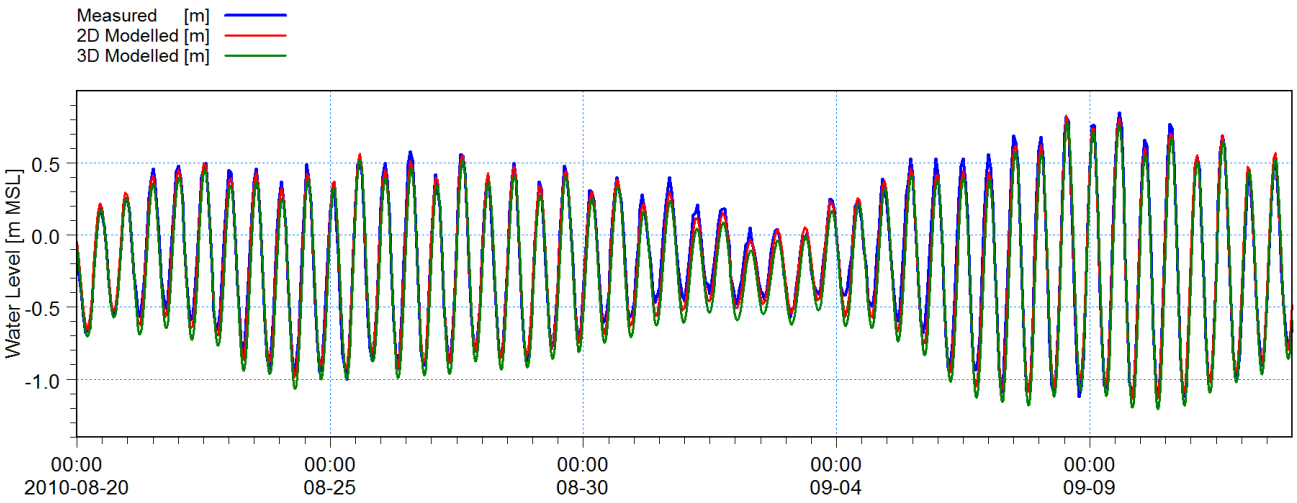

Figure 6-23: Time Series Comparison of Modelled (2D and 3D) and Measured Water Levels at Simons Town

From Figure 6-23, the time series plot shows that the 2D model accurately reproduces the predicted tidal water levels.

6.4.1.3 Currents

Currents were compared with Gordons Bay ADCP measurements (refer to Figure 4-1) and the 3D model results to assess the level of agreement with the 2D model results. A time series comparison of 3D modelled, 2D modelled and measured depth averaged current speed, current direction is presented in Figure 6-24. In addition, current rose plots are provided for all considered datasets in Figure 6-25.

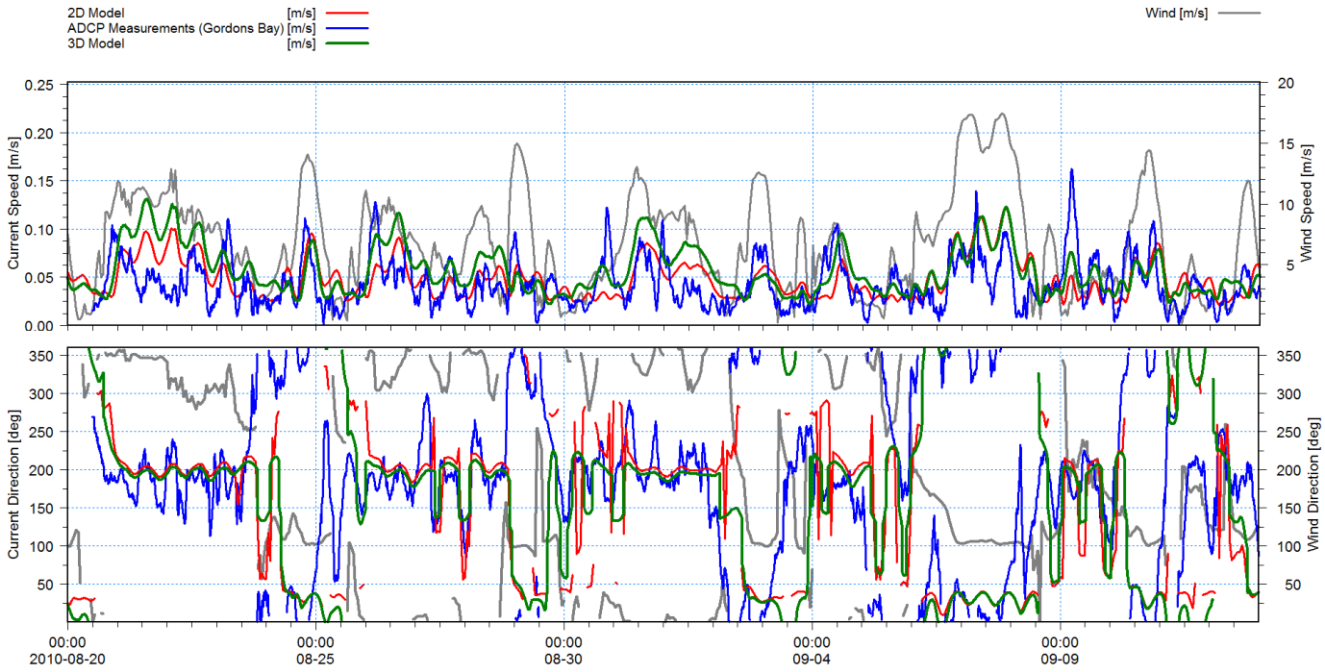

Figure 6-24: Depth-averaged Current Speed and Direction Time Series Comparison at Gordons Bay

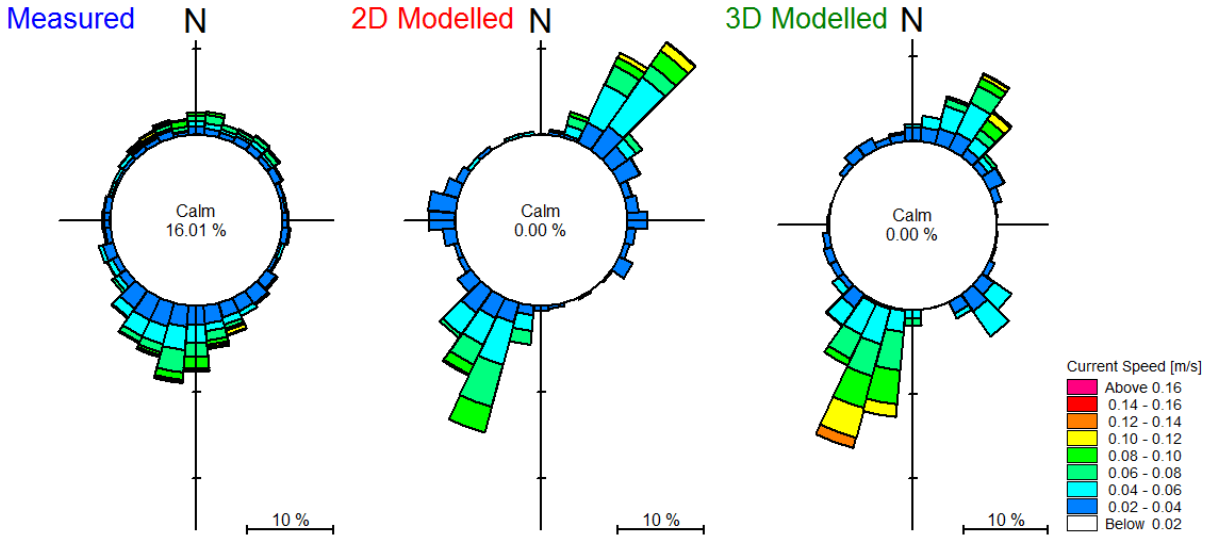

Figure 6-25: Depth-averaged Current Rose Comparison at Gordons Bay

Generally, depth-averaged currents in both measured and modelled results are fairly weak. Measured currents are also fairly “noisy” compared to model results. Generally, weaker currents show higher variability (or “noise”) in current direction and are therefore more difficult to measure with ADCP instruments.

Overall, the 2D model time series and rose results show good agreement with the 3D model results under well-mixed conditions. Depth-averaged current speeds slightly under-predict both measurements and 3D model results.

To assess currents spatially, the 2D and 3D model results were compared on two separate contour plots comprising south-easterly and north-westerly wind conditions which are presented in Figure 6-26 and Figure 6-27 respectively.

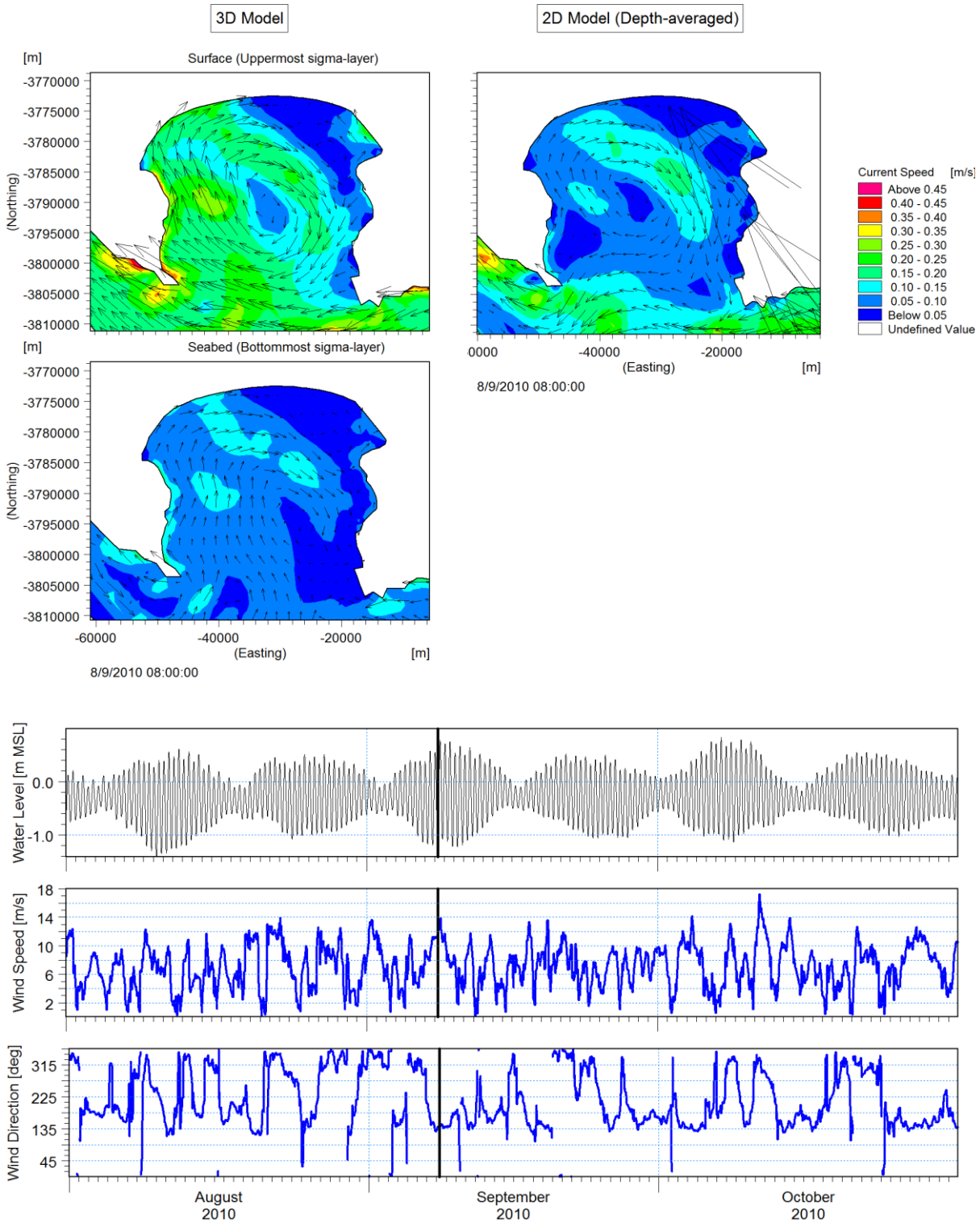

Figure 6-26: Comparison of 3D and 2D Model Results - Well-mixed South-easterly Generated Current Circulation Pattern

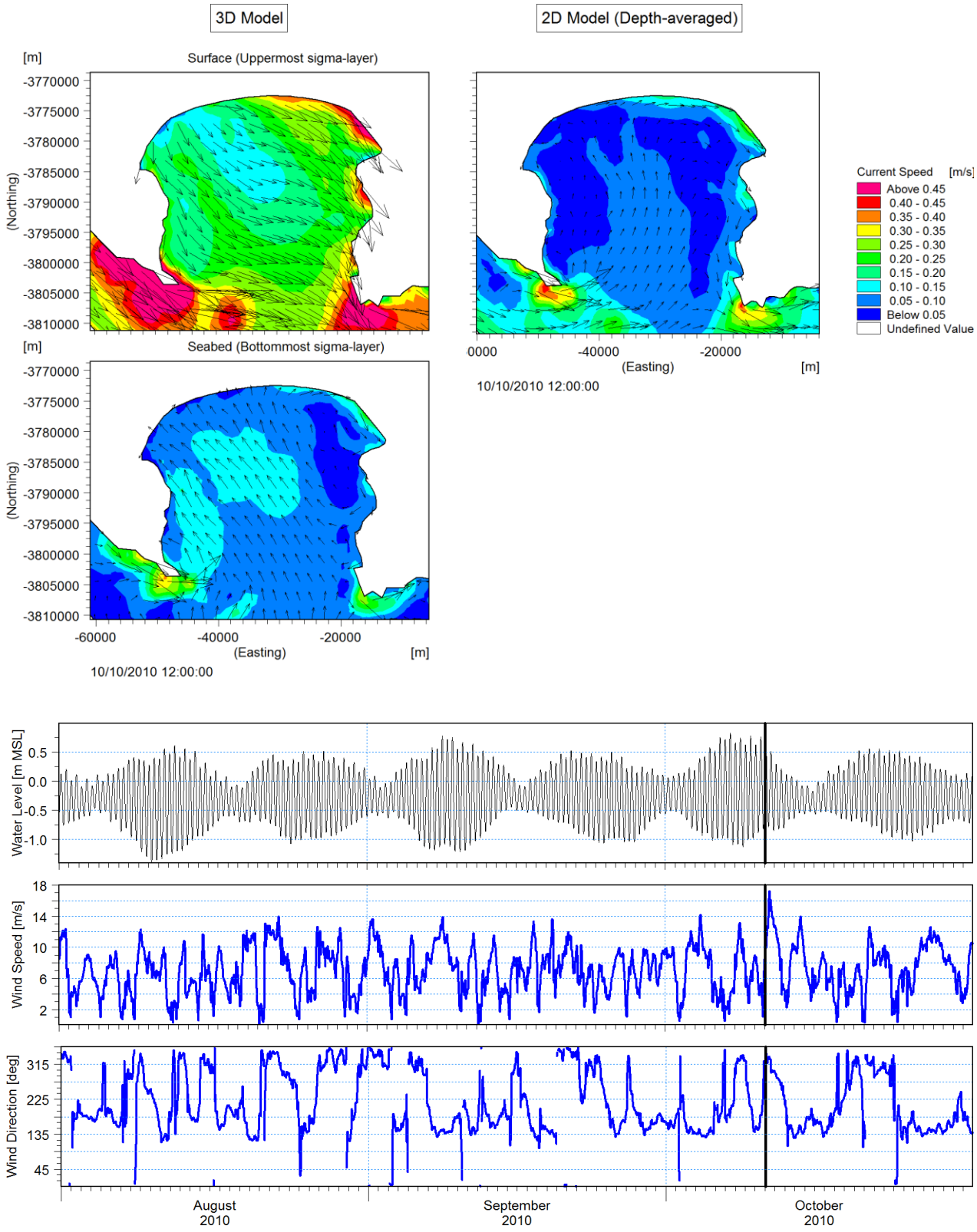

Figure 6-27: Comparison of 3D and 2D Model Results - Well-mixed North-westerly Generated Current Circulation Pattern

From Figure 6-26, the 2D model results are able to reproduce the clockwise circulation pattern under south-easterly conditions. Although the current field is vertically integrated, the 2D model correctly identifies the acceleration of current along the eastern shore. In addition, the "stagnant" zone along Strand and Gordons Bay is well represented in both models.

In contrast to south-easterly conditions, north-westerly conditions show less agreement when comparing circulation patterns. From Figure 6-27, the 2D model results exhibit a depth-averaged northward flow which is not consistent with the 3D model results. More specifically, surface layers in the 3D model show a strong south-east setting tendency which is not apparent from the 2D model results. Similarly, bottom currents show a north-west setting tendency which is not apparent in 2D model results. Overall, under well-mixed north-westerly conditions, the depth-averaged 2D model does not show any evidence of the decoupling of surface and bottom flows present in the 3D model results.

6.4.1.4 Discussion

The time series results indicated that, under well-mixed conditions, the 2D hydrodynamic model showed good agreement with both measurements and the 3D model results. Upon comparison of the circulation patterns between 3D and 2D models, good agreement was found when simulating south-easterly conditions. In addition, the 2D model captured the overall clockwise circulation pattern under well-mixed south-easterly conditions. However, under north-westerly conditions, the 2D model's depth averaged current field showed poorer agreement with the 3D model. Most notably, the 2D model was unable to resolve the decoupling of surface and bottom flows present in the 3D model. Therefore, it is recommended that, in potential future hydrodynamic simulations of False Bay, the modeller be mindful of the 2D model's lack of resolution when simulating hydrodynamics in False Bay under north-westerly conditions.

In summary, it is recommended that for engineering applications, where computation time needs to be optimised, that a 2D hydrodynamic model of False Bay be employed for the simulation of hydrodynamics under well-mixed south-easterly conditions. For comparison, the simulation of one year of hydrodynamics, the 3D model had a runtime of approximately 76 hours whereas the runtime for the 2D model was approximately 2.5 hours. If a full year of simulation is necessary, then it is recommended that a combination of 2D modelling and 3D modelling be considered. The 3D model would be dedicated to warmer months (i.e. November to April) where stratification and baroclinicity of the water column is present and the 2D model would be dedicated to colder months (May to October) considering a well-mixed water column. If computation time needs to be optimised, this combination of modelling methodologies could effectively reduce model runtime by approximately 50%. However, the modeller should be

cautious of simulating north-westerly conditions with a 2D model due to the significant discrepancies noted between the 2D and 3D models.

6.4.2 Comparison between Spatially-varying Wind and Uniform Wind Field

This section details the sensitivity analysis of spatially-varying and unidirectional wind forcing. This sensitivity analysis is intended to compare hydrodynamics under south-easterly wind conditions. Therefore, a fixed wind direction of 135º TN was considered for the setup of the unidirectionally wind-driven model. The wind speed time series input was sourced from the CSAG dataset at an extraction point near Cape Hangklip. The extraction point location is presented in Figure 6-28. In addition, the time series plot of wind speed at the extraction location is presented in Figure 6-29.

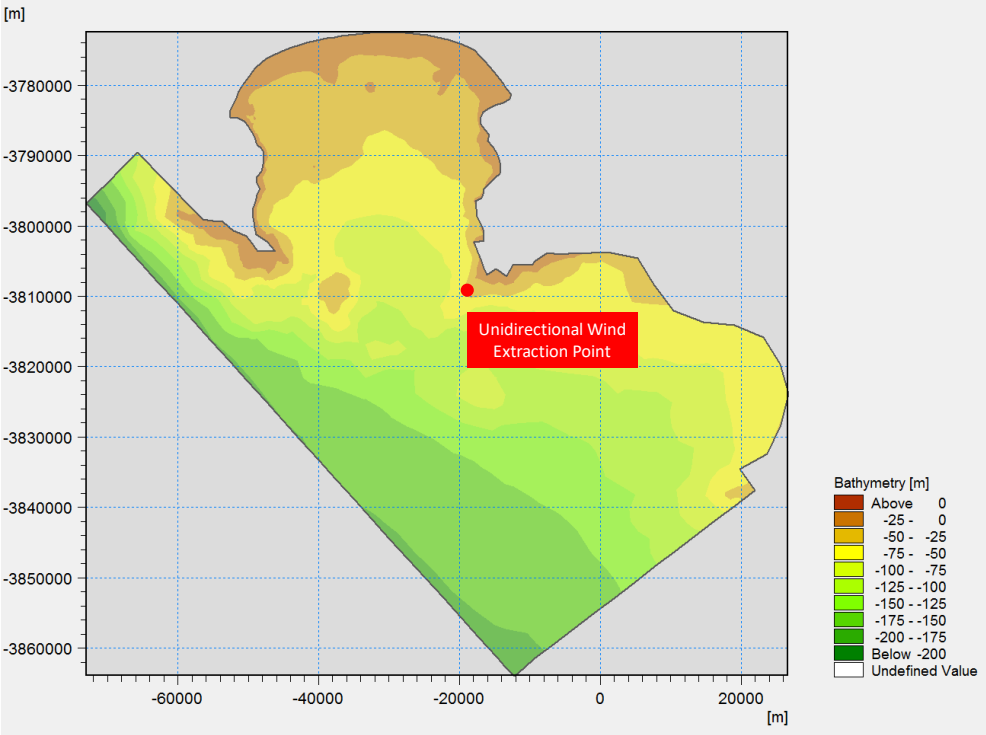

Figure 6-28: Extraction Location of Unidirectional Time Series

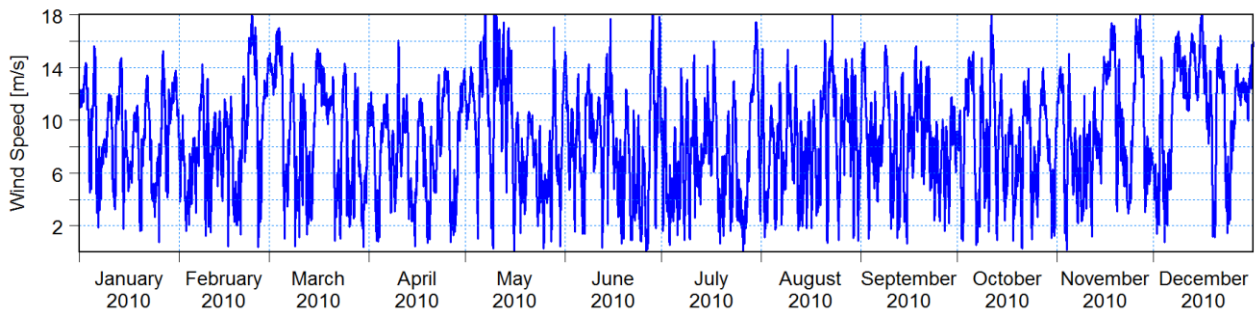

Figure 6-29: Unidirectional Wind Speed Time Series Plot extracted from CSAG Dataset

The major limitation of fixing wind direction is that differences in flow due to horizontal wind shear effects in False Bay will not be captured (Gründlingh et al., 1989). In addition, unidirectional wind forcing may introduce model artefacts as noted by Nicholson (2011) where results showed a large artificial upwelling cell at Gordons Bay. However, since wind directions are predominantly south-easterly in False Bay, a unidirectionally wind-driven model may be capable of resolving short-timescale hydrodynamics.

6.4.2.1 Water Levels

Modelled water levels were compared against measurements at Simons Town (refer to Figure 4-1 for measurement location). Figure 2-7 presents a time series comparison of measured and modelled water levels (CSAG wind forcing and constant wind forcing) at Simons Town.

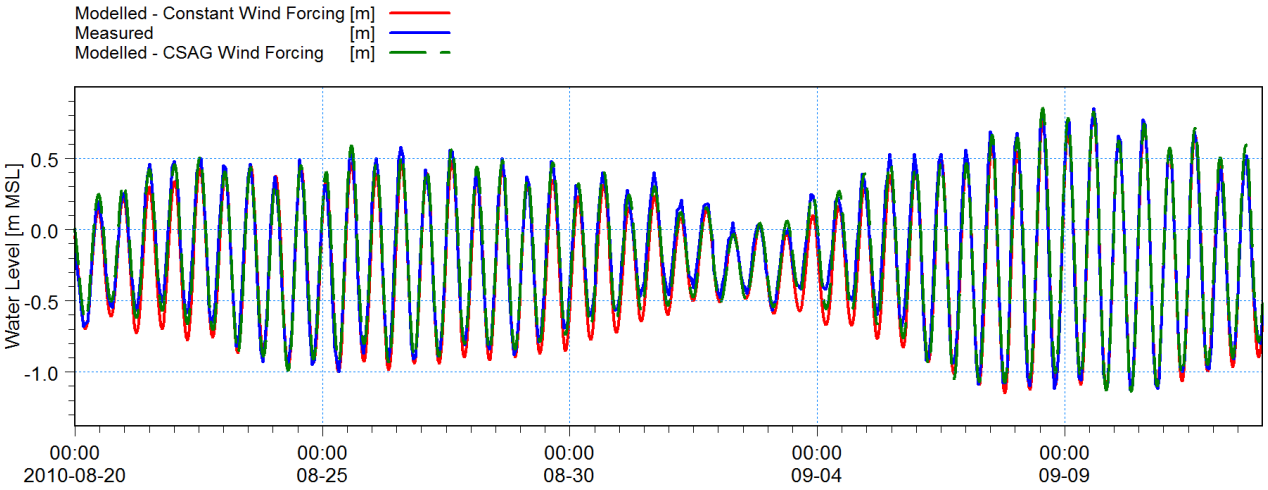

Figure 6-30: Time Series Comparison of Modelled (Constant and CSAG Wind Forcing) and Measured Water Levels at Simons Town

From Figure 6-30, the time series plot shows that the constant (or unidirectional) wind-driven model accurately reproduces the predicted tidal water levels.

6.4.2.2 Currents

Currents were compared with Gordons Bay ADCP measurements (refer to Figure 4-1) and the WASA (or CSAG) wind-driven model to assess the level of accuracy of the unidirectional (or constant) wind-driven model.

A time series comparison of surface (z=3) current speed and current direction considering modelled and measured results is presented in Figure 6-31. In addition, current rose plots are provided for all considered datasets in Figure 6-32.

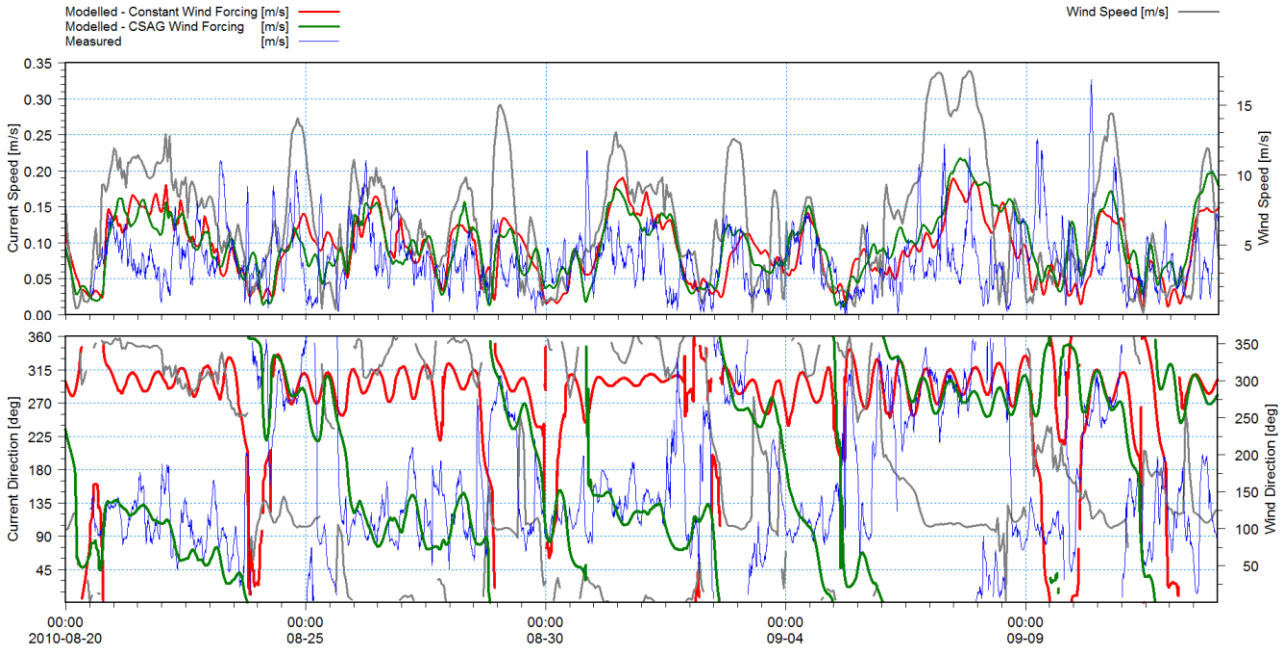

Figure 6-31: Surface (z=3) Current Speed and Direction Time Series Comparison of CSAG Wind Forcing and Constant Wind Forcing at Gordons Bay

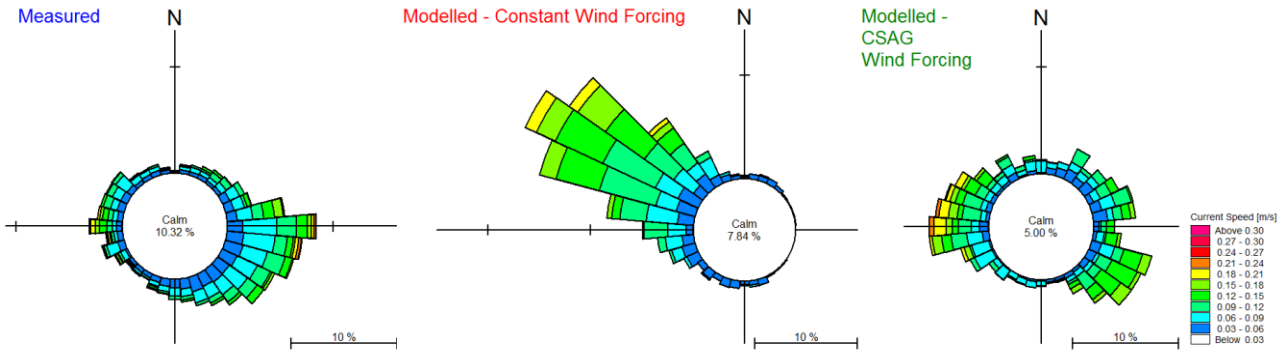

Figure 6-32: Surface (z=3) Current Rose Comparison of CSAG Wind Forcing and Constant Wind Forcing at Gordons Bay

A time series comparison of seabed (z=10) current speed and current direction considering modelled and measured results is presented in Figure 6-33. In addition, current rose plots are provided for all considered datasets in Figure 6-34.

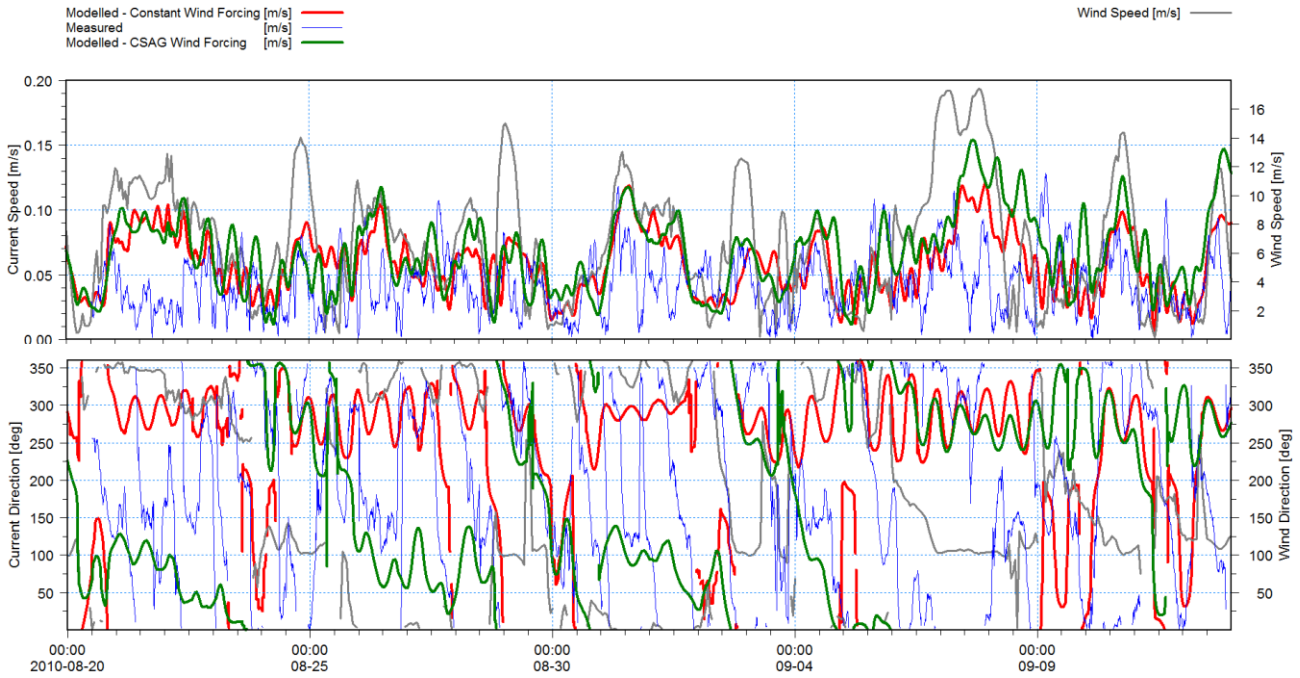

Figure 6-33: Near seabed (z=10) Current Speed and Direction Time Series Comparison of CSAG Wind Forcing and Constant Wind Forcing at Gordons Bay

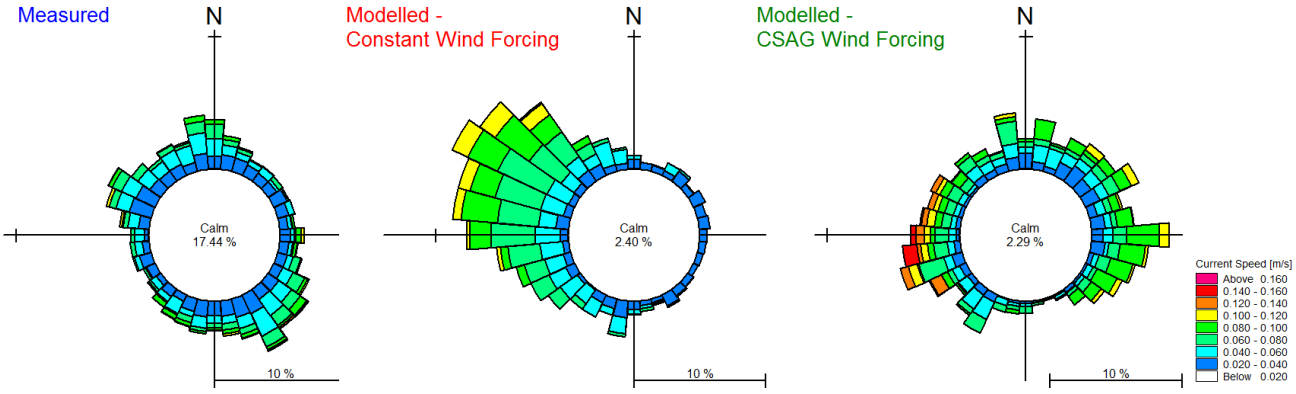

Figure 6-34: Surface (z=10) Current Rose Comparison of CSAG Wind Forcing and Constant Wind Forcing at Gordons Bay

Overall, current magnitudes show good agreement with measurements and the spatially varying wind-driven model. However, current directions showed poor agreement with measurements and the uniform wind-driven model. This conclusion was expected. However, under south-easterly wind conditions, the constant wind-driven model showed reasonable agreement with the spatially varying wind-driven model.

To evaluate how the two wind-driven models agree on a spatial scale, a contour plot comparison was undertaken. Figure 6-35 to Figure 6-38 presents contour plot comparisons of

current speed and seawater temperature under south-easterly conditions. Well-mixed and stratified conditions are considered. The plots show near surface and near seabed flows. To characterise the predominant wind climate, a time series was extracted from the WASA (CSAG) hindcast dataset at Roman Rock (refer to Figure 4-1).

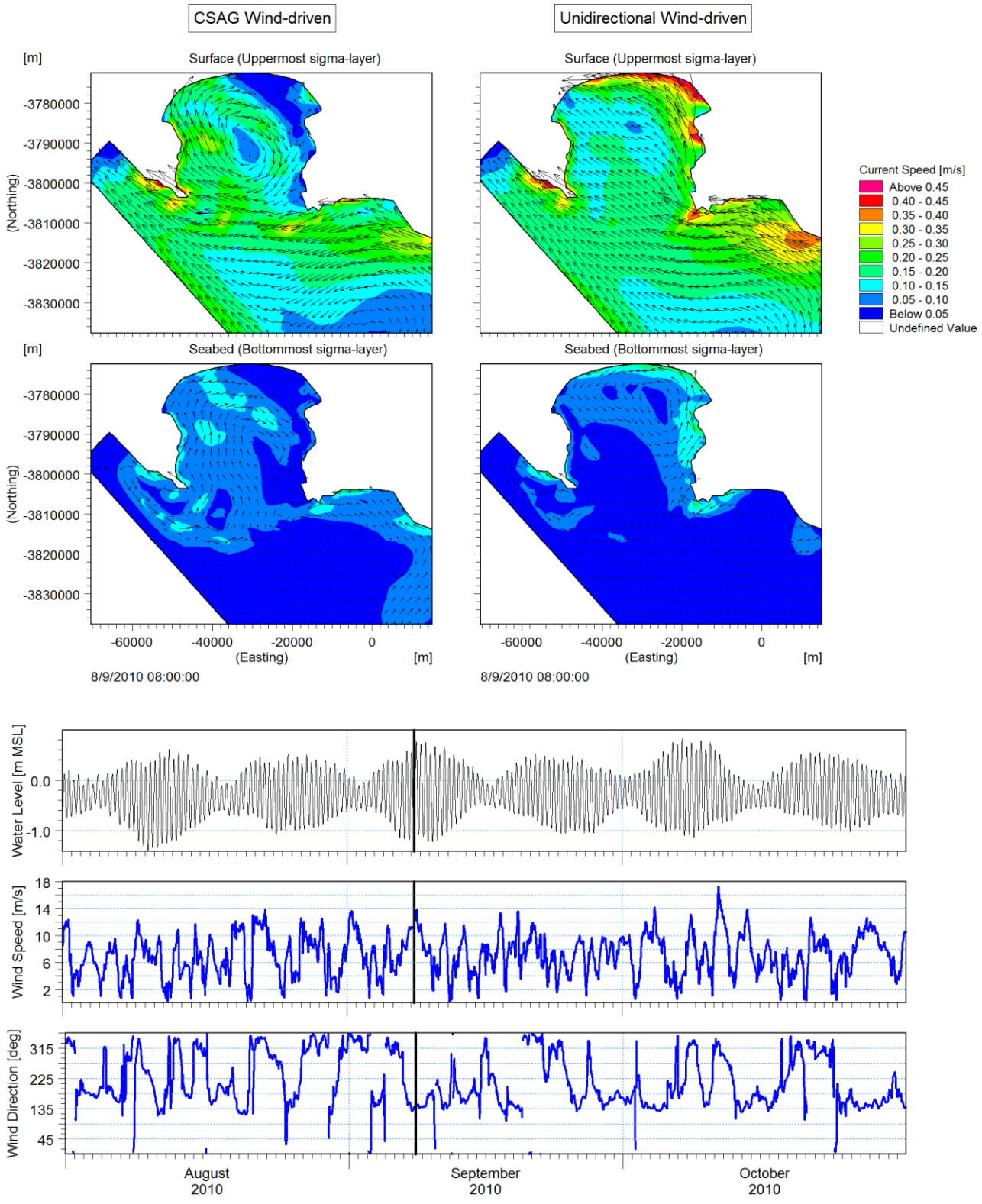

Figure 6-35: Comparison of CSAG and Unidirectional Model Results - Well-mixed South-easterly Generated Current Circulation Pattern

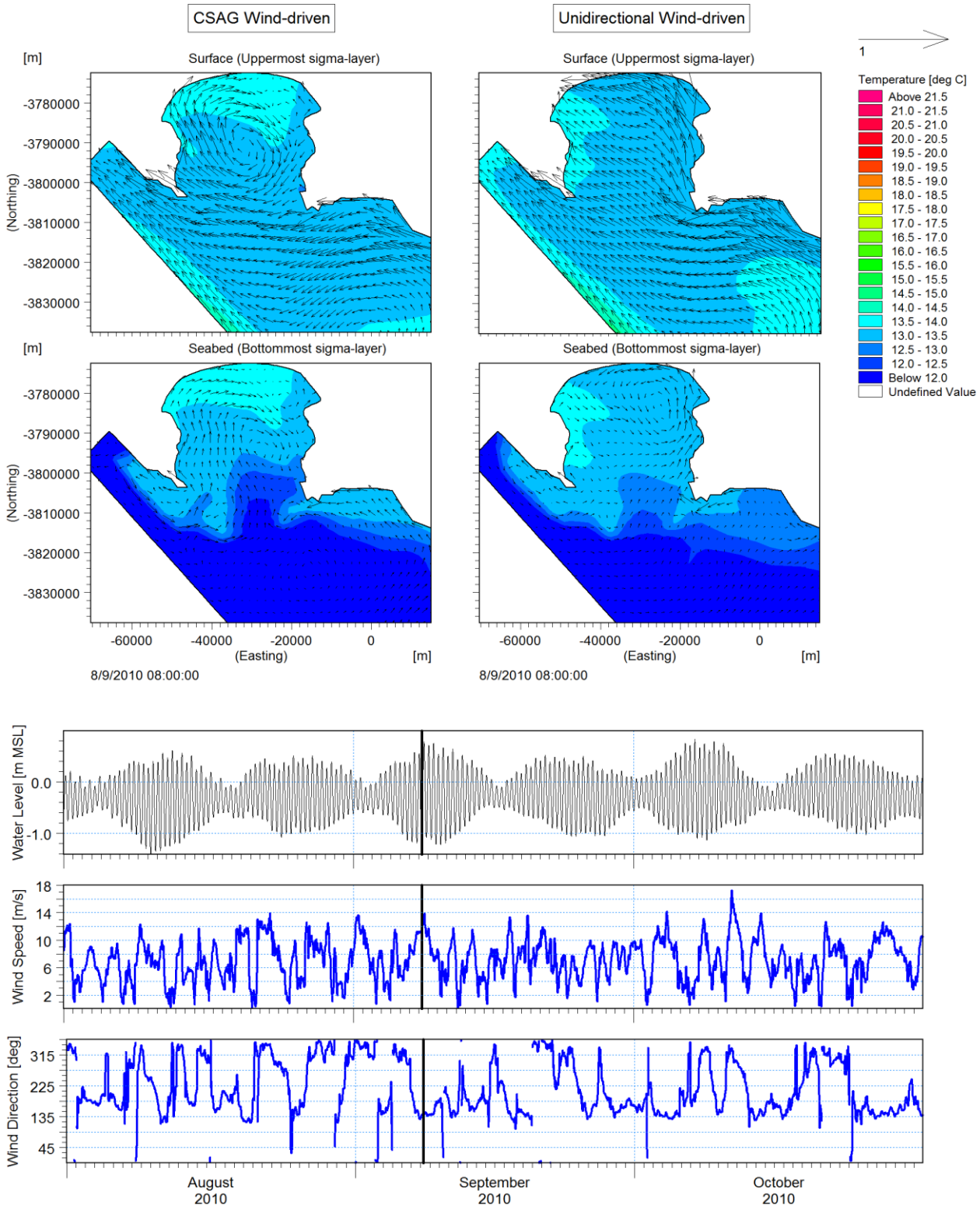

Figure 6-36: Comparison of CSAG and Unidirectional Model Results - Well-mixed South-easterly Generated Current Circulation Pattern with Temperature Overlay

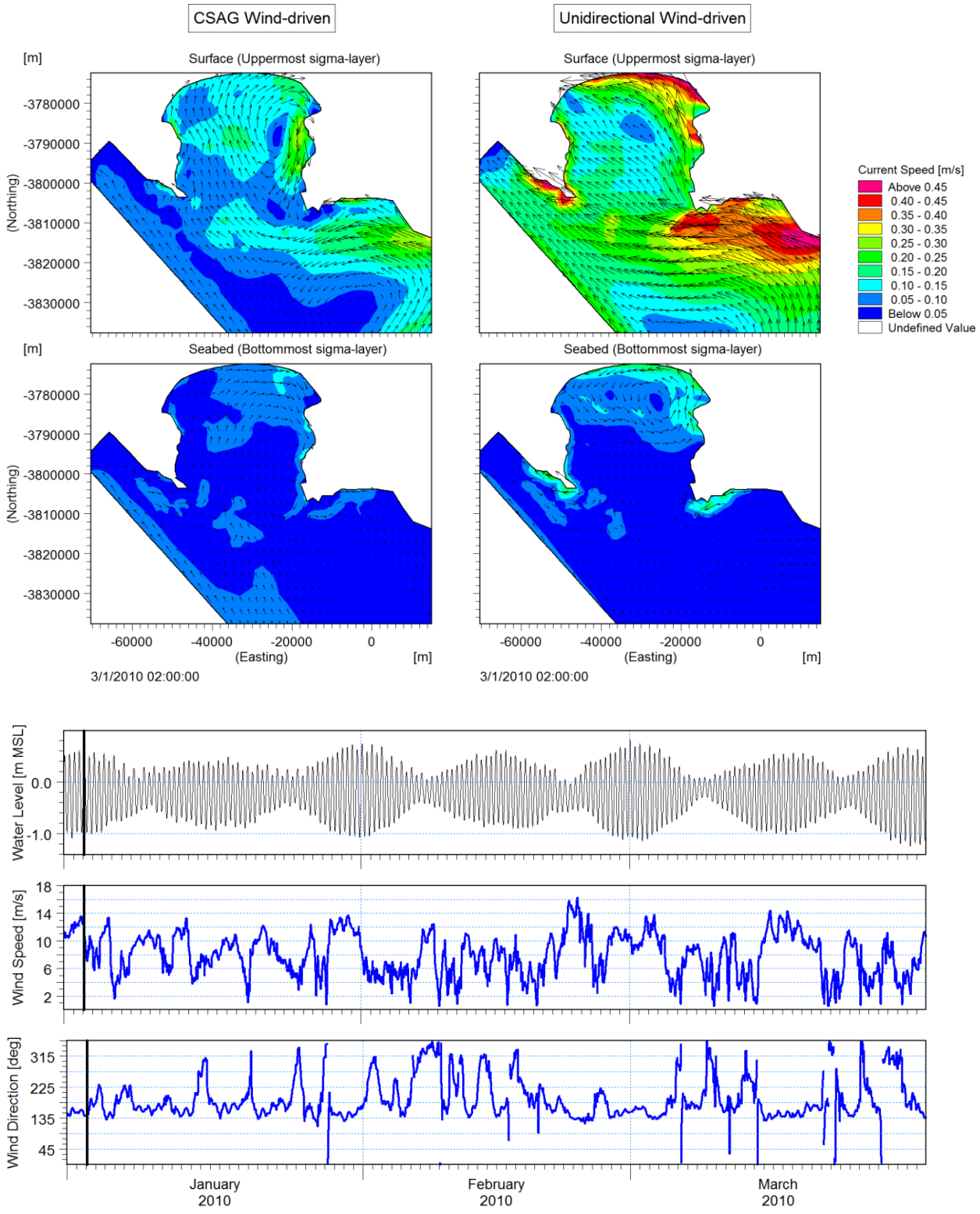

Figure 6-37: Comparison of CSAG and Unidirectional Model Results - Stratified South-easterly Generated Current Circulation Pattern

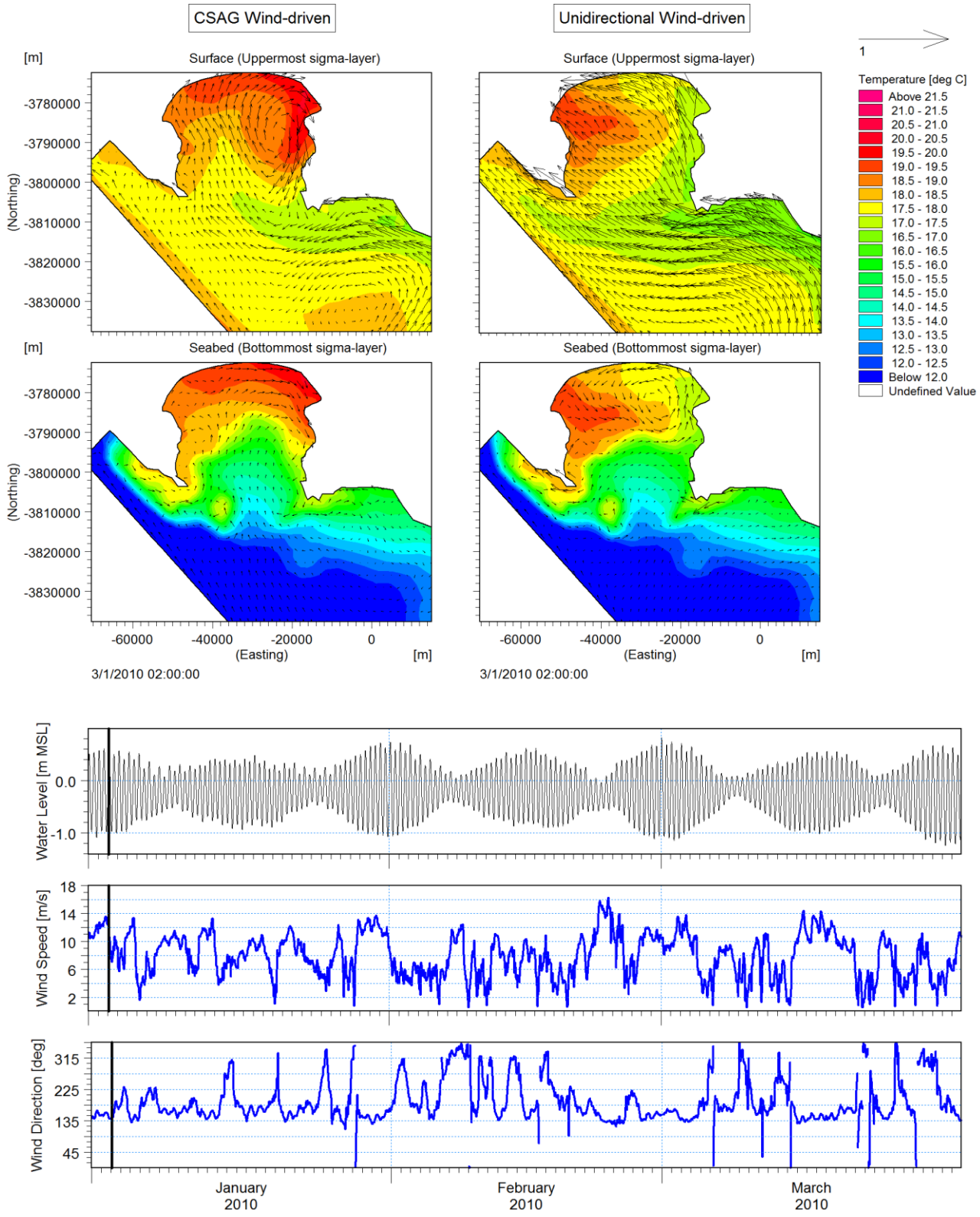

Figure 6-38: Comparison of CSAG and Unidirectional Model Results - Stratified South-easterly Generated Current Circulation Pattern with Temperature Overlay

Overall the unidirectional (or constant) wind-driven model shows poor correlation with the CSAG wind-driven model. The model is unable to form the cyclonic circulation pattern

associated with south-easterly wind conditions. Furthermore, the unidirectional wind-driven model results show the formation of an artificial anti-clockwise gyre near the seabed at Gordons Bay. Other artefacts are the formation of strong (0.4 m/s) surface currents at Cape Hangklip and along the eastern shorelone under both well-mixed and stratified conditions. The persistence of these currents leads to more mixing of the water column along the eastern shoreline. Under stratified conditions, this behaviour leads to the eastern shoreline exhibiting significantly colder temperatures (by 1-2℃) than the western shoreline. The comparison of seawater temperatures between the two models will be addressed in greater detail in Section 6.4.2.3.

6.4.2.3 Seawater Temperature

An intra-annual comparison of seawater temperature was undertaken between the CSAG wind-driven model and the constant wind-driven model. A time series comparison of the vertical thermal structure for the two datasets is presented in Figure 6-39. The location of the time series extraction points is provided in Figure 6-21. In addition, a monthly-averaged SST comparison of the two datasets is presented in Figure 6-40.

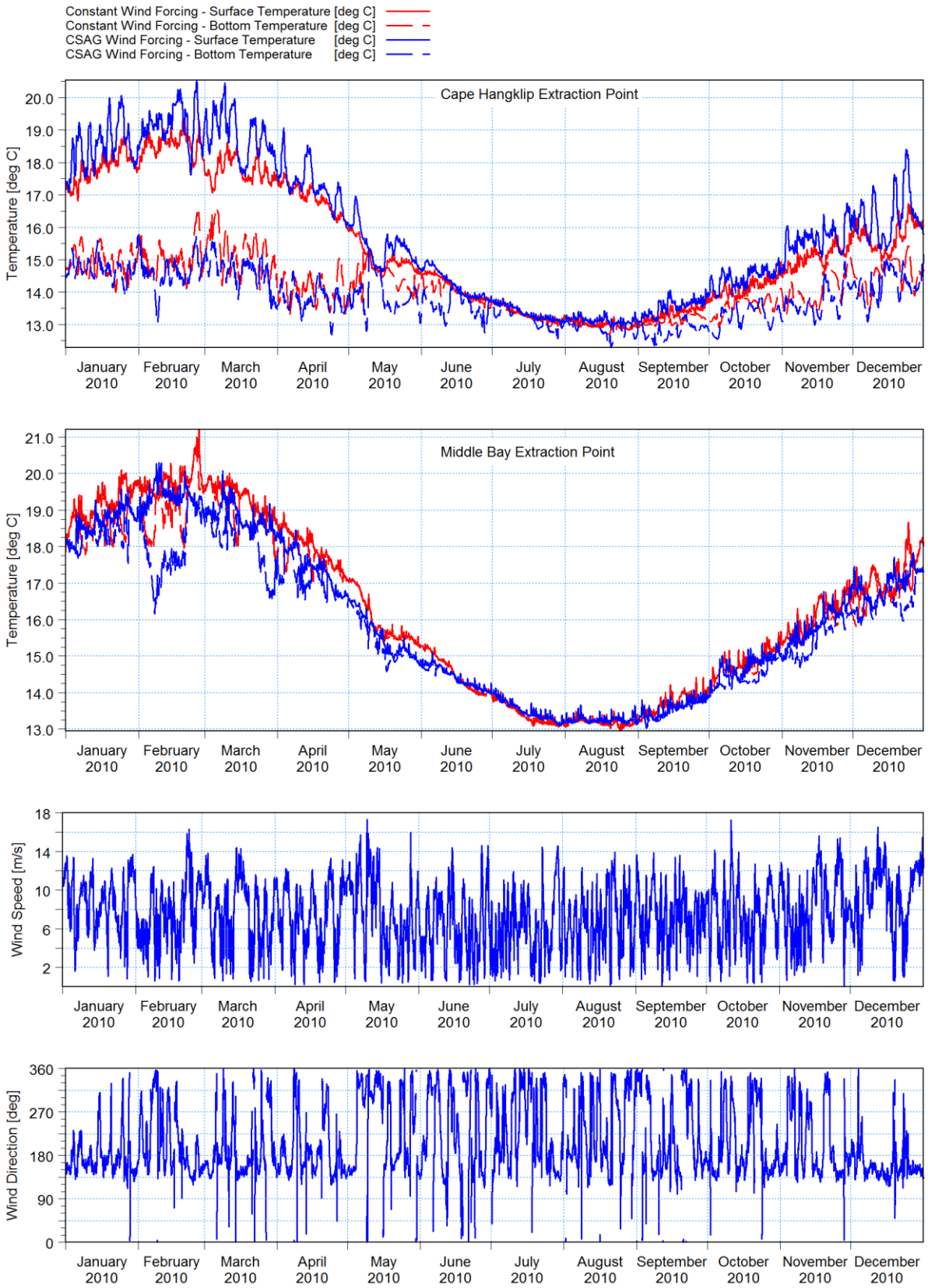

Figure 6-39: Time Series Comparison of Surface and Bottom Temperatures at a point near Cape Hangklip and in the Middle of the Bay – Constant Wind Forcing and CSAG Wind Forcing

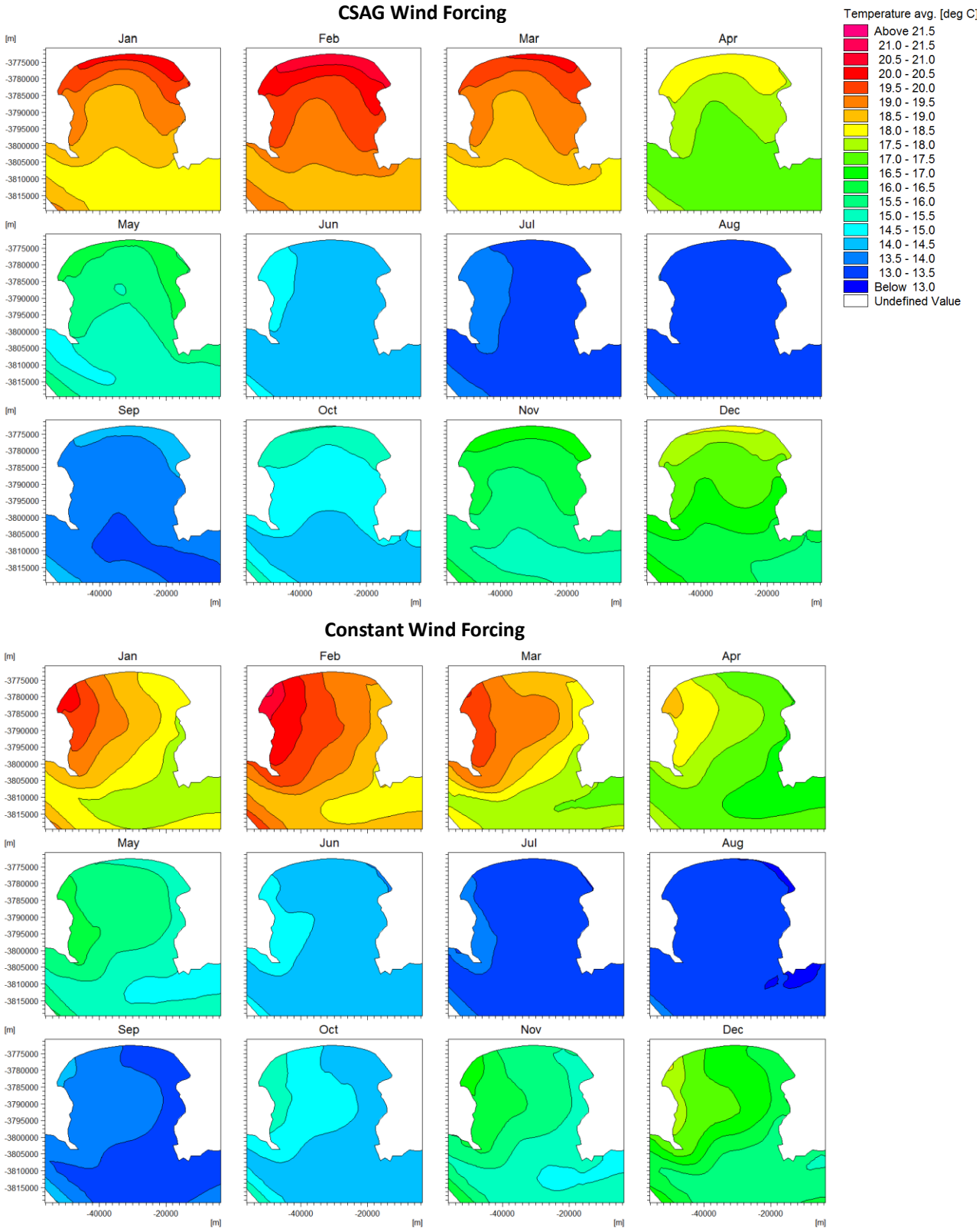

Figure 6-40: Comparison of Average SST per month for CSAG and Constant Wind Forcing over the Simulation Period Jan-Dec 2010

Overall, the unidirectional (constant) wind-driven model vertical temperatures show poor agreement with the CSAG wind-driven model results. During warmer months, the unidirectional wind-driven model results show colder seawater temperatures by 1-2℃ compared to the CSAG wind-driven model results. However, during colder months under well-mixed conditions, the difference between the two model results is marginal.

Upwelling events may be inferred by sharp fluctuations (2-3℃) in surface temperature. The CSAG wind-driven model results presented in Figure 6-39 clearly show evidence of upwelling events at Cape Hangklip and in the middle of the bay. However, it is evident that the constant wind-driven model results capture larger upwelling events at Cape Hangklip. The results instead show evidence of increased (or persistent) mixing of the water column due to the increased wind speed at this location. This interpretation is further supported by analysing surface water temperatures which are consistently colder under uniform wind forcing compared to the spatially varying forcing. Furthermore, when the surface temperatures at Cape Hangklip are analysed in combination with Figure 6-40, the constant wind-driven model shows a large persistent colder region at Cape Hangklip. The formation of this large colder region is an artefact. Similar cold regions are noted along the eastern shore. This finding is consistent with similar artefacts which were noted in a similar unidirectionally wind-driven model of False Bay (Nicholson (2011)).

Cold water intrusion events are represented in the middle bay time series by sharp drops (1-3℃) in bottom temperature. The CSAG wind-driven model results presented in Figure 6-39 clearly show evidence of cold water intrusion in the middle of the bay. However, these events are missing in the constant wind-driven results. This finding is expected since it has been determined in Section 6.1.3, that north-westerly wind conditions are responsible for cold water advection into the bay.

6.4.2.4 Discussion

The results indicated that the unidirectional wind-driven model was incapable of characterising the overall current regime within False Bay. Similarly, intra-annual spatial and temporal trends in False Bay seawater temperature were not consistent with the CSAG wind-driven model results. However, the time series comparison of model results showed that the unidirectional wind-driven model was able to accurately resolve currents under south-easterly wind conditions at a point near Gordons Bay. Therefore, it may be possible that unidirectional (or constant) wind-driven models would be more accurate considering a short-timescale and a limited spatial scale when characterising the hydrodynamics of False Bay.

Ultimately, the lack of agreement between model results shows how critical spatially varying wind-forcing is in defining the overall current regime and the vertical and horizontal thermal

structures within False Bay. At present, the lack of incorporation of spatially varying wind forcing has been a serious hindrance in providing robust simulation of the hydrodynamics of False Bay (Taljaard et al., 2000).

6.4.3 Comparison of HYCOM vs Monthly-averaged Temperature Boundaries

This section provides a comparison between temperature-depth profiles, namely HYCOM daily temperature-depth data and World Ocean Atlas (WOA) monthly-averaged temperature-depth data. World Ocean Atlas (WOA) is an objectively analysed climatological dataset based on in situ temperatures at annual, seasonal and monthly compositing periods for the global ocean. The WOA dataset considered in this study comprises a single temperature-depth profile at a monthly-averaged temporal resolution which is applied uniformly to all model boundaries. An example of the WOA monthly profile for February 2010 is presented in Figure 6-41.

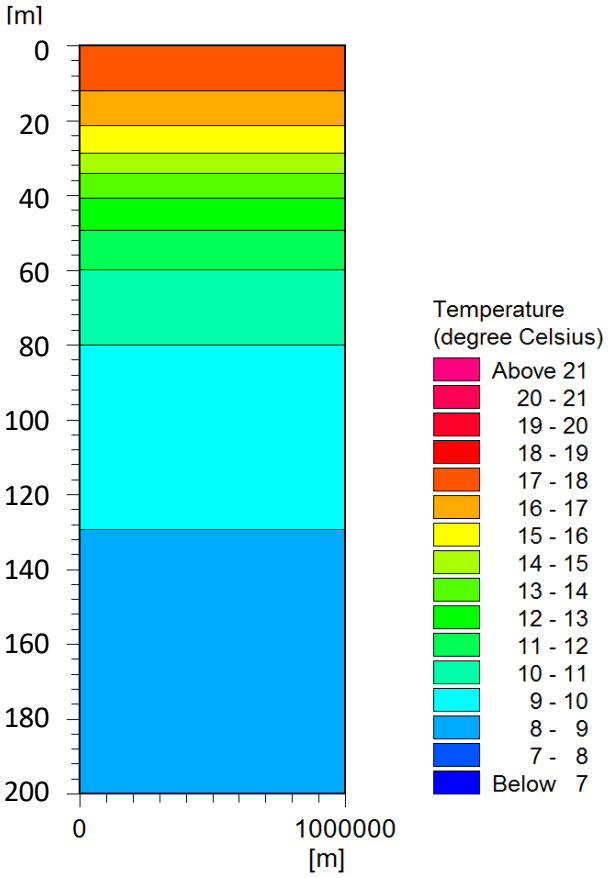

Figure 6-41: WOA February 2010 Temperature-depth Profile

The main risk of considering monthly-averaged temperature profile data on the model boundaries is that, due to precluding the finer temporal resolution, the model may be less capable of capturing event scale hydrodynamics. However, increased resolution in input data does not necessarily guarantee more accurate model results (Sutherland et al., 2004).

6.4.3.1 Water Levels

Modelled water levels were compared against measurements at Simons Town (refer to Figure 4-1 for measurement location). Figure 6-42 presents a time series comparison of measured and modelled water levels (WOA boundaries and HYCOM boundaries) at Simons Town.

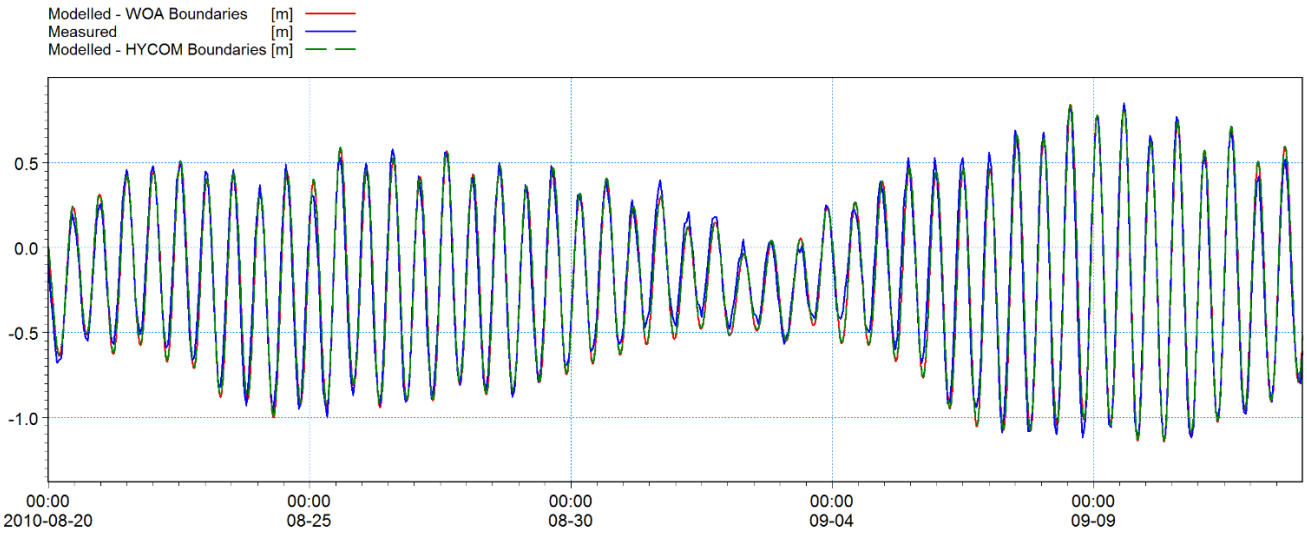

Figure 6-42: Time Series Comparison of Modelled (WOA and HYCOM boundaries) and Measured Water Levels at Simons Town

From Figure 6-42, the time series plot shows that the WOA driven model accurately reproduces the predicted tidal water levels.

6.4.3.2 Currents

Currents were compared with Gordons Bay ADCP measurements (refer to Figure 4-1) and the HYCOM-driven model to assess the level of accuracy of the WOA-driven model.

A time series comparison of surface (z=3) current speed and current direction considering modelled and measured results is presented in Figure 6-43. In addition, current rose plots are provided for all considered datasets in Figure 6-44.

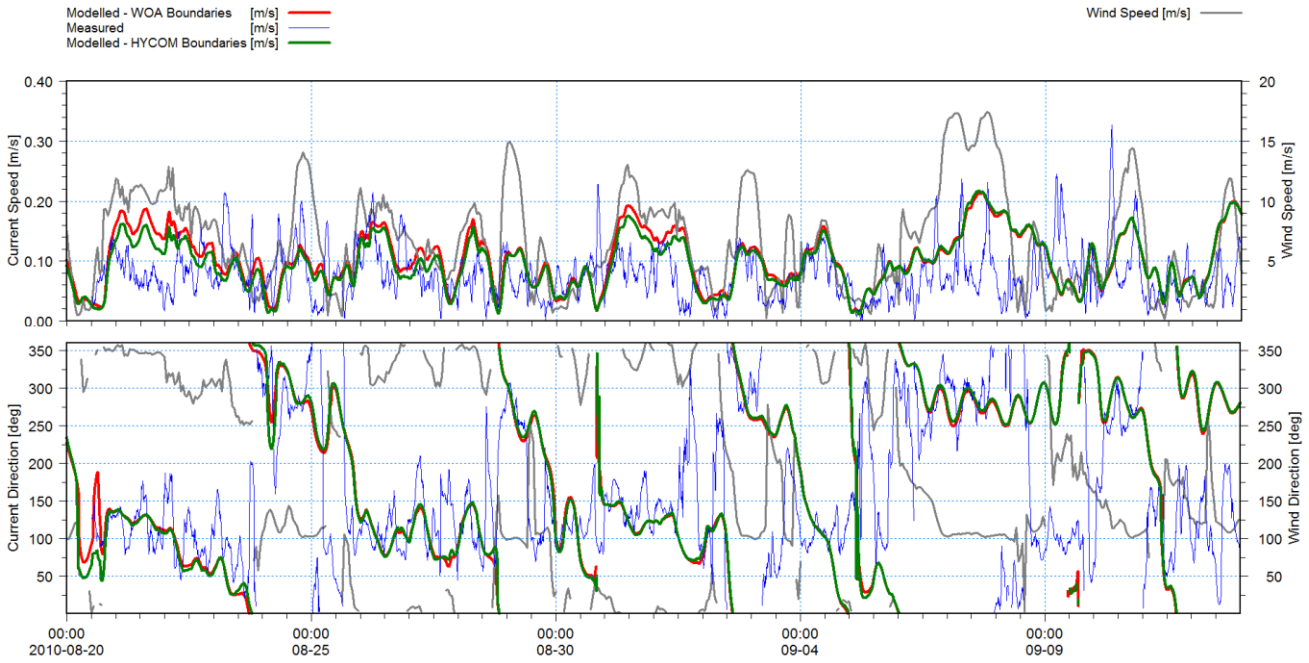

Figure 6-43: Surface (z=3) Current Speed and Direction Time Series Comparison at Gordons Bay – WOA and HYCOM boundaries

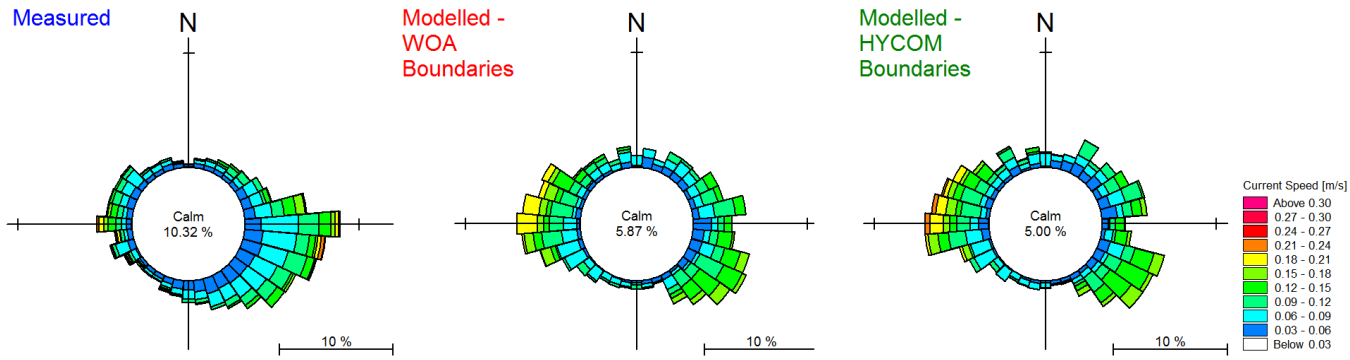

Figure 6-44: Surface (z=3) Current Rose Comparison at Gordons Bay – WOA and HYCOM boundaries

A time series comparison of seabed (z=10) current speed and current direction considering modelled and measured results is presented in Figure 6-45. In addition, current rose plots are provided for all considered datasets in Figure 6-46.

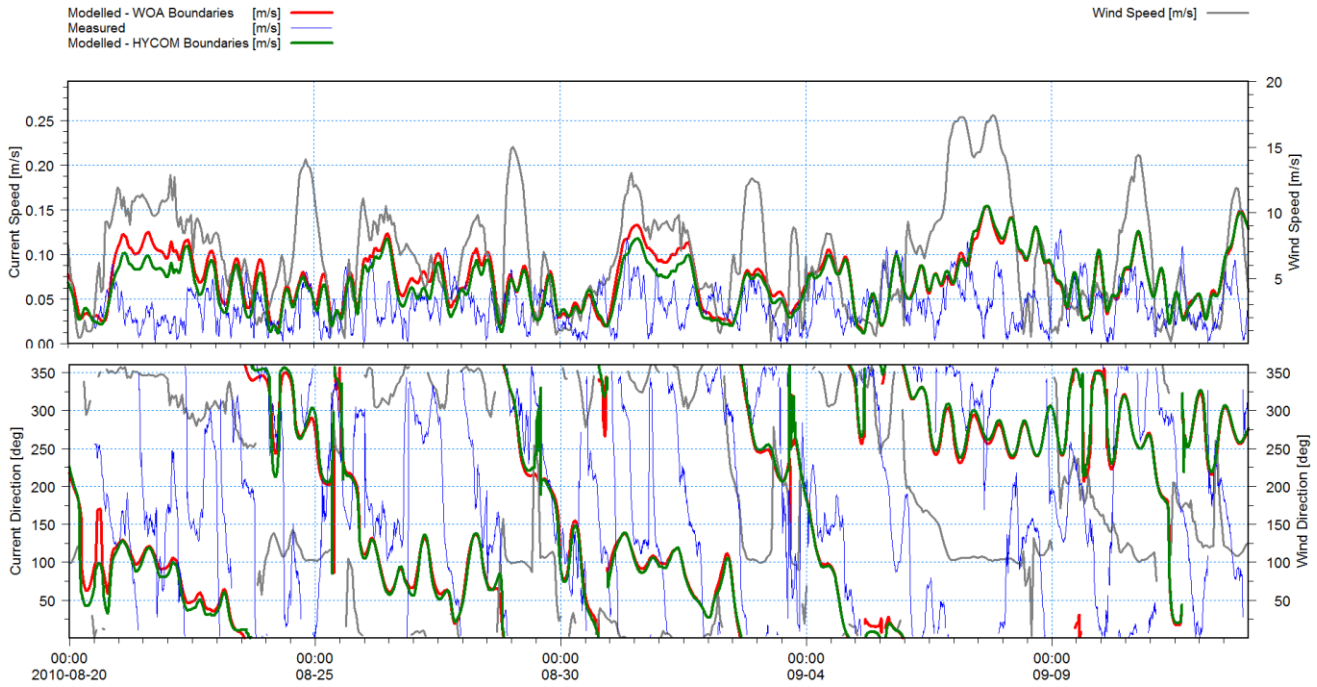

Figure 6-45: Surface (z=10) Current Speed and Direction Time Series Comparison at Gordons Bay – WOA and HYCOM boundaries

.

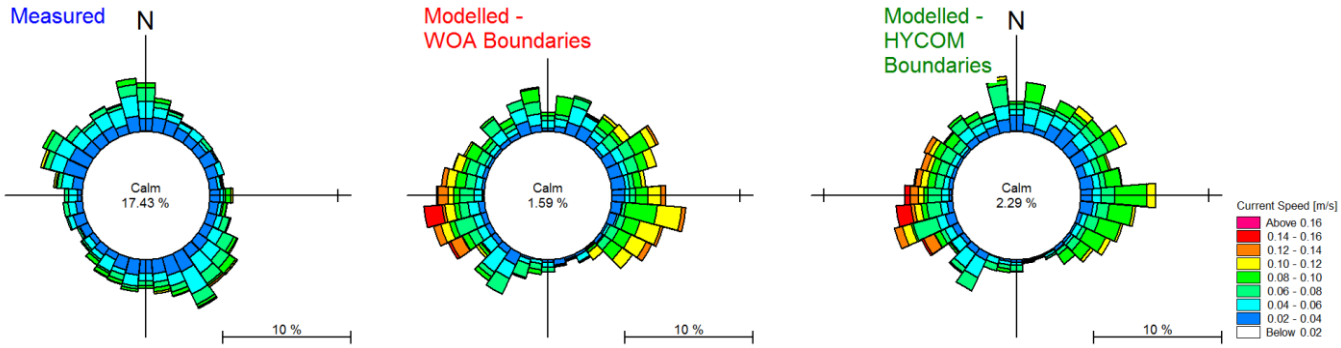

Figure 6-46: Surface (z=10) Current Rose Comparison at Gordons Bay – WOA and HYCOM boundaries

Overall, the WOA-driven model time series results show good agreement with the 3D modelled results under well-mixed conditions. To evaluate how the two models agree on a spatial scale, a contour plot comparison was undertaken. Figure 6-47 to Figure 6-50 show contour plot comparisons of current speed and seawater temperature under south-easterly conditions. Well-mixed and stratified conditions are considered. The plots show near surface and near seabed flows. To characterise the predominant wind climate, a time series was extracted from the WASA (CSAG) hindcast dataset at Roman Rock (refer to Figure 4-1).

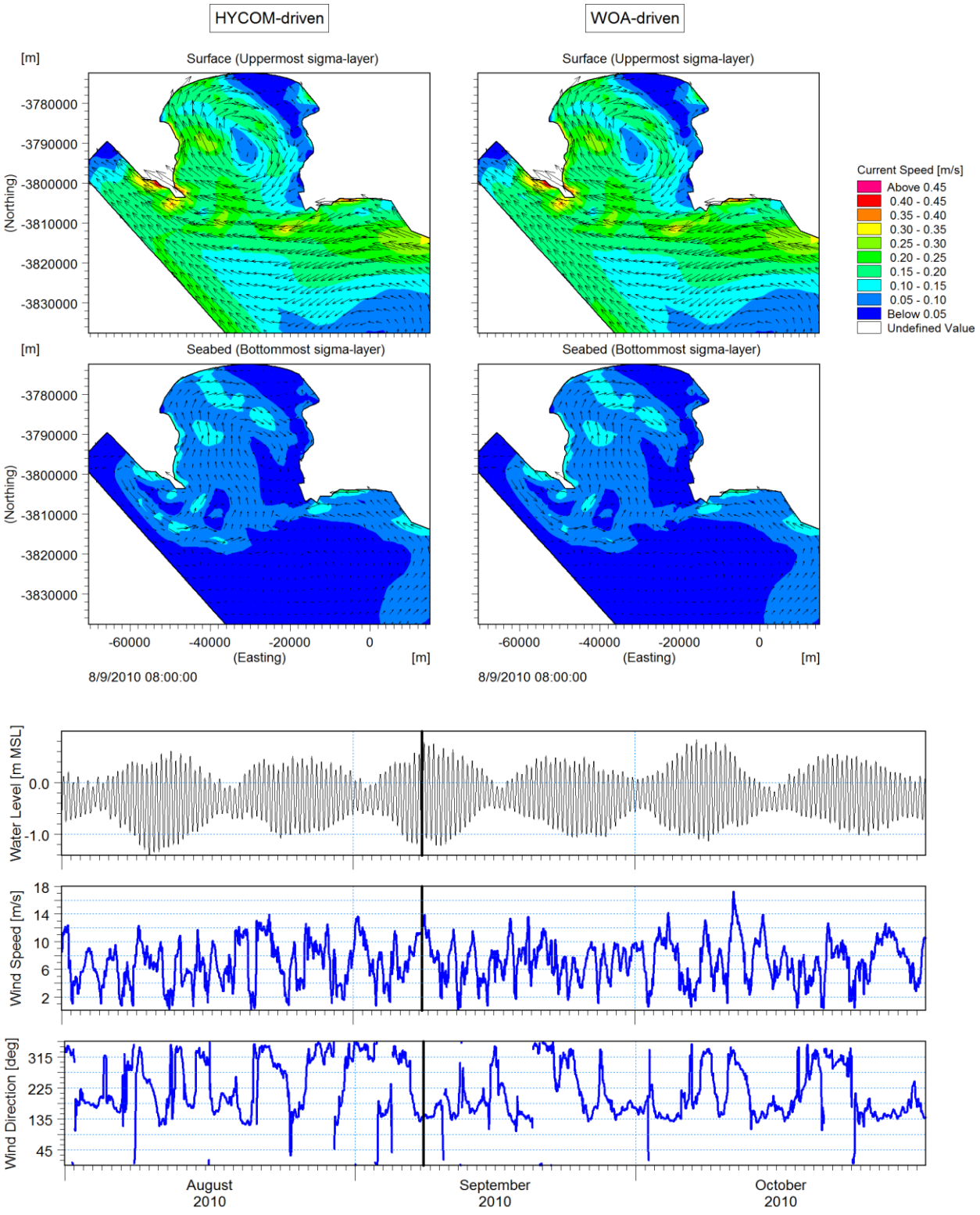

Figure 6-47: Comparison of HYCOM and WOA Model Results - Well-mixed South-easterly Generated Current Circulation Pattern

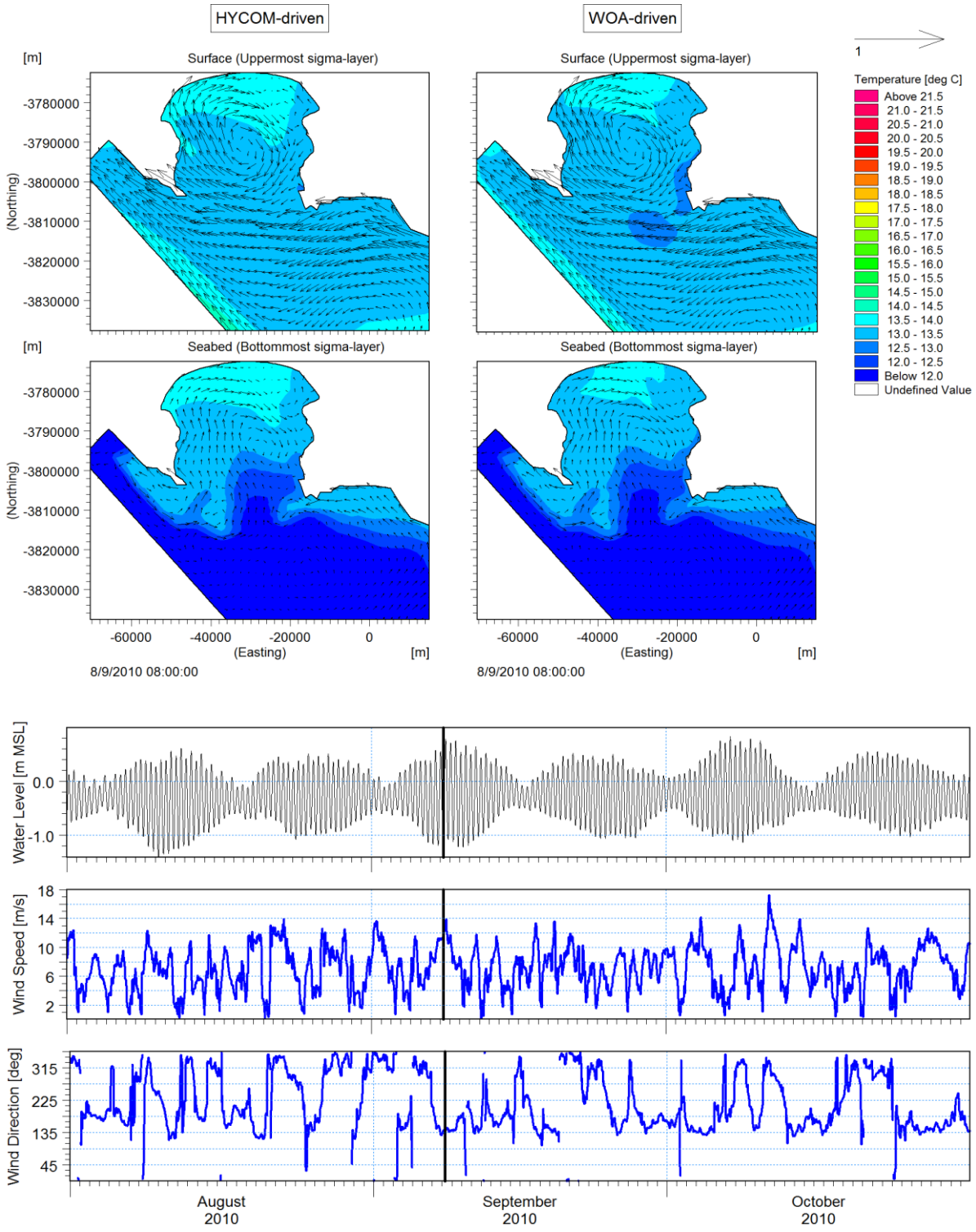

Figure 6-48: Comparison of HYCOM and WOA Model Results - Well-mixed South-easterly Generated Current Circulation Pattern with Temperature Overlay

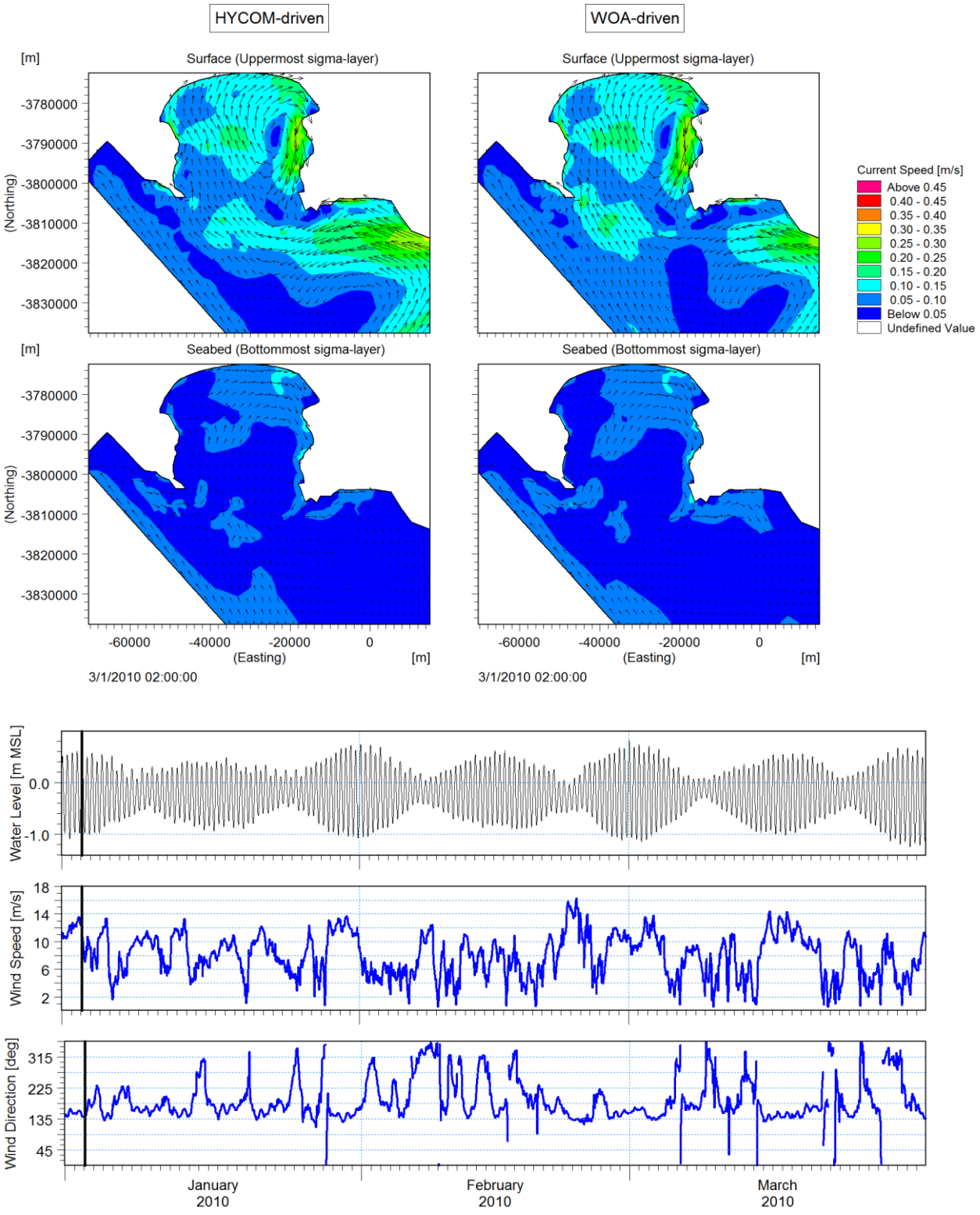

Figure 6-49: Comparison of HYCOM and WOA Model Results - Stratified South-easterly Generated Current Circulation Pattern

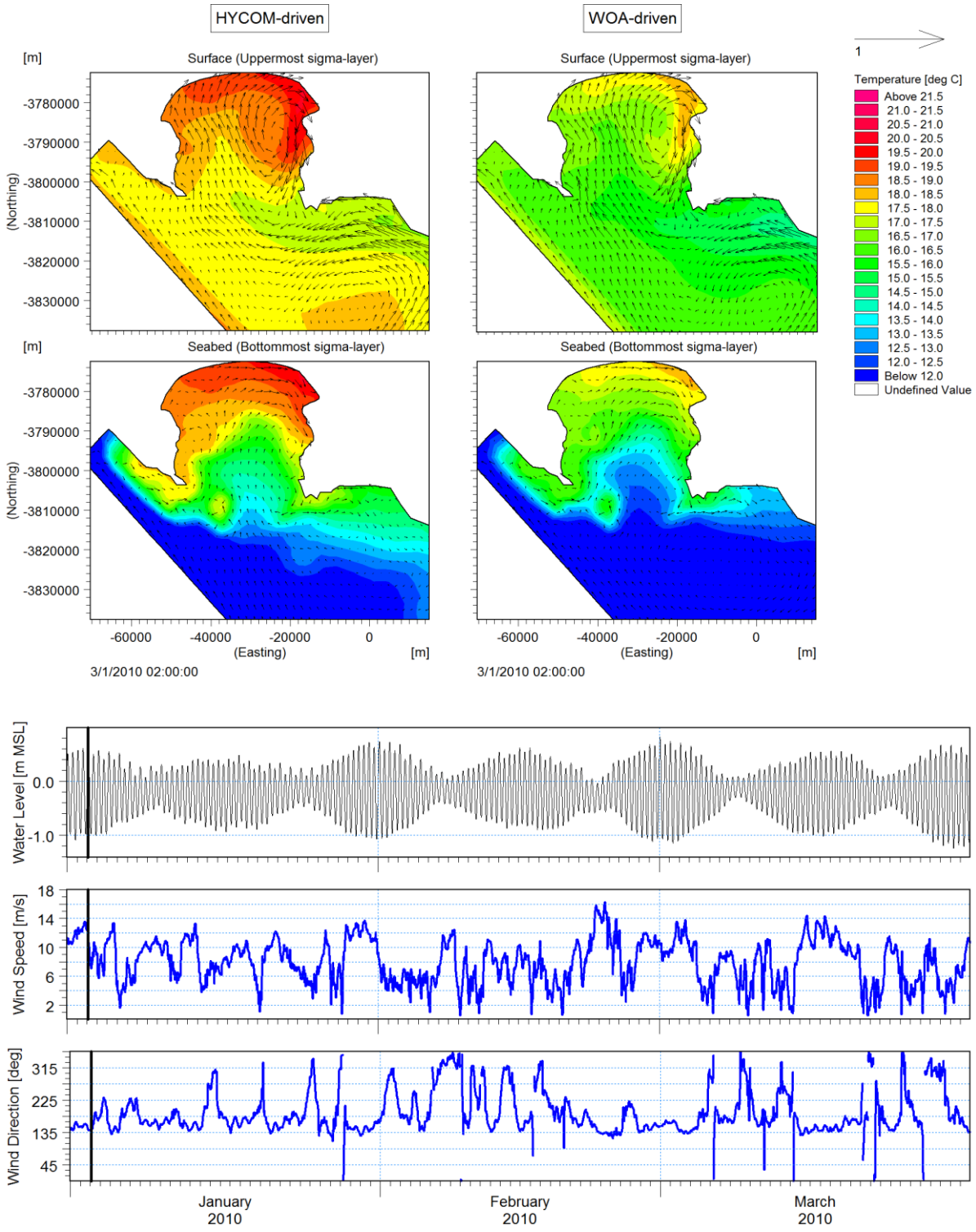

Figure 6-50: Comparison of HYCOM and WOA Model Results - Stratified South-easterly Generated Current Circulation Pattern with Temperature Overlay

Figure 6-51 to Figure 6-54 show contour plot comparisons of current speed and seawater temperature under north-westerly conditions. Well-mixed and stratified conditions are considered. The plots show near surface and near seabed flows. To characterise the

predominant wind climate, a time series was extracted from the WASA (CSAG) hindcast dataset at Roman Rock (refer to Figure 4-1).

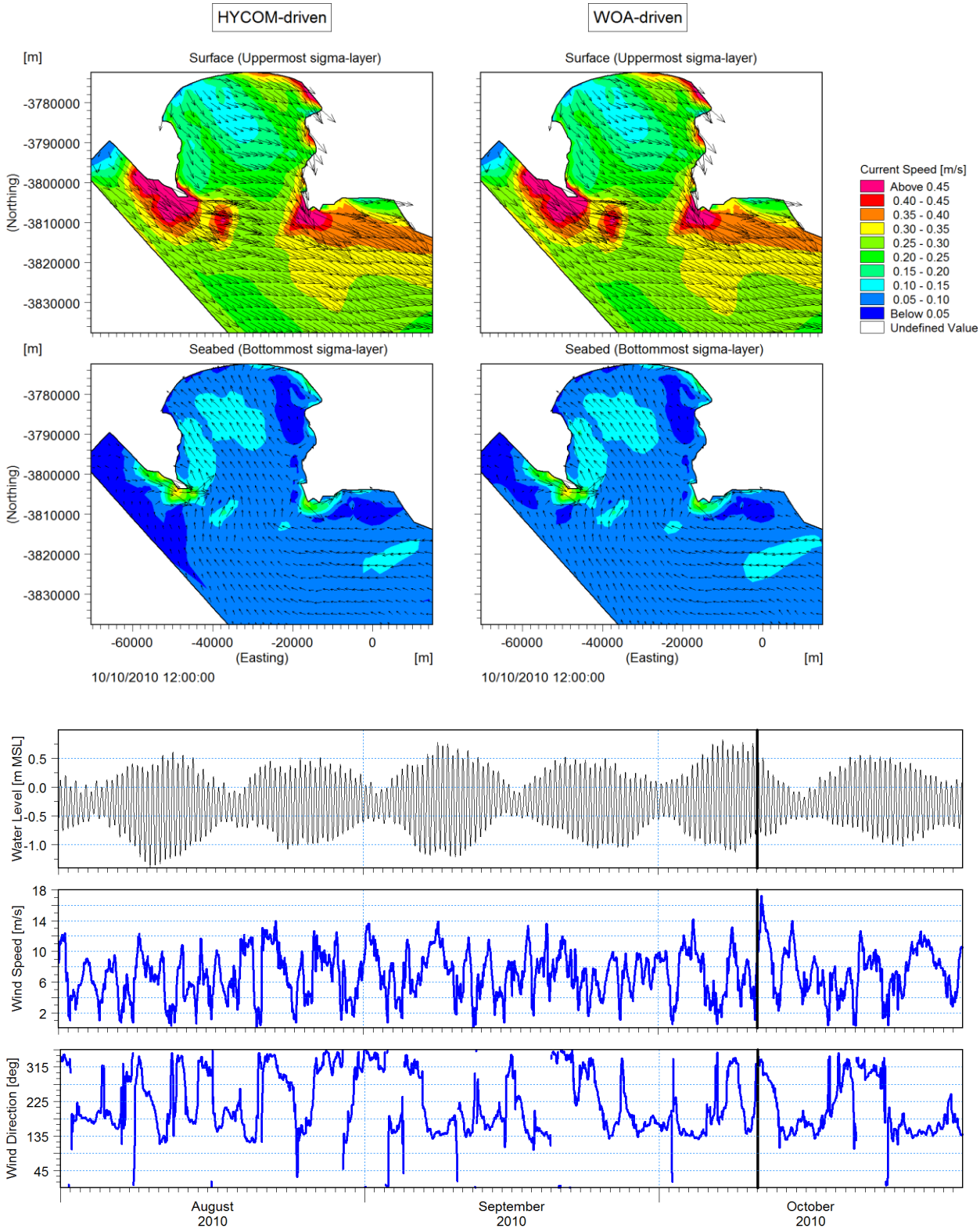

Figure 6-51: Comparison of HYCOM and WOA Model Results - Well-mixed North-westerly Generated Current Circulation Pattern

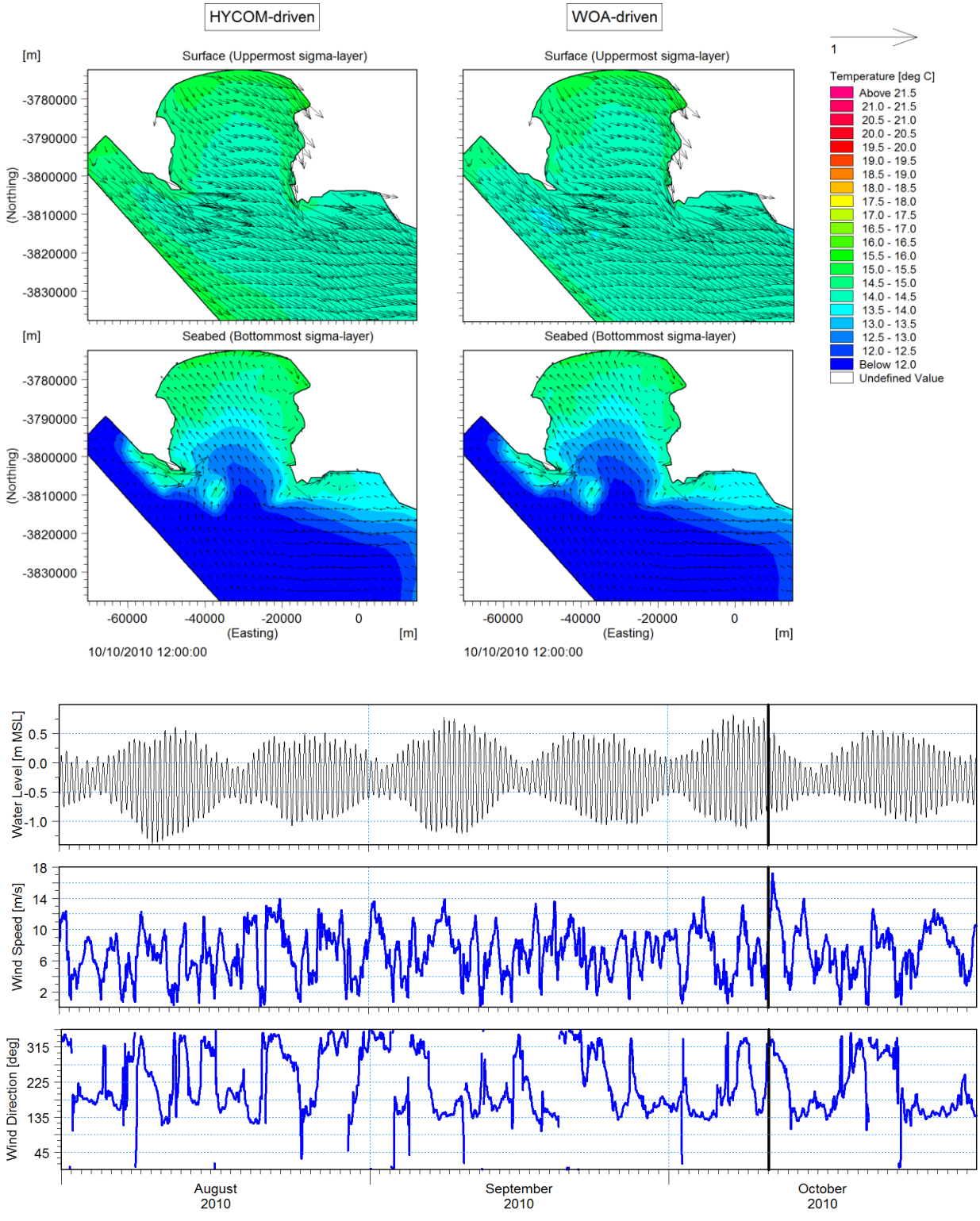

Figure 6-52: Comparison of HYCOM and WOA Model Results - Well-mixed North-westerly Generated Current Circulation Pattern with Temperature Overlay

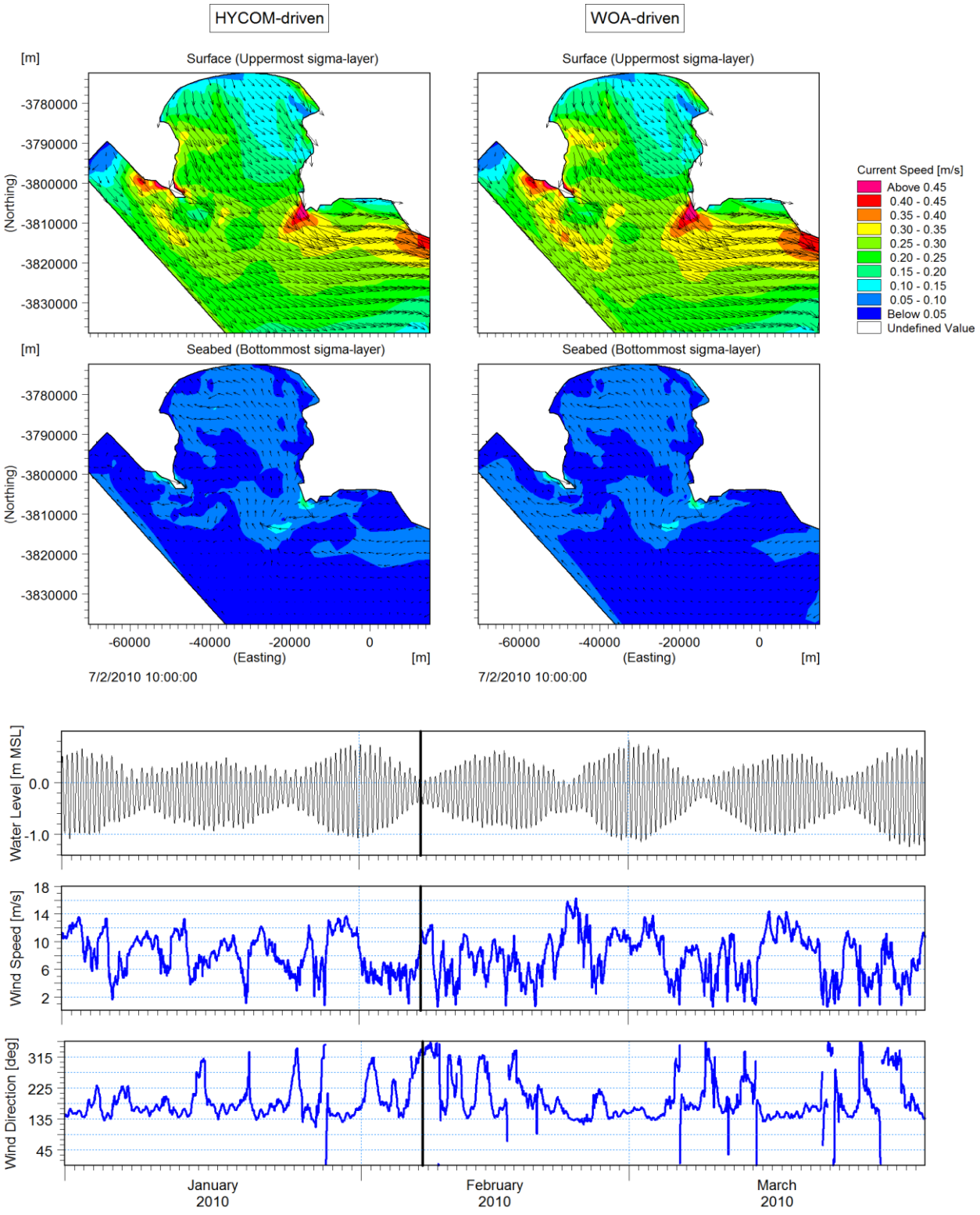

Figure 6-53: Comparison of HYCOM and WOA Model Results - Stratified North-westerly Generated Current Circulation Pattern

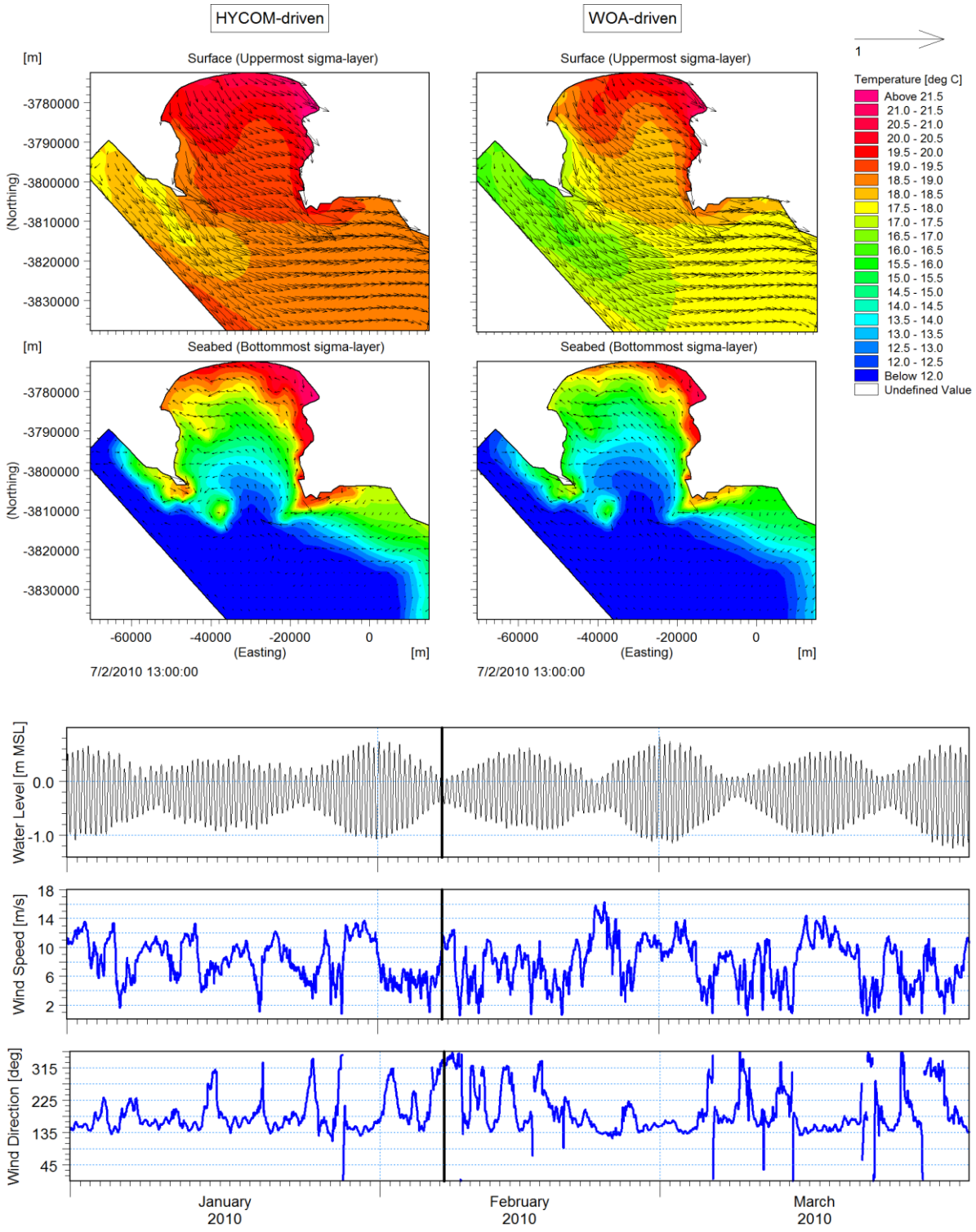

Figure 6-54: Comparison of HYCOM and WOA Model Results - Stratified North-westerly Generated Current Circulation Pattern

Overall, under south-easterly conditions, the HYCOM and WOA driven models show good agreement. Current magnitudes and directions are nearly identical in both model results under well-mixed and stratified conditions.

However, the WOA-driven model does show seawater temperatures (surface and bottom) which are 0.5-1.0℃ colder than the HYCOM dataset. This discrepancy will be addressed in greater detail in Section 6.4.3.3. Despite the difference in seawater temperature, the WOA-driven model results capture the overall cyclonic circulation pattern under south-easterly conditions.

Under north-westerly conditions, the HYCOM and WOA driven models show good agreement. Current magnitudes and directions are nearly identical in both model results under well-mixed and stratified conditions. Overall, the WOA-driven model captures the spatially-uniform current field under north-westerly conditions.

6.4.3.3 Seawater Temperature

An intra-annual comparison of seawater temperature was undertaken between the WOA-driven model and HYCOM-driven model. A time series comparison of the vertical thermal structure for the two datasets is presented in Figure 6-55. The location of the time series extraction points is provided in Figure 6-21. In addition, a monthly-averaged and monthly-minimum SST comparison of the two datasets is presented in Figure 6-56 and Figure 6-57 respectively.

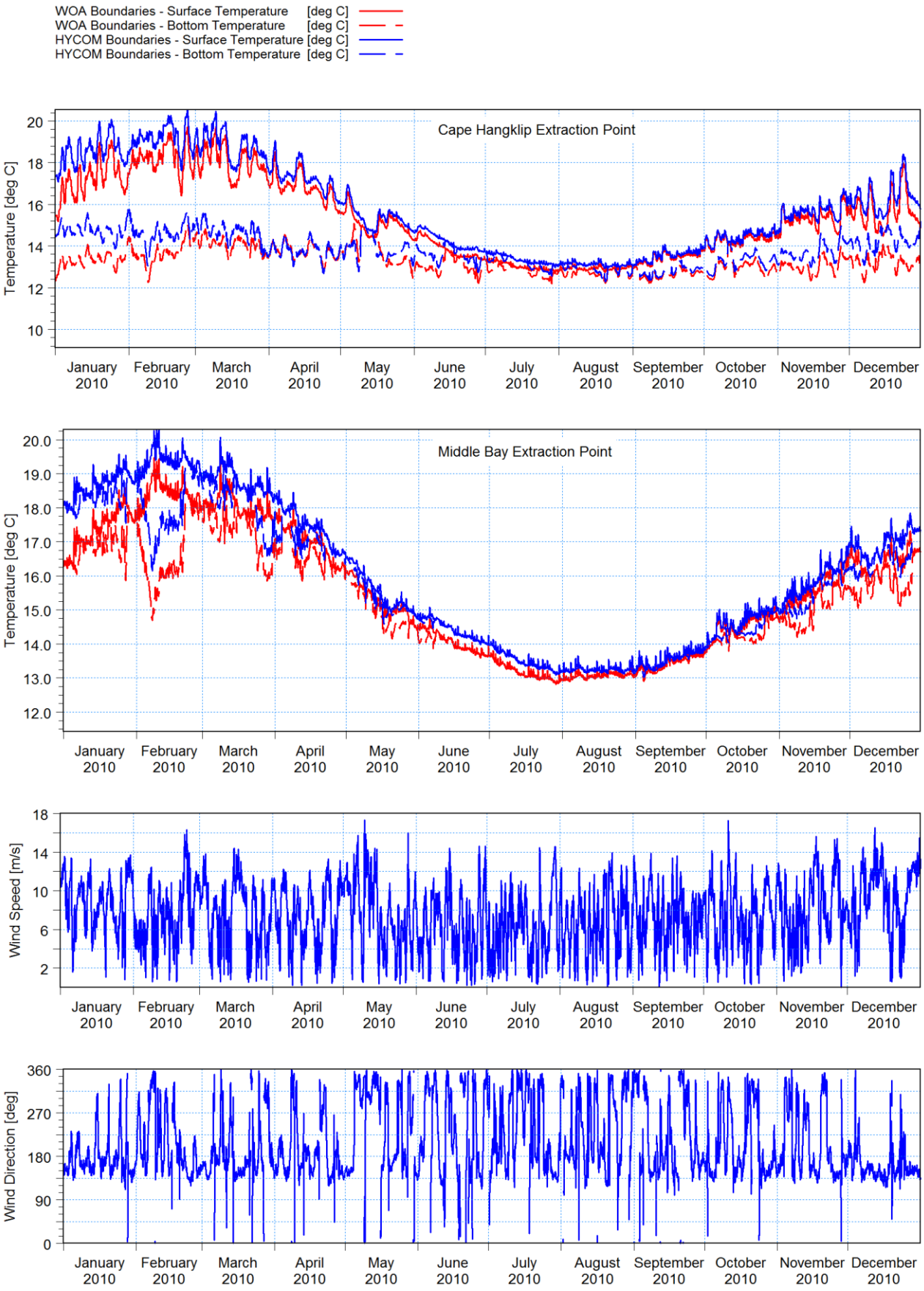

Figure 6-55: Time Series Comparison of Surface and Bottom Temperatures at a Point near Cape Hangklip and in the Middle of the Bay for WOA Boundaries and HYCOM Boundaries

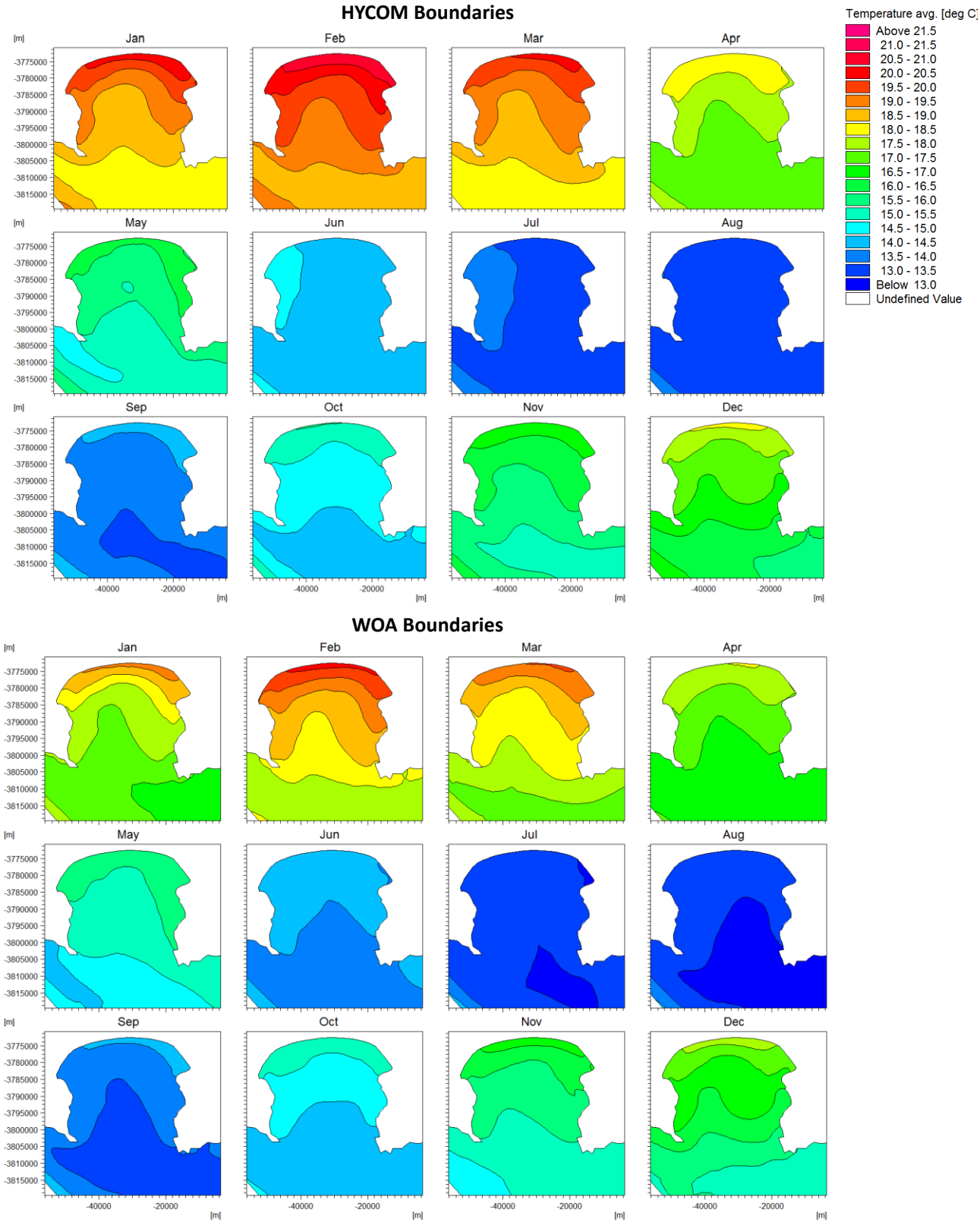

Figure 6-56: Comparison of Average SST per month for HYCOM and WOA Model Boundaries over the Simulation Period Jan-Dec 2010

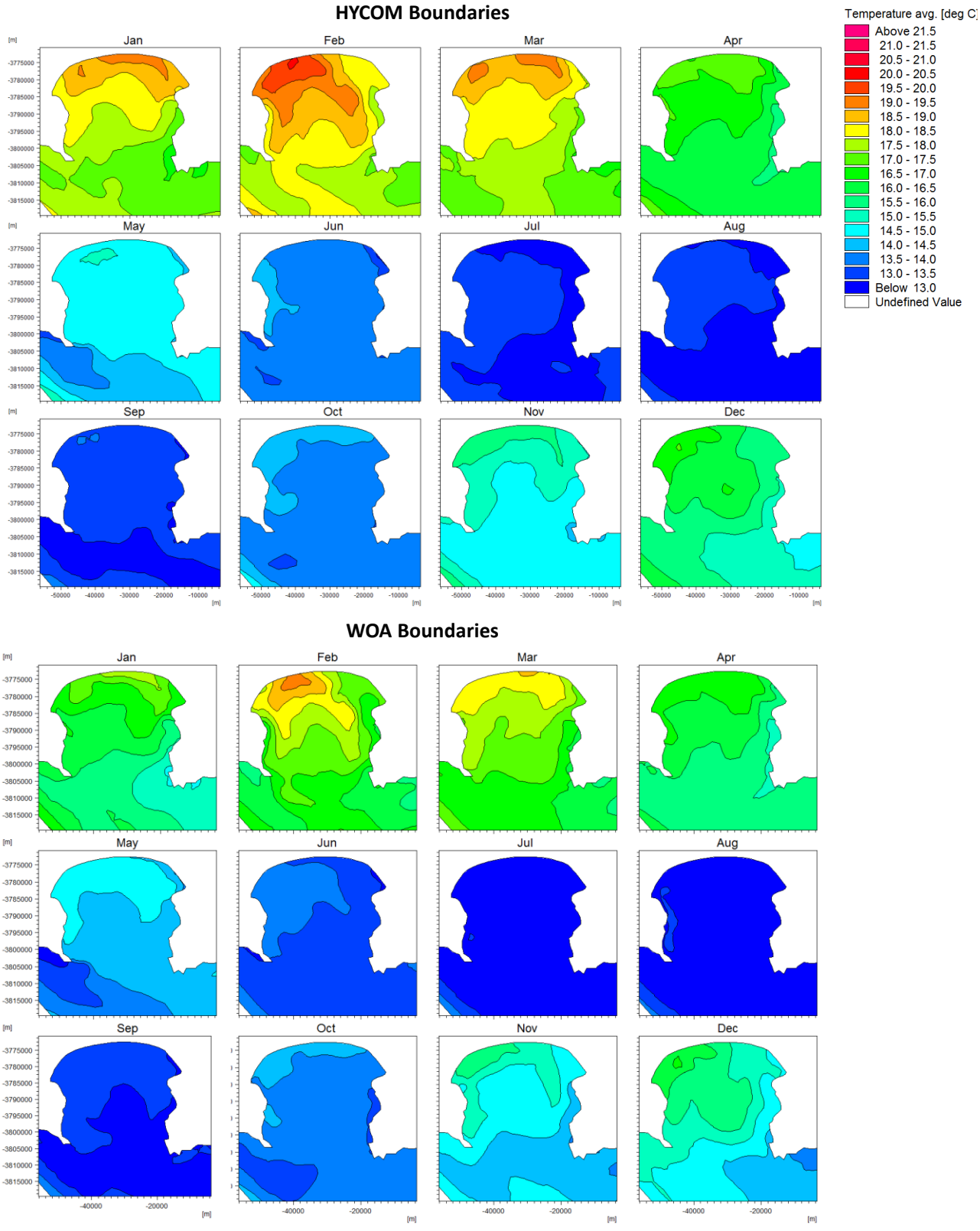

Figure 6-57: Comparison of Minimum SST per month for HYCOM and WOA Model Boundaries over the Simulation Period Jan-Dec 2010

Overall the WOA-driven model results were able to capture the increase in seawater temperature when transitioning from winter to summer months. In addition, the model is able to capture event-scale fluctuations in seawater temperature (such as upwelling and cold water intrusion events) which were consistent with the HYCOM-driven model results.

Upwelling events may be inferred from model results by sharp (2-3℃) vertical fluctuations in surface temperature. From Figure 6-55, the WOA-driven model results capture upwelling events at Cape Hangklip. However, during warmer months, the WOA results consistently under-predict seawater temperatures by up to approximately 1℃ compared to the HYCOM-driven model. When cross-compared with Figure 6-56, the WOA-driven model results under-predict seawater temperatures throughout the bay domain. In addition, during warmer months, upwelling cells are less apparent in the WOA-driven model. However, from Figure 6-57, the WOA results do correctly reproduce upwelling cells at Cape Point, Cape Hangklip and along the eastern shore which is consistent with the HYCOM-driven model and historical studies (Cram, (1970); Jury, (1985); Wainman et al., (1987); Taljaard et al., (2000)). During colder months, under well-mixed conditions, the WOA-driven results show closer agreement with the HYCOM-driven model results.

Cold water intrusion events are represented in the mid-bay time series by sharp drops (1-3℃) in bottom temperature. From Figure 6-55, these events are present in both models during warmer months.

6.4.3.4 Discussion

Overall the WOA-driven model results show good agreement with the HYCOM-driven model results. Although the WOA monthly timescale is comparatively lower in temporal resolution, the results indicate that higher temporal resolution temperature-depth datasets are not necessarily more accurate. In addition, when modelling hydrodynamic processes (particularly the circulation) in False Bay, it may be inferred that the temperature profiles on the boundaries are not the most critical model input parameter, at least when compared to the influence of spatially-varying wind forcing.

Based on the results of sensitivity testing of temperature boundaries, it is recommended that if the HYCOM dataset is unavailable when considering a future potential engineering application of hydrodynamic modelling in False Bay, that the WOA monthly averaged dataset be considered instead.

CHAPTER 7: CONCLUSIONS AND RECOMMENDATIONS

7.1 Conclusions

During the 1970s to early 1990s False Bay was the focus of many observational studies (Shannon et al., (1983); Jury, (1985); Jury, (1986); Botes, (1988); Gründlingh et al., (1989); Gründlingh & Largier, (1991); Gründlingh & Potgieter, (1993)) focusing on the collection of measurement data and establishing a database and understanding of the broader physical characteristics of the bay, particularly current circulation patterns. However, despite these numerous studies comprising the analysis of circulation in the bay, and the physical processes driving it, there remains significant uncertainty mainly due to:

- The short duration of measurement campaigns underpinning these studies; and
- The limited spatial scale of measurement campaigns.

The main objective of this thesis is to add to the existing body of knowledge on False Bay's physical processes with particular emphasis on bay circulation and hydrodynamic processes such as spatially varying wind forcing and intra-annual variability of sea temperature. In addition, this thesis was developed to assist with potential engineering applications of hydrodynamic modelling of False Bay. Lastly, it is envisaged that this thesis will serve as a basis for the potential development of an operational forecast model(s).

To meet the objectives above, a hydrodynamic model was developed which simulated a complete year and investigated the following primary physical processes in False Bay:

- Current circulation;
- Horizontal thermal structure (sea surface temperatures); and
- Vertical thermal structure.

In addition, sensitivity analyses were undertaken to investigate the potential engineering application of hydrodynamic modelling of False Bay. It cannot be guaranteed that all the input data sources considered in this study (e.g. CSAG hindcast wind dataset) will be available for future investigations/studies. Therefore, the sensitivity analyses considered the effects of including or neglecting certain processes or variability, and evaluated the potential errors if such processes/variations are necessarily omitted. The main conclusions obtained from the study's modelling approach is summarised in this chapter.

7.2 Current circulation

Overall, the circulation pattern results were consistent with historical studies on False Bay which noted the formation of a clockwise gyre under predominant south-easterly wind conditions. Model results correctly reproduced the decoupling of surface and bottom flows

which were noted in historical studies. Decoupling of flows refers to surface flows being significantly influenced by wind-forcing compared to weaker bottom flows which flow in a different direction. While the surface flow forms a stronger clockwise (or cyclonic) gyre, the bottom flows show a weaker cyclonic flow. Under south-easterly wind conditions, the model results show the formation of a weak anticyclonic gyre near Gordons Bay. This zone shows evidence of a “wind shadow” in this region which stretches from Strand along the eastern shore up to Cape Hangklip. The overall circulation pattern is similar under both stratified and well-mixed (isothermic) conditions.

Under north-westerly conditions, the model results showed that the anti-cyclonic circulation pattern presented in historical observational studies was absent. Instead, the north-westerly wind condition induces a spatially-uniform current field with no distinct gyres forming in the bay. A possible explanation for this current regime could be the formation of the north-westerly wind condition which is less spatially-complex than the south-easterly wind condition. Unlike south-easterly winds which are influenced by complex orographic features surrounding False Bay, north-westerly winds are mainly influenced by Table Mountain which is further from False Bay. North westerly winds tend to deflect around Table Mountain and across the bay uniformly until they are steered westerly at the mouth of the bay at Cape Point and Cape Hangklip. The results show that under north-westerly wind conditions, north-westerly-setting bottom return currents are generated throughout the bay domain. These return currents force bottom water from the entrance to the middle of the bay. The overall circulation pattern is similar under both stratified and well-mixed (isothermic) conditions.

7.3 Horizontal Thermal Structure (Sea Surface Temperatures)

Model results and composite satellite measurements in the bay showed good agreement. The model results showed that during warmer months (November to March), upwelling cells are noted at Cape Point, along the eastern shore and at Cape Hangklip with surface temperatures being approximately 0.5-1℃ less than surrounding sea surface temperatures (SST). In addition, during warmer months a strong shoreward gradient was noted. During colder months (June to August), spatially uniform SSTs were present.

7.4 Vertical thermal structure

From the deep-water entrance to the shallower northern shore, seawater temperatures become progressively warmer. The model results indicated that at the entrance of False Bay, the influence of Rocky Bank is very apparent. The feature segregates warmer western and colder eastern waters. Due to the asymmetry of bathymetry at the entrance, bottom waters are approximately 1-2℃ colder east of Rocky Bank under well-mixed (isothermic) and stratified conditions.

Under south-easterly wind conditions, colder surface waters are advected from offshore through the entrance of the bay at Cape Point toward the middle of the bay. The cyclonic circulation pattern results in warmer nearshore water being advected through the entrance (near Cape Hangklip) toward offshore. Ultimately, this results in surface seawater temperatures along the eastern shore being colder than the western shore.

North-westerly winds result in a spatially-uniform surface current field in the direction of the wind. The formation of this surface current field then induces a bottom return current field in the opposite direction i.e. north-west setting currents. The surface currents force warmer nearshore waters offshore. The induced bottom return currents then advect colder bottom waters from offshore into middle of the bay. This decoupling mechanism between surface and bottom flows leads to significant stratification during warmer months.

7.5 Model Sensitivities

7.5.1 Comparison of 2D vs. 3D Hydrodynamic Modelling of False Bay

Based on the sensitivity results, it was recommended that for engineering applications, where computation time needs to be optimised, that a 2D hydrodynamic model of False Bay be employed for the simulation of hydrodynamics under well-mixed south-easterly conditions. If a full year of simulation (or similarly long duration) is necessary, then it is recommended that a combination of 2D modelling and 3D modelling be considered. If computation time needs to be optimised, this combination of modelling methodologies could effectively reduce model runtime by approximately 50%. However, the modeller should be cautious of simulating north-westerly conditions with a 2D model due to the significant discrepancies noted between the 2D and 3D models.

7.5.2 Comparison between Spatially-varying Wind and Uniform Wind Field

The sensitivity results indicated a general lack of agreement between model results and ultimately proved how critical spatially varying wind-forcing was in defining the overall current regime and the vertical and horizontal thermal structures within False Bay. At present, the lack of incorporation of spatially varying wind forcing has been a serious hindrance in providing robust simulation of the hydrodynamics of False Bay

7.5.3 Comparison of HYCOM vs Monthly-averaged Temperature Boundaries

Overall the WOA-driven model (monthly-averaged temperature) results show good agreement with the HYCOM-driven model (daily-averaged temperature) results. Based on the results of sensitivity testing of temperature boundaries, it was recommended that if the HYCOM dataset is unavailable when considering a future potential engineering application of hydrodynamic modelling in False Bay, that the WOA monthly averaged dataset be considered instead.

7.6 Limitations of study

The model was developed as a three-dimensional (3D) hydrodynamic model which considers wind forcing, tidal forcing, temperature-depth profiles on the boundary and atmospheric input. However, the model does not consider wave coupling and the resulting physical processes such as wave breaking and the generation of longshore currents. Longshore currents add to the circulation within False Bay. It is expected that the influence of wave-driven circulation is significant in shallower regions of the bay, more specifically the gently sloping northern beaches (Taljaard et al., 2000). These wave-driven currents tend to generate a net clockwise circulation pattern along the shores of the bay (CSIR, 1982). However, the influence of wind-driven currents are more significant than wave-driven currents in deeper water which comprises the majority of the bay.

Although the model calibration and verification showed reasonable agreement with available current measurements, the measurement datasets spanned a short period (less than a month) and were located in relatively sheltered locations. More specifically, the Gordons Bay ADCP instrument location was located in a shallow region which is susceptible to a wind shadow stretching along the eastern shore. In addition, the ADCP measurment periods were undertaken in isothermic (well-mixed) conditions. Therefore, the calibration and verification with the available ADCP datasets may not be sufficient enough to characterise conditions which include stratification of the water column.

The modelled water levels were found to agree well with measurements at Simons Town. However, comparisons with modelled and measured currents showed reasonable to poor agreement. This was partly due to ADCP current measurements showing considerable “noise” in the dataset. It is possible that this “noise” may result from the influence of unaccounted for water level constituents such as coastally trapped waves (remote forcing), long waves, short waves, smaller timescale gusting events etc. By excluding these constituents, this means that perturbations in water level and subsequently current variation are not captured in the model results. Another possible reason for the “noise” in the ADCP measurements may be instrument-specific namely, weaker currents show higher variability (or “noise”) in current direction and are therefore more challenging to measure with ADCP instruments.

7.7 Recommendations for Future Studies

All of the major model input parameters presented in this study, i.e. water levels on the boundary (DTU), atmospheric input (ECMWF), spatially varying wind field (CSAG) and temperature boundaries (HYCOM), may be run in forecast modes. Therefore, in order to facilitate the development of operational forecasting models within False Bay, it is

recommended that the findings and results of this study be incorporated into the development of these models.

To evaluate and quantify the influence of wave-driven circulation in shallower waters within the bay, it is recommended that a wave-coupled hydrodynamic model be considered as a further development of this study. The results and findings of this study may be used as a basis for the development of this work.

It is recommended that, in a future study, if the verification and calibration of the model is to be improved, that a measurement campaign considering multiple measurement locations over a long duration be integrated into the research work. Multiple measurements are necessary to characterise the complex circulation regime within the bay. In addition, by integrating the modelling and measurement campaign, “data integrity” is more likely to be consistent across measurements datasets.

Lastly, it is recommended that the effect of additional water level constituents within False Bay such as coastally trapped waves (remote forcing), long waves, short waves, smaller timescale gusting events etc. be investigated in more detail. Furthermore, an in-depth analysis of tidal gauges and available water level measurements would be useful in providing an increased level of accuracy to the simulation of water levels within False Bay.

CHAPTER 8: REFERENCES

Apel, J. R. (1999). *Principles of Ocean Physics* (1st ed., Vol. 38). Academic Press.

Atkins, G. (1970a). Thermal structure and salinity of False Bay. *Transactions of the Royal Society of South Africa*, 39:2, 117-128.

Atkins, G. (1970b). Wind and current patterns in False Bay. *Transactions of the Royal Society of South Africa*, 39:2, 139-148.

Botes, W. (1988). Shallow water current meters comparative study: False Bay. *CSIR Report T/SEA 8803*, 14.

Cheng, P., Valle-Levinson, A., Winant, C. D., Ponte, A., Gutierrez de Velasco, G., & Winters, K. B. (2010a). Upwelling-enhanced seasonal stratification in a semiarid bay. *Continental Shelf Research*, 30:1241-1249.

Cheng, Y., & Andersen, O. B. (2010a). Improvement in global ocean tide model in shallow water regions. *Poster, SV.1-68 45, OSTST*.

Cram, D. L. (1970). A Suggested Origin for the Cold Surface Water in Central False Bay. *Transactions of the Royal Society of South Africa*, 39:2, 129-137 .

CSIR. (1982). *Status Report on pollution in False Bay, CSIR Report C/SEA 8241.* Stellebosch, South Africa: CSIR.

Cummings, J. A., & Smedstad, O. M. (2013). Variational Data Assimilation for the Global Ocean. *Data Assimilation for Atmospheric, Oceanic and Hydrologic Applications, 2*, 303-343.

DHI. (2017a, June 17). *MIKE 3 Flow Model: Hydrodynamic - Module (Scientific Documentation).* Denmark: DHI. Retrieved from MIKE 21 Products: https://www.mikepoweredbydhi.com/products/mike-21/hydrodynamics

DHI. (2017b, June 17). *Hydrodynamics*. Retrieved from MIKE 21 Products: https://www.mikepoweredbydhi.com/products/mike-21/hydrodynamics

DHI. (2017c). *MIKE C-MAP: Extraction of World Wide Bathymetry Data and Tidal Information, User Guide.* Denmark: DHI.

Dufois, F., & Rouault, M. (2012). Sea surface temperature in False Bay (South Africa): Towards a better understanding of its seasonal and inter-annual variability. *Continental Shelf Research*, 34, 24-35.

ECMWF. (2017, September 19). *European Centre for Medium-Range Weather Forecasts. ERA-Interim Project. Research Data Archive at the National Center for Atmospheric Research,*

Computational and Information Systems Laboratory. Retrieved from http://apps.ecmwf.int/datasets/data/interim-full-daily/

Gaines, S. (2017). *Upwelling*. Retrieved from NOAA Ocean Explorer: http://oceanexplorer.noaa.gov/explorations/02quest/background/upwelling/upwelling.html

Gao, G. (2011). *A Numerical Modeling Study of Storm Surge and Inundation in the Chesapeake Bay during the November 2009 Mid-Atlantic Nor'easter.* MSc. Thesis, The College of William and Mary in Virginia.

Gründlingh, M., & Largier, J. (1991). Physical oceanography of False Bay: A Review. *Transactions of the Royal Society of South Africa*, 47, 387–400.

Gründlingh, M., & Potgieter, E. (1993). Unique thermal record in False Bay. *South African Journal of Science*, 89, 510–512.

Gründlingh, M., Hunter, I., & Potgieter, E. (1989). Bottom currents at the entrance to False Bay. *Continental Shelf Research*, 9:12, 1029–1048.

Hall, E. (2008). *Hydrodynamic Modelling of Lake Ontario (Masters Thesis).* Queen's University, Department of Civil Engineering, Ontario, Canada.

Halliwell, G. (2002). *HYCOM Overview.* Retrieved from HYCOM: https://hycom.org/attachments/067_overview.pdf

Hearn, C. (2008). *The Dynamics of Coastal Models* (1st ed.). New York: Cambridge University Press.

Jones, G. (2008). *A field guide to the marine animals of the Cape Peninsula.* Cape Town: SURG.

Jury, M. (1984). Wind Shear and Differential Upwelling Along the SW Tip of Africa. *PhD Thesis in Physical Oceanography, University of Cape Town*.

Jury, M. (1985). Mesoscale variations in summer winds over the Cape Columbine- St Helena Bay region. *South African Journal of Marine Science*, 3, 77-88.

Jury, M. (1986). The Sudden Decay of Upwelling off the Cape Peninsula, South Africa: A Case Study. *South African Journal of Marine Science*, 4, 111-118.

Nam, P. T., Larson, M., Hanson, H., & Hoan, L. X. (2011). A numerical model of beach morphological evolution due to waves and currents in the vicinity of coastal structures. *Coastal Engineering*, 58, 863–876.

Nicholson, S. A. (2011). *The Circulation and Thermal Structure of False Bay: A Process-Oriented Numerical Modelling and Observational Study (Masters Thesis).* Department of Physical Oceanography. Cape Town: University of Cape Town.

NOAA. (2017). *How Hydrodynamic Models Are Used*. Retrieved April 14, 2017, from Office of Coastal Survey: https://www.nauticalcharts.noaa.gov/csdl/learn_models.html

Penven, P., & Tan, T. (2007). *ROMSTOOLS user guide.* Retrieved from Institut de Recherche pour le Development (IRD): http://roms.mpl.ird.fr/

Penven, P., G.B Brundrit, A., Colin de Verdiere, P., Freon, A. S., Johnson, J. R., & Shillington, F. A. (2001). A regional hydrodynamic model of up- welling in the Southern Benguela. *South African Journal of Science* , 97, 472–475.

Pond, S., & Pickard, G. (1978). *Introductory Dynamical Oceanography* (1st ed.). London: Pergamon Press.

Rundgren, C. D. (1992). *Aspects of Pollution in False Bay, South Africa (With Special Reference to Subtidal Pollution) (Masters Thesis).* Cape Town: University of Cape Town.

Shannon, L., & Chapman, P. (1983). Suggested mechanism for the chronic pollution by oil of beaches east of Cape Agulhas. *South African Journal of Marine Science*, 1:1, 231-244 .

Shannon, L., Walters, N., & Moldan , A. (1983). Some features in two Cape bays as deduced from satellite ocean-colour imagery. *South African Journal of Marine Science*, 1:1, 111-122.

Smit, A. J., Roberts, M., Anderson, R. J., Dufois, F., Dudley, S., Bornman, T. G., . . . Bolton, J. J. (2013). A Coastal Seawater Temperature Dataset for Biogeographical Studies: Large Biases between In Situ and Remotely-Sensed Data Sets around the Coast of South Africa. *PLOS ONE*, 8:12, 1-13.

Sutherland, J., Walstra, D. J., Chesher, T. J., van Rijn, L. C., & Southgate, H. N. (2004). Evaluation of coastal area modelling systems at an estuary mouth. *Coastal Engineering*, 51, 119–142.

Taljaard, S., van Ballegooyen, R., & Morant, P. (2000). *Special Assessments and Inventories of Available Literature and Data, CSIR Report ENV-S-C 2000-086/2.* Stellenbosch: CSIR.

Wainman, C. K., Polito, A., & Nelson, G. (1987). Winds and Subsurface Currents in the False Bay Region, South Africa. *South African Journal of Marine Science*, 5:1, 337-346.

WASA. (2014). *Wind Atlas For South Africa: Report to the WASA Project Steering Committee.* Sandton: SANEDI.

Annexure A: Wind Verification

1 INTRODUCTION

1.1 Scope of Wind Calibration

The wind hindcast dataset sourced from the WASA (2014) project was verified against existing weather stations around False Bay. The main objective of the verification of wind data was to assess the level of agreement with measurements and to determine whether processing would be required prior to input into the hydrodynamic model.

Table 1-1: Summary of Available Wind Measurement Data Considered

Data Type	Data Source	Data Location(s)	Dataset Period
Wind	CSIR	Cape Point	1994-1997 (4 years)
		Seal Island	1987-1988 (1 year)
		Simons Town (IMT)	1995 (3 months)
		Roman Rock	1995 (2 months)
		Steenbras	1995 (2 months)
	UCT CSAG	Atmospheric Model*	2005 - 2013 (8 years)
	South African Weather Service Data	Cape Point	1973-2017 (44 years)
		Cape Town International Airport	1949-2017 (68 years)
		Simons Town (IMT)	1949-1950 (1 year)
		Slangkop	1998-2017 (19 years)
		Strand	2000-2017 (17 years)
	IMT	Roman Rock	2007-2013 (6 years)

*Hindcast dataset derived from the WASA project

The datasets provided in Table 1-1 refer to multiple measurement locations within False Bay. An overview of these measurement locations are provided in Figure 1-1.

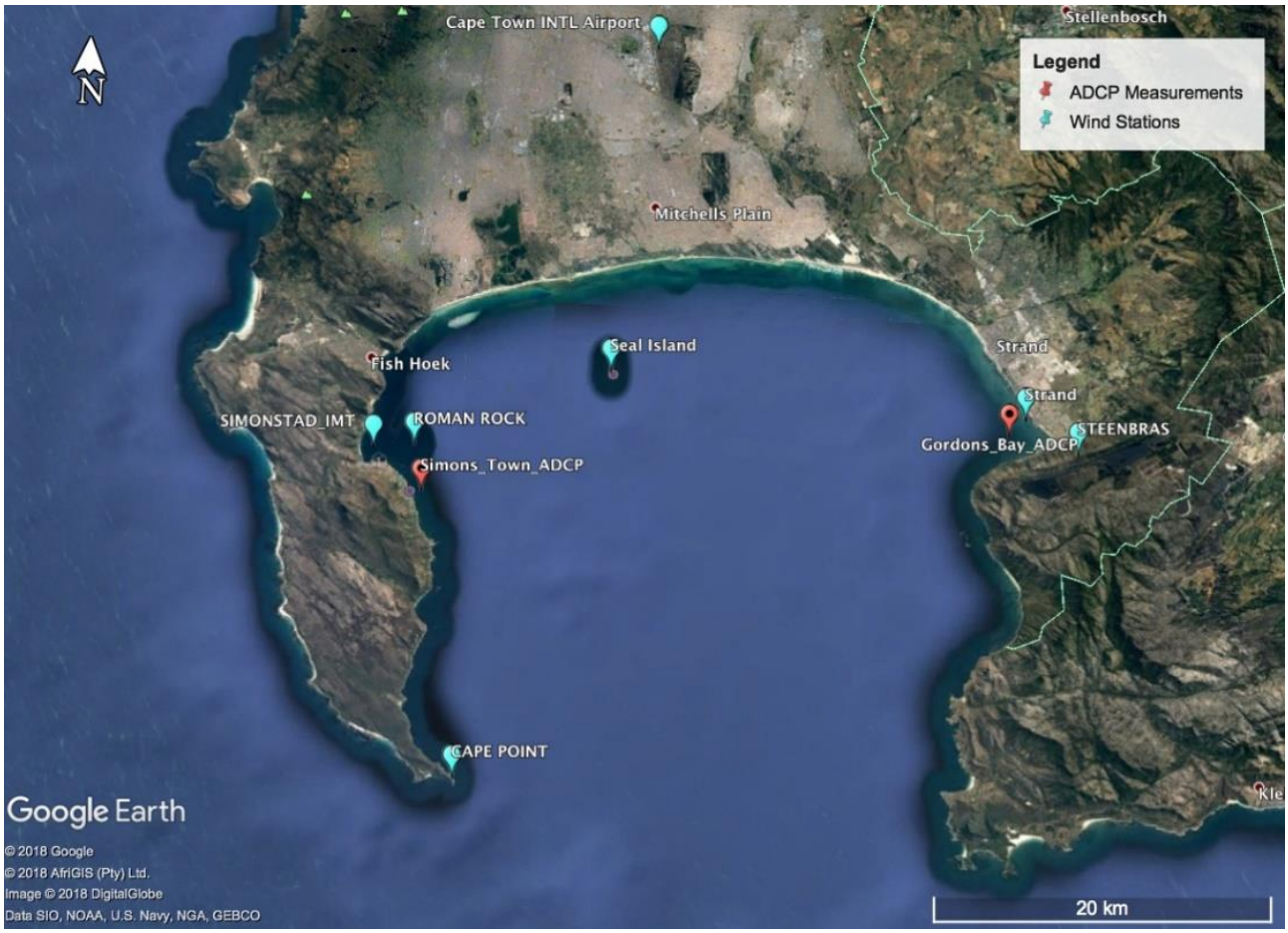

Figure 1-1: Overview of Measurement Locations in False Bay

2 WIND VERIFICATION RESULTS

2.1 Cape Town International Airport

A wind timeseries and wind rose comparison of the CSAG and Weather Station data over the calibration period is presented in Figure 2-2 and Figure 2-2 respectively.

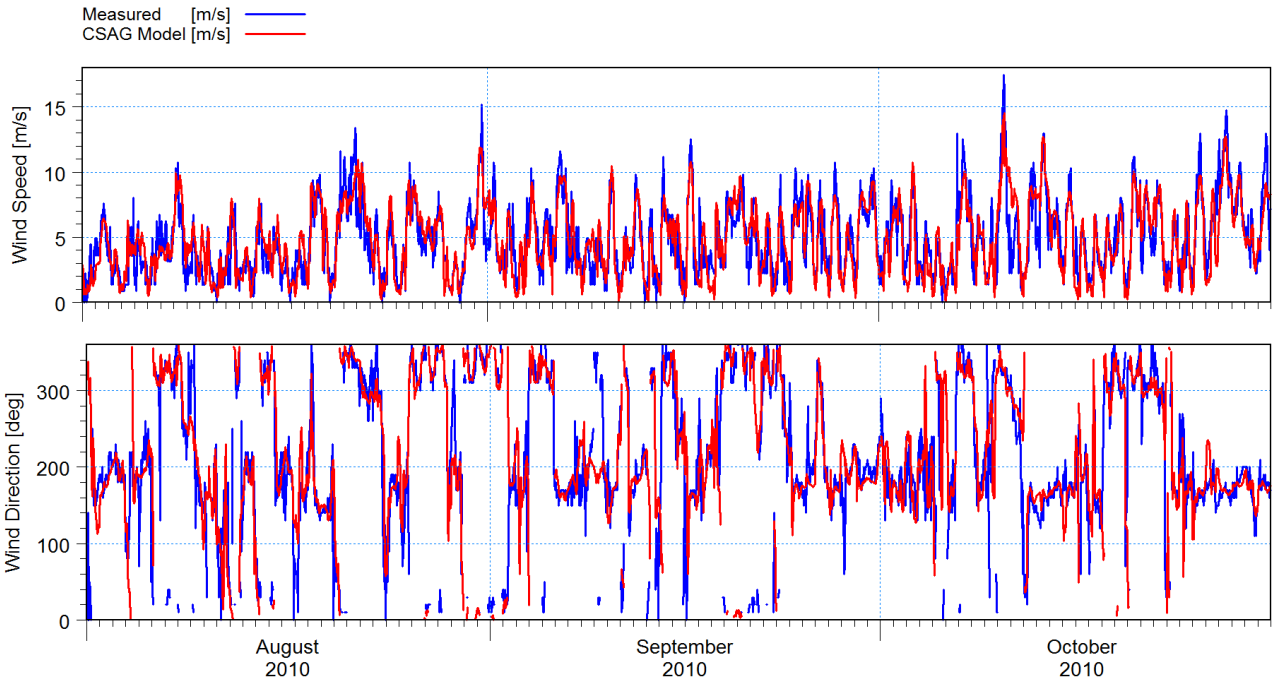

Figure 2-1: Wind Speed and Direction Timeseries comparison of Measured (+10 m AGL) and Modelled (+10 m AGL) Datasets – Cape Town International Airport

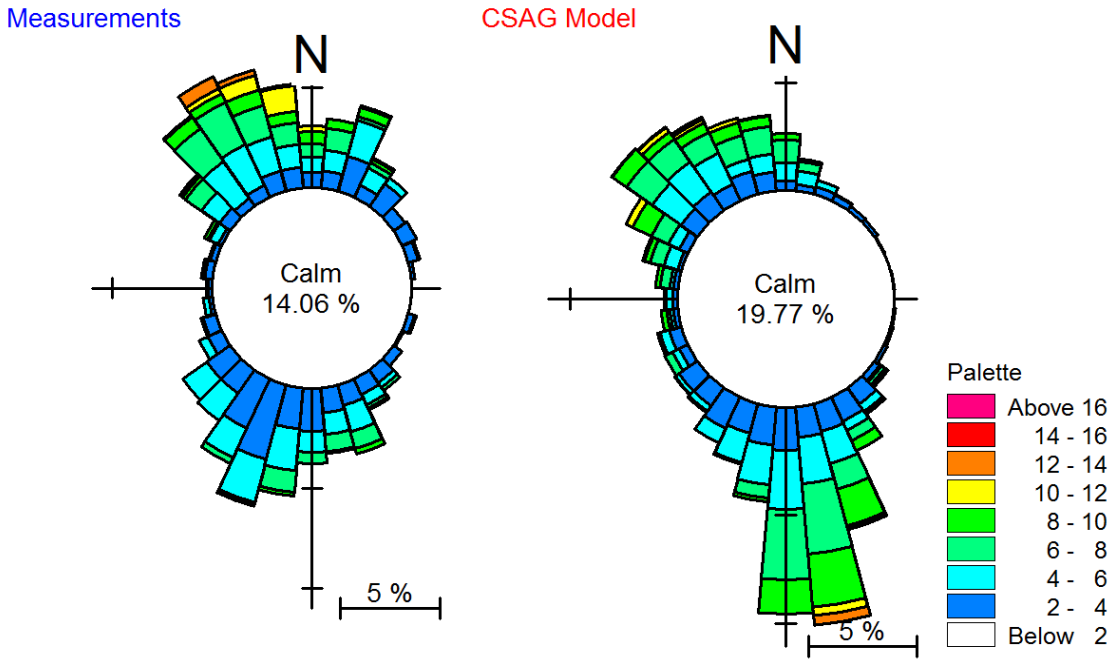

Figure 2-2: Wind Rose Comparison between Measured (+10 m AGL) and Modelled (+10 m AGL) Datasets – Cape Town International Airport

Overall, the CSAG model wind timeseries and roses shows good agreement with the weather station measurements at Cape Town International Airport.

2.2 Roman Rock

A wind timeseries and wind rose comparison of the CSAG and Weather Station data over the calibration period is presented in Figure 2-2 and Figure 2-2 respectively.

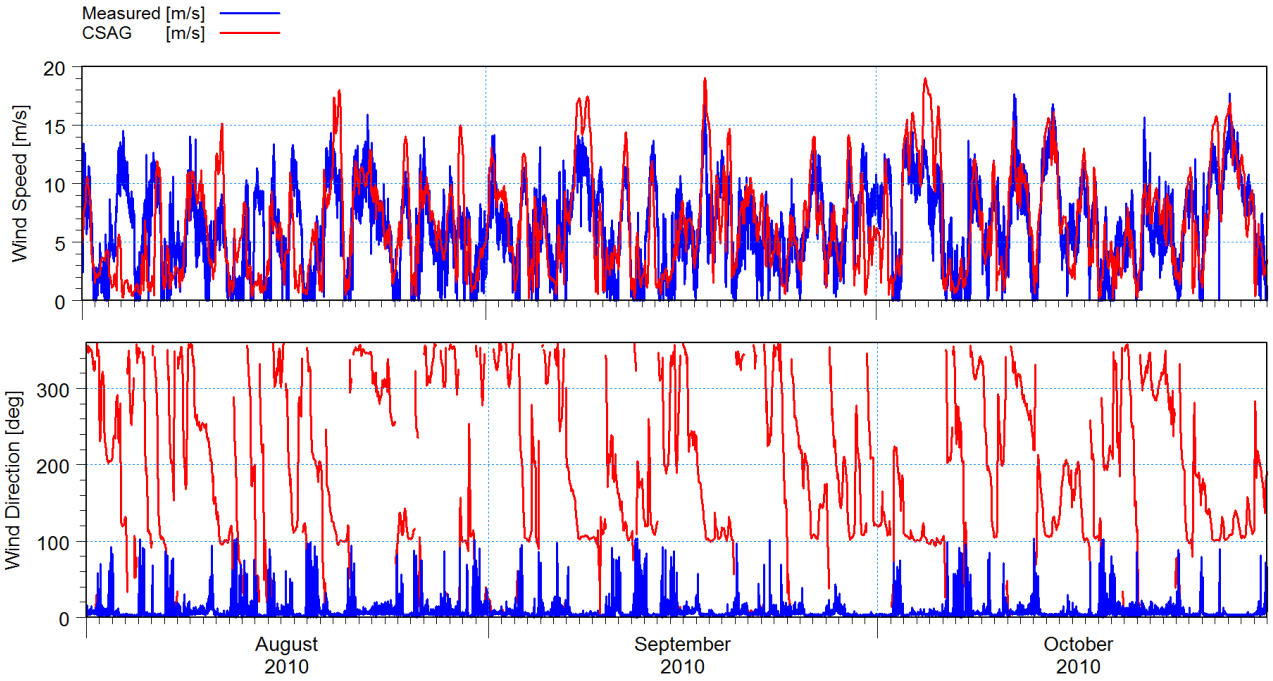

Figure 2-3: Wind Speed and Wind Direction Timeseries comparison of Measured (+10 m AGL) and Modelled (+10 m AGL) Datasets – Roman Rock

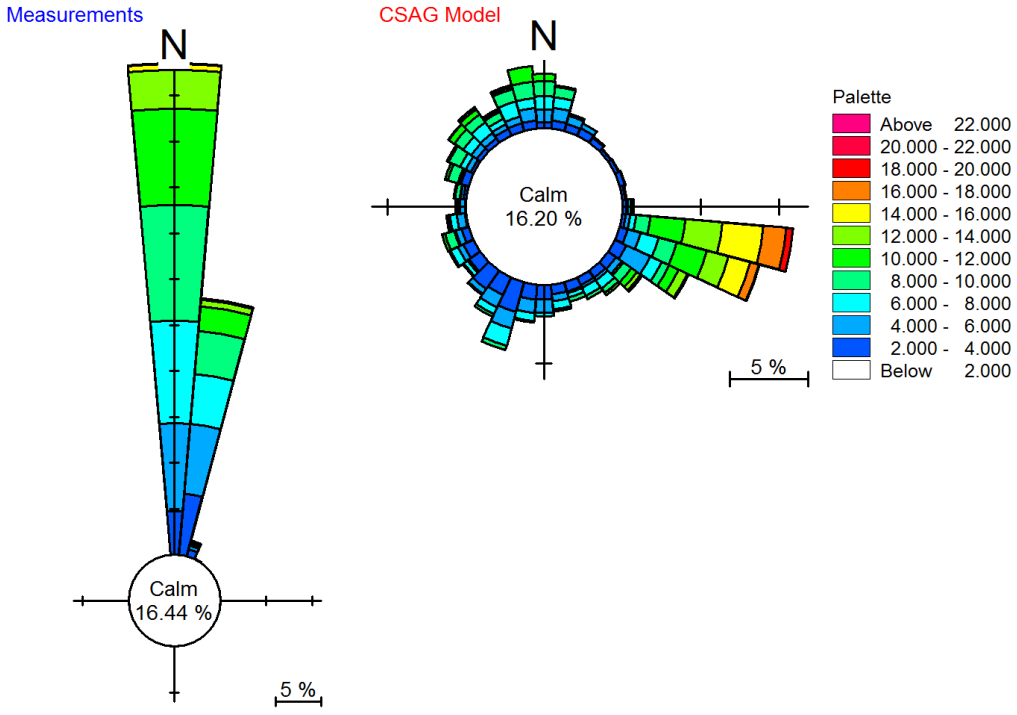

Figure 2-4: Wind Rose Comparison between Measured (+10 m AGL) and Modelled (+10 m AGL) Datasets – Roman Rock

From Figure 2-3, the CSAG model wind speed timeseries shows good agreement with the weather station measurements at Roman Rock. However, wind direction shows poor agreement as noted in the timeseries and wind rose plots. This discrepancy is due to instrument failure(s) within the measurement dataset.

2.3 Strand

A wind timeseries and wind rose comparison of the CSAG and Weather Station data over the calibration period is presented in Figure 2-6 and Figure 2-5 respectively.

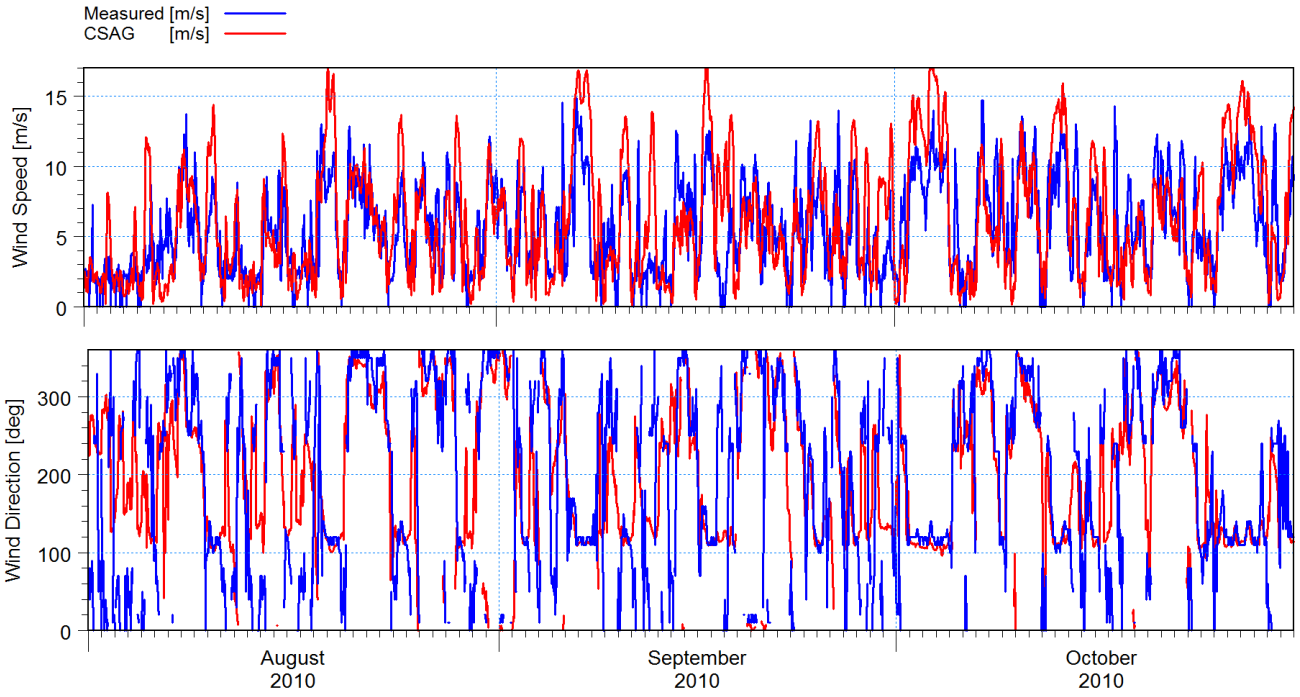

Figure 2-5: Wind Speed and Wind Direction Timeseries comparison of Measured (+10 m AGL) and Modelled (+7 m AGL) Datasets – Strand

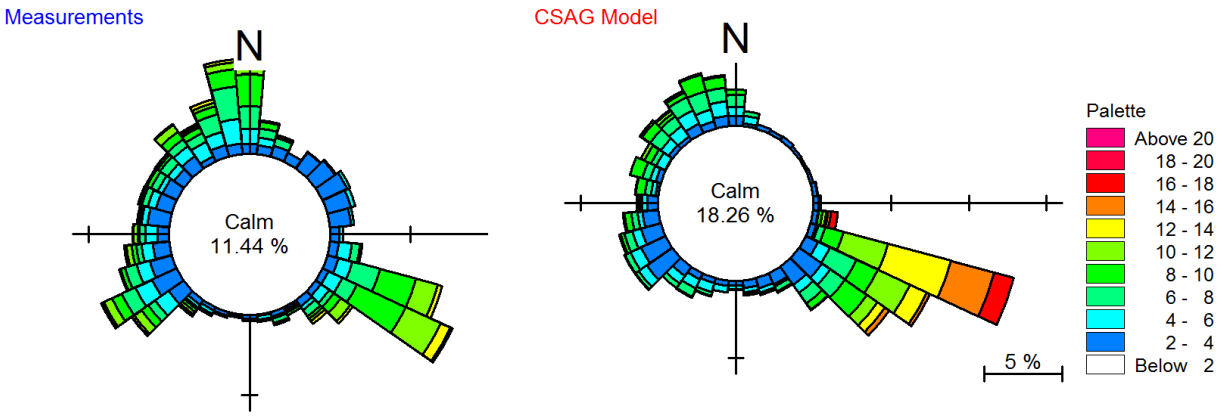

Figure 2-6: Wind Rose Comparison between Measured (+7 m AGL) and Modelled (+10 m AGL) Datasets – Strand

Overall, the CSAG model wind timeseries and roses shows good agreement with the weather station measurements at Strand. The model tends to slightly over-predict wind speed due to

the height difference between datasets. The CSAG dataset is at +10 m AGL while the Strand dataset is at +7 m AGL.

2.4 Cape Point

A wind timeseries and wind rose comparison of the CSAG and Weather Station data over the calibration period is presented in Figure 2-7 and Figure 2-8 respectively.

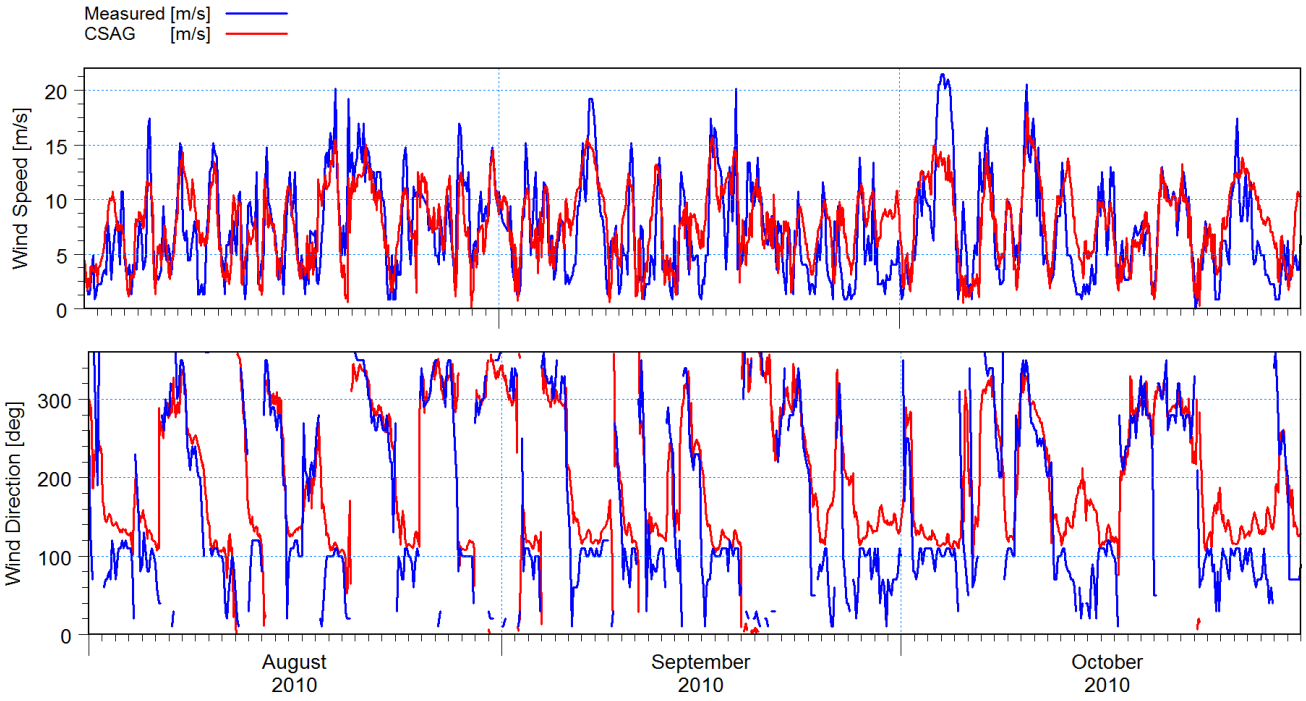

Figure 2-7: Wind Speed and Wind Direction Timeseries comparison of Measured (+10 m AGL) and Modelled (+10 m AGL - assumed) Datasets

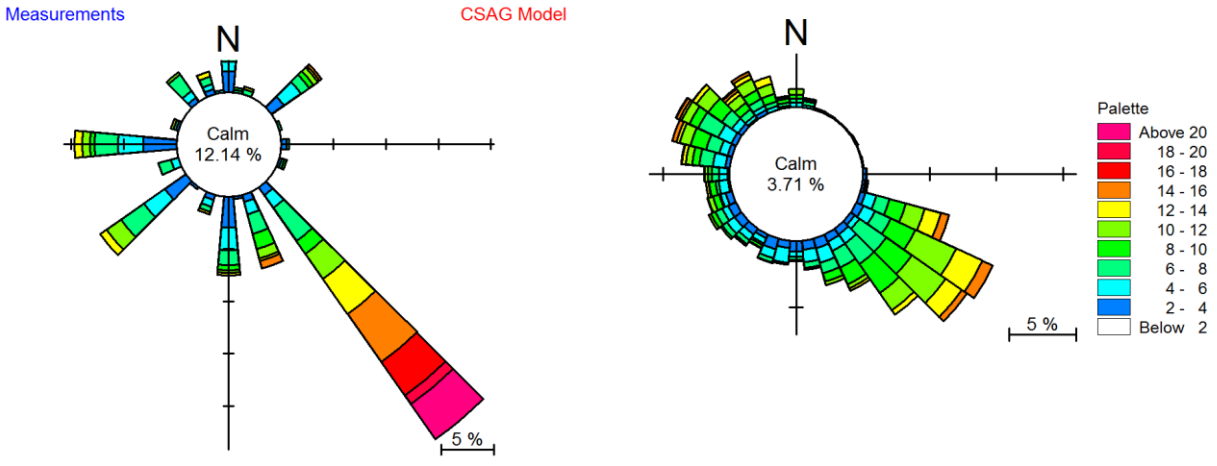

Figure 2-8: Wind Rose Comparison between Measured (+10 m AGL) and Modelled (+10 m AGL - assumed) Datasets

Overall, the CSAG model wind timeseries shows good agreement with the weather station measurements at Cape Point. The wind rose comparison reveals the limited number of wind

direction bins of the Cape Point weather station. This is likely due to instrument measurement limits.

2.5 Discussion

Overall, the timeseries comparison over the hydrodynamic model calibration period shows the CSAG hindcast dataset following wind trends quite well across weather stations and was deemed acceptable with no pre-processing undertaken.

3 REFERENCES

WASA. (2014). *Wind Atlas For South Africa: Report to the WASA Project Steering Committee.* Sandton: SANEDI.

Annexure B: Wind Formation and Atmospheric Models

1 WIND FORMATION AND BEHAVIOUR

1.1 Background

Generally, wind is generated by air flowing from high pressure systems to low pressure systems. On a macroscopic level, due to the rotation of the Earth, wind flow is dictated by the location of the pressure system.

A high-pressure system or anticyclone is a region where the atmospheric pressure at the surface is higher than its surrounding environment. The air at the center of a high pressure descends until it reaches the surface where it diverges from the center toward the edges (Heidorn, 2002). Conversely, low pressure cells are characterized by converging air flow at the surface which draw surface air from the center and which creates an ascending air current. In both low and high-pressure systems, air does not directly flow upward or downward. Instead, air currents deflect due to the Coriolis effect and instead circulate around these zones. Wind flow is deflected to the left in the Northern Hemisphere and to the right in the Southern Hemisphere.

When high pressure zones and low-pressure zones are relatively close to each other, large pressure gradients are present which in turn leads to strong winds (Heidorn, 2002). Similar to contour maps, weather maps show lines of constant pressure, termed “isobars” which indicate lines of constant pressure. The closer isobars are together, the stronger the wind generation.

Winds are fundamental in driving surface currents. When wind blows perpendicular to the coastline and surface water is pushed offshore, deep colder water is drawn to the surface to displace the surface water (Gaines, 2018). This phenomenon is known as coastal upwelling which is crucial for several biological processes. Upwelling supplies nutrient rich waters to the surface which facilitates the growth of marine food sources such as phytoplankton and seaweed. Therefore, upwelling regions are usually associated with marine ecosystems (Gaines, 2018). Regions like False Bay exhibit complex upwelling patterns due to the spatially varying wind pattern and the mountainous topography along the coastline.

1.2 Estimation of Spatially Varying Wind

In bay systems where coastal upwelling, mixing and transport is predominantly governed by a wind forced process (Gill, 1982), the setup of hydrodynamic models of these systems would need to consider boundary conditions that are realistic in relation to space-time varying meteorological effects. Therefore, multiple measurement locations are required around the bay which explicitly account for the space-time varying nature of atmosphere-

water fluxes (Rueda F. et al., 2009). There are several methods for determining spatially varying wind field parameters at locations where measurement data is incomplete or scarce. One approach is to build spatially varying wind fields by interpolating the wind record data from around the bay (Rueda F. et. al, 2009). This method presumes that the large scale meteorological behaviour of the bay can be captured by interpolation. This approach usually requires a number of reliable wind records that are situated directly above the water surface or measurement data that takes into account local environmental effects (termed local correction) during the processing of raw data e.g. data factoring differences in roughness between land and water (Hsu, 1981). Local correction typically involves boundary layer flow effects which account for the transition from land to water (Taylor & Lee, 1984). Other methods for estimating spatially varying environments have been proposed (Richards et. al (1966); Schwab (1978); Phillips & Irbe (1978)), however these methods are generally site specific and empirical. Moreover, these methods have been subject to a high degree of uncertainty (Schwab & Morton, 1984). The task of estimating spatially varying wind fields is therefore a complicated task due to the difficulty and uncertainty in converting over-land wind measurement to over-sea measurements. When over-sea wind approximations are generated from over-land measurements, the interpolation between multiple meteorological stations is formulated deterministically and serves as inputs into spatially varying wind models (Pan et. al (2001); Laval et. al (2003); Rubbert & Kongeter (2005); Rueda et. al (2005)). In these applications, the uncertainty is not accounted for which has a bearing on the quality of model predictions. The following is a list of approaches for determining uncertainty in model parameters (Rueda, Vidal, & Schladow, 2009):

- Conventional approaches such as the mean value first-order second moment (MFOSM) (Melching, 1995) which is based on analysing model behavior in a region of the parameter space near the “best” parameter set obtained from calibration (Rueda, Vidal, & Schladow, 2009);
- Regional approaches based on Monte Carlo sampling, such as the generalized likelihood uncertainty estimation (GLUE) (Beven & Binley, 1992), the Monte Carlo set membership (MCSM) (Van Straten & Keesman, 1991), and the prediction uncertainty (Klepper & Scholten, 1991); and
- Stochastic approaches based on Bayesian techniques (Omlin & Reichert, 1999).

An alternative to empirically determining spatially varying wind fields is to consider global or regional atmospheric models.

2 ATMOSPHERIC MODELS

2.1 Overview

Atmospheric models are nearly identical to hydrodynamic mathematical models that have been constructed for the purpose of solving the set of primitive equations that govern flow (or atmospheric flow in the case of atmospheric models), namely:

- The continuity equation – conservation of mass;
- Conservation of momentum – Navier-Stokes equations; and
- Thermal energy equation – relating the overall temperature of the system to heat sources and sinks.

Spatially, atmospheric models may be global, covering the Earth, or regional covering a section of the Earth. Depending on application, atmospheric models are capable of forecasting or providing hindcast data. In forecast mode, the model needs to be initialised by input from available observational data. Observational data generally comprises measurements, such as radiosondes, weather satellites, aircraft and ships, etc. (Gao, 2011).

These models are capable of predicting meteorological phenomena such as cyclones by supplementing the primitive equations above with parameters considering solar radiation, moist processes, heat exchange, soil, vegetation, surface water, the effects of terrain, and convection (Gao, 2011). High resolution or regional atmospheric models are termed “microscale models”. (WASA, 2014).

Due to the nonlinear nature of the primitive equations, analytical methods are unable to solve them. On this basis, numerical methods are employed in atmospheric models and hydrodynamic models to find approximate solutions.

2.2 Wind Atlas of South Africa (WASA)

The Wind Atlas of South Africa (WASA) project comprises one of the major regional atmospheric models available in South Africa. The WASA project commenced in 2009 as an initiative of the South African Department of Energy with the South African National Energy Research Institute (SANERI) as the executing partner (WASA, 2014). SANERI contracted with the implementation partners consisting of the South African Council for Scientific and Industrial Research (CSIR), University of Cape Town (Climate Systems Analysis Group), South African Weather Service (SAWS) and Department of Wind Energy, Technical University of Denmark (DTU Wind Energy). The principal funders are the Global Environment Facility (GEF) with UNDP support through the South African Wind Energy

Programme (SAWEP) which funded the CSIR activities and co-funded by the Royal Danish Embassy which funded the SANERI, SAWS, UCT and DTU activities (WASA, 2014).

The primary objective of the project was the development of a mesoscale atmospheric model which is calibrated with 10 wind stations (or masts) around South Africa (WASA, 2014). The model was developed with the intention of long term planning of large-scale exploitation of wind power in South Africa comprising wind farm planning, siting and wind resource assessments. The scope of work of the WASA project included the following:

- Setup and development of mesoscale wind modelling;
- Establishing wind measurement systems which included design, procurement, construction and operation etc.;
- Setup and development of microscale wind modelling;
- Application for wind resource assessment including workshops for invited stakeholders from e.g. authorities, planners, developers, banks, scientists, etc.;
- Estimation of extreme wind climates; and
- Documentation and dissemination including the preparation and dissemination of research publications and seminars.

The calibrated WASA Weather Research and Forecasting (WRF) model's domain extends beyond 10 wind stations and may be applied to most of South Africa. Wind data is available in two resolutions including either 3 km x 3 km or 5 km x 5 km resolution datasets. The 3 km x 3 km resolution model domain is presented in Figure 2-1.

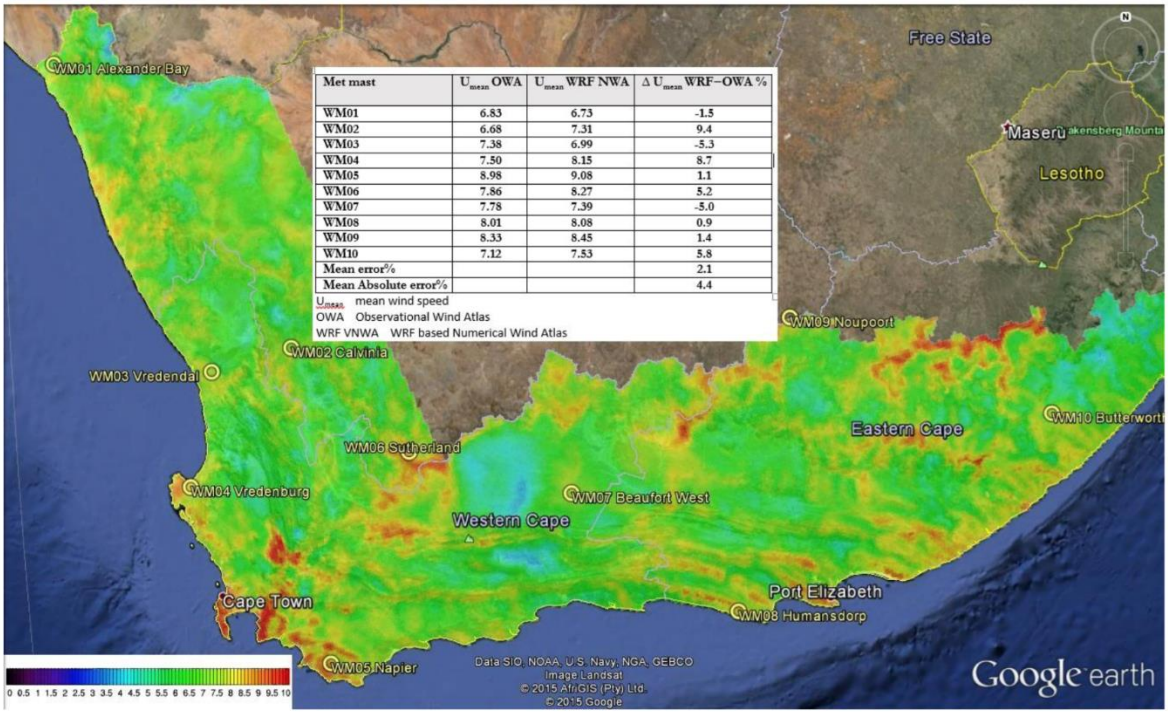

Met mast	U_{mean} OWA	U_{mean} WRF NWA	ΔU_{mean} WRF−OWA %
WM01	6.83	6.73	-1.5
WM02	6.68	7.31	9.4
WM03	7.38	6.99	-5.3
WM04	7.50	8.15	8.7
WM05	8.98	9.08	1.1
WM06	7.86	8.27	5.2
WM07	7.78	7.39	-5.0
WM08	8.01	8.08	0.9
WM09	8.33	8.45	1.4
WM10	7.12	7.53	5.8
Mean error%			2.1
Mean Absolute error%			4.4

U_{mean} mean wind speed
OWA Observational Wind Atlas
WRF VNWA WRF based Numerical Wind Atlas

Figure 2-1: Calibrated Model Domain of 3 km x 3 km Resolution

The diurnal and annual cycle of wind speed at each mast were compared with data from each respective model grid cell where the mast would be situated. An overview showing the summary statistics at the 10 mast site locations is provided in Table 2-1.

Table 2-1: Summary Statistics at 10 Mast Site Locations (WASA, 2014)

Mast	Mean Bias ($m\,s^{-1}$)	RMSE ($m\,s^{-1}$)	Mean absolute cycle bias ($m\,s^{-1}$)	Pearson correlation coefficient hourly	daily	monthly
WM01	−0.04	2.4	0.46	0.78	0.82	0.87
WM02	0.47	2.5	0.61	0.74	0.87	0.88
WM03	−0.46	2.1	0.52	0.78	0.85	0.90
WM04	0.04	1.9	0.48	0.83	0.93	0.97
WM05	−0.65	2.2	0.66	0.86	0.93	0.89
WM06	0.45	2.3	0.55	0.79	0.92	0.91
WM07	−0.14	2.3	0.38	0.72	0.86	0.78
WM08	−0.08	2.5	0.47	0.76	0.89	0.86
WM09	0.42	2.4	0.45	0.84	0.91	0.97
WM10	−0.02	2.7	0.66	0.74	0.83	0.89

From Table 2-1, the mean bias, root-mean-square error (RMSE) and mean absolute cycle bias were calculated using hourly data. The Pearson correlation is calculated using hourly, daily and monthly wind speed averages. Overall the WRF model simulated the diurnal and seasonal wind climate to a high degree of accuracy with a Pearson correlation coefficient near unity.

3 REFERENCES

Beven, K. J., & Binley, A. M. (1992). The future of distributed models: Model calibration and uncertainty prediction. *Hydrological Processes*, 6, 279-298.

Gaines, S. (2018, October 21). Upwelling. Santa Barbara, California, United States of America. Retrieved from NOAA Ocean Explorer: http://oceanexplorer.noaa.gov/explorations/02quest/background/upwelling/upwelling.html

Gao, G. (2011). *A Numerical Modeling Study of Storm Surge and Inundation in the Chesapeake Bay during the November 2009 Mid-Atlantic Nor'easter.* MSc. Thesis, The College of William and Mary in Virginia.

Gill, A. E. (1982). *Atmosphere–Ocean Dynamics.* San Diego: Academic Press.

Heidorn, K. C. (2002). *Suite 101: Science of the Sky.* http://www.islandnet.com/~see/weather/elements/glory.htm.

Hsu, S. A. (1981). Models for estimating offshore winds from onshore meteorological measurements. *Boundary Layer Meteorol.*, 20:3, 341–351.

Klepper, O., & Scholten, H. (1991). Prediction uncertainty in an ecological model of the Oosterschelde estuary. *Journal of Forecasting*, 10:1-2, 191-209.

Laval, B., Imberger, J., & Hodges, B. R. (2003). Modelling Circulation in Lakes: Spatial and Temporal Variations. *Limnology and Oceanography*, 48:3, 983-994.

Melching, C. S. (1995). *Reliability estimation, in Computer Models of Watershed Hydrology.* Water Resources Publications.

Omlin, M., & Reichert, P. (1999). A comparison of techniques for the estimation of model prediction uncertainty. *Ecological Modelling*, 115:1, 45-59.

Pan, H., Avissar, H. R., & Haidvogel, D. B. (2001). Summer Circulation and Temperature Structure in Lake Kinneret. *Jouranl of Physical Oceanography*, 32:1, 295-313 .

Phillips, D. W., & Irbe, J. G. (1978). *Lake to land comparison of wind, temperature, and humidity on Lake Ontario during the International Field Year for the Great Lakes (IFYGL).* Fisheries and Environment Canada, Atmospheric Environment.

Richards, T. L., Dragert, H., & McIntyre, D. R. (1966). Influence of atmospheric stability and overwater fetch on winds over the Great Lakes. *Monthly Weather Review*, 94:7, 448-453.

Rubbert, S., & Kongeter, J. (2005). Measurements and three-dimensional simulations of flow in a shallow reservoir subject to small-scale wind field inhomogeneities induced by sheltering. *Aquatic Sciences*, 67:1, 104–121.

Rueda, F. J., Schladow, G. S., Monismith, S. G., & Stacey, M. T. (2005). On the effects of topography on wind and the generation of currents in a large multi-basin lake. *Hydrobiologia*, 532:1–3, 139–151.

Rueda, F., Vidal, J., & Schladow, G. (2009). Modeling the effect of size reduction on the stratification of a large wind-driven lake using an uncertainty-based approach. *Water Resources Research*, 45, 1-15.

Schwab, D. J. (1978). Simulation and forecasting of Lake Erie storm surges. *Monthly Weather Review*, 106, 1476-1487.

Schwab, D. J., & Morton, J. A. (1984). Estimation of overlake wind speed from overland wind speed: A comparison of three methods. *Journal of Great Lakes Research*, 10:1, 68-72.

Taylor, P. A., & Lee, R. J. (1984). Simple guidelines for estimating wind speed variations due to small-scale topographic features. *Climatology Bulletin*, 23:1, 1-12.

Van Straten, G., & Keesman, K. J. (1991). Uncertainty propagation and speculation in projective forecasts of environmental change: A lake eutrophication example. *Journal of Forecasting*, 10:1-2, 163-190.

WASA. (2014). *Wind Atlas For South Africa: Report to the WASA Project Steering Committee.* SANEDI.